Modelling and numerical simulation of compressible multicomponent flows

Pratik Rai

INSTITUT POLYTECHNIQUE DE PARIS

NNT : 2021IPPAX040

Thèse de doctorat

Modelling and numerical simulation of compressible multicomponent flows

Thèse de doctorat de l'Institut Polytechnique de Paris
préparée à l'Ecole polytechnique

École doctorale n°574 ECOLE DOCTORALE DE MATHÉMATIQUES HADAMARD (EDMH)
Spécialité de doctorat: Mathématiques Appliquées

Thèse présentée et soutenue à Paris, le 23 julliet 2021, par

PRATIK RAI

Composition du Jury :

Rémi Abgrall Professeur des Universitiés, Institut für Mathematik & Computational Science, Universität Zürich	Président
Bruno Després Professeur des Universitiés, Laboratoire Jacques-Louis-Lions, Sorbonne Université	Rapporteur
Raphaël Loubère Directeur de recherche, Institut de Mathématiques de Bordeaux, Université de Bordeaux	Rapporteur
Siddhartha Mishra Professeur des Universités, Seminar für Angewandte Mathematik, ETH Zürich	Examinateur
Edwige Godlewski Professeur des Universitiés, Laboratoire Jacques-Louis-Lions, Sorbonne Université	Examinateur
Vincent Giovangigli Directeur de recherche, Centre de Mathématiques Appliquées, École Polytechnique	Directeur de thèse
Frédéric Coquel Directeur de recherche, Centre de Mathématiques Appliquées, École Polytechnique	Co-directeur de thèse
Florent Renac Maître de recherche, Méthodes Numériques pour la mécanique des Fluides, ONERA	Encadrant
Christophe Chalons Professeur des Universitiés, Laboratoire de Mathématiques de Versailles, Université de Versailles	Invité

Dedicated to my parents
for their love and sacrifice

A NOTE OF THANKS

At this juncture, marking the end of my doctoral research, I would like to thank the people who supported me, both technically and emotionally, and whose efforts are integral to the success of this thesis.

First of all, I would like to thank my supervisor, Florent Renac, for introducing me to the design of sophisticated numerical schemes for hyperbolic partial differential equations, and for his complete involvement in guiding me through this thesis. Florent and I, have interacted countless times during the course of this thesis, and it was amongst our many technical discussions that I gathered a sense of mathematical rigor, a skill that will certainly stand me in good stead, and I sincerely thank him for honing it in me. Working at ONERA also gave me the opportunity to collaborate with Claude Marmignon and I thank him for the long hours he dedicated in answering my queries and for his insight on the physics of compressible multiphase flows. I am also grateful to have met Vincent Couaillier, with whom I enjoyed many conversations, both, over lunch and often in the corridor. Being the head of the unit, he generally remains very occupied, yet he always made sure that all resources were made available to me, for the successful completion of my research.

I would like to express my sincere gratitude to the directors of this thesis, Prof. Frédéric Coquel and Prof. Vincent Giovangigli, for their time and dedication in following the progress of this thesis, and for kindling in me a curiosity for mathematics, in general, through our many stimulating conversations. It was extremely unfortunate that, during the later part of this thesis, Frédéric's health started deteriorating significantly and our interaction came to a sudden halt. I sincerely hope that Frédéric makes a full recovery and rejoin the academic community at the earliest.

I would also like to extend my sincere thanks to all the members of the jury, for their interest in my research and for accepting to be a part of the evaluation process, and I must also thank the Ecole Polytechnique for enrolling me as a doctoral researcher in the Hadamard school of Mathematics (EDMH) and to the scientific board at ONERA for accepting to fund this research endeavour. Here, I would like to especially mention Prof. Nizar Touzi from the laboratory of Applied Mathematics (CMAP), who I happened to meet at a truly difficult moment in my doctoral research and it was through his advice and counselling that I was able to sail through those troubled times. I will, therefore, be forever be indebted to him for his support.

My stay in Paris allowed me to make some wonderful friends, Javier, Fabio, Francesca, Rocco, Matteo, Luc, who left an indelible impression on me. I will forever miss our lunch at ONERA, our chat during the 4 pm coffee breaks and the weekend pizza nights. I hope that with the advancement of our careers in the coming years we still remain connected.

Finally, I would like to mention a special person in my life, Rishav, who stood by me and supported me through thick and thin, and without whose love and warmth I would have never complete this thesis successfully. I must admit that being distant from each other, for

all these year, has taken a heavy toll on us, and in the coming months I promise to move closer to you.

To everyone involved, I hope to have made you proud. Thank you.

Abstract

This thesis addresses two main objectives: the modelling of compressible multiphase and multicomponent flows, and the design of novel numerical schemes for their accurate simulation.

In the first part of this work, we propose a novel Baer-Nunziato-like hyperbolic model for reactive non-equilibrium gas-liquid flows, where the governing equations account for mass transfer, interfacial drag, mechanical nonequilibrium and thermal transfer between the phases. The exchange of information between the phases is governed my the material interface which are defined using general closure laws. The model is Galilean invariant and entropy dissipative and maintain these properties at compete non-equilibrium.

We, then, focus on the design of novel high-order numerical schemes for hyperbolic multiphase and multicomponent flows, involving nonconservative products. Here, the discretization framework is based on the discontinuous Galerkin spectral elements method (DGSEM), which involves the collocation of quadrature and interpolation points. The DGSEM uses the summation-by-parts operators, with simultaneous approximation terms (SBP-SAT), in the numerical quadrature for approximating the integrals over discretization elements. We use the SBP-SAT operators to modify the volume integral over cell elements and replace the physical fluxes with entropy conservative fluxes in fluctuation form, while applying entropy stable fluxes at the cell interfaces. This modification allows us to establish a semi-discrete entropy inequality, for a given entropy function, while still ensuring high-order accuracy of the numerical scheme. For high-order integration in time, we rely on explicit strong-stability preserving Runge-Kutta schemes that retain the properties of first order time integration schemes.

We, first, apply the semi-discrete DGSEM to the discretization of the homogeneous Baer-Nunziato model where we derive entropy conservative and entropy stable fluxes for the model. We show that these fluxes also satisfy the Abgrall criterion and preserve the discrete kinetic energy. The numerical scheme guarantees the positivity of the cell-averaged solutions, which is ensured by imposing conditions on the numerical parameters. The positivity of the solution is further transferred to nodal values through the use of a posteriori limiters.

The DGSEM is, further, applied to the discretization of the gamma-based multicomponent model of Shyue (1998). Here, we propose a novel high-order entropy stable scheme that enables a sharp resolution of material discontinuities, while also maintaining high-order accuracy and entropy stability. We derive contact-preserving numerical fluxes and entropy conservative fluxes that are applied in the volume integral based on the values of a troubled-cell indicator function, while at the cell-interfaces we derive a HLLC approximate Riemann solver. The numerical scheme resolves shock solutions accurately, preserves uniform states across contact discontinuities and maintains positivity of the cell-averaged solutions.A posteriori limiters are further applied that enforce positivity at nodal values.

Résumé

Cette thèse a deux objectifs principaux : la modélisation des écoulements compressibles multiphasiques et multi-composants, et la conception de nouveaux schémas numériques pour leur simulation d'ordre élevé.

En ce qui concerne la modélisation des écoulements multiphasiques, nous nous concentrons sur le modèle de non-équilibre de type Baer-Nunziato et proposons un nouveau modèle pour les écoulements impliquant un mélange réactif de gaz et de liquide. Notre modèle est hyperbolique et prend en compte le transfert de masse, la traînée interfaciale, le déséquilibre mécanique ainsi que le transfert thermique entre les phases. Le modèle est invariant par transformations galiléennes et dissipe l'entropie.

En ce qui concerne la conception de nouveaux schémas pour les écoulements compressibles, nous nous concentrons sur les modèles hyperboliques d'écoulement multiphasiques et multi-composants sous forme non-conservative. Nous choisissons comme cadre de discrétisation la méthode des éléments spectraux de Galerkin discontinus (DGSEM), basée sur la collocation des points de quadrature et d'interpolation. La méthode DGSEM utilise des opérateurs de sommation par parties (SBP) dans la quadrature numérique pour approcher les intégrales sur les éléments de discrétisation. Dans notre cas, nous modifions l'intégrale sur les éléments de la cellule en remplaçant les flux physiques par des flux aux fluctuations conservant l'entropie tout en appliquant des flux dissipant l'entropie aux interfaces du maillage. Cela nous permet d'établir un schéma semi-discret qui est précis à l'ordre élevé et qui satisfait à une inégalité d'entropie semi-discrète. Pour l'intégration temporelle d'ordre élevé, nous nous appuyons sur des schémas explicites de Runge-Kutta préservant la stabilité et conservant les propriétés des schémas d'intégration temporelle au premier ordre.

Nous appliquons ce schéma à la discrétisation du modèle homogène de Baer-Nunziato, où nous dérivons des flux conservant et dissipant l'entropie mathématique pour le modèle. Nous montrons également que la conception des flux numériques préserve formellement l'énergie cinétique au niveau discret. En analysant le schéma discret, nous imposons des conditions sur les paramètres numériques qui restreignent le pas de temps et garantissent la positivité des solutions moyennées par cellule. La positivité de la solution moyenne de la cellule est renforcée aux valeurs nodales en appliquant des limiteurs.

Le schéma DGSEM est également appliqué pour la discrétisation du modèle multi-composants de Shyue (1998) pour des lois d'état de type gaz raidis. Nous proposons ici un nouveau schéma d'ordre élevé qui dissipe l'entropie et qui permet une résolution précise des discontinuités matérielles. À cette fin, nous dérivons des flux dissipant l'entropie et des flux préservant les contacts qui sont appliqués dans l'intégrale de volume, sur la base d'un senseur de chocs. Pour les flux numériques à l'interface, nous concevons un solveur de type HLLC pour le modèle multi-composants. Nous montrons que le schéma DG satisfait à inégalité d'entropie semi-discrète pour les solutions de choc, préserve les profils uniformes à travers les contacts et les interfaces matérielles et maintient la positivité de la solution.

Contents

List of Figures

List of Tables

Chapter 1

Introduction

1.1 Motivation

The study of compressible multiphase flows finds use in several engineering and physical problems. Historically, there are numerable evidences to them being used to study geophysical flows involving sediments and clouds, and fluid flows through porous media. Approximately, around the middle of the twentieth century, the modelling and simulation of multiphase models started gathering interest from the nuclear and the aeronautical industries. Typically, in the nuclear industry, the targeted applications have been to investigate the normal operating mode of pressurized water reactors and incidental configurations, such as the departure from nucleate boiling, the loss of coolant accident (LOCA) or the re-flooding phase following a LOCA. While in the aeronautical and aerospace industries, compressible multiphase models were used to study the complex flows physics occurring inside jet engines or through the propulsion system of re-entry space vehicles. In the particular example of a jet engine, multiphase flows can be found in the combustion chamber, where air from the compression phase is received and mixed with dispersed aviation fuel to create a combustible air-fuel mixture which is then ignited. The unburnt mixture and the burnt gaseous product then travels through the turbine and, finally, exit through the nozzle. This motion of the fluid mixture through the different stages of the jet engine is a complex phenomenon, where the fluid mixture experiences compression, expansion, ignition, interfacial drag, heat and mass transfer. A thorough understanding of such complex flows by means of physical experiment can entail heavy monitory expenses and resources. Thus creating a need for mathematical models and design of numerical schemes which enable the study of complex flow physics by means of mathematical analysis and computer simulations.

In this thesis, we study compressible multiphase flows through diffuse interface models, examples of which can be found in [4, 7, 10, 99, 101, 119, 122]. Diffuse interface models aim to resolve the interface, between the involved phases or species, numerically in diffused surrounding zones. One main challenge of this approach lies in the fact that the computation of interfaces separating two immiscible phases with different thermodynamics has no physical viscous regularization, as seen in shock-capturing schemes. The model may contain external driving forces, also known as source terms, which usually govern the disequilibria between the phases (or species). These disequilibria terms can be related to compaction, heat transfer, interfacial drag or mechanical transfer. Diffuse interface models can be further categorized

into interface-based models and multicomponent (or multispecies) models. In the case of interface-based models, each phase is assigned its own set of governing equations and the phases interact with each other through the material interface. Such models also provide an explicit and clean treatment of the material interface which is necessary as an interface is the physical location where the flow parameters are close to the limits of validity of the equation of state. In contrast, a multicomponent model is based on the mixture quantities of the flow. Here the system of equations do not explicitly treat the material interface and one may either consider gas mixture where all the species occupy the same volume, or immiscible mixture where the components occupy different volumes in a given control volume. However, in contrast to interface-based models, the number of equations in multicomponent models may not depend on the number of components. This makes them highly computationally efficient.

The governing equations of multiphase models are, usually, represented by a system of first order nonlinear hyperbolic partial differential equations (PDEs), for which the Cauchy problem lead to breakdown of classical solutions in finite time, even for sufficiently smooth initial data. As a result, global existence of solutions requires working with a class of discontinuous functions where the system of equations is interpreted in their distributional sense. We explore these fundamental notions by briefly recalling the mathematical theory around hyperbolic systems. This in turn will help in better understanding the forthcoming discussions in this thesis. The main ideas presented here are borrowed from the seminal works of Lax [88, 89] and from the books by Godlewski and Raviart [61], as well as by Dafermos [39].

Let us consider a bounded domain $\Omega \subseteq \mathbb{R}^d$ in d space dimensions with Lipschitz boundary $\partial\Omega \subseteq \mathbb{R}^{d-1}$ and unit outward normal $\mathbf{n} \in S^{d-1}$. The production of an external vector valued quantity $\mathbf{u}$, that takes values in an open set $\Omega_* \subset \mathbb{R}^N$, within the domain, is given by the following balance law

$$\frac{d}{dt}\int_\Omega \mathbf{u}(\mathbf{x},t)d\mathbf{x} + \int_{\partial\Omega} \mathbf{f}(\mathbf{u})\cdot\mathbf{n}\, d\Gamma(\mathbf{x}) + \int_\Omega \mathbf{c}(\mathbf{u})\nabla\mathbf{u}d\mathbf{x} = \int_\Omega \mathbf{s}(\mathbf{x},t)d\mathbf{x}, \quad t>0, \tag{1.1}$$

where $\mathbf{f}(\mathbf{u}) : \Omega_* \to \mathbb{R}^{N\times d}$ is the called the flux function, that acts through the boundaries of the domain, $\mathbf{c}(\mathbf{u})\nabla\mathbf{u} : \Omega_* \to \mathbb{R}^N$ is the nonconservative product and $\mathbf{s}(\mathbf{x},t) : \Omega_* \to \mathbb{R}^N$ is the vector of driving forces, that is also known as the source term. Note that both $\mathbf{f}(\mathbf{u})$ and $\mathbf{c}(\mathbf{u})$ are smooth functions. In the particular case where the source terms and the nonconservative product are absent, $\mathbf{c}(\mathbf{u})\nabla\mathbf{u} \equiv \mathbf{s}(\mathbf{x},t) \equiv 0$, the quantity $\mathbf{u}$ is said to be conserved. The application of the divergence theorem then leads to the system of *conservation laws* for $N-$variables

$$\partial_t\mathbf{u} + \nabla\cdot\mathbf{f}(\mathbf{u}) = 0, \quad \mathbf{x}\in\mathbb{R}^d,\ t>0. \tag{1.2}$$

The system (1.2) is said to be *hyperbolic* if the matrix valued function $\mathbf{A}(\mathbf{u}) = \sum_{j=1}^d \frac{\partial}{\partial\mathbf{u}}\mathbf{f}_j(\mathbf{u})n_j : \Omega_* \ni \mathbf{u} \mapsto \mathbb{R}^{N\times N}$ for smooth solutions of (1.2) that admits real eigenvalues $\lambda_1(\mathbf{u}), \lambda_2(\mathbf{u}), \cdots, \lambda_N(\mathbf{u})$ and corresponding linearly independent (right) eigenvectors $\mathbf{r}_1(\mathbf{u}), \mathbf{r}_2(\mathbf{u}), \cdots, \mathbf{r}_N(\mathbf{u})$, such that

$$\mathbf{A}(\mathbf{u})\mathbf{r}_k(\mathbf{u}) = \lambda_k(\mathbf{u})\mathbf{r}_k(\mathbf{u}), \quad \mathbf{u}\in\Omega_*,\ 1\le k\le N. \tag{1.3}$$

As a result, hyperbolicity of a system of PDEs can be interpreted as the propagation of N distinct weak waves in space at (finite) speeds corresponding to the eigenvalues, also known as *characteristic speeds*. If the eigenvalues are distinct then (1.2) is said to be *strictly*

hyperbolic.

Definition 1.1.1. *The $k-th$ characteristic field is said to be genuinely nonlinear if*

$$D\lambda_k(\mathbf{u})\cdot\mathbf{r}_k(\mathbf{u}) \neq 0, \quad \forall \mathbf{u}\in\Omega_*,$$

and it is said to be linearly degenerate if

$$D\lambda_k(\mathbf{u})\cdot\mathbf{r}_k(\mathbf{u}) = 0, \quad \forall \mathbf{u}\in\Omega_*,$$

where $D\lambda_k(\mathbf{u})\cdot\mathbf{r}_k(\mathbf{u})$ is the directional derivative of $\lambda_k(\mathbf{u})$ in the direction $\boldsymbol{r}_k(\mathbf{u})$.

If (1.2) is provided with sufficiently smooth initial conditions

$$\mathbf{u}(\mathbf{x},0) = \mathbf{u}_0(\mathbf{x}), \tag{1.4}$$

then we arrive at the Cauchy problem for (1.2).

Notion of weak solutions for conservation laws

Hyperbolic systems may develop discontinuous solutions in finite time even for sufficiently smooth initial data, where the notion of the derivative becomes too strong. We illustrate this loss of regularity by considering the inviscid Burger's equation in single spatial dimension

$$\partial_t u + \partial_x\left(\frac{u^2}{2}\right) = 0, \tag{1.5a}$$

$$u(x,0) = u_0(x) = \frac{1}{1+x^2}. \tag{1.5b}$$

For t $>$ 0, but small, the solution can be found by the method of characteristics. Indeed, if u is smooth, (1.5a) is equivalent to

$$\partial_t u + u\partial_x u = 0. \tag{1.6}$$

Geometrically, this means that the directional derivative of u along the vector $(1,u)$ vanishes. Therefore u must be constant along the characteristic lines in $x-t$ plane:

$$t \mapsto (x + tu_0(x), t) = \left(x + \frac{t}{1+x^2}, t\right). \tag{1.7}$$

These lines do not intersect for $t < T = 8/\sqrt{27}$, and the solution of the Cauchy problem is thus given by

$$u\left(x + \frac{t}{1+x^2}, t\right) = \frac{1}{1+x^2}. \tag{1.8}$$

However, for $t > T$ the characteristic lines start interacting and the map

$$x \mapsto x + \frac{t}{1+x^2}, \tag{1.9}$$

is no longer one-to-one. Hence (1.8) does not define a single-valued solution for the Cauchy problem (1.5).

Note that a classical solution is a Lipschitz continuous function that satisfies (1.2) almost everywhere in Ω_*. However, it is clear from our concise demonstration that global solutions cannot be defined in a classical sense, hence we interpret (1.2) in the sense of distributions.

Definition 1.1.2. *Let $\mathbf{u}_0(\mathbf{x}) \in \boldsymbol{L}^1_{loc}(\mathbb{R}^d)$ be a vector-valued initial condition that takes values in Ω_* and $\boldsymbol{\phi}(\boldsymbol{x},t) \in \boldsymbol{C}^1_0(\mathbb{R}^d \times [0,+\infty))^N$ be a test function, then a function $\mathbf{u}(\mathbf{x},t)$ is a weak solution to the Cauchy problem (1.2),(1.4) if it satisfies the following relation in the sense of distributions*

$$\int_0^\infty \int_\Omega \left(\mathbf{u}\cdot\partial_t\boldsymbol{\phi} + \mathbf{f}(\mathbf{u})\cdot\nabla\boldsymbol{\phi}\right) d\mathbf{x}\,dt + \int_\Omega \mathbf{u}_0(\mathbf{x})\cdot\boldsymbol{\phi}(\mathbf{x},0)\,d\mathbf{x} = 0, \tag{1.10}$$

for all $\boldsymbol{\phi}(\boldsymbol{x},t) \in \boldsymbol{C}^1_0(\mathbb{R}^d \times [0,+\infty))^N$.

Alternatively, $\mathbf{u}(\mathbf{x},t)$ is a weak solution if it is piecewise differentiable over submanifolds of $\mathbb{R}^d \times [0,+\infty)$, with normals $(\mathbf{n},-\sigma) \in S^{d-1}\times\mathbb{R}$, and satisfy (1.2) at its points of differentiability, while satisfying the Rankine-Hugoniot jump condition

$$\mathbf{n}\cdot[\![\mathbf{f}(\mathbf{u})]\!] = \sigma[\![\mathbf{u}]\!], \tag{1.11}$$

at each surface of discontinuity.

Here, the terms $[\![\mathbf{u}]\!] := \mathbf{u}^+ - \mathbf{u}^-$ denotes the jump operation and

$$\mathbf{u}^\pm(\mathbf{x},t) := \lim_{\epsilon\downarrow 0,\epsilon>0} \mathbf{u}(\mathbf{x}(t)\pm\epsilon\mathbf{n}, t\pm\epsilon\sigma),$$

are the traces of $\mathbf{u}$ at the surface of discontinuity.

We now show that the distributional interpretation of the conservation law (1.2) is too weak and does not lead to uniqueness. As an example, we again consider the Burger's equation (1.5a) and complement it with Riemann initial data

$$u_0(x) = \begin{cases} 0, & x<0,\\ 1, & x>0. \end{cases} \tag{1.12}$$

This leads to the Cauchy problem emanating piecewise constant data on the $x-t$ plane that are separated by jump discontinuities. This is called as a *Riemann problem.* A continuous solution of th Riemann problem is given by

$$u_1(x,t) = \begin{cases} 0, & x<0,\\ x/t, & 0\le x<t,\\ 1 & t\le x. \end{cases} \tag{1.13}$$

However, using the Rankine-Hugoniot conditions (1.11), one can easily come up with more weak solutions, such as

$$u_2(x,t) = \begin{cases} 0, & x<t/2,\\ 1, & x\ge t/2 \end{cases} \qquad \text{and} \quad u_3(x,t) = \begin{cases} 0, & x<t/4,\\ 1/2, & t/4\le x\le 3t/4,\\ 1, & x\ge 3t/4, \end{cases}$$

where u_2 and u_3 trivially satisfy the conservation law (1.5a) in regions where it is constant, whereas along the the lines of discontinuity $x = t/2$ and $x = t/4, x = 3t/4$, respectively, the condition (1.11) holds, with shock speeds $\sigma = 1/2$ and $\sigma = 1/4, \sigma = 3/4$, respectively.

From this example, it is evident that additional constraints are needed to guarantee uniqueness of solution for (1.2), which we describe below.

Mathematical entropy and admissible solutions

Admissible solutions, among weak solutions for (1.2), must satisfy a companion relation known as the *entropy condition*. The entropy condition is defined in terms of a convex entropy function $\eta(\mathbf{u}) \in \mathbf{C}^2(\Omega_*, \mathbb{R})$ and an entropy flux $\mathbf{q}(\mathbf{u}) \in \mathbf{C}^2(\Omega_*, \mathbb{R}^d)$.

Definition 1.1.3. *Let $(\eta(\mathbf{u}), \mathbf{q}(\mathbf{u}))$ be an entropy-entropy flux pair and $\mathbf{v}(\mathbf{u}) := \frac{\partial}{\partial \mathbf{u}}\eta(\mathbf{u})$ be the entropy variables such that*

$$\boldsymbol{q}_j(\mathbf{u})^\top = \mathbf{v}(\mathbf{u})^\top \mathbf{f}_j'(\mathbf{u}), \quad \forall \mathbf{u} \in \Omega_*,\ j = 1, \cdots, d. \tag{1.14}$$

Then admissible weak solutions $\mathbf{u}(\mathbf{x}, t)$ to the Cauchy problem (1.2), (1.4) must satisfy an entropy inequality (1.15) for all test functions $\boldsymbol{\phi}(\boldsymbol{x}, t) \in \boldsymbol{C}_0^1(\mathbb{R}^d \times [0, +\infty))$ in the sense of distributions

$$\int_0^\infty \int_\Omega \left(\eta(\mathbf{u})\partial_t \boldsymbol{\phi} + \mathbf{q}(\mathbf{u}) \cdot \nabla \boldsymbol{\phi}\right) d\mathbf{x}dt + \int_\Omega \eta(\mathbf{u}_0(\mathbf{x}))\boldsymbol{\phi}(\mathbf{x}, 0)d\mathbf{x} \geq 0. \tag{1.15}$$

Note that this entropy condition is useful only if some nontrivial convex entropy function for (1.2) is known. Furthermore, (1.14) is a system of $N \times d$ linear PDEs for $d+1$ unknowns $\eta(\mathbf{u})$ and $\mathbf{q}(\mathbf{u})$. Therefore, in the case of scalar conservation law $N = 1$ in arbitrary spatial dimensions, any convex function can be considered as the entropy. While for systems $N > 1$, the entropy-entropy flux pairs can only be determined for $N = 2$ and $d = 1$. For any system, where $N > 2$ in $d > 1$, the relation (1.14) is overdetermined. Interestingly, however, hyperbolic systems arising from continuum mechanics are known to be endowed with an entropy function which satisfies the second law of thermodynamics. A classic example for such a system is the compressible Euler equations of gas dynamics, where the mathematical entropy function is usually considered as the negative of the concave physical entropy.

Theorem 1.1.1 (Godunov [62])**.** *Let $\eta(\mathbf{u})$ be a strictly convex function, then it qualifies as an entropy function for the conservation law (1.2) if the $N \times N$ matrix $\eta''(\mathbf{u})\mathbf{f}_j'(\mathbf{u}), 1 \leq j \leq d$ is symmetric positive definite.*

The entropy condition (1.15) can equivalently be written in the divergence form as

$$\partial_t \eta(\mathbf{u}) + \nabla \cdot \mathbf{q}(\mathbf{u}) \leq 0. \tag{1.16}$$

In the case of smooth solutions, (1.16) turns into a conservation law for the entropy function, while for solutions in the form of shocks the entropy solution is the limit of a vanishing viscosity. Additionally, it can be said that weak solutions are admissible it they satisfy the the following entropy jump condition across discontinuities

$$\mathbf{n} \cdot [\![\mathbf{q}(\mathbf{u})]\!] \leq \sigma [\![\eta(\mathbf{u})]\!]. \tag{1.17}$$

We end this brief recollection of the theory of hyperbolic conservation laws by commenting on the entropy variable, which appeared in Definition 1.1.3.

Theorem 1.1.2 (Mock [100]). *If $\eta(\mathbf{u})$ is a strictly convex entropy function then the mapping $\mathbf{u} \mapsto \mathbf{v}(\mathbf{u})$ is one-to-one, and the change of variable $\mathbf{u}(\mathbf{v})$ symmetrizes (1.2)*

Through the change of variables, the conservation law can be written in terms of the entropy variables

$$\partial_t \mathbf{u}(\mathbf{v}) + \partial_x \mathbf{f}(\mathbf{u}(\mathbf{v})) = 0. \tag{1.18}$$

This system is symmetric in the sense that the matrix $\mathbf{u}'(\mathbf{v}) = \left(\eta''\left(\mathbf{u}(\mathbf{v})\right)\right)^{-1}$ is symmetric positive definite, and $\mathbf{f}'(\mathbf{u}(\mathbf{v}))$ is symmetric.

MODELLING OF TWO-PHASE FLOWS

One of the pioneering works, in the context of two-phase flows, involves the model proposed by Baer and Nunziato [7], where the governing equations describe the flow of a mixture of energetic granular material embedded in gaseous combustion product under complete disequilibria. Their model was derived by bypassing the discrete nature of separate phases through the use of averaging techniques from [45, 75]. In single spatial dimension, the Baer-Nunziato model is a set of seven hyperbolic partial differential equations, where each phase has its own governing equations for the evolution of partial mass, momentum and energy, while the phases are coupled through the transport equation for the void fraction. It must be noted that such models require explicit treatment of the material interface as the closure of the interfacial variables can significantly impact the well-posedness of the Cauchy problem, see [115].

In our work, we focus on deriving a Baer-Nunziato-like disequilibrium model for reactive gas-liquid flows. In a slightly general context, the authors in [115] were the first to propose a non-equilibrium model for compressible gas-liquid flows. Their model was derived by applying the averaging technique in [44] to compressible flows, where the authors neglected the mass and thermal transfer between the phases. This led to numerous works where the authors have modified the model proposed in [115] to include either mass transfer or thermal transfer or both, see [43, 53, 56, 92, 97, 117, 118, 120]. Note, however, that even today there is no general consensus on the choice of the source terms that accurately depicts the physics of the flow. As a result, in our work we resort to the assumptions made in [10] for the choice of source terms for reactive mixtures. However, even though there is sufficient freedom in the choice of the source terms, yet there exists a major constraint which takes the form of the entropy balance. Essentially, for a convex entropy function, the contribution of the source terms should lead to an entropy decay. This is particularly difficult when mass transfer is included in the model, as the difference of the Gibbs free energy between the phases appears as an additional driving force in the entropy balance [10, 144]. The difficulties are however not limited to the presence of Gibbs free energy terms, as we show that the entropy balance is susceptible to change in the inertial frame of reference, and corrective source terms are necessary in order to achieve Galilean invariance.

Through this thesis, we propose a novel two-phase flow model for gas-liquid reactive flows that is both Galilean invariant and entropy dissipative. The model exhibits these capabilities while accounting for disequilibria in chemical transfer, interfacial drag, pressure

and heat transfer between the phases. To the best of our knowledge, no other model for reactive two-phase flows exhibits such properties at complete disequilibria.

Nonconservative hyperbolic systems and their numerical discretization

In the context of designing novel numerical schemes, we focus on the discretization of compressible multiphase and multicomponent flows, which are governed by nonliear hyperbolic . Here we are interested in the Cauchy problem for a one-dimensional nonlinear nonconservative hyperbolic system of the form

$$\partial_t \mathbf{u} + \partial_x \mathbf{f}(\mathbf{u}) + \mathbf{c}(\mathbf{u})\partial_x \mathbf{u} = 0, \quad x \in \mathbb{R},\ t > 0, \tag{1.19a}$$

$$\mathbf{u}(\mathbf{x}, 0) = \mathbf{u}_0(\mathbf{x}), \quad x \in \mathbb{R}. \tag{1.19b}$$

An integral form of this equation in d space dimensions space has been introduced in (1.1), however here we only consider the homogeneous system and ignore the source terms. Note that even though $\mathbf{c}(\mathbf{u})$ is assumed to be smooth, $\mathbf{u}$ can be discontinuous. This makes it difficult to meaningfully define the nonconservative product $\mathbf{c}(\mathbf{u})\partial_x \mathbf{u}$ at the point of discontinuity using the standard framework of weak solution arising from conservation laws.

To overcome this predicament, LeFloch and collaborators [40] extended the work done on quasilinear PDEs with discontinuous functions by Volpert [137] to define the weak solution of nonconservative products as Borel measures on the set where the state vector is continuous, while at the discontinuities the measure is defined based on a family of Lipschitz paths connecting the left and right states. LeFloch [90] has also shown that this family of paths can be derived from a parabolic regularization of (1.19) by means of smooth viscous profiles. Indeed, the family of paths depends on the given regularization and this non-uniqueness is a specific feature of nonconservative hyperbolic systems. Nevertheless, the definition of weak solution does not guarantee uniqueness of the solution and so solutions of (1.19) must satisfy the entropy condition, as seen in the case of conservation laws (1.16).

Numerical schemes that approximate hyperbolic systems, in general, should ideally recover admissible solutions by satisfying a discrete entropy condition [69, 88]. This property of the numerical scheme is known as entropy stability. In the case of conservation laws, Tadmor [128] provided the framework for entropy conservative and entropy stable numerical fluxes which allow for either conservation or dissipation of entropy by three-point finite volume schemes. This was extended to nonconservative systems in [24, 103] by the use of fluctuation fluxes and the theory of connecting paths [40]. However, path-consistent schemes do not always converge to the right admissible solutions as the solutions are dependent on the choice of path which defines the jump relation and hence the viscous profile used to attain entropy stability [3, 22, 26]. Entropy stable schemes using fluctuation fluxes to discretize nonconservative hyperbolic systems can be found in [25, 71, 108] and we refer to [91] for a review.

High-order accuracy of the numerical scheme is another exceedingly desirable quality that one seeks. Though not exhaustive, we refer to finite volume schemes using the path-consistent framework and either reconstruction operators [21], or central schemes [23]; to discontinuous Galerkin (DG) methods [54, 55, 113]; or to ADER methods [46, 49]. Among these, the DG methods have gained substantial popularity over the years. The DG method

approximates the solution with a piecewise polynomial solution over an unstructured mesh, see Figure 1-1 for a representation in one space dimension. The semi-discrete form of the DG method is proven to satisfy an entropy inequality for square entropy functions in scalar conservation laws [79], which was extended to symmetric systems in [72].

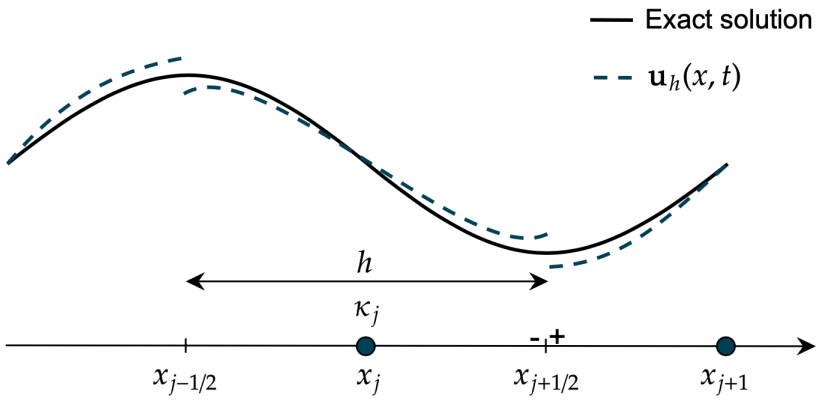

Figure 1-1: A one-dimensional representation of the mesh with cell κ_j of size h. The left and right interfaces of cell κ_j are at $x_{j\mp\frac{1}{2}}$.

In [59], Gassner and coauthors have proposed an entropy stable high-order scheme for the compressible Euler equations using the discontinuous Galerkin spectral elements method (DGSEM), which was extended to general conservation laws in [30]. They used the general framework for conservative elementwise flux differencing schemes [52] satisfying a semi-discrete entropy inequality for the cell-averaged entropy. The DGSEM is based on collocation of quadrature nodes with interpolation points using the Gauss-Lobatto quadrature rules and Lagrange interolation polynomials to span the function space [86]. The scheme was shown to satisfy the summation-by-parts (SBP) property [57] for the discrete operators which allows to take into account, in the semi-discrete entropy inequality, the numerical quadrature that approximates integrals compared to other techniques that require their exact evaluation [70, 71, 79]. Such a form of the nodal DG method has found tremendous use in the development of entropy stable high-order schemes for the compressible Euler equations [30, 59] and multicomponent Euler equations [110], the shallow water equations [141], the magnetohydrodynamic (MHD) equations [15, 94, 142] and gradient flows [127]. In the case of nonconservative systems, a semi-discrete framework was proposed in [108] based on the DGSEM formulation that proves to be entropy stable and high-order accurate.

THE BAER-NUNZIATO MODEL

One of the models that we discretize in this work is the two-velocity, two-pressure, two-temperature Baer-Nunziato model for two-phase flows [7]. In general, the model is a system that describes two-phase flows in complete disequilibrium with respect to the chemical,

mechanical, thermal, and thermodynamic processes. The interaction between the phases are governed by the presence of nonconservative products and zeroth order relaxation source terms. However, in this work, we restrict the numerical discretization to the convective part of the model and ignore the source terms. The homogeneous model that we consider is fairly general using closure laws for the interface velocity and pressure [34, 56] as well as stiffened gas equations of states (EOS) for both the phases.

In the Eulerian framework, many Godunov-type methods computing the homogeneous BN two-phase flow model have been proposed, including the operator splitting method [27, 36, 41, 130, 131, 133], the unsplit Roe-type wave-propagation method [8, 82, 95, 114] and the path-conservative scheme [48]. However all these methods are limited to first order accuracy. In the DG community high-order schemes were proposed in [47, 54, 55, 84, 102], but they do not prove a discrete entropy inequality.

In the present work we utilize the framework from [108] and focus on the design of a high-order entropy stable scheme for the Baer-Nunziato model. This framework is here extended to systems that contain both space derivatives in divergence form and nonconservative products, which is based on a direct generalization of the frameworks of entropy stable finite volume schemes for conservation laws [128] and for nonconservative systems [24]. Such generalization has already been proposed for balance laws in [24] in the case of three-point schemes. This generalization allows the design of discretizations that reduce to conservative schemes using conservative numerical fluxes when the nonconservative products vanish as it is the case away from material fronts in the Baer-Nunziato model. Using this framework, we modify the integration over cell elements using the SBP operator and replace the physical fluxes with two-point entropy conservative fluxes in fluctuation form [24], while we use entropy stable fluxes at the cell interfaces [24, 108]. The entropy conservative fluxes are derived by using the entropy condition [24], and we add upwind-type dissipation as advocated in [76] to obtain the entropy stable numerical fluxes. Let us stress that such choice of numerical fluxes at interfaces is not unique and may be replaced by other numerical fluxes from the literature that guaranty entropy stability and robustness [36, 71]. The scheme is also kinetic energy preserving at the discrete level. The present method is introduced in one space dimension for the sake of clarity and we provide details on its extension to multiple space dimensions on Cartesian meshes in the appendices. The extension of the DGSEM to quadrangles and hexahedra is direct and based on tensor products of one-dimensional basis functions and quadrature rules.

We then focus on high-order integration in time for which we rely on strong stability-preserving explicit Runge-Kutta methods [63, 121] which are defined as convex combinations of first-order schemes and keep their properties under some condition on the time step. We analyze the properties of the fully discrete one-step scheme and derive explicit conditions on the time step and numerical parameters to maintain the positivity of the cell-averaged partial densities and a maximum principle for the cell-averaged void fraction. Positivity of the solution is then enforced at nodal values by the use of a posteriori limiters [145, 146]. Numerical tests in one and two space dimensions are finally performed to assess the properties of the present scheme.

The gamma-based multicomponent model and its discretization using DGSEM

Multicomponent flow models [2, 4, 123, 124], with equations for the mixture quantities, have an innate capability to cope with an arbitrary number of fluid species without changes in the number of governing equations. This particular quality makes them incredibly flexible and computationally efficient when simulating complex phenomena. These models are, generally, considered in their nonconservative form to prevent strong oscillations across material interfaces as in discretely conservative schemes. The design of numerical schemes, predominantly, involves two issues that need special care. Firstly, the equation of state of the mixture should not acquire nonphysical values near material interfaces. Secondly, the numerical scheme should resolve strong shocks without excessive oscillations.

With the above objectives, it becomes reasonable to subject nonconservative multicomponent models to the high-order entropy stable DGSEM framework that we utilise in this work. For the choice of model, here we discretize the gamma-based model for compressible multicomponent flows by Shyue [121], which will be henceforth called as the gamma-model. This model is an extension of the gamma-model which was originally proposed by Abgrall [1], to include the stiffened gas equation of state. The model is a system of compressible Euler equation which are augmented with the transport equations for the EOS parameters $\Gamma = 1/(\gamma - 1)$ and $\Pi = \gamma p_\infty/(\gamma - 1)$, with $\gamma > 1$ the adiabatic exponent and $p_\infty > 0$ a pressure-like constant for the mixture. The introduction of explicit evolutionary equations for Γ and Π, allow an accurate computation of the pressure across material interfaces, which is necessary to preserve invariant domains.

In recent times, there have been a number of works [31, 42, 51, 64, 96, 105, 106, 138] using the DG method that primarily focus on sharp resolution of the material interface for diffuse interface models, however they do not provably satisfy an entropy inequality. In this work, we propose a novel high-order scheme for the gamma-model [122] that preserves uniform velocity and pressure profiles across contact and material discontinuities while proving to be entropy stable across shocks. We utilize the DGSEM framework introduced in this work to modify the volume integral over cell elements and replace the physical fluxes with entropy conservative fluxes for shock solutions, while applying contact preserving fluxes everywhere else. We show that no single numerical flux for the gamma-model can exhibit the qualities of entropy conservation and contact preservation, therefore a choice needs to be made for applying the numerical fluxes in the volume integral based on the local solution. Our algorithm makes this choice through a pressure-based troubled-cell indicator function [78]. At the cell interfaces, we apply the HLLC approximate Riemann solver for the gamma-model. We show that the HLLC solver preserves uniform profiles across contact discontinuities, satisfies a discrete entropy inequality and maintains positivity of the solution. Together with entropy conservative numerical fluxes in the volume integral and the HLLC fluxes at the cell interface, the semi-discrete DG scheme is shown to be entropy stable across shocks. Furthermore, we include a posteriori limiters that enforce the positivity of the solution at nodal values. A series of test cases for both one- and two-dimensional problems are provided to verify the accuracy, stability and robustness of the proposed method.

The DG code AGHORA

All numerical schemes that were designed as part of this thesis were implemented in the ONERA DG code AGHORA [112].

Aghora is a high-resolution numerical solver for the simulation of unsteady compressible turbulent flows with different turbulence modelling (RANS, hybrid RANS-LES, LES, DNS), mutli-species and multi-phase models. The space discretization is based on high-order discontinuous Galerkin methods, with different function space representations, on unstructured mutli-element meshes in two and three space dimensions with high-order approximation of curved boundaries. High-order explicit and implicit methods are used for the time integration. The Aghora solver also uses local mesh and approximation order adaptation techniques for local high resolution simulation of flow features.

1.2 PUBLICATIONS

- The work performed in Chapter 4 was presented at the European workshop on high order numerical methods for evolutionary PDEs: theory and applications, Madrid 2019, and has been published as the below article:

  F. Coquel, C. Marmignon, P. Rai, F. Renac. An entropy stable high-order discontinuous Galerkin spectral element method for the Baer-Nunziato two-phase flow model. J. Comput. Phys., 431 (2021). DOI: https://doi.org/10.1016/j.jcp.2021.110135

- The DGSEM discretization of the gamma-based multicomponent flow model in Chapter 5, will be submitted as the following article:

  A contact preserving and entropy stable discontinuous Galerkin spectral element method for multicomponent flows. In preparation.

- The work in Chapter 2 on the novel Galilean invariant and entropy dissipative model for reactive gas-liquid flows is being extended to include the asymptotic analysis of the model, and will be submitted as the following article:

  A Galilean invariant and entropy dissipative model for gas-liquid reactive flows and its asymptotic analysis. In preparation.

Chapter 2

A Galilean invariant entropy dissipative two-phase flow model for gas-liquid reactive flows

Résumé du chapitre

Dans ce chapitre, nous nous intéressons à la modélisation des écoulements diphasiques à l'aide de lois d'équilibre hyperboliques non linéaires contenant des produits non-conservatifs. Nous commençons l'étude par le modèle non-équilibre de type Baer-Nunziato proposé par Saurel et Abgrall[115] où le modèle est dérivé en utilisant la procédure de moyenne d'ensemble de Drew [44]. Ce modèle évolue dans l'espace et dans le temps sous l'influence des déséquilibres en vitesse et en pression entre les phases, alors qu'il ne tient pas compte du transfert chimique. Les phases interagissent en raison du terme source et du produit non-conservatif. Ces modèles sans équilibre sont appelés modèles moyennés et les lois d'équilibre qui en résultent sont sous-déterminées. Par conséquent, pour tenir compte de la perte d'information, des conditions de fermeture supplémentaires sont nécessaires qui garantissent également l'hyperbolicité et la cohérence thermodynamique, voir Coquel et al. [34, 35], Gallouët et al. [56], Hantke et Müller [68].

Notre objectif avec ce travail est de proposer un modèle d'écoulements réactifs, qui rend compte des déséquilibres complets dans les processus chimiques, mécaniques et thermodynamiques. Pour cela, nous modifions le modèle proposé dans [115] avec des termes sources supplémentaires afin de satisfaire cet objectif. Il faut mentionner qu'une attention particulière est nécessaire lors de l'introduction de nouveaux termes sources dans un modèle existant, car le choix global des termes sources influence grandement le caractère bien posé du modèle. Pour les variables interfaciales, qui apparaissent dans le produit non-conservatif, nous nous appuyons sur les lois de fermeture proposées par Coquel et al. [34], Gallouët et al. [56] qui assurent la positivité des fractions volumiques, des fractions de masse et des énergies internes des phases. De plus, nous démontrons que nos modifications conduisent à un modèle invariant par transformations galiléennes qui est également dissipateur d'entropie pour un choix d'une fonction d'entropie convexe.

2.1 Short description and outline of the chapter

In this chapter we discuss the modelling of two-phase flows using nonlinear hyperbolic balance laws that contain nonconservative products. Our starting point is the Baer-Nunziato-like non-equilibrium model proposed in [115] where the model is derived using the ensemble averaging procedure of [44]. The model assumes thermal equilibrium and does not account for chemical transfer, while it evolves in space and time under the influence of the disequilibrium in velocity and pressure between the phases. The phases interact as a result of the source term and the nonconservative product. Such non-equilibrium models are averaged models, and the resulting balance laws are underdetermined. Therefore, in order to account for the loss of information, additional closure conditions are necessary that also guarantee hyperbolicity and thermodynamical consistency [34, 35, 56, 68].

Our aim with this work is to propose a model for reactive flows, which accounts for complete disequilibria in the chemical, mechanical and thermodynamic processes. For this purpose we modify the model proposed in [115] with additional source terms in order to satisfy our objective. It must be mentioned that significant care is needed while introducing new source terms in an existing model, as the overall choice of the source terms greatly influence the well-posedness of the model. For the interfacial variables, that appear in the nonconservative product, we rely on the closure laws proposed in [34, 56] that ensure the positivity of the void fractions and the mass fractions, as well as, the internal energies of the phases. Additionally, we demonstrate that our modifications lead to a Galilean invariant model which is also entropy dissipative the convex physical entropy.

The plan of the chapter is as follows. section 2.2 describes the main mathematical and physical properties of the non-equilibrium model, along with the introduction of new source terms. In section 2.3 we describe the entropy condition for systems with relaxation source terms and demonstrate that the new source terms do not guarantee an entropy dissipative and Galilean invariant model. section 2.4 describes remedies to the model in the form of corrective source terms, that allow us to propose a Galilean invariant entropy dissipative non-equilibrium model. We end this this chapter by summarising our work in section 2.5.

2.2 Governing equations of the non-equilibrium model

The non-equilibrium model that we intend to modify is the two-velocity, two-pressure two-phase flow model presented in [115], which is obtained by similar averaging techniques as done for the incompressible case in [44]. The model bears resemblance to the well known Baer-Nunziato model [7], except that here the source terms are responsible for the interaction between a liquid and a gaseous phases. Note that, in what follows, the physical quantities and constants related to the gaseous phase are subscript as 1 while for the liquid phase they have been subscript as 2.

In one space dimension the model is a set of seven first order hyperbolic balance laws

$$\partial_t \mathbf{u} + \partial_x \mathbf{f}(\mathbf{u}) + \mathbf{c}(\mathbf{u})\partial_x \mathbf{u} = \mathbf{s}(\mathbf{u}), \quad x \in \mathbb{R}, t > 0, \tag{2.1}$$

where

$$\mathbf{u} \coloneqq \begin{pmatrix} \alpha_1 \\ \alpha_1\rho_1 \\ \alpha_1\rho_1 u_1 \\ \alpha_1\rho_1 E_1 \\ \alpha_2\rho_2 \\ \alpha_2\rho_2 u_2 \\ \alpha_2\rho_2 E_2 \end{pmatrix}, \quad \mathbf{f}(\mathbf{u}) \coloneqq \begin{pmatrix} 0 \\ \alpha_1\rho_1 u_1 \\ \alpha_1(\rho_1 u_1^2 + \mathrm{p}_1) \\ \alpha_1 u_1(\rho_1 E_1 + \mathrm{p}_1) \\ \alpha_2\rho_2 u_2 \\ \alpha_2(\rho_2 u_2^2 + \mathrm{p}_2) \\ \alpha_2 u_2(\rho_2 E_2 + \mathrm{p}_2) \end{pmatrix}, \quad \mathbf{c}(\mathbf{u})\partial_x\mathbf{u} \coloneqq \begin{pmatrix} \mathrm{u_I} \\ 0 \\ -\mathrm{p_I} \\ -\mathrm{p_I u_I} \\ 0 \\ \mathrm{p_I} \\ \mathrm{p_I u_I} \end{pmatrix} \partial_x\alpha_1, \tag{2.2}$$

and

$$\mathbf{s}(\mathbf{u}) \coloneqq \begin{pmatrix} -\Theta \mathrm{p}_r \\ 0 \\ \Lambda u_r \\ \Theta \mathrm{p_I p}_r + \Lambda \mathrm{u_I} u_r \\ 0 \\ -\Lambda u_r \\ -\left(\Theta \mathrm{p_I p}_r + \Lambda \mathrm{u_I} u_r\right) \end{pmatrix} \tag{2.3}$$

represent the vector of the state variables, the physical fluxes, the nonconservative products, and the zeroth order source terms, respectively. The phase densities are ρ_i, the velocities are u_i, and the specific total energies are $E_i = e_i + u_i^2/2$ where e_i is the specific internal energy and $i = 1, 2$ refers to the ith phase. The void fraction of each phase is denoted as α_i and the two void fractions are related through the saturation condition

$$\alpha_1 + \alpha_2 = 1. \tag{2.4}$$

The solution $\mathbf{u}$ belongs to the phase space

$$\Omega_{\text{noneq}} = \left\{\mathbf{u} \in \mathbb{R}^7 : 0 < \alpha_i < 1,\ \rho_i > 0,\ u_i \in \mathbb{R},\ \rho_i e_i > \mathrm{p}_{\infty,i},\ i = 1, 2\right\}, \tag{2.5}$$

where $\mathrm{p}_{\infty,i}$ is a pressure-like constant. Space variations of the physical quantities are governed by the flux function $\mathbf{f} : \Omega_{\text{noneq}} \ni \mathbf{u} \mapsto \mathbf{f}(\mathbf{u}) \in \mathbb{R}^7$ and the nonconservative product $\mathbf{c}(\mathbf{u})\partial_x\mathbf{u}$, with $\mathbf{c} : \Omega_{\text{noneq}} \ni \mathbf{u} \mapsto \mathbf{c}(\mathbf{u}) \in \mathbb{R}^{7\times 7}$, where both $\mathbf{f}(\mathbf{u})$ and $\mathbf{c}(\mathbf{u})$ are smooth. The nonconservative product couples the phases and hinders the system (2.1) to be written in divergence form. Observe that if α_i is uniform in space, the phases decouple into separate systems of compressible Euler equations. The right hand source terms $\mathbf{s}(\mathbf{u}) \in L^\infty(\Omega_{\text{noneq}}) : \Omega_{\text{noneq}} \ni \mathbf{u} \mapsto \mathbb{R}^7$ act as driving forces, and together with the nonconservative product, are responsible for the phase interaction. Note that within the vector of source terms there are relative quantities

$$\mathrm{p}_r = \mathrm{p}_2 - \mathrm{p}_1, \quad u_r = u_2 - u_1 \tag{2.6}$$

of pressure and velocity, respectively, that arise as a result of the non-equilibria associated to the mechanical and drift processes. Furthermore, the terms Θ and Λ are represent the compaction viscosity and the drag coefficient, respectively, and govern the rate of relaxation of the respective processes.

In this work we modify the source vector (2.3), from [115], so that the resulting model accounts for chemical transfer and non-equilibrium in temperature, in addition to the non-equilibria in the mechanical and drift processes. Therefore, we introduce the chemical po-

tential $\mathcal{M}$ and the heat transfer coefficient $\mathcal{K}$ to the source vector

$$\mathbf{s}_{\text{mod}}(\mathbf{u}) := \begin{pmatrix} -\Theta \mathrm{p}_r \\ -\mathcal{M} \\ \Lambda u_r \\ \Theta \mathrm{p}_\mathrm{I} \mathrm{p}_r + \Lambda \mathrm{u}_\mathrm{I} u_r + \mathcal{K} T_r \\ \mathcal{M} \\ -\Lambda u_r \\ -\left(\Theta \mathrm{p}_\mathrm{I} \mathrm{p}_r + \Lambda \mathrm{u}_\mathrm{I} u_r + \mathcal{K} T_r\right) \end{pmatrix}, \tag{2.7}$$

where

$$\mathcal{M} = \nu(\psi_1 - \psi_2), \tag{2.8}$$

ψ_i is the Gibbs free energy for the phases $i = 1, 2$, and $\nu > 0$ is the coefficient for the relaxation of the Gibbs free energy. The relative temperature is defined as

$$T_r = T_2 - T_1. \tag{2.9}$$

Note that, at a material interface, the phases attain local equilibrium and the terms for relative pressure, temperature and velocity vanish.

Assumptions. In this work, we assume that Θ, Λ and $\mathcal{K}$ are positive parameters, while $\mathcal{M}$ is negative. The chemical potential is considered to be negative as we impose

$$\psi_2 > \psi_1, \tag{2.10}$$

which represents a change of phase 1 (liquid) to phase 2 (gas) through chemical reactions, see [10]. Here it is also worth mentioning that the pressure relaxation is the fastest among the different process to reach equilibrium, followed by the drag relaxation and then the thermal relaxation while the chemical transfer is the slowest. This cascading rate of relaxation of the source terms are based on physical experiments and interested readers can refer to [7, 10, 81, 115] for further details.

Closure laws. The pressure of each phase p_i is related to the density and internal energy through a stiffened gas EOS:

$$\mathrm{p}_i(\rho_i, e_i) = (\gamma_i - 1)\rho_i e_i - \gamma_i \mathrm{p}_{\infty,i}, \tag{2.11}$$

where $\gamma_i = \mathrm{C}_{\mathrm{p}_i}/\mathrm{C}_{\mathrm{v}i} > 1$ is the ratio of specific heats of phase i and $\mathrm{p}_{\infty,i} \geq 0$ are some constants. Note that, for the gaseous phase, $\mathrm{p}_{\infty_1} = 0$ and the polytropic ideal gas EOS is retrieved.

System (2.1) is supplemented with closure laws for the interfacial velocity and pressure, u_I and p_I, respectively, that govern the exchange of information at the interface of the two phases. In this work, we use definitions of the interfacial velocity and pressure based on convex combinations of the velocities and pressures of the two phases [34, 56] and adapted to the treatment of discontinuous solutions:

$$\mathrm{u}_\mathrm{I} := \beta u_1 + (1 - \beta) u_2, \tag{2.12a}$$

$$\mathrm{p}_\mathrm{I} := \mu \mathrm{p}_1 + (1 - \mu) \mathrm{p}_2, \tag{2.12b}$$

where the weights are

$$\beta = \frac{\chi\alpha_1\rho_1}{\chi\alpha_1\rho_1 + (1-\chi)\alpha_2\rho_2}, \quad \mu = \frac{(1-\beta)T_2}{\beta T_1 + (1-\beta)T_2}, \quad \chi \in \{0, \tfrac{1}{2}, 1\}. \tag{2.13}$$

Under the particular choice for the closures (2.12) and (2.13), the characteristic field associated to the eigenvalue $\mathrm{u_I}$ for the matrix-valued function $\mathbf{A} : \Omega_{\text{noneq}} \ni \mathbf{u} \mapsto \mathbf{A}(\mathbf{u}) = \mathbf{f}'(\mathbf{u}) + \mathbf{c}(\mathbf{u}) \in \mathbb{R}^{7\times 7}$ of (2.1) is linearly degenerate (LD) [34]. This allows to close the jump relation across an isolated material interface since $\mathrm{u_I}$ is now continuous across it.

In the remaining discussions in this chapter, we will demonstrate that the non-equilibrium model (2.1) with source terms (2.7) does not guarantee a Galilean invariant entropy dissipative model, and additional corrective terms are necessary. Furthermore, for the sake of simplification, we will henceforth use the following general notation:

$$\mathbf{u} = \begin{pmatrix} \alpha_i \\ \alpha_i\rho_i \\ \alpha_i\rho_i u_i \\ \alpha_i\rho_i E_i \end{pmatrix}, \quad \mathbf{f}(\mathbf{u}) = \begin{pmatrix} 0 \\ \alpha_i\rho_i u_i \\ \alpha_i(\rho_i u_i^2 + \mathrm{p}_i) \\ \alpha_i u_i(\rho_i E_i + \mathrm{p}_i) \end{pmatrix}, \quad \mathbf{c}(\mathbf{u})\partial_x\mathbf{u} = \begin{pmatrix} \mathrm{u_I} \\ 0 \\ -\mathrm{p_I} \\ -\mathrm{p_I u_I} \end{pmatrix} \partial_x\alpha_i, \tag{2.14a}$$

$$\mathbf{s}_{\text{mod}}(\mathbf{u}) := (-1)^{i-1} \begin{pmatrix} -\Theta \mathrm{p}_r \\ -\mathcal{M} \\ \Lambda u_r \\ \Theta \mathrm{p_I p}_r + \Lambda \mathrm{u_I} u_r + \mathcal{K} T_r \end{pmatrix}, \quad i = 1, 2, \tag{2.14b}$$

without ambiguity due to the saturation condition (2.4).

2.3 Entropy in dissipative relaxation

In the smooth regime, we consider the quasilinear form of the system (2.1):

$$\partial_t\mathbf{u} + \partial_x\mathbf{A}(\mathbf{u})\partial_x\mathbf{u} = \mathbf{s}(\mathbf{u}), \quad x \in \mathbb{R}, t > 0, \tag{2.15}$$

where $\mathbf{s}(\mathbf{u})$ is stiff. The system (2.15) is hyperbolic over the phase space (2.5) and $\mathbf{A}(\mathbf{u})$ admits real eigenvalues

$$\begin{aligned} &\lambda_1(\mathbf{u}) = u_1 - c_1,\ \lambda_2(\mathbf{u}) = u_2 - c_2,\ \lambda_3(\mathbf{u}) = u_1, \\ &\lambda_4(\mathbf{u}) = \mathrm{u_I},\ \lambda_5(\mathbf{u}) = u_2,\ \lambda_6(\mathbf{u}) = u_1 + c_1,\ \lambda_7(\mathbf{u}) = u_2 + c_2, \end{aligned} \tag{2.16}$$

associated to linearly independent eigenvectors. Here $c_i(\rho_i, e_i)^2 = \gamma_i(\gamma_i - 1)(\rho_i e_i - p_{\infty,i})/\rho_i$ is the speed of sound for the EOS (2.11). Observe, in (2.16), that λ_3, λ_4 and λ_5 are associated to linearly degenerate (LD) fields, whereas $\lambda_1, \lambda_2, \lambda_6$ and λ_7, are associated to genuinely nonlinear (GNL) fields. Additionally, (2.15) is only weakly hyperbolic when $\mathrm{u_I}$ is equal to one of the transport velocities, u_1 or u_2, for $\chi = 1$ or 0 in (2.13).

Uniqueness of solutions of (2.15) relies on the existence of a convex entropy function $\eta(\mathbf{u})$ and an entropy flux $q(\mathbf{u})$ such that physically relevant weak solutions satisfy an admissibility

criteria in the sense of distributions

$$\partial_t \eta(\mathbf{u}) + \partial_x q(\mathbf{u}) = \frac{\partial}{\partial \mathbf{u}} \eta(\mathbf{u}) \cdot \mathbf{s}(\mathbf{u}). \tag{2.17}$$

This amounts to the following necessary conditions:

$$\mathbf{v}(\mathbf{u})^\top \mathbf{A}(\mathbf{u}) = \frac{\partial}{\partial \mathbf{u}} q(\mathbf{u}), \tag{2.18a}$$

$$\mathbf{v}(\mathbf{u})^\top \mathbf{s}(\mathbf{u}) \leq 0, \tag{2.18b}$$

where $\mathbf{v}(\mathbf{u}) = \frac{\partial}{\partial \mathbf{u}} \eta(\mathbf{u})$ is the vector of entropy variables. Convex entropy functions play a stabilizing role in relaxation [29, 143] and this has been extensively analyzed in [17, 67, 143].

In the case of systems, such as (2.1) that have a thermodynamic origin, there exists a physical entropy function for each phase

$$s_i(\rho_i, \theta_i) = -\mathrm{C_{v}}_i \ln\left(\frac{\mathrm{p}+\mathrm{p}_{\infty,i}}{\rho_i^{\gamma_i}}\right) = -\mathrm{C_{v}}_i\Big(\ln \frac{1}{T_i} + (\gamma_i - 1)\ln \rho_i\Big), \quad i = 1, 2. \tag{2.19}$$

This definition of the phasic entropies can easily be derived by using the relation

$$\rho_i \mathrm{C_{v}}_i T_i = \rho_i e_i - \mathrm{p}_{\infty,i} = \frac{\mathrm{p}_i + \mathrm{p}_{\infty,i}}{\gamma_i - 1}, \quad i = 1, 2. \tag{2.20}$$

If one considers only the homogeneous part of (2.1), with (2.2), then it is easy to verify that for smooth solutions the total entropy of the mixture is conserved since

$$\partial_t \sum_{i=1}^{2} \alpha_i \rho_i s_i + \partial_x \sum_{i=1}^{2} \alpha_i \rho_i s_i u_i = \sum_{i=1}^{2} \frac{(\mathrm{p_I} - \mathrm{p}_i)(\mathrm{u_I} - u_i)}{T_i} \partial_x \alpha_i, \tag{2.21}$$

where the nonconservative product on the right-hand side vanishes for the closure of interfacial quantities (2.12) and (2.13):

$$\sum_{i=1}^{2} \frac{(\mathrm{p_I} - \mathrm{p}_i)(\mathrm{u_I} - u_i)}{T_i} \partial_x \alpha_i = 0. \tag{2.22}$$

Additionally, in the case of non-smooth solutions, such as shocks, given a convex entropy pair (η, q), where

$$\eta(\mathbf{u}) := -\sum_{i=1}^{2} \alpha_i \rho_i s_i, \quad q(\mathbf{u}) := -\sum_{i=1}^{2} \alpha_i \rho_i s_i u_i, \tag{2.23}$$

admissible weak solutions must satisfy a nonlinear stability condition

$$\partial_t \eta(\mathbf{u}) + \partial_x q(\mathbf{u}) \leq 0. \tag{2.24}$$

Lemma 2.3.1. *The two-phase flow model (2.15) with source terms (2.7) and closure laws (2.11)-(2.13) does not guarantee entropy dissipation and is not Galilean invariant.*

Proof. We recall the fundamental relation for the second law of thermodynamics

$$T_i ds_i = de_i + \frac{\mathrm{p}_i}{\rho_i^2} d\rho_i, \quad i = i, 2, \tag{2.25}$$

which can be re-cast as

$$T_i d\alpha_i\rho_i s_i = d\alpha_i\rho_i E_i + \left(\frac{u_i^2}{2} - \psi_i\right) d\alpha_i\rho_i - u_i d\alpha_i\rho_i u_i + \mathrm{p_i} d\alpha_i, \tag{2.26}$$

where $\psi_i = e_i + \frac{\mathrm{p}}{\rho_i} - T_i s_i$ denotes the Gibbs free energy.

Using the equations for the void fraction, mass, momentum and energy equations from (2.1)-(2.2) with source terms (2.7) we get

$$\begin{aligned} &T_i\partial_t\alpha_i\rho_i s_i + \partial_x\alpha_i u_i(\rho_i E_i + \mathrm{p_i}) - u_i\partial_x\alpha_i(\rho_i u_i^2 + \mathrm{p_i}) + (\frac{u_i^2}{2} - \psi_i)\partial_x\alpha_i\rho_i u_i + (\mathrm{p_I} u_i + \mathrm{p_i u_I} - \mathrm{p_I u_I})\partial_x\alpha_i \\ &\qquad = (-1)^{i-1}\left(\Theta(\mathrm{p_I} - \mathrm{p_i})\mathrm{p}_r + \Lambda(\mathrm{u_I} - u_i)u_r - \mathcal{M}\left(\frac{u_i^2}{2} - \psi_i\right) + \mathcal{K}T_r\right), \end{aligned} \tag{2.27}$$

where the space derivatives can be further simplified to get

$$\begin{aligned} &T_i\partial_t\alpha_i\rho_i s_i + \partial_x\alpha_i\rho_i e_i u_i + \alpha_i\mathrm{p_i}\partial_x u_i + \left(\mathrm{p_I}(u_i - \mathrm{u_I}) + \mathrm{p_i u_I}\right)\partial_x\alpha_i + s_i T_i\partial_x\alpha_i\rho_i u_i \\ &\quad - e_i\partial_x\alpha_i\rho_i u_i - \alpha_i\mathrm{p_i}\partial_x u_i - \frac{\alpha_i\mathrm{p_i}u_i}{\rho_i}\partial_x\rho_i - \mathrm{p_i}u_i\partial_x\alpha_i \\ &\quad = (-1)^{i-1}\left(\Theta(\mathrm{p_I} - \mathrm{p_i})\mathrm{p}_r + \Lambda(\mathrm{u_I} - u_i)u_r - \mathcal{M}\left(\frac{u_i^2}{2} - \psi_i\right) + \mathcal{K}T_r\right), \end{aligned} \tag{2.28}$$

which eventually leads to

$$\begin{aligned} &\partial_t\alpha_i\rho_i s_i + \partial_x\alpha_i\rho_i s_i u_i - \frac{(\mathrm{p_i} - \mathrm{p_I})(u_i - \mathrm{u_I})}{T_i}\partial_x\alpha_i \\ &\qquad = \frac{(-1)^{i-1}}{T_i}\left(\Theta(\mathrm{p_I} - \mathrm{p_i})\mathrm{p}_r + \Lambda(\mathrm{u_I} - u_i)u_r - \mathcal{M}\left(\frac{u_i^2}{2} - \psi_i\right) + \mathcal{K}T_r\right). \end{aligned} \tag{2.29}$$

We then set $\eta(\mathbf{u}) := -\sum_{i=1}^{2}\alpha_i\rho_i s_i$ as the convex entropy function and $q(\mathbf{u}) := -\sum_{i=1}^{2}\alpha_i\rho_i s_i u_i$ as the entropy flux and apply the relation (2.22) to get the following balance law:

$$\begin{aligned} \partial_t\eta(\mathbf{u}) + \partial_x q(\mathbf{u}) = &-\Theta\mathrm{p}_r^2\left(\frac{1-\mu}{T_1} + \frac{\mu}{T_2}\right) - \Lambda u_r^2\left(\frac{1-\beta}{T_1} + \frac{\beta}{T_2}\right) - \mathcal{K}\frac{T_r^2}{T_1 T_2} \\ &+ \mathcal{M}\left(\frac{\psi_2}{T_2} - \frac{\psi_1}{T_1} + \frac{1}{2}\left(\frac{u_1^2}{T_1} - \frac{u_2^2}{T_2}\right)\right). \end{aligned} \tag{2.30}$$

Observe that the algebraic relations involving relaxation in pressure, velocity and temperature are all positive, given that the temperature of each phase T_i is positive and the coefficient of pressure, velocity and thermal relaxations are positive. Additionally, these terms have a negative sign in front of them therefore they correctly contribute to the entropy dissipation.

However, the term related to the chemical potential $\mathcal{M} < 0$ has the quantities $\frac{\psi_2}{T_2} - \frac{\psi_1}{T_1}$ and $\frac{u_1^2}{T_1} - \frac{u_2^2}{T_2}$ which can attain both positive and negative values and are not bounded. The latter

term also prevent Galilean invariance of (2.30). These terms need to be bounded in order to ensure a correct contribution towards the entropy balance. Therefore the model (2.15) with source terms (2.7) does not to qualify as Galilean invariant and entropy dissipative. □

The entropy balance (2.30) shows that the Gibbs free energy appears as an additional driving force, which is also indicated in [10] for reactive systems. In order to control its contribution towards the entropy balance, at complete non-equilibria, we introduce the notion of interfacial Gibbs free energy in the following way

$$\psi_{\mathrm{I}} = (1-\omega)\psi_1 + \omega\psi_2, \quad 0 \le \omega \le 1. \tag{2.31}$$

The interfacial Gibbs free energy will, eventually, combine with the phasic Gibbs energy terms appearing in the last part of the source term in (2.30) and will allow to control its contribution towards the entropy dissipation.

2.4 A corrected model

Since we cannot control the sign of the last term in (2.30), corrective source terms are necessary and will be applied through the chemical potential. Note that we also aim to annihilate the effects of the velocity terms in (2.30) so that the entropy dissipation retains Galilean invariance. Additionally, we intend to impose a control on the sign of the Gibbs free energy in the source terms of (2.30), so that entropy balance exhibits dissipation at complete non-equilibria.

Lemma 2.4.1. *Let $\tilde{\Lambda}\mathcal{M}$ and $(\psi_{\mathrm{I}}+\tilde{m})\mathcal{M}$ be the corrective source terms that are introduced to the momentum and energy equations*

$$\mathbf{s}_{\mathrm{cor}}(\mathbf{u}) = (-1)^{i-1}\begin{pmatrix} -\Theta \mathrm{p}_r \\ -\mathcal{M} \\ \Lambda u_r - \tilde{\Lambda}\mathcal{M} \\ \Theta \mathrm{p}_{\mathrm{I}}\mathrm{p}_r + \Lambda \mathrm{u}_{\mathrm{I}} u_r + \mathcal{K}T_r - (\psi_{\mathrm{I}}+\tilde{m})\mathcal{M} \end{pmatrix}, \quad i = 1,2. \tag{2.32}$$

Then the non-equilibrium model (2.1)-(2.2), with source terms (2.32), is entropy dissipative for the convex entropy pair defined in (2.23) if $\tilde{\Lambda} = \frac{u_1+u_2}{2}$ and $\tilde{m} = \frac{u_1 u_2}{2}$.

Proof. The entropy balance is evaluated with source terms (2.32)

$$\begin{aligned} \partial_t \eta(\mathbf{u}) + \partial_x q(\mathbf{u}) = &-\Theta \mathrm{p}_r^2\left(\frac{1-\mu}{T_1}+\frac{\mu}{T_2}\right) - \Lambda u_r^2\left(\frac{1-\beta}{T_1}+\frac{\beta}{T_2}\right) - \mathcal{K}\frac{T_r^2}{T_1T_2} \\ &+ \mathcal{M}\left(\frac{\psi_2}{T_2}-\frac{\psi_1}{T_1}+\frac{1}{2}\left(\frac{u_1^2}{T_1}-\frac{u_2^2}{T_2}\right)\right) + \mathcal{M}\tilde{\Lambda}\left(\frac{u_2}{T_2}-\frac{u_1}{T_1}\right) + \mathcal{M}(\psi_{\mathrm{I}}+\tilde{m})\left(\frac{1}{T_1}-\frac{1}{T_2}\right), \end{aligned} \tag{2.33}$$

where the interfacial Gibbs energy is introduced through the corrective source terms. Upon

collecting the terms, we get

$$\begin{aligned}\partial_t\eta(\mathbf{u})+\partial_x q(\mathbf{u}) = &-\Theta \mathrm{p}_r^2\left(\frac{1-\mu}{T_1}+\frac{\mu}{T_2}\right)-\Lambda u_r^2\left(\frac{1-\beta}{T_1}+\frac{\beta}{T_2}\right)-\mathcal{K}\frac{T_r^2}{T_1T_2}\\ &+\mathcal{M}\Bigg(\frac{\psi_2}{T_2}-\frac{\psi_1}{T_1}+\psi_{\mathrm{I}}\left(\frac{1}{T_1}-\frac{1}{T_2}\right)\\ &+\frac{1}{2T_1}(u_1^2+2(\tilde{m}-\tilde{\Lambda}u_1))-\frac{1}{2T_2}(u_2^2+2(\tilde{m}-\tilde{\Lambda}u_2))\Bigg).\end{aligned} \tag{2.34}$$

Now, we only need to solve the following simultaneous equations

$$u_1^2+2(\tilde{m}-\tilde{\Lambda}u_1)=0, \tag{2.35a}$$

$$u_2^2+2(\tilde{m}-\tilde{\Lambda}u_2)=0, \tag{2.35b}$$

in order to annihilate the unbounded velocity terms associated to the chemical potential, which leads to $\tilde{\Lambda}=\frac{u_1+u_2}{2}$ and $\tilde{m}=\frac{u_1u_2}{2}$.

The entropy balance now reads

$$\begin{aligned}\partial_t\eta(\mathbf{u})+\partial_x q(\mathbf{u}) = &-\Theta \mathrm{p}_r^2\left(\frac{1-\mu}{T_1}+\frac{\mu}{T_2}\right)-\Lambda u_r^2\left(\frac{1-\beta}{T_1}+\frac{\beta}{T_2}\right)-\mathcal{K}\frac{T_r^2}{T_1T_2}\\ &+\mathcal{M}(\psi_2-\psi_1)\left(\frac{1-\omega}{T_2}+\frac{\omega}{T_1}\right)\le 0,\quad (\mu,\omega,\beta)\in[0,1],\end{aligned} \tag{2.36}$$

which is both Galilean invariant and entropy dissipative under the assumptions placed on the model from section 2.2. □

Theorem 2.4.1. *The non-equilibrium hyperbolic two-phase flow model*

$$\partial_t\mathbf{u}+\partial_x\mathbf{f}(\mathbf{u})+\mathbf{c}(\mathbf{u})\partial_x\mathbf{u}=\mathbf{s}_{\mathrm{cor}}(\mathbf{u}),\quad x\in\mathbb{R},t>0, \tag{2.37}$$

where

$$\mathbf{u}=\begin{pmatrix}\alpha_i\\ \alpha_i\rho_i\\ \alpha_i\rho_i u_i\\ \alpha_i\rho_i E_i\end{pmatrix},\quad \mathbf{f}(\mathbf{u})=\begin{pmatrix}0\\ \alpha_i\rho_i u_i\\ \alpha_i(\rho_1 u_i^2+\mathrm{p}_i)\\ \alpha_i u_i(\rho_i E_i+\mathrm{p}_i)\end{pmatrix},\quad \mathbf{c}(\mathbf{u})\partial_x\mathbf{u}=\begin{pmatrix}\mathrm{u}_{\mathrm{I}}\\ 0\\ -\mathrm{p}_{\mathrm{I}}\\ -\mathrm{p}_{\mathrm{I}}\mathrm{u}_{\mathrm{I}}\end{pmatrix}\partial_x\alpha_i, \tag{2.38a}$$

$$\mathbf{s}_{\mathrm{cor}}(\mathbf{u})=(-1)^{i-1}\begin{pmatrix}-\Theta\mathrm{p}_r\\ -\mathcal{M}\\ \Lambda u_r-\frac{u_1+u_2}{2}\mathcal{M}\\ \Theta\mathrm{p}_{\mathrm{I}}\mathrm{p}_r+\Lambda\mathrm{u}_{\mathrm{I}}u_r+\mathcal{K}T_r-(\psi_{\mathrm{I}}+\frac{u_1u_2}{2})\mathcal{M}\end{pmatrix},\quad i=1,2. \tag{2.38b}$$

is Galilean invariant and entropy dissipative for the convex entropy pair (2.23).

The model is closed with the stiffened gas EOS (2.11) that defines the pressure of each phase, while the interfacial variables are closed using general closure laws (2.11)-(2.13) and (2.31).

2.5 Summary

The discussion in this chapter can be summarized as follows. We propose a two-phase flow model for a reactive mixture of gas and liquid, where the chemical, mechanical and thermodynamical processes are in complete disequilibria. This model is derived from the Baer-Nunziato-like model proposed in [115], where chemical and heat transfers were not accounted for. In our work we introduce novel source terms that allows the exchange or chemicals and heat across the phases. In doing so we highlight that introduction of new source terms to an existing model is a problem which is far from trivial, as the choice of source terms affect the well-posedness of the model. Therefore additional correction is necessary so that the resulting model is Galilean invariant and entropy dissipative. We thus arrive a two-phase flow model for reactive immiscible fluids that is Galilean invariant and entropy dissipative at complete disequilibria.

Chapter 3

Hyperbolic systems in nonconservative form: theory and discretization

Résumé du chapitre

Les discussions de ce chapitre concernent des EDP hyperboliques non linéaires avec des produits non conservatifs où nous ne tenons pas compte des termes sources, contrairement au Chapter 2. Nous nous intéressons ici au problème de Cauchy pour un système hyperbolique non linéaire non conservatif à une dimension. Nous supposons que (3.1) est strictement hyperbolique et admet des valeurs propres réelles et distinctes avec un ensemble complet de vecteurs propres.

Il est bien connu que les systèmes hyperboliques non linéaires peuvent conduire à la rupture des solutions classiques en temps fini, même pour des conditions initiales suffisamment lisses. On s'appuie alors sur des solutions faibles qui sont définies au sens des distributions. Cependant, dans le cas de systèmes non conservatifs, le cadre standard des solutions faibles, découlant des lois de conservation, ne s'applique pas car il est difficile de définir de manière significative le produit non conservatif au point de discontinuité. De plus, les systèmes hyperboliques sont souvent obtenus comme la limite de viscosité nulle d'une régularisation parabolique. Par conséquent, le choix de la famille de chemins dépend du profil visqueux. Cependant, les solutions faibles ne garantissent pas l'unicité, c'est pourquoi une contrainte supplémentaire sous la forme d'une condition d'entropie est introduite, qui permet de sélectionner des solutions faibles physiquement pertinentes. En conséquence, dans ce chapitre, nous rappelons la notion de solutions faibles dans le contexte des systèmes hyperboliques non-conservatifs: [40, 90], où le produit non-conservatif est défini comme une mesure de Borel bornée à une discontinuité basée sur une famille de chemins de Lipschitz reliant les états gauche et droit. Nous montrons ensuite l'existence de la solution de [90] pour les données initiales de Riemann et commentons la condition d'entropie.

Le système non conservatif décrit dans ce chapitre est discrétisé à l'aide de la méthode des éléments spectraux de Galerkin discontinue (DGSEM)[57, 59, 86] avec les règles de quadrature de Gauss-Lobatto, qui sont basées sur la collocation des points d'interpolation. Nous décrivons ici le cadre DGSEM, ainsi que sa propriété de sommation par parties (SBP), de manière très détaillée ; en conséquence, ce chapitre sert également de base à la conception des schémas numériques réalisés dans cette thèse. Nous rappelons également les résultats

obtenus dans [108] pour les systèmes non-conservatifs généraux et décrivons la notion de flux numériques qui conservent et ceux qui dissipent l'entropie [24]. Le cadre DGSEM permet de proposer un schéma semi-discret pour le problème de Cauchy (3.1). Nous modifions l'intégration sur les éléments cellulaires en utilisant les opérateurs SBP et nous remplaçons les flux physiques par des flux conservant d'entropie tout en appliquant des flux dissipant d'entropie à l'interface. Cela permet de prouver une inégalité semi-discrète pour l'entropie moyenne de la cellule, tout en maintenant une précision d'ordre élevé.

Nous décrivons également le schéma d'intégration temporelle qui sera utilisé dans tous les chapitres à venir. Dans cette thèse, nous nous appuyons sur des schémas de Runge-Kutta explicites préservant la stabilité [63, 121] qui sont définis comme des combinaisons convexes de schémas du premier ordre et conservent leurs propriétés sous certaines conditions sur le pas de temps. Il faut noter que ces schémas d'intégration temporelle sont particulièrement utiles lors de l'analyse du schéma entièrement discret car ils permettent d'imposer des conditions sur les paramètres numériques qui garantissent la positivité de la solution.

3.1 Short description and outline of the chapter

The discussions in this chapter involve nonlinear hyperbolic PDEs with nonconservative products where we disregard the source terms, unlike Chapter 2.

Here we are interested in the Cauchy problem for a one-dimensional nonlinear nonconservative hyperbolic system of the form

$$\partial_t \mathbf{u} + \partial_x \mathbf{f}(\mathbf{u}) + \mathbf{c}(\mathbf{u})\partial_x \mathbf{u} = 0, \qquad x \in \mathbb{R},\ t > 0, \tag{3.1a}$$

$$\mathbf{u}(x,0) = \mathbf{u}_0(x), \quad x \in \mathbb{R}, \tag{3.1b}$$

where $\mathbf{u}(x,t)$ is the state vector that takes values in an open convex set $\Omega_* \subset \mathbb{R}^N$, $\mathbf{f}(\mathbf{u}) : \Omega_* \ni \mathbf{u} \mapsto \mathbf{f}(\mathbf{u}) \in \mathbb{R}^N$ is the flux function and $\mathbf{c}(\mathbf{u})\partial_x \mathbf{u}$ is the nonconservative product with $\mathbf{c}(\mathbf{u}) : \Omega_* \to \mathbb{R}^{N\times N}$. Note that both $\mathbf{f}(\mathbf{u})$ and $\mathbf{c}(\mathbf{u})$ are assumed to be smooth.

The system (3.1a) can be expressed in a quasilinear form

$$\partial_t \mathbf{u} + \mathbf{A}(\mathbf{u})\partial_x \mathbf{u} = 0. \tag{3.2}$$

where $\mathbf{A}(\mathbf{u}) := \nabla_{\mathbf{u}}\mathbf{f}(\mathbf{u}) + \mathbf{c}(\mathbf{u}) : \Omega_* \ni \mathbf{u} \mapsto \mathbf{A}(\mathbf{u}) \in \mathbb{R}^{N\times N}$ is a smooth, locally bounded map that cannot be considered as the Jacobian matrix due to the presence of the nonconservative product. Here we assume that (3.2) is strictly hyperbolic and $\mathbf{A}(\mathbf{u})$ admits real and distinct eigenvalues with a complete set of eigenvectors.

It is well known that nonlinear hyperbolic systems may lead to breakdown of classical solutions in finite time, even for sufficiently smooth initial conditions. We then rely on for weak solutions that are defined in the sense of distributions. However, in the case of nonconservative systems the standard framework of weak solutions, arising from conservation laws, does not apply as it is difficult to meaningfully define the nonconservative product at the point of discontinuity. Additionally, hyperbolic systems are often obtained as the vanishing-viscosity limit of a parabolic regularization. Therefore the choice of family of paths depends on the viscous profile. However, weak solutions do not guarantee uniqueness therefore an additional constraint in the form of an entropy condition is introduced, that allows to select physically relevant weak solutions. As a result in this chapter we recall the

notion of weak solutions in the context of nonconservative hyperbolic systems [40, 90], where the nonconservative product is defined as a bounded Borel measure at a discontinuity based on a family of Lipschitz paths connecting the left and right states. Then we show existence of solution from [90] for Riemann initial data and comment on the entropy condition.

The nonconservative system described in this chapter is discretized using the discontinuous Galerkin spectral element method (DGSEM)[57, 59, 86] with Gauss-Lobatto quadrature rules, that are based on the collocation of interpolation points. Here we describe the DGSEM framework, along with its summation-by-parts (SBP) property, in extensive detail as a result this chapter also acts a foundation for the design of numerical schemes performed in this thesis. We also recall the results obtained in [108] for general nonconservative systems and describe the notion of entropy conservative [24] and entropy stable fluxes. The DGSEM framework allows to propose a semi-discrete scheme for the Cauchy problem (3.1). We modify the integration over cell elements using the SBP operators and replace the physical fluxes with entropy conservative fluxes while applying entropy stable fluxes at the interface. This allows to prove a semi-discrete inequality for the cell-averaged entropy, while maintaining high-order accuracy.

We also describe the time integration scheme that will used in all forthcoming chapters. In this thesis, we rely on strong stability-preserving explicit Runge-Kutta schemes [63, 121] which are defined as convex combinations of first-order schemes and keep their properties under some condition on the time step. It must be noted that these time integration schemes are especially useful when analysing the fully discrete scheme as they allow to impose conditions on the numerical parameters that guarantees the positivity of the solution.

This chapter is organised as follows. In section 3.2, we recall the definition of weak solutions for nonconservative systems from [90]. Then, in section 3.3, we demonstrate that weak solutions are dependent on the viscous profile and expose the entropy condition for nonconservative systems as an admissibility criterion to select the physically relevant solutions. In section 3.4 we introduce the DGSEM framework and the semi-discrete scheme. section 3.5 introduces the notion of entropy conservative and entropy stable numerical fluxes in fluctuation form and highlights the properties of the semi-discrete scheme. We end this chapter by describing the strong-stability preserving explicit Runge-Kutta time integration in section 3.7.

3.2 Notion of weak solutions

We, first, define the nonconservative product $\mathbf{A}(\mathbf{u})d_x\mathbf{u}$ as a bounded measure at the point of discontinuity and then demonstrate, through a simple example, that the definition of the product depends on the family of Lipschitz paths.

Lemma 3.2.1 (DLM [40])**.** *Let* $\mathbf{u} :]a, b[\to \mathbb{R}^N$ *be a function of bounded variation which is discontinuous at a point* $x_0 \in]a, b[$*, such that the discontinuity separates two constant states to the left and right,* $\mathbf{u}_L :]a, x_0^-[\to \mathbb{R}^N$ *and* $\mathbf{u}_R :]x_0^+, b[\to \mathbb{R}^N$*, respectively. Then the nonconservative product* $\mathbf{A}(\mathbf{u})d_x\mathbf{u}$ *at* x_0 *can be defined as a bounded measure that depends on a family of Lipschitz paths connecting the left and right states.*

To illustrate this idea, we consider a single discontinuity for $\mathbf{u}$ at the point x_0 separating

two continuous states on the left and right, $\mathbf{u}_L$ and $\mathbf{u}_R$, such that

$$\mathbf{u} = \mathbf{u}_L + \mathrm{H}(x - x_0)[\![\mathbf{u}]\!], \quad x \in]a, b[, \tag{3.3}$$

where $\mathrm{H} : \mathbb{R} \to \mathbb{R}$ is the heavyside function and $[\![\mathbf{u}]\!] := \mathbf{u}_R - \mathbf{u}_L$ represents the jump operation over the function $\mathbf{u}$. Furthermore, to the function $\mathbf{A}(\mathbf{u})$, we introduce a smooth regularisation $\mathbf{u}^\epsilon$, such that if the total variation of $\mathbf{u}^\epsilon$ is uniformly bounded then

$$\mathbf{A}(\mathbf{u})d_x\mathbf{u} \equiv \lim_{\epsilon \to 0} \mathbf{A}(\mathbf{u}^\epsilon)d_x\mathbf{u}^\epsilon, \tag{3.4}$$

which defines the nonconservative product as a bounded measure. For the sake of completeness of the argument let us also recall the definition of the total variation of a BV function $\mathbf{u}$:

$$TV(\mathbf{u}) = \int_a^b \left| \frac{d\mathbf{u}}{dx} \right| < +\infty. \tag{3.5}$$

Let us introduce a Lipschitz continuous path $\boldsymbol{\Psi} : [s; \mathbf{u}_L, \mathbf{u}_R] \to \Omega_*$ satisfying $\Psi(0) = \mathbf{u}_L$ and $\Psi(1) = \mathbf{u}_R$, such that for every $\epsilon > 0$, $\mathbf{u}^\epsilon$ is defined as

$$\mathbf{u}^\epsilon(x,t) = \begin{cases} \mathbf{u}_L, & a < x < x_0 - \epsilon, \\ \boldsymbol{\Psi}\left(\dfrac{x - x_0 + \epsilon}{2\epsilon}; \mathbf{u}_L, \mathbf{u}_R \right), & x_0 - \epsilon < x < x_0 + \epsilon, \\ \mathbf{u}_R, & b > x > x_0 + \epsilon, \end{cases} \tag{3.6}$$

such that at the limit $\epsilon \to 0$,

$$\mathbf{A}(\mathbf{u}^\epsilon)d_x\mathbf{u}^\epsilon \rightharpoonup \mathbf{C}\delta_{x_0}, \tag{3.7}$$

in the sense of measures on $]a, b[$, where δ_{x_0} is the Dirac measure placed at x_0 and

$$\mathbf{C} = \int_0^1 \mathbf{A}(\boldsymbol{\Psi}(s))\boldsymbol{\Psi}'(s)ds. \tag{3.8}$$

Here we see a clear dependence of the definition of the nonconservative product on the chosen family of paths connecting the left and right states. Now, assuming that we choose a family of locally Lipschitz paths, $\boldsymbol{\Psi}(s; \mathbf{u}_L, \mathbf{u}_R) : [0,1] \times \Omega_* \times \Omega_* \to \Omega_*, \forall \mathbf{u}_L, , \mathbf{u}_R \in \Omega_*, \forall s \in [0,1]$, that satisfies the following consistency and regularity properties:

(Hyp.1): $\boldsymbol{\Psi}(0; \mathbf{u}_L, \mathbf{u}_R) = \mathbf{u}_L, \quad \boldsymbol{\Psi}(1; \mathbf{u}_L, \mathbf{u}_R) = \mathbf{u}_R,$

(Hyp.2): $\exists k > 0, \quad \left| \partial_s \boldsymbol{\Psi}(s; \mathbf{u}_L, \mathbf{u}_R) \right| \leqslant k \left| \mathbf{u}_R - \mathbf{u}_L \right|,$

(Hyp.3): $\exists k > 0, \quad \left| \partial_s \boldsymbol{\Psi}(s; \mathbf{u}_L, \mathbf{u}_R) - \partial_s \boldsymbol{\Psi}(s; \mathbf{u}_L^*, \mathbf{u}_R^*) \right| \leqslant k \left(|\mathbf{u}_L - \mathbf{u}_L^*| + |\mathbf{u}_R - \mathbf{u}_R^*| \right),$

then the nonconservative product can be defined based on the family of paths $\boldsymbol{\Psi}(s; \mathbf{u}_L, \mathbf{u}_R)$.

Theorem 3.2.1 (DLM [40])**.** *Let the state vector be defined on the space of BV functions $\mathbf{u} \in \mathbf{BV}(]a, b[, \mathbb{R}^N)$ and $\mathbf{A}(\mathbf{u})$ be a $N \times N$ matrix-valued function, then for a chosen family of Lipschitz paths , there exits a unique real-valued Borel measure μ, such that*

- *if $\mathbf{u}$ is continuous on some Borel set $\mathcal{O} \subset \mathbb{R}$, then*

$$\mu(\mathcal{O}) = \int_{\mathcal{O}} \mathbf{A}(\mathbf{u}) \frac{d\mathbf{u}}{dx}, \tag{3.9}$$

- *if* $\mathbf{u}$ *is discontinuous at a point* x_0*, then*

$$\mu(x_0) = \int_0^1 \mathbf{A}(\mathbf{\Psi}(s;\mathbf{u}_L,\mathbf{u}_R))\partial_s\mathbf{\Psi}(s;\mathbf{u}_L,\mathbf{u}_R)ds. \tag{3.10}$$

The interpretation of the nonconservative product as a Borel measure is central to the definition of weak solutions for (3.2) and henceforth we will denote it as $\left[\mathbf{A}(\mathbf{u})d_x\mathbf{u}\right]_{\mathbf{\Psi}}$.

Note that the above theorem coincides with the definition of the nonconservative product introduced by Volpert [137] if the family of paths are considered as straight lines. More precisely, in such a case the nonconservative product can be defined as the product of the averaged superposition $\hat{\mathbf{A}}$ of $\mathbf{u} \in \mathbf{BV}(]a,b[,\mathbb{R}^N)$ by the smooth function $\mathbf{A}(\mathbf{u})$ and the Borel measure $\frac{d\mathbf{u}}{dx}$

$$\left[\mathbf{A}(\mathbf{u})d_x\mathbf{u}\right]_{\mathbf{\Psi}} = \hat{\mathbf{A}}(\mathbf{u})\frac{d\mathbf{u}}{dx}, \tag{3.11}$$

where

$$\hat{\mathbf{A}}(\mathbf{u}) = \int_0^1 \mathbf{A}\left(\mathbf{u}_L + s\left(\mathbf{u}_R - \mathbf{u}_L\right)\right)ds, \tag{3.12}$$

and the family of paths are defined as

$$\mathbf{\Psi}(s;\mathbf{u}_L,\mathbf{u}_R) = \mathbf{u}_L + s(\mathbf{u}_R - \mathbf{u}_L). \tag{3.13}$$

It has been proved in [137] that $\hat{\mathbf{A}}(\mathbf{u})$ is a measurable function with respect to the Borel measure $\frac{d\mathbf{u}}{dx}$ and the resulting product is a bounded Borel measure.

We will now move to the original point of interest, namely to describe the notion of weak solutions of (3.1) and (3.2), based on the definition of the nonconservative product in Theorem 3.2.1. Note that now we consider the vector of unknowns $\mathbf{u}$ as a function of space and time, and therefore the product $\left[\mathbf{A}(\mathbf{u}(\cdot,t))\partial_x\mathbf{u}(\cdot,t)\right]_{\mathbf{\Psi}}$ is defined for every $t > 0$ as a Borel measure on $\mathbb{R}$ and is a bounded Lebesgue-measurable function.

Definition 3.2.1. *A function* $\mathbf{u} \in \mathbf{L}^\infty(\mathbb{R}^+,\mathbf{BV}(\mathbb{R},\mathbb{R}^N))$ *is called a weak solution of (3.1) if for any* $\boldsymbol{\phi} \in \boldsymbol{C}_0^1(\mathbb{R}\times\mathbb{R}^+,\mathbb{R})$ *it satisfies*

$$\begin{aligned}\int_{\mathbb{R}^+}\int_{\mathbb{R}} \mathbf{u}(x,t)\partial_t\boldsymbol{\phi}(x,t)dxdt - \int_{\mathbb{R}^+}\left(\int_{\mathbb{R}} \boldsymbol{\phi}(x,t)\left[\mathbf{A}(\mathbf{u}(x,t))\partial_x\mathbf{u}(x,t)\right]_{\mathbf{\Psi}}dx\right)dt \\ + \int_{\mathbb{R}} \boldsymbol{\phi}(x,0)\mathbf{u}_0(x)dx = 0,\end{aligned} \tag{3.14}$$

where $\mathbf{A}(\mathbf{u})$ *is defined in (3.2).*

Consequently, for a discontinuity travelling at the finite speed $\sigma \in \mathbb{R}$*, the weak solution must satisfy the generalized Rankine-Hugoniot condition*

$$\sigma[\![\mathbf{u}]\!] = \left[\mathbf{A}(\mathbf{u})\partial_x\mathbf{u}\right]_{\mathbf{\Psi}}, \tag{3.15}$$

where $[\![\mathbf{u}]\!] = \mathbf{u}_R - \mathbf{u}_L$ *and* $\mathbf{u}_L$*,* $\mathbf{u}_R$ *are the respective left and right states at the discontinuity.*

Remark 3.2.1. *In the case that (3.1a) is a conservation law, i.e.* $\boldsymbol{c}(\mathbf{u}) \equiv 0$*, the matrix-valued function is indeed a Jacobian of the physical flux* $\mathbf{A}(\mathbf{u}) = \partial_{\mathbf{u}}\mathbf{f}(\mathbf{u})$ *and the relation (3.15) simplifies to the standard notion of the Rankine-Hugoniot jump condition*

$$\sigma[\![\mathbf{u}]\!] = [\![\mathbf{f}(\mathbf{u})]\!], \tag{3.16}$$

for weak solutions in the sense of distributions. Note that the jump condition for conservation laws is independent of the family of paths introduced earlier.

3.3 Existence of solution and the entropy condition

We state the existence results obtained in [40] for Riemann initial data

$$\mathbf{u}_0(x) = \begin{cases} \mathbf{u}_L, & x < 0, \\ \mathbf{u}_R, & x > 0, \end{cases} \tag{3.17}$$

in the case where the jump $|\mathbf{u}_L - \mathbf{u}_R|$ is small.

Theorem 3.3.1 (DLM [40])**.** *Let there be family of paths* $\mathbf{\Psi}$ *satisfying* **(Hyp.1)-(Hyp.3)**. *Assume that (3.2) is strictly hyperbolic with either genuinely nonlinear, or linearly degenerate characteristic fields, and that* $\mathbf{\Psi}$ *satisfies*

$$\frac{\partial \mathbf{\Psi}}{\partial \mathbf{u}_R}(1; \mathbf{u}_L, \mathbf{u}_L) - \frac{\partial \mathbf{\Psi}}{\partial \mathbf{u}_R}(0; \mathbf{u}_L, \mathbf{u}_L) = \mathrm{Id}, \quad \forall \mathbf{u}_L \in \Omega_*. \tag{3.18}$$

Then, for $|\mathbf{u}_L - \mathbf{u}_R|$ *small enough, the Riemann problem for (3.2) with initial data (3.17) has a solution with bounded variation* $\mathbf{u}$ *that depends only on* $\frac{x}{t}$ *and has the Lax's structure:* $\mathbf{u}$ *consists of* $N+1$ *constant states separated by shock waves, rarefaction waves or contact discontinuities.*

Let us now interpret the family of paths from a parabolic regularization. This leads to the notion that the choice of family of paths depends on the viscous profile. In order to demonstrate this, let us consider the parabolic regularization of (3.2), we have, for $\epsilon > 0$

$$\partial_t \mathbf{u}^\epsilon + \mathbf{A}(\mathbf{u}^\epsilon)\partial_x \mathbf{u}^\epsilon = \epsilon \partial_x \left(\mathbf{D}(\mathbf{u}^\epsilon)\partial_x \mathbf{u}^\epsilon \right), \tag{3.19}$$

where the right hand elliptic operator is termed as the viscous profile and $\mathbf{D}$ is a smooth positive semi-definite matrix.

Assuming that $\mathbf{u}$ is still a BV function, which is piecewise smooth [137], then for smooth solutions as $\epsilon \to 0$, we formally have

$$\mathbf{u}^\epsilon \to \mathbf{u}, \quad \mathbf{A}(\mathbf{u}^\epsilon)\partial_x \mathbf{u}^\epsilon \rightharpoonup \mathbf{A}(\mathbf{u})\partial_x \mathbf{u}, \quad \epsilon \partial_x \left(\mathbf{D}(\mathbf{u}^\epsilon)\partial_x \mathbf{u}^\epsilon \right) \to 0, \tag{3.20}$$

almost everywhere, under suitable estimates on the derivatives of $\mathbf{u}^\epsilon$.

In the case of travelling wave solutions of (3.19), $\mathbf{u}^\epsilon(x,t) = \mathbf{w}(\xi), \xi = \frac{x-\sigma t}{\epsilon}$, that satisfy

$$\lim_{\xi \to -\infty} \mathbf{w}(\xi) = \mathbf{u}_L, \quad \lim_{\xi \to +\infty} \mathbf{w}(\xi) = \mathbf{u}_R, \quad \lim_{\xi \to \pm\infty} \mathbf{w}'(\xi) = 0, \tag{3.21}$$

the viscous profile must satisfy the following ordinary differential equation

$$\left(\mathbf{A}(\mathbf{w}(\mathbf{s})) - \sigma \right) \mathbf{w}'(\xi) = \left(\mathbf{D}(\mathbf{w}(\mathbf{s}))\mathbf{w}'(\xi) \right)', \tag{3.22}$$

which can be integrated, see [24], to deduce

$$\sigma[\![\mathbf{w}]\!] = \int_{-\infty}^{+\infty} \mathbf{A}(\mathbf{w}(\xi))\mathbf{w}'(\xi)d\xi, \tag{3.23}$$

where it is evident that the jump condition depends on the choice of viscous profile $\mathbf{w}(\xi)$.

It must be mentioned, however, that weak solution in Definition 3.2.1 do not guarantee uniqueness, and, therefore, additional constraints need to be enforced in order to select admissible solutions. These constraints come in the form of *entropy conditions*.

Definition 3.3.1. *Let $\eta(\mathbf{u}) : \Omega_* \to \mathbb{R}$ be a smooth convex function and $q(\mathbf{u}) : \Omega_* \to \mathbb{R}$ be the smooth entropy flux, then admissible smooth solutions of (3.2) must satisfy an additional conservation law*

$$\boldsymbol{\eta}'(\mathbf{u})\left(\partial_t\mathbf{u} + \mathbf{A}(\mathbf{u})\partial_x\mathbf{u}\right) = \partial_t\eta(\mathbf{u}) + \partial_x q(\mathbf{u}) = 0, \forall \mathbf{u} \in \Omega_*, \tag{3.24}$$

such that

$$\boldsymbol{q}'(\mathbf{u})^\top = \boldsymbol{\eta}'(\mathbf{u})^\top\mathbf{A}(\mathbf{u}), \tag{3.25}$$

where $\boldsymbol{\eta}'(\mathbf{u})^\top = \partial_{\mathbf{u}}\eta(\mathbf{u})$ are the entropy variables and the mapping $\mathbf{u} \to \mathbf{v}(\mathbf{u})$ is one-to-one.

Additionally, let $(\mathbf{u}^\epsilon)_\epsilon$ be a sequence of sufficiently smooth solutions to (3.19) such that

- $\|\mathbf{u}^\epsilon\|_{\boldsymbol{L}^\infty(\mathbb{R}^+,\boldsymbol{BV}(\mathbb{R},\mathbb{R}^N))} < +\infty$,
- $\mathbf{u}^\epsilon \to \mathbf{u}$ *as* $\epsilon \to 0$ *almost everywhere in* $\mathbb{R} \times [0, +\infty[$,

then as $\epsilon \to 0$, admissible weak solutions of (3.19) must satisfy the entropy condition

$$\partial_t\eta(\mathbf{u}) + \partial_x q(\mathbf{u}) \leq 0. \tag{3.26}$$

In the sense of distributions $\forall \boldsymbol{\phi} \in \boldsymbol{C}_0^1(\mathbb{R}^+, \mathbb{R})$:

$$\int_{\mathbb{R}^+}\int_{\mathbb{R}} \eta(\mathbf{u}(x,t))\partial_t\boldsymbol{\phi}(x,t) + q(\mathbf{u}(x,t))\partial_x\boldsymbol{\phi}(x,t)dxdt + \int_{\mathbb{R}} \eta(\mathbf{u}_0(x))\boldsymbol{\phi}(x,0)dx \geq 0. \tag{3.27}$$

3.4 NUMERICAL SOLUTION

In this section we introduce the discontinuous Galerkin spectral element method (DGSEM) that we use to discretize (3.1).

Let us consider the Cauchy problem (3.1) over a computational grid $\Omega_h := \cup_{j\in\mathbb{Z}}\kappa_j$ containing cells $\kappa_j = [x_{j-\frac{1}{2}}, x_{j+\frac{1}{2}}]$, $x_{j+\frac{1}{2}} = jh$ with cell size $h > 0$, where the mesh is assumed to be uniform without loss of generality, see Figure 3-1.

We seek approximate solutions of (3.1) in the function space of piecewise polynomials

$$\mathcal{V}_h^p = \left\{v_h \in L^2(\Omega_h) : v_h|_{\kappa_j} \in \mathcal{P}_p(\kappa_j), \kappa_j \in \Omega_h\right\}, \tag{3.28}$$

where $\mathcal{P}_p(\kappa_j)$ denotes the space of polynomials of degree at most p in the element κ_j. The

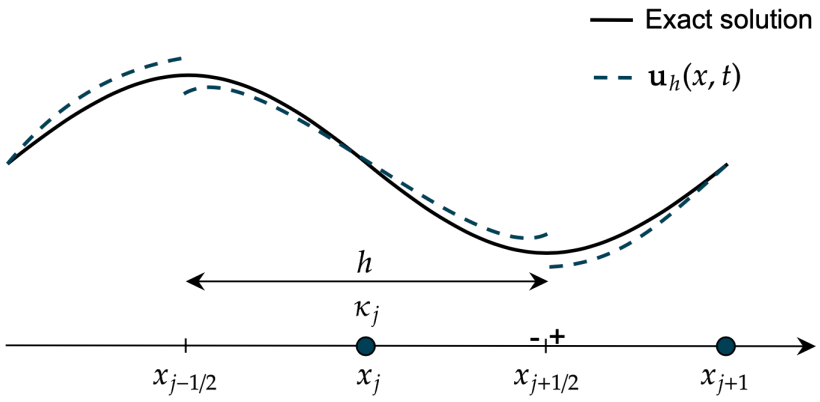

Figure 3-1: A one-dimensional representation of the mesh with cell κ_j of size h. The left and right interfaces of cell κ_j are at $x_{j\mp\frac{1}{2}}$, and the left and right traces are represented at $x_{j+\frac{1}{2}}$.

polynomial approximate solution is defined as

$$\mathbf{u}_h(x,t) := \sum_{k=0}^{p} \phi_j^k(x)\mathbf{U}_j^k(t) \quad \forall x \in \kappa_j, \kappa_j \in \Omega_h, t \geq 0, \tag{3.29}$$

where $(\phi_j^0, ..., \phi_j^p)$ constitutes a basis of $\mathcal{V}_h^p$ restricted onto κ_j and $\mathbf{U}_j^{0\leqslant k\leqslant p}$ are the $p+1$ degrees of freedom (DOFs) in κ_j.

Here we use the Lagrange interpolation polynomials $\ell_{0\leqslant k\leqslant p}$, see Figure 3-2, associated to the Gauss-Lobatto (GL) nodes over the reference element $I = [-1, 1]$: $-1 = \xi_0 < \xi_1 < \cdots < \xi_p = 1$:

$$\ell_k(\xi) = \prod_{l=0, l\neq k}^{p} \frac{\xi - \xi_l}{\xi_k - \xi_l}, \tag{3.30a}$$

$$\ell_k(\xi_l) = \delta_{kl}, \qquad 0 \leqslant k, l \leqslant p. \tag{3.30b}$$

Observe that the GL nodes take into account the boundary points $\xi = -1$ and $\xi = 1$ and satisfy the summation-by-parts (SBP) property. The basis functions with support in a given element κ_j are written as

$$\phi_j^k(x) = \ell_k(\sigma_j(x)), \quad \sigma_j(x) = 2(x - x_j)/h, \tag{3.31}$$

where $x_j = (x_{j+\frac{1}{2}} + x_{j-\frac{1}{2}})/2$ denotes the center of the element.

The DOFs in (3.29) thus correspond to the point values of the solution: given $0 \leqslant k \leqslant p$, $j \in \mathbb{Z}$, and $t \geq 0$, we have

$$\mathbf{u}_h(x_j^k, t) = \mathbf{U}_j^k(t) \tag{3.32}$$

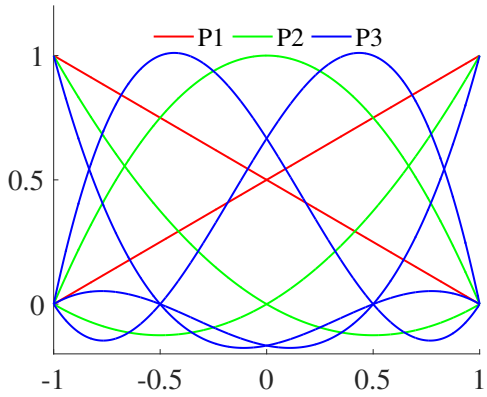

Figure 3-2: The plot of the Lagrange basis functions on the bi-unit reference element $I = [-1, 1]$ for $p = 1, 2,$ and 3.

for $x_j^k = x_j + \xi_k h/2$. Likewise, the left and right traces of the solution at the element interfaces read

$$\mathbf{u}_h(x_{j+1/2}^-, t) = \mathbf{U}_j^p(t), \quad \mathbf{u}_h(x_{j-1/2}^+, t) = \mathbf{U}_j^0(t), \tag{3.33}$$

respectively. The integrals over the elements are based on the Gauss-Lobatto quadrature rule where the quadrature and interpolation points are collocated:

$$\int_{\kappa_j} f(x)dx = \frac{h}{2}\int_{-1}^{1} f(x_j + \frac{h}{2}\xi)d\xi \approx \frac{h}{2}\sum_{l=0}^{p}\omega_l f(x_j^l), \tag{3.34}$$

where $\omega_l > 0$ with $\sum_{l=0}^{p}\omega_l = 2$, are the quadrature weights and x_j^l are the quadrature points. The discrete inner product within the element is defined as

$$\langle f, g\rangle_j^p := \frac{h}{2}\sum_{l=0}^{p}\omega_l f(x_j^l)g(x_j^l). \tag{3.35}$$

Let us also introduce the discrete difference matrix

$$D_{kl} = \ell_l'(\xi_k) = \frac{h}{2}d_x\phi_j^l(x_j^k), \quad 0 \leqslant k, l \leqslant p, \tag{3.36}$$

where the property $\sum_{l=0}^{p}\ell_l \equiv 1$ implies

$$\sum_{l=0}^{p} D_{kl} = 0 \quad \forall 0 \leqslant k \leqslant p. \tag{3.37}$$

The discrete difference matrix is known to satisfy the summation-by-parts (SBP) property, as observed in [86]. The SBP is the discrete analogue of the following integration-by-parts

$$\int_{\kappa_j}\phi_j^k(x)d_x\phi_j^l(x)dx + \int_{\kappa_j} d_x\phi_j^k(x)\phi_j^l(x)dx = \Big(\phi_j^k(x)\phi_j^l(x)\Big)_{x_{j+1/2}^-} - \Big(\phi_j^k(x)\phi_j^l w(x)\Big)_{x_{j-1/2}^+}, \tag{3.38}$$

where we use (3.34) and (3.36) to get

$$\omega_k D_{kl} + \omega_l D_{lk} = \delta_{kp}\delta_{lp} - \delta_{k0}\delta_{l0} \quad \forall 0 \leqslant k, l \leqslant p. \tag{3.39}$$

Indeed, the approximation (3.34) is exact for polynomial integrands up to degree $2p-1$ which is the case in (3.39).

3.4.1 SEMI-DISCRETE FORM

Let $\mathbf{u}_h \in (\mathcal{V}_h^p)^N$ be the approximate solution of (3.1a) then, under the DGSEM framework [54, 113], the semi-discrete form of (3.1) can be written as

$$\begin{aligned}\sum_{\kappa_j\in\Omega_h}\int_{\kappa_j}\partial_t v_h \mathbf{u}_h dx - \sum_{\kappa_j\in\Omega_h}\int_{\kappa_j}\mathbf{f}(\mathbf{u}_h)\partial_x v_h dx + \sum_{\kappa_j\in\Omega_h}\int_{\kappa_j}\mathbf{c}(\mathbf{u}_h)\partial_x \mathbf{u}_h dx \\ + \sum_{j\in\mathbb{Z}} v^-_{j+1/2}\Big(\mathbf{h}(\mathbf{U}^p_j,\mathbf{U}^0_{j+1}) + \mathbf{d}^-(\mathbf{U}^p_j,\mathbf{U}^0_{j+1})\Big) \\ + \sum_{j\in\mathbb{Z}} v^+_{j+1/2}\Big(\mathbf{d}^+(\mathbf{U}^p_{j-1},\mathbf{U}^0_j) - \mathbf{h}(\mathbf{U}^p_{j-1},\mathbf{U}^0_j)\Big) = 0, \quad \forall v_h \in \mathcal{V}_h^p.\end{aligned} \tag{3.40}$$

We again perform integration-by-parts to get

$$\begin{aligned}\sum_{\kappa_j\in\Omega_h}\int_{\kappa_j}\partial_t v_h \mathbf{u}_h dx + \sum_{\kappa_j\in\Omega_h}\int_{\kappa_j} v_h\big(\partial_x\mathbf{f}(\mathbf{u}_h) + \mathbf{c}(\mathbf{u}_h)\partial_x\mathbf{u}_h\big)dx \\ + \sum_{j\in\mathbb{Z}} v^-_{j+1/2}\Big(\mathbf{h}(\mathbf{U}^p_j,\mathbf{U}^0_{j+1}) - \mathbf{f}(\mathbf{U}^p_j) + \mathbf{d}^-(\mathbf{U}^p_j,\mathbf{U}^0_{j+1})\Big) \\ + \sum_{j\in\mathbb{Z}} v^+_{j+1/2}\Big(\mathbf{f}(\mathbf{U}^0_j) - \mathbf{h}(\mathbf{U}^p_{j-1},\mathbf{U}^0_j) + \mathbf{d}^+(\mathbf{U}^p_{j-1},\mathbf{U}^0_j)\Big) = 0, \quad \forall v_h \in \mathcal{V}_h^p,\end{aligned} \tag{3.41}$$

where $\mathbf{h}(\mathbf{u}^-,\mathbf{u}^+)$ are the numerical fluxes for the physical flux function, $\mathbf{f}(\mathbf{u}^\pm)$ are the traces of the physical flux at the interfaces, and $\mathbf{d}^\pm(\mathbf{u}^-,\mathbf{u}^+)$ are the fluctuation fluxes for the nonconservative product. Note that here we consider solutions which are only piecewise smooth, therefore the operation $\big(\mp\mathbf{h}(\mathbf{u}^-,\mathbf{u}^+) \pm \mathbf{f}(\mathbf{u}^\pm)\big)$ splits the Dirac mass placed at the interface.

The projection of the initial condition (3.1b) onto $(\mathcal{V}_h^p)^N$ reads

$$\sum_{\kappa_j\in\Omega_h}\int_{\kappa_j} v_h \mathbf{u}_h(x,0)dx = 0, \quad \forall v_h \in \mathcal{V}_h^p. \tag{3.42}$$

In this work, we replace the numerical fluxes in (3.41) with fluctuation fluxes $\mathbf{D}(\cdot,\cdot)$ and substitute v_h for the Lagrange interpolation polynomials (3.30). Furthermore, we consider the quadrature rule (3.34) and the difference matrix (3.36) to get a semi-discrete scheme for (3.1a):

$$\begin{aligned}\frac{\omega_k h}{2}\frac{d}{dt}\mathbf{U}^k_j + \omega_k\sum_{l=0}^{p} D_{kl}\big(\mathbf{f}(\mathbf{U}^l_j) + \mathbf{c}(\mathbf{U}^k_j)\mathbf{U}^l_j\big) \\ + \delta_{kp}\mathbf{D}^-(\mathbf{U}^p_j,\mathbf{U}^0_{j+1}) + \delta_{k0}\mathbf{D}^+(\mathbf{U}^p_{j-1},\mathbf{U}^0_j) = 0, \quad t>0, \quad \forall j\in\mathbb{Z}, \quad 0\leqslant k\leqslant p,\end{aligned} \tag{3.43}$$

along with the projection of the initial condition (3.1b) on the function space:

$$\mathbf{U}_j^k(0) = \mathbf{u}_0(x_j^k) \quad \forall j \in \mathbb{Z}, 0 \leqslant k \leqslant p. \tag{3.44}$$

The fluctuation fluxes satisfy the consistency property

$$\mathbf{D}^{\pm}(\mathbf{u}, \mathbf{u}) = 0, \quad \forall \mathbf{u} \in \Omega_*. \tag{3.45}$$

Note that our aim is to recover physically relevant solutions of (3.1) using the scheme (3.43). Therefore the concept of entropy weak solutions needs to be considered. In the following section we comment on the numerical fluxes and describe the conditions that allow them to satisfy a semi-discrete entropy inequality.

3.5 NUMERICAL FLUXES

We rely on numerical fluxes in fluctuation form [103] that satisfy the properties of entropy conservation and entropy stability for the semi-discrete scheme (3.43). Here we recall their definition from [24].

Definition 3.5.1. *Let $\mathbf{D}_{ec}^{\pm}$ be consistent numerical fluxes in fluctuation form, $\mathbf{D}_{ec}^{\pm}(\mathbf{u}, \mathbf{u}) = 0$ for all $\mathbf{u}$ in Ω_*, and (η, q) be an entropy-entropy flux pair for (3.1a), then $\mathbf{D}_{ec}^{\pm}$ are said to be entropy conservative if they satisfy the following relation:*

$$\mathbf{v}(\mathbf{u}^-)^\top \mathbf{D}_{ec}^-(\mathbf{u}^-, \mathbf{u}^+) + \mathbf{v}(\mathbf{u}^+)^\top \mathbf{D}_{ec}^+(\mathbf{u}^-, \mathbf{u}^+) = q(\mathbf{u}^+) - q(\mathbf{u}^-) \quad \forall \mathbf{u}^{\pm} \in \Omega_*, \tag{3.46}$$

where $\mathbf{v}(\mathbf{u}^{\pm}) = \eta'(\mathbf{u}^{\pm})$ are the entropy variables.

In this work we are interested in entropy conservative fluxes of the following form

$$\mathbf{D}_{ec}^-(\mathbf{u}^-, \mathbf{u}^+) = \mathbf{h}(\mathbf{u}^-, \mathbf{u}^+) - \mathbf{f}(\mathbf{u}^-) + \mathbf{d}^-(\mathbf{u}^-, \mathbf{u}^+), \tag{3.47a}$$
$$\mathbf{D}_{ec}^+(\mathbf{u}^-, \mathbf{u}^+) = \mathbf{f}(\mathbf{u}^+) - \mathbf{h}(\mathbf{u}^-, \mathbf{u}^+) + \mathbf{d}^+(\mathbf{u}^-, \mathbf{u}^+), \tag{3.47b}$$

where the numerical fluxes satisfy the consistency conditions:

$$\mathbf{h}(\mathbf{u}, \mathbf{u}) = \mathbf{f}(\mathbf{u}), \quad \mathbf{d}^{\pm}(\mathbf{u}, \mathbf{u}) = 0 \quad \forall \mathbf{u} \in \Omega_*, \tag{3.48}$$

and may also satisfy the path-conservative property

$$\mathbf{d}^-(\mathbf{u}^-, \mathbf{u}^+) + \mathbf{d}^+(\mathbf{u}^-, \mathbf{u}^+) = \int_0^1 \mathbf{c}(\mathbf{\Psi}(s, \mathbf{u}^-, \mathbf{u}^+)) \partial_s \mathbf{\Psi}(s, \mathbf{u}^-, \mathbf{u}^+) ds, \quad \forall \mathbf{u}^{\pm} \in \Omega_*, \quad j \in \mathbb{Z}. \tag{3.49}$$

Using (3.47), the condition for entropy conservation now becomes

$$\mathbf{v}(\mathbf{u}^-)^\top \mathbf{d}^-(\mathbf{u}^-, \mathbf{u}^+) + \mathbf{v}(\mathbf{u}^+)^\top \mathbf{d}^+(\mathbf{u}^-, \mathbf{u}^+) + [\![\mathbf{v}^\top \mathbf{f} - q]\!] = \mathbf{h}(\mathbf{u}^-, \mathbf{u}^+)^\top [\![\mathbf{v}]\!] \quad \forall \mathbf{u}^{\pm} \in \Omega_*, \tag{3.50}$$

where $\overline{a} = \frac{a^+ + a^-}{2}$ is the arithmetic mean and $[\![a]\!] = a^+ - a^-$ at a point x and $a^{\pm} = \lim_{\varepsilon \downarrow 0} a(x \pm \varepsilon)$. This relation is a direct generalization of entropy conditions in [24, 128] to systems with both conservative and nonconservative terms (3.1a).

Furthermore, we apply entropy stable fluxes [76] at the interfaces that dissipate the

entropy for shock solutions.

Definition 3.5.2. *Fluctuation fluxes* $\mathbf{D}^{\pm}$ *of the form*

$$\mathbf{D}^{\pm}(\mathbf{u}^-,\mathbf{u}^+) = \mathbf{D}^{\pm}_{ec}(\mathbf{u}^-,\mathbf{u}^+) \pm \mathbf{D}_{\nu}(\mathbf{u}^-,\mathbf{u}^+), \tag{3.51}$$

are said to be entropy stable if they satisfy the following relation:

$$\mathbf{v}(\mathbf{u}^-)^{\top}\mathbf{D}^-(\mathbf{u}^-,\mathbf{u}^+) + \mathbf{v}(\mathbf{u}^+)^{\top}\mathbf{D}^+(\mathbf{u}^-,\mathbf{u}^+) \geq q(\mathbf{u}^+) - q(\mathbf{u}^-) \quad \forall \mathbf{u}^{\pm} \in \Omega_*, \tag{3.52}$$

where $\mathbf{D}_{\nu}(\mathbf{u}^-,\mathbf{u}^+)$ *is a numerical dissipation that satisfies the consistency and entropy dissipation*

$$\mathbf{D}_{\nu}(\mathbf{u},\mathbf{u}) = 0, \quad [\![\mathbf{v}(\mathbf{u})]\!]^{\top}\mathbf{D}_{\nu}(\mathbf{u}^-,\mathbf{u}^+) \geqslant 0 \quad \forall \mathbf{u},\mathbf{u}^{\pm} \in \Omega_*. \tag{3.53}$$

Observe that in the semi-discrete form (3.43), the discrete volume integral

$$\omega_k \sum_{l=0}^{p} D_{kl}\big(\mathbf{f}(\mathbf{U}_j^l) + \mathbf{c}(\mathbf{U}_j^k)\mathbf{U}_j^l\big)$$

does not bear proper constraints towards entropy conservation or dissipation. In other words, we cannot control the sign of its scalar product with the entropy variables. Therefore, we modify the volume integral and replace it with entropy conservative fluctuation fluxes, as in [108]. The semi-discrete scheme now reads

$$\frac{\omega_k h}{2}\frac{d\mathbf{U}_j^k}{dt} + \mathbf{R}_j^k(\mathbf{u}_h) = 0, \tag{3.54}$$

where

$$\mathbf{R}_j^k(\mathbf{u}_h) = \omega_k \sum_{l=0}^{p} D_{kl}\tilde{\mathbf{D}}(\mathbf{U}_j^k,\mathbf{U}_j^l) + \delta_{kp}\mathbf{D}^-(\mathbf{U}_j^p,\mathbf{U}_{j+1}^0) + \delta_{k0}\mathbf{D}^+(\mathbf{U}_{j-1}^p,\mathbf{U}_j^0), \tag{3.55}$$

and

$$\tilde{\mathbf{D}}(\mathbf{u}^-,\mathbf{u}^+) := \mathbf{D}^-_{ec}(\mathbf{u}^-,\mathbf{u}^+) - \mathbf{D}^+_{ec}(\mathbf{u}^+,\mathbf{u}^-), \tag{3.56a}$$

$$\overset{(3.47)}{=} \mathbf{h}(\mathbf{u}^-,\mathbf{u}^+) + \mathbf{h}(\mathbf{u}^+,\mathbf{u}^-) + \mathbf{d}^-(\mathbf{u}^-,\mathbf{u}^+) - \mathbf{d}^+(\mathbf{u}^+,\mathbf{u}^-). \tag{3.56b}$$

Note that in the above relation we do not require $\mathbf{h}$ to be symmetric as in [30, 52], but rather use the symmetrizer $\frac{1}{2}\big(\mathbf{h}(\mathbf{u}^-,\mathbf{u}^+) + \mathbf{h}(\mathbf{u}^+,\mathbf{u}^-)\big)$. Indeed this symmetrizer still satisfies the consistency (3.48) and entropy conservation (3.50) conditions.

3.5.1 Properties of the semi-discrete scheme

The modification to the integrals over cell elements in (3.55) allows for an entropy stable numerical scheme that preserves the high-order accuracy of the scheme. These properties have been proven in [30, Theorem 3.3] for the conservative terms and [108, Theorems 3.1 and 3.2] for the nonconservative ones, however we recall them for systems that contain both the conservative and nonconservative terms.

Theorem 3.5.1. *Let* $\tilde{\mathbf{D}}$ *be defined as (3.56) using consistent and entropy conservative fluctuation fluxes (3.48) and (3.46), respectively, and let* $\mathbf{D}^{\pm}$ *be entropy stable fluxes that satisfies*

(3.52). Then, the semi-discrete numerical scheme (3.54) satisfies an entropy inequality for the entropy-entropy flux pair (η, q)*:*

$$h\frac{d}{dt}\langle\eta\rangle_j + Q(\mathbf{U}_j^p, \mathbf{U}_{j+1}^0) - Q(\mathbf{U}_{j-1}^p, \mathbf{U}_j^0) \leqslant 0, \tag{3.57}$$

where $\langle\eta\rangle_j(t) = \sum_{k=0}^p \frac{\omega_k}{2}\eta\big(\boldsymbol{U}_j^k(t)\big)$ *is the cell averaged entropy and the conservative numerical entropy flux is defined by*

$$Q(\mathbf{u}^-, \mathbf{u}^+) = \frac{q(\mathbf{u}^-) + q(\mathbf{u}^+)}{2} + \frac{1}{2}\mathbf{v}(\mathbf{u}^-)^\top \mathbf{D}^-(\mathbf{u}^-, \mathbf{u}^+) - \frac{1}{2}\mathbf{v}(\mathbf{u}^+)^\top \mathbf{D}^+(\mathbf{u}^-, \mathbf{u}^+), \tag{3.58}$$

which are also consistent.

Further assuming that $\mathbf{d}^\pm$ *in (3.56b) have the form*

$$\mathbf{d}^\pm(\mathbf{u}^-, \mathbf{u}^+) = \mathcal{C}^\pm(\mathbf{u}^-, \mathbf{u}^+)[\![\mathbf{u}]\!], \tag{3.59a}$$

$$\mathcal{C}(\mathbf{u}^-, \mathbf{u}^+) \coloneqq \mathcal{C}^+(\mathbf{u}^-, \mathbf{u}^+) + \mathcal{C}^-(\mathbf{u}^-, \mathbf{u}^+), \tag{3.59b}$$

$$\mathcal{C}(\mathbf{u}^-, \mathbf{u}^+) + \mathcal{C}(\mathbf{u}^+, \mathbf{u}^-) = \mathbf{c}(\mathbf{u}^-) + \mathbf{c}(\mathbf{u}^+), \tag{3.59c}$$

$$\mathcal{C}(\mathbf{u}, \mathbf{u}) = \mathbf{c}(\mathbf{u}), \tag{3.59d}$$

where $[\![\mathbf{u}]\!] = \mathbf{u}^+ - \mathbf{u}^-$*, then semi-discrete DGSEM (3.54) is a high-order approximation in space of smooth solutions for the nonconservative system (3.1a) that satisfies*

$$h\frac{d}{dt}\langle\mathbf{u}_h\rangle_j + \langle\mathbf{c}(\mathbf{u}_h), d_x\mathbf{u}_h\rangle_j^p + \mathbf{D}^-(\mathbf{U}_j^p, \mathbf{U}_{j+1}^0) + \mathbf{f}(\mathbf{U}_j^p) + \mathbf{D}^+(\mathbf{U}_{j-1}^p, \mathbf{U}_j^0) - \mathbf{f}(\mathbf{U}_j^0) = 0, \tag{3.60}$$

for the cell averaged solution

$$\langle\mathbf{u}_h\rangle_j(t) \coloneqq \frac{1}{h}\int_{\kappa_j} \mathbf{u}_h(x,t)dx = \frac{1}{2}\sum_{k=0}^p \omega_k \mathbf{U}_j^k(t). \tag{3.61}$$

Proof. The proof for semi-discrete entropy stability follows the same technique as deriving an entropy condition for the quasi-linear system in addition to employing some of the DGSEM identities mentioned earlier. Therefore, we left multiply $\boldsymbol{\eta}'(\mathbf{U}_j^k)^\top$ to (3.54) and by summing over $0 \leqslant k \leqslant p$ obtain

$$\begin{aligned} h\frac{d}{dt}\langle\eta\rangle_j + \sum_{k,l=0}^p \omega_k \boldsymbol{\eta}'(\mathbf{U}_j^k)^\top \tilde{\mathbf{D}}(\mathbf{U}_j^k, \mathbf{U}_j^l) D_{kl} + \boldsymbol{\eta}'(\mathbf{U}_j^p)^\top \mathbf{D}^-(\mathbf{U}_j^p, \mathbf{U}_{j+1}^0) \\ + \boldsymbol{\eta}'(\mathbf{U}_j^0)^\top \mathbf{D}^+(\mathbf{U}_{j-1}^p, \mathbf{U}_j^0) = 0, \end{aligned} \tag{3.62}$$

where attention should be given to resolving the volume term

$$\begin{aligned}
\sum_{k,l=0}^{p} \omega_k \boldsymbol{\eta}'(\mathbf{U}_j^k)^\top \tilde{\mathbf{D}}(\mathbf{U}_j^k, \mathbf{U}_j^l) D_{kl} &\overset{(5.24a)}{=} \sum_{k,l=0}^{p} \omega_k \boldsymbol{\eta}'(\mathbf{U}_j^k)^\top \left(\mathbf{D}_{ec}^-(\mathbf{U}_j^k, \mathbf{U}_j^l) - \mathbf{D}_{ec}^+(\mathbf{U}_j^l, \mathbf{U}_j^k) \right) D_{kl} \\
&\overset{(3.39)}{=} \sum_{k,l=0}^{p} \omega_k \boldsymbol{\eta}'(\mathbf{U}_j^k)^\top \mathbf{D}_{ec}^-(\mathbf{U}_j^k, \mathbf{U}_j^l) D_{kl} + \omega_l \boldsymbol{\eta}'(\mathbf{U}_j^k)^\top \mathbf{D}_{ec}^+(\mathbf{U}_j^l, \mathbf{U}_j^k) D_{lk} \\
&\quad - \delta_{kl}(\delta_{kp} - \delta_{k0}) \eta'(\mathbf{U}_j^k)^\top \mathbf{D}_{ec}^+(\mathbf{U}_j^l, \mathbf{U}_j^k) \\
&\overset{(3.45)}{\underset{k \leftrightarrow l}{=}} \sum_{k,l=0}^{p} \omega_k \left(\boldsymbol{\eta}'(\mathbf{U}_j^k)^\top \mathbf{D}_{ec}^-(\mathbf{U}_j^k, \mathbf{U}_j^l) + \boldsymbol{\eta}'(\mathbf{U}_j^l)^\top \mathbf{D}_{ec}^+(\mathbf{U}_j^k, \mathbf{U}_j^l) \right) D_{kl} \\
&\overset{(3.46)}{=} \sum_{k,l=0}^{p} \omega_k \left(q(\mathbf{U}_j^l) - q(\mathbf{U}_j^k) \right) D_{kl} \\
&\underset{(3.37)}{\overset{(3.39)}{=}} q(\mathbf{U}_j^p) - q(\mathbf{U}_j^0).
\end{aligned}$$

In the above, $k \leftrightarrow l$ indicates the inversion of the indices k and l in some of the terms.

The relation (3.62), thus, simplifies to

$$h \frac{d}{dt} \langle \eta \rangle_j + q(\mathbf{U}_j^p) - q(\mathbf{U}_j^0) + \boldsymbol{\eta}'(\mathbf{U}_j^p)^\top \mathbf{D}^-(\mathbf{U}_j^p, \mathbf{U}_{j+1}^0) + \boldsymbol{\eta}'(\mathbf{U}_j^0)^\top \mathbf{D}^+(\mathbf{U}_{j-1}^p, \mathbf{U}_j^0) = 0, \tag{3.63}$$

which can equivalently be expressed as

$$\begin{aligned}
h \frac{d}{dt} \langle \eta \rangle_j &+ \frac{1}{2} \left(q(\mathbf{U}_j^p) + q(\mathbf{U}_{j+1}^0) \right) - \frac{1}{2} \left(q(\mathbf{U}_{j+1}^0) - q(\mathbf{U}_j^p) \right) \\
&- \frac{1}{2} \left(q(\mathbf{U}_{j-1}^p) + q(\mathbf{U}_j^0) \right) + \frac{1}{2} \left(q(\mathbf{U}_{j-1}^p) - q(\mathbf{U}_j^0) \right) \\
&+ \boldsymbol{\eta}'(\mathbf{U}_j^p)^\top \mathbf{D}^-(\mathbf{U}_j^p, \mathbf{U}_{j+1}^0) - \boldsymbol{\eta}'(\mathbf{U}_{j+1}^p)^\top \mathbf{D}^+(\mathbf{U}_j^p, \mathbf{U}_{j+1}^0) + \boldsymbol{\eta}'(\mathbf{U}_{j+1}^p)^\top \mathbf{D}^+(\mathbf{U}_j^p, \mathbf{U}_{j+1}^0) \\
&+ \boldsymbol{\eta}'(\mathbf{U}_j^0)^\top \mathbf{D}^+(\mathbf{U}_{j-1}^p, \mathbf{U}_j^0) - \boldsymbol{\eta}'(\mathbf{U}_{j-1}^p)^\top \mathbf{D}^-(\mathbf{U}_{j-1}^p, \mathbf{U}_j^0) + \boldsymbol{\eta}'(\mathbf{U}_{j-1}^p)^\top \mathbf{D}^-(\mathbf{U}_{j-1}^p, \mathbf{U}_j^0) = 0,
\end{aligned} \tag{3.64}$$

where we collect the terms and use (3.58) to get

$$\begin{aligned}
&h \frac{d}{dt} \langle \eta \rangle_j + Q(\mathbf{U}_j^p, \mathbf{U}_{j+1}^0) - Q(\mathbf{U}_{j-1}^p, \mathbf{U}_j^0) \\
&= \frac{1}{2} \left(q(\mathbf{U}_j^0) - q(\mathbf{U}_{j-1}^p) - \boldsymbol{\eta}'(\mathbf{U}_j^0)^\top \mathbf{D}^+(\mathbf{U}_{j-1}^p, \mathbf{U}_j^0) - \boldsymbol{\eta}'(\mathbf{U}_{j-1}^p)^\top \mathbf{D}^-(\mathbf{U}_{j-1}^p, \mathbf{U}_j^0) \right) \\
&+ \frac{1}{2} \left(q(\mathbf{U}_{j+1}^0) - q(\mathbf{U}_j^p) - \boldsymbol{\eta}'(\mathbf{U}_{j+1}^0)^\top \mathbf{D}^+(\mathbf{U}_j^p, \mathbf{U}_{j+1}^0) - \boldsymbol{\eta}'(\mathbf{U}_j^p)^\top \mathbf{D}^-(\mathbf{U}_j^p, \mathbf{U}_{j+1}^0) \right) \\
&\overset{(3.52)}{\leq} 0 \quad .
\end{aligned} \tag{3.65}$$

High-order accuracy [37, 108]. In order to prove that the DGSEM scheme (3.54) is high-order accurate it is sufficient to prove that the modification to the volume integral (3.55)-(3.56) provide a high-order approximation of $\int_{\kappa_j} \phi_j \left(\partial_x \mathbf{f}(\mathbf{u}_h) + \mathbf{c}(\mathbf{u}_h) \partial_x \mathbf{u}_h \right) dx$.

Let $\pi_h^p : L^2(\Omega) \cap C(\Omega) \ni u \to \pi_h^p(u) \in \mathcal{V}_h^p$ be the Lagrange projection onto the reference domain. Since the Lagrange interpolation error is of order $\mathcal{O}(h^{p+1})$, we have the following

result for the product of u and v in $\mathcal{C}^{p+1}(\Omega_h)$:

$$d_x\pi_h^p(uv)(x) = u(x)d_xv(x) + v(x)d_xu(x) + \mathcal{O}(h^p), \quad \forall x \in \Omega_h. \tag{3.66}$$

Furthermore, let $\mathbf{c}_h^k(x) := \sum_{l=0}^p \mathcal{C}^-(\mathbf{U}_j^k, \mathbf{U}_j^l)\phi^l(x)$ be the interpolation polynomial, then we have $\mathbf{c}_h^k(x_j^k) = \mathcal{C}^-(\mathbf{U}_j^k, \mathbf{U}_j^k)$ and $d_x\mathbf{c}_h^k(x_h^k) = \frac{2}{h}\sum_{l=0}^p \mathcal{C}^-(\mathbf{U}_j^k, \mathbf{U}_j^l)D_{kl}$ by using (3.39). Then by applying (3.66) to $\mathbf{c}_h^k\mathbf{u}_h$, we obtain

$$\frac{2}{h}\sum_{l=0}^p \mathcal{C}^-(\mathbf{U}_j^k, \mathbf{U}_j^l)\mathbf{U}_j^l D_{kl} = \frac{2}{h}\sum_{l=0}^p \Big(\mathcal{C}^-(\mathbf{U}_j^k, \mathbf{U}_j^k)\mathbf{U}_j^l + \mathcal{C}^-(\mathbf{U}_j^k, \mathbf{U}_j^l)\mathbf{U}_j^k\Big) D_{kl} + \mathcal{O}(h^p). \tag{3.67}$$

Similarly, an expression for $\mathbf{c}_h^k(x) := \sum_{l=0}^p \mathcal{C}^+(\mathbf{U}_j^l, \mathbf{U}_j^k)\phi^l(x)$ can also be derived. As a result (3.56) can be written as

$$\begin{aligned}
&\frac{2}{h}\sum_{k,l=0}^p \tilde{\mathbf{D}}(\mathbf{U}_j^k, \mathbf{U}_j^l)D_{kl} \\
&= \frac{2}{h}\sum_{k,l=0}^p \Big(2\mathbf{h}(\mathbf{U}_j^k, \mathbf{U}_j^l) + \mathbf{d}^-(\mathbf{U}_j^k, \mathbf{U}_j^l) - \mathbf{d}^+(\mathbf{U}_j^l, \mathbf{U}_j^k)\Big) D_{kl} \\
&\overset{(3.59a)}{=} \frac{2}{h}\sum_{k,l=0}^p \Big(\mathbf{h}(\mathbf{U}_j^k, \mathbf{U}_j^l) + \mathbf{h}(\mathbf{U}_j^l, \mathbf{U}_j^k) + \Big(\mathcal{C}^-(\mathbf{U}_j^k, \mathbf{U}_j^l) + \mathcal{C}^+(\mathbf{U}_j^l, \mathbf{U}_j^k)\Big)\Big(\mathbf{U}_j^l - \mathbf{U}_j^k\Big)\Big) D_{kl} \\
&\underset{(3.37)}{\overset{(3.67)}{=}} \partial_x\tilde{\mathbf{f}}(\mathbf{u}_h(x_j^k)) + \frac{2}{h}\sum_{k,l=0}^p \Big(\mathcal{C}^-(\mathbf{U}_j^k, \mathbf{U}_j^k) + \mathcal{C}^+(\mathbf{U}_j^k, \mathbf{U}_j^k)\Big)\mathbf{U}_j^l D_{kl} + \mathcal{O}(h^p) \\
&\underset{(3.36)}{\overset{(3.59c)}{=}} \partial_x\tilde{\mathbf{f}}(\mathbf{u}_h(x_j^k)) + \mathcal{C}(\mathbf{U}_j^k, \mathbf{U}_j^k)\partial_x\mathbf{u}_h(x_j^k) + \mathcal{O}(h^p) \\
&\overset{(3.59d)}{=} \partial_x\tilde{\mathbf{f}}(\mathbf{u}_h(x_j^k)) + \mathbf{c}(\mathbf{u}_h(x_j^k))\partial_x\mathbf{u}_h(x_j^k) + \mathcal{O}(h^p).
\end{aligned}$$

Finally we prove (3.60) by summing (3.55) over $0 \leqslant k \leqslant p$, we obtain

$$h\frac{d\langle \mathbf{u}_h\rangle_j}{dt} + \sum_{k=0}^p\sum_{l=0}^p \omega_k D_{kl}\tilde{\mathbf{D}}(\mathbf{U}_j^k, \mathbf{U}_j^l) + \mathbf{D}^-(\mathbf{U}_j^p, \mathbf{U}_{j+1}^0) + \mathbf{D}^+(\mathbf{U}_{j-1}^p, \mathbf{U}_j^0) = 0,$$

where

$$\begin{aligned}
&\sum_{k,l=0}^p \omega_k D_{kl}\tilde{\mathbf{D}}(\mathbf{U}_j^k, \mathbf{U}_j^l) \\
&\overset{(3.56b)}{=} \sum_{k,l=0}^p \omega_k D_{kl}\Big(\mathbf{h}(\mathbf{U}_j^k, \mathbf{U}_j^l) + \mathbf{d}^-(\mathbf{U}_j^k, \mathbf{U}_j^l)\Big) + \sum_{k,l=0}^p \omega_k D_{kl}\Big(\mathbf{h}(\mathbf{U}_j^l, \mathbf{U}_j^k) - \mathbf{d}^+(\mathbf{U}_j^l, \mathbf{U}_j^k)\Big) \\
&\underset{(3.48)}{\overset{(3.39)}{=}} \sum_{k,l=0}^p \omega_k D_{kl}\Big(\mathbf{h}(\mathbf{U}_j^k, \mathbf{U}_j^l) + \mathbf{d}^-(\mathbf{U}_j^k, \mathbf{U}_j^l)\Big) - \sum_{k,l=0}^p \omega_l D_{lk}\Big(\mathbf{h}(\mathbf{U}_j^l, \mathbf{U}_j^k) \\
&- \mathbf{d}^+(\mathbf{U}_j^l, \mathbf{U}_j^k)\Big) + \mathbf{f}(\mathbf{U}_j^p) - \mathbf{f}(\mathbf{U}_j^0) \\
&\underset{(3.59b)}{\overset{(3.59a)}{=}} \sum_{k,l=0}^p \omega_k D_{kl}\mathcal{C}(\mathbf{U}_j^k, \mathbf{U}_j^l)(\mathbf{U}_j^l - \mathbf{U}_j^k) + \mathbf{f}(\mathbf{U}_j^p) - \mathbf{f}(\mathbf{U}_j^0)
\end{aligned}$$

$$
\begin{aligned}
&\overset{(3.39)}{\underset{(3.59d)}{=}} \sum_{k,l=0}^{p} \omega_k D_{kl} \mathcal{C}(\mathbf{U}_j^k, \mathbf{U}_j^l)\mathbf{U}_j^l + \sum_{k,l=0}^{p} \omega_l D_{lk} \mathcal{C}(\mathbf{U}_j^k, \mathbf{U}_j^l)\mathbf{U}_j^k \\
&\quad - \mathbf{c}(\mathbf{U}_j^p)\mathbf{U}_j^p + \mathbf{c}(\mathbf{U}_j^0)\mathbf{U}_j^0 + \mathbf{f}(\mathbf{U}_j^p) - \mathbf{f}(\mathbf{U}_j^0) \\
&\overset{(3.59c)}{=} \sum_{k,l=0}^{p} \omega_k D_{kl} \big(\mathbf{c}(\mathbf{U}_j^k) + \mathbf{c}(\mathbf{U}_j^l)\big)\mathbf{U}_j^l - \mathbf{c}(\mathbf{U}_j^p)\mathbf{U}_j^p \\
&\quad + \mathbf{c}(\mathbf{U}_j^0)\mathbf{U}_j^0 + \mathbf{f}(\mathbf{U}_j^p) - \mathbf{f}(\mathbf{U}_j^0) \\
&\overset{(3.39)}{=} \sum_{k,l=0}^{p} \omega_k D_{kl} \mathbf{c}(\mathbf{U}_j^k)\mathbf{U}_j^l - \sum_{k,l=0}^{p} \omega_k D_{kl} \mathbf{c}(\mathbf{U}_j^k)\mathbf{U}_j^k + \mathbf{f}(\mathbf{U}_j^p) - \mathbf{f}(\mathbf{U}_j^0) \\
&\overset{(3.37)}{\underset{(3.35)}{=}} \langle \mathbf{c}(\mathbf{u}_h), d_x \mathbf{u}_h \rangle_j^p + \mathbf{f}(\mathbf{U}_j^p) - \mathbf{f}(\mathbf{U}_j^0)
\end{aligned}
$$

□

3.6 DGSEM IN MULTIPLE SPACE DIMENSIONS

We here extend the DGSEM to multiple space dimensions and restrict ourselves to Cartesian meshes. For the sake of clarity we introduce the scheme in two space dimensions, $d = 2$, on uniform grids without loss of generality.

The physical domain Ω is discretized with a Cartesian grid Ω_h with elements $\kappa_{i,j} = [x_{i-\frac{1}{2}}, x_{i+\frac{1}{2}}] \times [y_{j-\frac{1}{2}}, y_{j+\frac{1}{2}}]$ with $x_{i+\frac{1}{2}} = ih_x$, $y_{j+\frac{1}{2}} = jh_y$, where $h_x > 0$ and $h_y > 0$ are the space steps.The Cartesian coordinate system is denoted as $(0, \mathbf{e_x}, \mathbf{e_y})$. Each element $\kappa_{i,j}$ is defined through the mapping $\mathbf{x}_{i,j} : I^2 \ni (\xi, \eta) \mapsto \mathbf{x} = \mathbf{x}_{i,j}(\xi, \eta) \in \kappa_{i,j}$ with $I^2 = [-1, 1]^2$. The function space $\mathcal{V}_h^p$ restricted onto an element $\kappa_{i,j}$ is spanned with functions defined as tensor products of one-dimensional Lagrange polynomials associated to the Gauss-Lobatto nodes (see section 3.4):

$$\phi_{i,j}^{kl}\big(\mathbf{x}_{i,j}(\xi, \eta)\big) := \ell_k(\xi)\ell_l(\eta), \quad 0 \leqslant k, l \leqslant p,$$

which satisfy the cardinality relation $\ell_k(\xi_{\tilde{k}})\ell_l(\eta_{\tilde{l}}) = \delta_{\tilde{k}k}\delta_{\tilde{l}l}$ for $0 \leqslant \tilde{k}, k, \tilde{l}, l \leqslant p$. The approximate solution is now represented as

$$\mathbf{u}_h(\mathbf{x}, t) := \sum_{k,l=0}^{p} \phi_{i,j}^{kl}(\mathbf{x})\mathbf{U}_{i,j}^{kl}(t) \quad \forall \mathbf{x} \in \kappa_{i,j},\ t \geqslant 0.$$

The integrals over the physical elements and faces are approximated with Gauss-Lobatto quadratures:

$$\int_{\kappa_{i,j}} f(\mathbf{x})dV \approx \sum_{k,l=0}^{p} \omega_k\omega_l \frac{h_x h_y}{4} f(\mathbf{x}_{i,j}^{kl}), \quad \int_e f(\mathbf{x})dS \approx \sum_{k=0}^{p} \omega_k \frac{|e|}{2} f(\mathbf{x}_e^k),$$

where ω_k and $\omega_k\omega_l$ are the Gaussian weights, and $|e|$ is the length of e.

The semi-discrete DGSEM for the discretization of (4.37) then reads

$$\frac{h_x h_y}{4} \frac{d\mathbf{U}_{i,j}^{kl}}{dt}$$

$$+\omega_l \frac{h_y}{2}\left(\sum_{m=0}^{p}\omega_k D_{km}\tilde{\mathbf{D}}(\mathbf{U}_{i,j}^{kl},\mathbf{U}_{i,j}^{ml},\mathbf{e_x})+\delta_{kp}\mathbf{D}^{-}(\mathbf{U}_{i,j}^{pl},\mathbf{U}_{i+1,j}^{0l},\mathbf{e_x})+\delta_{k0}\mathbf{D}^{+}(\mathbf{U}_{i-1,j}^{pl},\mathbf{U}_{ij}^{0l},\mathbf{e_x})\right)$$
$$+\omega_k \frac{h_x}{2}\left(\sum_{m=0}^{p}\omega_l D_{lm}\tilde{\mathbf{D}}(\mathbf{U}_{i,j}^{kl},\mathbf{U}_{i,j}^{km},\mathbf{e_y})+\delta_{lp}\mathbf{D}^{-}(\mathbf{U}_{i,j}^{kp},\mathbf{U}_{i,j+1}^{k0},\mathbf{e_y})+\delta_{l0}\mathbf{D}^{+}(\mathbf{U}_{i,j-1}^{kp},\mathbf{U}_{ij}^{k0},\mathbf{e_y})\right)=0,$$

with

$$\tilde{\mathbf{D}}(\mathbf{u}^-,\mathbf{u}^+,\mathbf{n}) \coloneqq \mathbf{D}_{ec}^{-}(\mathbf{u}^-,\mathbf{u}^+,\mathbf{n})-\mathbf{D}_{ec}^{+}(\mathbf{u}^+,\mathbf{u}^-,\mathbf{n}).$$

3.7 TIME INTEGRATION

The DG formulation provides the ability to compute high-order accurate solutions in space, therefore it is expected that the temporal integration is also high-order accurate. In this work we rely on strong-stability preserving Runge-Kutta (SSP-RK) methods [63] that preserves the properties of first order forward Euler method under some condition on the time step.

To demonstrate this, let us discretize the scheme (3.54) using the forward Euler method

$$\mathbf{u}_h^{(n+1)} = \mathbf{u}_h^{(n)} + \Delta t \mathbf{R}(\mathbf{u}_h^{(n)}), \tag{3.68}$$

where $\mathbf{u}_h^{(n)}$ is the vector of DOFs, $\mathbf{R}(\mathbf{u}_h^n, t^n)$ is the vector of residuals (3.55) and $t^{(n)} = n\Delta t$, $\Delta t > 0$ is the time step. Additionally the explicit s stage Runge-Kutta method can be written as

$$\begin{cases} \mathbf{v}^{(0)} = \mathbf{u}_h^{(n)} \\ \mathbf{v}^{(i)} = \sum_j^{i-1} \alpha_{ij}\mathbf{v}^{(j)} + \beta_{ij}\Delta t \mathbf{R}\left(\mathbf{v}^{(j)}, t^n + \Delta t\right), \\ \mathbf{v}^{(s)} = \mathbf{u}_h^{(n+1)}, \end{cases} \tag{3.69}$$

where the values of α_{ij} and β_{ij} are found such that the order conditions are satisfied [19, 66, 121]. For consistency, we must have

$$\sum_{l=0}^{i-1}\alpha_{il} = 1.$$

Observe that if α_{ij} and β_{ij} are positive in (3.69) then the RK method is a convex combination of the forward Euler steps

$$\mathbf{v}^{(i)} = \sum_{j=0}^{i-1}\alpha_{ij}\left(\mathbf{v}^{(j)} + \frac{\beta_{ij}}{\alpha_{ij}}\Delta t \mathbf{R}\left(\mathbf{v}^{(j)}, t^n + \Delta t\right)\right).$$

As a result, if Δt_E is the time step for the Euler method, then we can directly rely on that result at high order, provided that the maximum time step is bounded as

$$\Delta t_{RK} \leqslant \min_{ij}\frac{\alpha_{ij}}{\beta_{ij}}\Delta t_E.$$

This describes the SSP-RK methods which are particularly important for problems involving shocks and discontinuities.

In our work we use the SSP-RK method proposed in [121], which can be written as

$$\begin{aligned}
\mathbf{v}^{(1)} &= \mathbf{u}_h^n + \Delta t \mathbf{R}\left(\mathbf{v}^{(0)}, t^n + \Delta t\right), \\
\mathbf{v}^{(2)} &= \frac{1}{4}\left(3\mathbf{u}_h^{(n)} + \mathbf{v}^{(1)} + \Delta t \mathbf{R}\left(\mathbf{v}^{(1)}, t^n + \Delta t\right)\right), \\
\mathbf{v}^{(3)} &= \frac{1}{3}\left(\mathbf{u}_h^{(n)} + 2\mathbf{v}^{(2)} + 2\Delta t \mathbf{R}\left(\mathbf{v}^{(2)}, t^n + \frac{1}{2}\Delta t\right)\right),
\end{aligned} \tag{3.70}$$

and $\mathbf{u}_h^{(n+1)} = \mathbf{v}^{(3)}$.

Chapter 4

An entropy stable high-order discontinuous Galerkin spectral element method for the Baer-Nunziato two-phase flow model

Résumé du chapitre

Dans ce chapitre, nous proposons une discrétisation d'ordre élevé du modèle d'écoulement diphasique de Baer-Nunziato [7] avec des fermetures pour la vitesse et la pression à l'interface adaptées au traitement de solutions discontinues, et des équations d'état des gaz raidies. Nous utilisons la méthode des éléments spectraux de Galerkin discontinue (DGSEM), basée sur la collocation des points de quadrature et d'interpolation [86]. La DGSEM utilise des opérateurs de sommation par parties (SBP) dans la quadrature numérique pour approximer les intégrales sur les éléments de discrétisation [20, 59]. Ici, nous nous appuyons sur le cadre fourni dans [108] pour les systèmes hyperboliques non-conservatifs afin de modifier l'intégration sur les éléments de cellule en utilisant les opérateurs SBP et de remplacer les flux physiques par des flux de fluctuation conservant de l'entropie de [24], tandis que nous dérivons des flux numériques qui dissipe l'entropie aux interfaces. Cela permet de prouver une inégalité semi-discrète pour l'entropie physique moyenne de la cellule, tout en conservant une précision d'ordre élevé. La conception des flux numériques préserve aussi formellement l'énergie cinétique au niveau discret. L'intégration temporelle d'ordre élevé est réalisée à l'aide de schémas de Runge-Kutta préservant la stabilité et nous proposons des conditions sur les paramètres numériques pour la positivité de la fraction de vide et des densités partielles moyennées par cellule. La positivité de la solution moyenne de la cellule est étendue aux valeurs nodales par l'utilisation d'un limiteur a posteriori. La précision d'ordre élevé, la stabilité non linéaire et la robustesse du présent schéma sont évaluées par plusieurs expériences numériques en une et deux dimensions spatiales.

4.1 Short description and outline of the chapter

In this chapter we propose a high-order discretization of the Baer-Nunziato two-phase flow model [7] with closures for interface velocity and pressure adapted to the treatment of discontinuous solutions, and stiffened gas equations of states. We use the discontinu-

ous Galerkin spectral element method (DGSEM), based on collocation of quadrature and interpolation points [86]. The DGSEM uses summation-by-parts (SBP) operators in the numerical quadrature for approximating the integrals over discretization elements [20, 59]. Here, we build upon the framework provided in [108] for nonconservative hyperbolic systems to modify the integration over cell elements using the SBP operators and replace the physical fluxes with entropy conservative fluctuation fluxes from [24], while we derive entropy stable numerical fluxes applied at interfaces. This allows to prove a semi-discrete inequality for the cell-averaged physical entropy, while keeping high-order accuracy. The design of the numerical fluxes also formally preserves the kinetic energy at the discrete level. High-order integration in time is performed using strong stability-preserving Runge-Kutta schemes and we propose conditions on the numerical parameters for the positivity of the cell-averaged void fraction and partial densities. The positivity of the cell-averaged solution is extended to nodal values by the use of an a posteriori limiter. The high-order accuracy, nonlinear stability, and robustness of the present scheme are assessed through several numerical experiments in one and two space dimensions.

The plan of this chapter is as follows. In Section 4.2 we recall the essential properties of the Baer-Nunziato model that are relevant to this work. The derivation of entropy conservative and entropy stable numerical fluxes are given in section 4.3. The properties of the scheme and the limiters are described in section 4.4. The results of the numerical experiments in one space dimension are presented in section 4.5, while those in two space dimensions are presented in section 4.6. Finally, we summarize the present work in section 4.7.

4.2 The Baer-Nunziato model

Here we only recall specific properties of the Baer-Nunziato model that are relevant to this chapter. This is done in order to avoid repetitiveness. For complete details on the physical aspects of the model, we refer to Chapter 2.

We consider the Cauchy problem to the model (2.1), without the zeroth order source terms [5, 6, 48, 132]

$$\partial_t \mathbf{u} + \partial_x \mathbf{f}(\mathbf{u}) + \mathbf{c}(\mathbf{u})\partial_x \mathbf{u} = 0, \qquad x \in \mathbb{R}, t > 0, \tag{4.1a}$$

$$\mathbf{u}(x,0) = \mathbf{u}_0(x), \quad x \in \mathbb{R}, \tag{4.1b}$$

where

$$\mathbf{u} = \begin{pmatrix} \alpha_i \\ \alpha_i\rho_i \\ \alpha_i\rho_i u_i \\ \alpha_i\rho_i E_i \end{pmatrix}, \quad \mathbf{f}(\mathbf{u}) = \begin{pmatrix} 0 \\ \alpha_i\rho_i u_i \\ \alpha_i(\rho_1 u_i^2 + \mathrm{p}_i) \\ \alpha_i u_i(\rho_i E_i + \mathrm{p}_i) \end{pmatrix}, \quad \mathbf{c}(\mathbf{u})\partial_x \mathbf{u} = \begin{pmatrix} \mathrm{u}_\mathrm{I} \\ 0 \\ -\mathrm{p}_\mathrm{I} \\ -\mathrm{p}_\mathrm{I}\mathrm{u}_\mathrm{I} \end{pmatrix} \partial_x \alpha_i, \quad i = 1, 2. \tag{4.2}$$

represent the variable vector, the vector of physical fluxes, and nonconservative products, respectively. The phase densities are ρ_i, the velocities are u_i, and the specific total energies are $E_i = e_i + u_i^2/2$ where e_i is the specific internal energy and $i = 1, 2$ refers to the ith phase. The void fraction of each individual phase is denoted as α_i and we assume that both satisfy the saturation condition

$$\alpha_1 + \alpha_2 = 1. \tag{4.3}$$

In one space dimension, the model is a system of seven equations including the evolution equations for the mass, momentum and energy of each phase, along with a transport equation for the void fraction. The solution $\mathbf{u}$ belongs to the phase space

$$\Omega_{\text{BNM}} = \big\{\mathbf{u} \in \mathbb{R}^7 : 0 < \alpha_i < 1,\ \rho_i > 0,\ u_i \in \mathbb{R},\ \rho_i e_i > \mathrm{p}_{\infty,i},\ i = 1, 2\big\}, \tag{4.4}$$

where $\mathrm{p}_{\infty,i} \geq 0$ is a pressure-like constant.

Closure laws. We use the same closure laws for the pressure and the interfacial variables as in (2.11)-(2.12) with (2.13). Therefore the pressure of each phase is related to the density and internal energy through the stiffened gas EOS:

$$\mathrm{p}_i(\rho_i, e_i) = (\gamma_i - 1)\rho_i e_i - \gamma_i \mathrm{p}_{\infty,i}, \tag{4.5}$$

where $\gamma_i = \mathrm{C}_{\mathrm{p}_i}/\mathrm{C}_{\mathrm{v}i} > 1$ is the ratio of specific heats of phase i, while we use general closure laws from [34, 56]:

$$\mathrm{u}_\mathrm{I} := \beta u_1 + (1 - \beta)u_2, \tag{4.6a}$$
$$\mathrm{p}_\mathrm{I} := \mu \mathrm{p}_1 + (1 - \mu)\mathrm{p}_2, \tag{4.6b}$$

where

$$\beta = \frac{\chi\alpha_1\rho_1}{\chi\alpha_1\rho_1 + (1-\chi)\alpha_2\rho_2}, \quad \mu = \frac{(1-\beta)T_2}{\beta T_1 + (1-\beta)T_2}, \quad \chi \in \{0, \tfrac{1}{2}, 1\}, \tag{4.7}$$

are the convex weights and T_i denotes the temperature of the ith phase, which is defined by

$$e_i = \mathrm{C}_{\mathrm{v}i} T_i + \frac{\mathrm{p}_{\infty,i}}{\rho_i}. \tag{4.8}$$

Entropy. The system (4.1a) is endowed with a physical entropy function

$$s_i(\rho_i, \theta_i) = -\mathrm{C}_{\mathrm{v}i} \ln\big(\tfrac{\mathrm{p}+\mathrm{p}_{\infty,i}}{\rho_i^{\gamma_i}}\big) = -\mathrm{C}_{\mathrm{v}i}\big(\ln\theta_i + (\gamma_i - 1)\ln\rho_i\big), \quad i = 1, 2, \tag{4.9}$$

where $\theta_i = \frac{1}{T_i}$ the inverse of temperature.

Smooth solutions of (4.1) satisfy

$$\partial_t \sum_{i=1}^{2} \alpha_i\rho_i s_i + \partial_x \sum_{i=1}^{2} \alpha_i\rho_i s_i u_i = \sum_{i=1}^{2} (\mathrm{p}_\mathrm{I} - \mathrm{p}_i)(\mathrm{u}_\mathrm{I} - u_i)\theta_i \partial_x \alpha_i, \tag{4.10}$$

where the right-hand side indeed vanishes for the closure of interfacial quantities (4.6) and (4.7):

$$\sum_{i=1}^{2} (\mathrm{p}_\mathrm{I} - \mathrm{p}_i)(\mathrm{u}_\mathrm{I} - u_i)\theta_i \partial_x \alpha_i = 0. \tag{4.11}$$

In the case of non-smooth solutions, such as shocks, admissible weak solutions of (4.1) must satisfy a nonlinear stability condition for the convex entropy function $\eta(\mathbf{u}) := -\sum_{i=1}^{2} \alpha_i\rho_i s_i$ and entropy flux $q(\mathbf{u}) := -\sum_{i=1}^{2} \alpha_i u_i \rho_i s_i$:

$$\partial_t \eta(\mathbf{u}) + \partial_x q(\mathbf{u}) \leqslant 0. \tag{4.12}$$

For smooth solutions, system (4.1a) can also be written in quasi-linear form as

$$\partial_t \mathbf{u} + \mathbf{A}(\mathbf{u})\partial_x \mathbf{u} = 0, \quad x \in \mathbb{R}, t > 0, \tag{4.13}$$

where $\mathbf{A} : \Omega_{\text{BNM}} \ni \mathbf{u} \mapsto \mathbf{A}(\mathbf{u}) = \mathbf{f}'(\mathbf{u}) + \mathbf{c}(\mathbf{u}) \in \mathbb{R}^{7\times 7}$ is a matrix-valued function for smooth solutions of (4.1). The system (4.13) is hyperbolic over the phase space (4.4) and $\mathbf{A}(\mathbf{u})$ admits real eigenvalues

$$\begin{aligned} &\lambda_1(\mathbf{u}) = u_1 - c_1,\ \lambda_2(\mathbf{u}) = u_2 - c_2,\ \lambda_3(\mathbf{u}) = u_1, \\ &\lambda_4(\mathbf{u}) = \mathrm{u_I},\ \lambda_5(\mathbf{u}) = u_2,\ \lambda_6(\mathbf{u}) = u_1 + c_1,\ \lambda_7(\mathbf{u}) = u_2 + c_2, \end{aligned} \tag{4.14}$$

associated to linearly independent eigenvectors. Here $c_i(\rho_i, e_i)^2 = \gamma_i(\gamma_i - 1)(\rho_i e_i - p_{\infty,i})/\rho_i$ is the speed of sound for the EOS (4.5). Observe, in (4.14), that λ_3, λ_4 and λ_5 are associated to LD fields, whereas the others ones, $\lambda_1, \lambda_2, \lambda_6$ and λ_7, are associated to genuinely nonlinear (GNL) fields. Note that (4.13) is only weakly hyperbolic when $\mathrm{u_I}$ is equal to one transport velocity, u_1 or u_2, for $\chi = 1$ or 0 in (4.7). In this work we assume that (4.13) is hyperbolic and well-posed and exclude resonance phenomena.

Definition 4.2.1. *A hyperbolic system (4.13) is said to be resonant if a linearly degenerate field interacts with a genuinely nonlinear field, resulting in the system to turn degenerate as the right eigenvectors no longer span the whole phase space.*

In our case, the eigenvalues of $\mathbf{A}(\mathbf{u})$ *in (4.13) are linearly independent iff*

$$\alpha_i \neq 0, \quad \mathrm{u_I} \neq u_i \pm c_i, \quad i = 1, 2. \tag{4.15}$$

During the remaining course of this chapter, we will discretize the initial value problem (4.1) using the DGSEM framework, which was introduced in section 3.4. Here we propose numerical fluxes in fluctuation form, refer section 3.5, for the model (4.1a) that satisfies the Theorem 3.5.1.

4.3 Numerical fluxes for the Baer-Nunziato model

Here we derive the numerical fluxes for the model (4.1a) that satisfy the entropy conservation (3.50) and dissipation (3.52) properties together with the assumptions in Theorem 3.5.1. An essential tool which would help in the algebraic manipulations are the Leibniz identities, which we recall here. Let $a^+, a^-, b^+, b^-, c^+, c^-$ in $\mathbb{R}$ have finite values, then we have

$$[\![ab]\!] = \overline{a}[\![b]\!] + \overline{b}[\![a]\!], \quad [\![abc]\!] = \overline{a}(\overline{b}[\![c]\!] + \overline{c}[\![b]\!]) + \overline{bc}[\![a]\!], \tag{4.16}$$

where $\overline{a} = \frac{a^+ + a^-}{2}$ is the arithmetic mean and $[\![a]\!] = a^+ - a^-$ at a point x and $a^\pm = \lim_{\varepsilon \downarrow 0} a(x \pm \varepsilon)$.

4.3.1 Entropy conservative fluxes

We begin by proposing entropy conservative numerical fluxes.

Proposition 4.3.1. *The numerical fluxes (3.47) with the following definitions are consistent and entropy conservative fluxes that satisfy the assumptions (3.59) of Theorem 3.5.1 for the*

Baer-Nunziato model (4.1a) with the EOS (4.5) and the interface variables (4.6).

$$\mathbf{h}(\mathbf{u}^-,\mathbf{u}^+) \coloneqq \begin{pmatrix} 0 \\ h_{\rho_i} \\ h_{\rho u_i} \\ h_{\rho E_i} \end{pmatrix} - \beta_s \frac{[\![\alpha_i]\!]}{2} \begin{pmatrix} 1 \\ \tilde{h}_{\rho_i} \\ \tilde{h}_{\rho u_i} \\ \tilde{h}_{\rho E_i} \end{pmatrix}, \quad \mathbf{d}^{\pm}(\mathbf{u}^-,\mathbf{u}^+) \coloneqq \frac{[\![\alpha_i]\!]}{2} \begin{pmatrix} \mathrm{u_I}^{\pm} \\ 0 \\ -\mathrm{p_I}^{\pm} \\ -\mathrm{p_I}^{\pm}\mathrm{u_I}^{\pm} \end{pmatrix}, \quad i = 1,2, \tag{4.17}$$

where

$$\begin{aligned} (h_{\rho_i}, h_{\rho u_i}, h_{\rho E_i}) &= \left(\overline{\alpha}_i \overline{u}_i \hat{\rho}_i,\ \overline{\alpha}_i \left(\overline{u}_i^2 \hat{\rho}_i + \overline{\frac{\mathrm{p}_i \theta_i}{\theta_i}} \right),\ \overline{\alpha}_i \overline{u}_i \left(\hat{\rho}_i \left(\frac{\mathrm{C_v}_i}{\hat{\theta}_i} + \frac{u_i^- u_i^+}{2} \right) + \overline{\frac{\mathrm{p}_i \theta_i}{\theta_i}} + \mathrm{p}_{\infty,i} \right) \right), \\ (\tilde{h}_{\rho_i}, \tilde{h}_{\rho u_i}, \tilde{h}_{\rho E_i}) &= \left(\hat{\rho}_i,\ \hat{\rho}_i \overline{u}_i,\ \hat{\rho}_i \left(\frac{\mathrm{C_v}_i}{\hat{\theta}_i} + \frac{u_i^- u_i^+}{2} \right) + \mathrm{p}_{\infty,i} \right), \end{aligned} \tag{4.18}$$

$\beta_s \geqslant 0$ *is defined in Theorem 4.4.2 and* $\hat{a} = \dfrac{[\![a]\!]}{[\![\ln a]\!]}$ *is the logarithmic mean [76].*

Proof. Consistency of the numerical flux $\mathbf{h}$ follows from consistency of the arithmetic and logarithmic means and the fact that $\rho_i e_i = \rho_i \mathrm{C_v}_i T_i + \mathrm{p}_{\infty,i}$ from

$$\rho_i \mathrm{C_v}_i T_i = \rho_i e_i - \mathrm{p}_{\infty,i} = \frac{\mathrm{p}_i + \mathrm{p}_{\infty,i}}{\gamma_i - 1}, \quad i = 1,2. \tag{4.19}$$

It can be easily checked that $\mathbf{d}^{\pm}$ satisfy (3.59) and consistency $\mathbf{d}^{\pm}(\mathbf{u},\mathbf{u}) = 0$.

Now let us recall the entropy variables associated to the entropy in (4.12):

$$\mathbf{v}(\mathbf{u}) = \begin{pmatrix} (-1)^i \left(\mathrm{p}_1 \theta_1 - \mathrm{p}_2 \theta_2 \right) \\ -s_i + \left(h_i - \dfrac{u_i^2}{2} \right) \theta_i \\ u_i \theta_i \\ -\theta_i \end{pmatrix}, \quad i = 1,2, \tag{4.20}$$

where $h_i(\rho_i, e_i) = e_i + \frac{\mathrm{p}_i(\rho_i,e_i)}{\rho_i} = \mathrm{C_p}_i T_i$ is the specific enthalpy for phase $i = 1,2$ and $\theta_i = 1/T_i$. Then, the discrete counterpart of (4.11) holds for the interface closures (4.6) and reads

$$\sum_{i=1}^{2} \overline{(\mathrm{p_I} - \mathrm{p}_i)(\mathrm{u_I} - u_i)\theta_i} [\![\alpha_i]\!] = 0. \tag{4.21}$$

Entropy conservation requires the fluxes (3.47) with (4.17) to satisfy (3.50) so we have to check that

$$\begin{aligned} \Delta Q(\mathbf{u}^-,\mathbf{u}^+) \coloneqq &-\mathbf{h}(\mathbf{u}^-,\mathbf{u}^+) \cdot [\![\mathbf{v}(\mathbf{u})]\!] + \mathbf{v}(\mathbf{u}^-) \cdot \mathbf{d}^-(\mathbf{u}^-,\mathbf{u}^+) + \mathbf{v}(\mathbf{u}^+) \cdot \mathbf{d}^+(\mathbf{u}^-,\mathbf{u}^+) \\ &+ [\![\mathbf{f}(\mathbf{u}) \cdot \mathbf{v}(\mathbf{u}) - q(\mathbf{u})]\!] = 0. \end{aligned} \tag{4.22}$$

Below we detail each term in the above relation by using the Liebniz identities (4.16) for

the numerical fluxes (4.17). Note that direct manipulations give

$$\llbracket \mathrm{p}_i\theta_i \rrbracket \overset{(4.5)}{=} (\gamma_i - 1)\mathrm{C}_{\mathrm{v}i}\llbracket \rho_i \rrbracket - \mathrm{p}_{\infty,i}\llbracket \theta_i \rrbracket, \tag{4.23a}$$

$$\llbracket h_i\theta_i \rrbracket = 0, \tag{4.23b}$$

$$\llbracket s_i \rrbracket \overset{(4.9)}{=} -\mathrm{C}_{\mathrm{v}i}\llbracket \ln\theta_i \rrbracket - (\gamma_i - 1)\mathrm{C}_{\mathrm{v}i}\llbracket \ln\rho_i \rrbracket, \tag{4.23c}$$

$$\overline{u}_i^2 - \overline{\frac{u_i^2}{2}} = \frac{u_i^- u_i^+}{2}. \tag{4.23d}$$

Then, by (4.17) and (4.20), we have

$$\begin{aligned}
&\llbracket \mathbf{v}(\mathbf{u}) \rrbracket \cdot \mathbf{h}(\mathbf{u}^-, \mathbf{u}^+) \\
&= \sum_{i=1}^{2} \overline{\alpha}_i\hat{\rho}_i\overline{u}_i\llbracket (h_i - u_i^2/2)\theta_i - s_i \rrbracket + \overline{\alpha}_i\left(\hat{\rho}_i\overline{u}_i^2 + \overline{\frac{\mathrm{p}_i\theta_i}{\theta_i}}\right)\llbracket u_i\theta_i \rrbracket \\
&- \overline{\alpha}_i\overline{u}_i\left(\hat{\rho}_i\left(\frac{\mathrm{C}_{\mathrm{v}i}}{\hat{\theta}_i} + \frac{u_i^- u_i^+}{2}\right) + \overline{\frac{\mathrm{p}_i\theta_i}{\theta_i}} + \mathrm{p}_{\infty,i}\right)\llbracket \theta_i \rrbracket \\
&- \beta_s\frac{\llbracket \alpha_i \rrbracket}{2}\left(-\llbracket \mathrm{p}_i\theta_i \rrbracket + \hat{\rho}_i\llbracket (h_i - u_i^2/2)\theta_i - s_i \rrbracket + \hat{\rho}_i\overline{u}_i\llbracket u_i\theta_i \rrbracket - \left(\hat{\rho}_i\left(\frac{\mathrm{C}_{\mathrm{v}i}}{\hat{\theta}_i} + \frac{u_i^- u_i^+}{2}\right) + \mathrm{p}_{\infty,i}\right)\llbracket \theta_i \rrbracket\right) \\
&\overset{(4.23)}{=} \sum_{i=1}^{2} -\overline{\alpha}_i\hat{\rho}_i\overline{u}_i\Big(\overline{u}_i\overline{\theta}_i\llbracket u_i \rrbracket + \overline{u_i^2/2}\llbracket \theta_i \rrbracket - \mathrm{C}_{\mathrm{v}i}\llbracket \ln\theta_i \rrbracket - (\gamma_i - 1)\mathrm{C}_{\mathrm{v}i}\llbracket \ln\rho_i \rrbracket\Big) \\
&+ \overline{\alpha}_i\left(\hat{\rho}_i\overline{u}_i^2 + \overline{\frac{\mathrm{p}_i\theta_i}{\theta_i}}\right)\llbracket u_i\theta_i \rrbracket - \overline{\alpha}_i\overline{u}_i\left(\hat{\rho}_i\left(\frac{\mathrm{C}_{\mathrm{v}i}}{\hat{\theta}_i} + \frac{u_i^- u_i^+}{2}\right) + \overline{\frac{\mathrm{p}_i\theta_i}{\theta_i}} + \mathrm{p}_{\infty,i}\right)\llbracket \theta_i \rrbracket \\
&- \beta_s\frac{\llbracket \alpha_i \rrbracket}{2}\Big(-(\gamma_i - 1)\mathrm{C}_{\mathrm{v}i}\llbracket \rho_i \rrbracket + \mathrm{p}_{\infty,i}\llbracket \theta_i \rrbracket + \hat{\rho}_i\overline{u}_i\left(\overline{u}_i\llbracket \theta_i \rrbracket + \overline{\theta}_i\llbracket u_i \rrbracket\right) - \left(\hat{\rho}_i\left(\frac{\mathrm{C}_{\mathrm{v}i}}{\hat{\theta}_i} + \frac{u_i^- u_i^+}{2}\right) + \mathrm{p}_{\infty,i}\right)\llbracket \theta_i \rrbracket \\
&- \hat{\rho}_i\left(\overline{u}_i\overline{\theta}_i\llbracket u_i \rrbracket + \overline{u_i^2/2}\llbracket \theta_i \rrbracket - \mathrm{C}_{\mathrm{v}i}\llbracket \ln\theta_i \rrbracket - (\gamma_i - 1)\mathrm{C}_{\mathrm{v}i}\llbracket \ln\rho_i \rrbracket\right)\Big) \\
&\underset{(4.23)}{\overset{(4.16)}{=}} \sum_{i=1}^{2} -\overline{\alpha}_i\overline{u}_i\hat{\rho}_i\Big(\overline{u}_i\overline{\theta}_i\llbracket u_i \rrbracket + \overline{u_i^2/2}\llbracket \theta_i \rrbracket - \mathrm{C}_{\mathrm{v}i}\llbracket \ln\theta_i \rrbracket - (\gamma_i - 1)\mathrm{C}_{\mathrm{v}i}\llbracket \ln\rho_i \rrbracket\Big) \\
&+ \overline{\alpha}_i\left(\overline{u}_i^2\hat{\rho}_i + \overline{\frac{\mathrm{p}_i\theta_i}{\theta_i}}\right)\left(\overline{u_i}\llbracket \theta_i \rrbracket + \overline{\theta}_i\llbracket u_i \rrbracket\right) - \overline{\alpha}_i\overline{u}_i\left(\hat{\rho}_i\left(\frac{\mathrm{C}_{\mathrm{v}i}}{\hat{\theta}_i} + \frac{u_i^- u_i^+}{2}\right) + \overline{\frac{\mathrm{p}_i\theta_i}{\theta_i}} + \mathrm{p}_{\infty,i}\right)\llbracket \theta_i \rrbracket.
\end{aligned} \tag{4.24}$$

Furthermore, using (4.17) we easily obtain

$$\mathbf{v}(\mathbf{u}^-)\cdot\mathbf{d}^-(\mathbf{u}^-, \mathbf{u}^+) + \mathbf{v}(\mathbf{u}^+)\cdot\mathbf{d}^+(\mathbf{u}^-, \mathbf{u}^+) = \sum_{i=1}^{2}\overline{(\mathrm{p}_{\mathrm{I}}\mathrm{u}_{\mathrm{I}} - \mathrm{p}_{\mathrm{I}}u_i - \mathrm{p}_i\mathrm{u}_{\mathrm{I}})\theta_i}\llbracket \alpha_i \rrbracket \overset{(4.21)}{=} -\sum_{i=1}^{2}\overline{\mathrm{p}_i u_i\theta_i}\llbracket \alpha_i \rrbracket, \tag{4.25}$$

and

$$
\begin{aligned}
&[\![\mathbf{f}(\mathbf{u})\cdot\mathbf{v}(\mathbf{u})-q(\mathbf{u})]\!]\\
&=\sum_{i=1}^{2}[\![-\alpha_i\rho_i u_i\big(s_i-(h_i-u_i^2/2)\theta_i\big)+\alpha_i(\rho_i u_i^2+\mathrm{p}_i)u_i\theta_i-\alpha_i(\rho_i E_i+\mathrm{p}_i)u_i\theta_i+\alpha_i\rho_i s_i u_i]\!]\\
&=\sum_{i=1}^{2}[\![\alpha_i\mathrm{p}_i u_i\theta_i]\!]\overset{(4.16)}{=}\sum_{i=1}^{2}\overline{\mathrm{p}_i u_i\theta_i}[\![\alpha_i]\!]+\overline{\alpha}_i\overline{\mathrm{p}_i\theta_i}[\![u_i]\!]+\overline{\alpha}_i\overline{u}_i[\![\mathrm{p}_i\theta_i]\!]\\
&\overset{(??)}{=}\sum_{i=1}^{2}\overline{\mathrm{p}_i u_i\theta_i}[\![\alpha_i]\!]+\overline{\alpha}_i\overline{\mathrm{p}_i\theta_i}[\![u_i]\!]+\overline{\alpha}_i\overline{u}_i\big((\gamma_i-1)\mathrm{C}_{\mathrm{v}i}[\![\rho_i]\!]-\mathrm{p}_{\infty,i}[\![\theta_i]\!]\big).
\end{aligned}
\tag{4.26}
$$

Substituting (4.24), (4.25) and (4.26) into (4.22) and collecting terms proportional to $[\![\rho_i]\!]$, $[\![u_i]\!]$, and $[\![\theta_i]\!]$, we get

$$
\begin{aligned}
&\Delta Q(\mathbf{u}^-,\mathbf{u}^+)\\
&\overset{(4.23)}{=}\sum_{i=1}^{2}\overline{\alpha}_i\left(\hat{\rho}_i\overline{u}_i^2\overline{\theta}_i-\left(\hat{\rho}_i\overline{u}_i^2+\frac{\overline{\mathrm{p}_i\theta_i}}{\overline{\theta}_i}\right)\overline{\theta}_i+\overline{\mathrm{p}_i\theta_i}\right)[\![u_i]\!]\\
&+\overline{\alpha}_i\overline{u}_i\left(\hat{\rho}_i\left(\frac{\overline{u_i^2}}{2}-\mathrm{C}_{\mathrm{v}i}\frac{[\![\ln\theta_i]\!]}{[\![\theta_i]\!]}\right)-\hat{\rho}_i\overline{u}_i^2-\frac{\overline{\mathrm{p}_i\theta_i}}{\overline{\theta}_i}+\hat{\rho}_i\left(\frac{\mathrm{C}_{\mathrm{v}i}}{\hat{\theta}_i}+\frac{u_i^-u_i^+}{2}\right)+\frac{\overline{\mathrm{p}_i\theta_i}}{\overline{\theta}_i}+\mathrm{p}_{\infty,i}-\mathrm{p}_{\infty,i}\right)[\![\theta_i]\!]\\
&-(\gamma_i-1)\mathrm{C}_{\mathrm{v}i}\overline{\alpha}_i\overline{u}_i\left(\hat{\rho}_i[\![\ln\rho_i]\!]-[\![\rho_i]\!]\right)=0,
\end{aligned}
$$

which concludes the proof. □

Remark 4.3.1. *The contributions to the volume integral in (3.55) of the terms associated to β_s in (4.17) vanish due to the symmetrizer $\mathbf{h}(\mathbf{u}^-,\mathbf{u}^+)+\mathbf{h}(\mathbf{u}^+,\mathbf{u}^-)$ in (3.56b). They will however play an important role in the design of the entropy stable fluxes at interfaces (see Theorem 4.4.2). They may be compared to the upwinding term in the Lax-Friedrichs flux derived in [116] for (4.1a). The main motivation for including this term was to introduce stabilizing mechanisms in the transport equation for the void fraction, as is evident from the first component of $\mathbf{h}$ in (4.17). However, $\mathrm{u_I}$ is associated to a LD field, so the remaining terms $\tilde{h}_{\rho_i}$, $\tilde{h}_{\rho u_i}$, and $\tilde{h}_{\rho E_i}$ are further included so that this dissipation does not affect the entropy balance as shown in the proof above.*

Remark 4.3.2. *Assuming perfect gas EOS in (4.5), $\mathrm{p}_{\infty,i}=0$, and uniform void fractions, $[\![\alpha_i]\!]=0$, then the numerical flux $\mathbf{h}(\mathbf{u}^-,\mathbf{u}^+)$ in (4.17) for both phases reduce to the entropy conservative Chandraskhar flux [28] for the compressible Euler equations. This numerical flux has been here extended to the stiffened gas EOS (4.5).*

4.3.2 ENTROPY STABLE FLUXES

We here follow the procedure in [76] and build entropy stable fluxes (3.52) by adding upwind-type dissipation to the entropy conservative numerical fluxes (3.47). We introduce numerical dissipation to the equations of mass, momentum and energy for each phase. The rationales for this particular choice of the numerical dissipation are as follows. First, we do not add numerical dissipation to the void fraction equation as it is associated to a LD field. We stress that the conservative flux in (4.17) already adds dissipation through an

upwinding term without altering the entropy balance (see Remark 4.3.1). Second, since we exclude resonance effects according to the assumption (4.15), the void fractions remain uniform across shocks leading to uncoupled phases. It is, thus, appropriate to include dissipation phase by phase.

Proposition 4.3.2. *A class of entropy stable fluxes (3.52) that satisfy*

$$\mathbf{D}_\nu(\mathbf{u},\mathbf{u}) = 0, \quad [\![\mathbf{v}(\mathbf{u})]\!]^\intercal \mathbf{D}_\nu(\mathbf{u}^-,\mathbf{u}^+) \geqslant 0 \quad \forall \mathbf{u},\mathbf{u}^\pm \in \Omega_*. \tag{4.27}$$

can be obtained for the Baer-Nunziato model (4.1a) where the numerical dissipation takes the form

$$\mathbf{D}_\nu(\mathbf{u}^-,\mathbf{u}^+) = \begin{pmatrix} 0 & 0 & 0 & 0 \\ 0 & k_{22} & 0 & 0 \\ 0 & k_{32} & k_{33} & 0 \\ 0 & k_{42} & k_{43} & k_{44} \end{pmatrix} \begin{pmatrix} 0 \\ [\![\rho_i]\!] \\ [\![u_i]\!] \\ [\![T_i]\!] \end{pmatrix},$$

where the matrix entries satisfy the following conditions

$$k_{22} \geqslant 0, \quad k_{33} \geqslant 0, \quad k_{44} \geqslant 0, \quad k_{32} = \overline{u_i} k_{22}, \quad k_{43} = \overline{u_i} k_{33}, \quad k_{42} = \left(\frac{\mathrm{C_{v}}i}{\hat{\theta}_i} + \frac{u_i^- u_i^+}{2} \right) k_{22}. \tag{4.28}$$

Proof. By construction we have $\mathbf{D}_\nu(\mathbf{u},\mathbf{u}) = 0$. Then, using (4.20) and (4.9), we get

$$\begin{aligned} [\![\mathbf{v}(\mathbf{u})]\!] \cdot \mathbf{D}_\nu(\mathbf{u}^-,\mathbf{u}^+) &= \sum_{i=1}^{2} k_{22}(\gamma_i - 1)\mathrm{C_{v}}i [\![\rho_i]\!][\![\ln \rho_i]\!] + k_{33}\overline{\theta_i}[\![u_i]\!]^2 - k_{44}[\![T_i]\!][\![\theta_i]\!] \\ &\quad + \overline{\theta_i}(k_{32} - k_{22}\overline{u_i})[\![\rho_i]\!][\![u_i]\!] - \left(k_{42} - \overline{u_i}k_{32} - k_{22}\left(\frac{\mathrm{C_{v}}i}{\hat{\theta}_i} - \frac{\overline{u_i^2}}{2} \right) \right) [\![\rho_i]\!][\![\theta_i]\!] \\ &\quad - (k_{43} - \overline{u_i}k_{33})[\![u_i]\!][\![\theta_i]\!] \\ &\overset{(4.28)}{=} \sum_{i=1}^{2} k_{22}(\gamma_i - 1)\mathrm{C_{v}}i [\![\rho_i]\!][\![\ln \rho_i]\!] + k_{33}\overline{\theta_i}[\![u_i]\!]^2 - k_{44}[\![T_i]\!][\![\theta_i]\!] \geqslant 0. \end{aligned}$$

□

Using dimensional arguments, we define $k_{33} = \overline{\rho}_i k_{22}$ and $k_{44} = \overline{\rho}_i \mathrm{C_{v}}i k_{22}$, and $k_{22} = \frac{\epsilon_\nu}{2} \max\left(\rho_{\mathbf{A}}(\mathbf{u}^-), \rho_{\mathbf{A}}(\mathbf{u}^+)\right)$, with $\epsilon_\nu \geqslant 0$ and $\rho_{\mathbf{A}}(\mathbf{u}) = \max_{i=1,2}(|u_i| + c_i)$ the spectral radius of $\mathbf{A}(\mathbf{u})$ in (4.13), to get the following numerical dissipation

$$\mathbf{D}_\nu(\mathbf{u}^-,\mathbf{u}^+) = \frac{\epsilon_\nu}{2} \max\left(\rho_{\mathbf{A}}(\mathbf{u}^-), \rho_{\mathbf{A}}(\mathbf{u}^+)\right) \begin{pmatrix} 0 \\ [\![\rho_i]\!] \\ [\![\rho_i u_i]\!] \\ \left(\frac{\mathrm{C_{v}}i}{\hat{\theta}_i} + \frac{u_i^- u_i^+}{2} \right) [\![\rho_i]\!] + \overline{\rho}_i [\![E_i]\!] \end{pmatrix}. \tag{4.29}$$

Remark 4.3.3. *Nonconservative systems may admit shocks which depend on small scale mechanisms such as viscosity and that numerical methods may fail to capture because the leading viscosity terms in the equivalent equation do not match these mechanisms [91]. The jump conditions indeed depend on the family of paths prescribed in the jump relations which*

should be consistent with the viscous profile. Using (4.29) the decay rate for the cell-averaged entropy (3.57) reads

$$h\frac{d\langle\eta(\mathbf{u}_h)\rangle_j}{dt}+Q(\mathbf{U}_j^p,\mathbf{U}_{j+1}^0)-Q(\mathbf{U}_{j-1}^p,\mathbf{U}_j^0)=-\frac{\epsilon_\nu}{2}\sum_{i=1}^{2}\frac{(\gamma_i-1)\mathrm{C_{v}}_i[\![\rho_i]\!]^2}{\hat{\rho}_i}+\overline{\rho_i}\overline{\theta_i}[\![u_i]\!]^2-\overline{\rho_i}\mathrm{C_{v}}_i[\![T_i]\!][\![\theta_i]\!]\leqslant 0,$$

where the two last terms in the RHS are analogous to the ones in the physical model [56] for a Prandtl number $Pr_i = 3\gamma_i/4$:

$$\partial_t\eta(\mathbf{u})+\partial_x q(\mathbf{u})=-\sum_i\frac{4\mu_i}{3}\left(\theta_i(\partial_x u_i)^2-\frac{3\mathrm{C_{p}}_i}{4Pr_i}\partial_x T_i\partial_x\theta_i\right),$$

and $\mu_i > 0$ is the dynamic viscosity coefficient and are therefore consistent with the small scale mechanisms. The first term in the RHS was seen to improve stability and robustness of the computations despite its lack of physical relevance.

4.4 PROPERTIES OF THE HIGH-ORDER DGSEM SCHEME FOR THE BAER-NUNZIATO MODEL

4.4.1 KINETIC ENERGY PRESERVATION

The equation for the kinetic energy of the model (4.1a) can be derived from the mass and momentum equations:

$$\partial_t K_i+\partial_x K_i u_i+u_i\partial_x\alpha_i\mathrm{p}_i-\mathrm{p_I}u_i\partial_x\alpha_i=0,\quad i=1,2,$$

where $K_i=\frac{1}{2}\alpha_i\rho_i u_i^2$ is the partial kinetic energy of the ith phase. These equations contain nonconservative terms of pressure work and energy transfer between the phases. The property of kinetic energy preservation by numerical schemes was introduced in [77] for the compressible Euler equations, where a general condition was provided to impose kinetic energy preservation for finite volume schemes, and was seen to be useful in turbulent flow simulations. Kinetic energy preservation was later extended to high-order nodal DG schemes in [58, 59] and we refer to [87] for split forms of the convective terms in the compressible Euler equations that lead to kinetic energy preserving schemes. According to [59, Theorem 2] it is sufficient to show that the volume terms of the advective part of the cell-averaged kinetic energy can be written in conservation form. This is done in the theorem below.

Theorem 4.4.1. *The discretization of the volume integral in (3.54)-(3.55) with the numerical fluxes (4.17) is kinetic energy preserving.*

Proof. Let us consider the time derivative and volume term of the advective parts of the mass and momentum equations of phase $i = 1, 2$ in (3.55). Using (4.17) they read

$$\Delta K_{i,j}^{\alpha\rho,k}=\tfrac{\omega_k h}{2}d_t(\alpha_{i,j}^k\rho_{i,j}^k)+\sum_{l=0}^{p}2\omega_k D_{kl}h_i^{\alpha\rho}(\mathbf{U}_j^k,\mathbf{U}_j^l),$$

$$\Delta K_{i,j}^{\alpha\rho u,k}=\tfrac{\omega_k h}{2}d_t(\alpha_{i,j}^k\rho_{i,j}^k u_{i,j}^k)+\sum_{l=0}^{p}2\omega_k D_{kl}\tfrac{u_{i,j}^k+u_{i,j}^l}{2}h_i^{\alpha\rho}(\mathbf{U}_j^k,\mathbf{U}_j^l),$$

with $h_i^{\alpha\rho}(\mathbf{u}^-,\mathbf{u}^+) = \frac{1}{2}\big(h_{\rho_i}(\mathbf{u}^-,\mathbf{u}^+) + h_{\rho_i}(\mathbf{u}^+,\mathbf{u}^-)\big) \overset{(4.17)}{=} \overline{\alpha}_i\overline{u}_i\hat{\rho}_i$.

Introducing $K_{i,j}^k = \frac{1}{2}\alpha_{i,j}^k\rho_{i,j}^k(u_{i,j}^k)^2$, we have

$$
\begin{aligned}
&\sum_{k=0}^{p} u_{i,j}^k \Delta K_{i,j}^{\alpha\rho u,k} - \frac{(u_{i,j}^k)^2}{2}\Delta K_{i,j}^{\alpha\rho,k} \\
&= \sum_{k=0}^{p} \frac{\omega_k h}{2} d_t(K_{i,j}^k) + \sum_{k,l=0}^{p} 2\omega_k D_{kl}\big(u_{i,j}^k \tfrac{u_{i,j}^k+u_{i,j}^l}{2} - \tfrac{(u_{i,j}^k)^2}{2}\big) h_i^{\alpha\rho}(\mathbf{U}_j^k,\mathbf{U}_j^l) \\
&= d_t\langle K_i(\mathbf{u}_h)\rangle_j + \sum_{k,l=0}^{p} 2\omega_k D_{kl}\tfrac{u_{i,j}^k u_{i,j}^l}{2} h_i^{\alpha\rho}(\mathbf{U}_j^k,\mathbf{U}_j^l) \\
&\overset{(3.39)}{=} d_t\langle K_i(\mathbf{u}_h)\rangle_j + \sum_{k,l=0}^{p} \omega_k D_{kl}\tfrac{u_{i,j}^k u_{i,j}^l}{2} h_i^{\alpha\rho}(\mathbf{U}_j^k,\mathbf{U}_j^l) \\
&- \sum_{k,l=0}^{p} \omega_l D_{lk}\tfrac{u_{i,j}^k u_{i,j}^l}{2} h_i^{\alpha\rho}(\mathbf{U}_j^k,\mathbf{U}_j^l) + u_{i,j}^p K_{i,j}^p - u_{i,j}^0 K_{i,j}^0 \\
&= d_t\langle K_i(\mathbf{u}_h)\rangle_j + u_{i,j}^p K_{i,j}^p - u_{i,j}^0 K_{i,j}^0,
\end{aligned}
$$

by symmetry of $h_i^{\alpha\rho}(\mathbf{u}^-,\mathbf{u}^+)$, which concludes the proof. □

4.4.2 Positivity of the numerical solution

High-order time integration is made through the use of strong stability-preserving explicit Runge-Kutta schemes [121] that are convex combinations of explicit first-order schemes in time, see section 3.7. Therefore, we focus on the fully discrete scheme by using a one-step first-order explicit time discretization.

We use the notation $t^{(n)} = n\Delta t$ with $\Delta t > 0$ the time step, and set $\lambda = \frac{\Delta t}{h}$, $\mathbf{u}_h^{(n)}(\cdot) = \mathbf{u}_h(\cdot,t^{(n)})$ and $\mathbf{U}_j^{k,n} = \mathbf{U}_j^k(t^{(n)})$. The fully discrete scheme reads

$$
\frac{\omega_k}{2}(\mathbf{U}_j^{k,n+1} - \mathbf{U}_j^{k,n}) + \lambda\mathbf{R}_j^k(\mathbf{u}_h^{(n)}) = 0, \tag{4.30}
$$

where $\mathbf{R}_j^k(\cdot)$ is defined in (3.55). Our analysis of the discrete scheme provides conditions on the numerical parameters that guarantee the positivity of the cell-averaged partial densities and a maximum principle on the cell-averaged void fraction. Unfortunately, we were not able to derive conditions for positivity of the partial internal energies, i.e., $\rho_i e_i > \mathrm{p}_{i,\infty}$, and we refer to [36] for a first-order scheme that guaranties such condition.

Theorem 4.4.2. *Assume that* $\rho_{i,j\in\mathbb{Z}}^{0\leqslant k\leqslant p,n} > 0$, $\alpha_{i,j\in\mathbb{Z}}^{0\leqslant k\leqslant p,n} > 0$ *for* $i = 1,2$ *and let* β_s, *in (4.17), be locally defined at element interfaces as*

$$
\beta_{s_{j+1/2}} := \max_{i=1,2}(|u_{i,j}^{p,n}|, |u_{i,j+1}^{0,n}|), \tag{4.31}
$$

then under the CFL condition

$$\lambda \max_{j\in\mathbb{Z}} \max_{i=1,2} \left(\max_{0\leqslant k\leqslant p} \frac{1}{\omega_k} \left(\langle \mathrm{u_I}_h^{(n)}, d_x\phi_j^k\rangle_j^p + \delta_{kp}\frac{\beta_{s_{j+1/2}} - \mathrm{u_I}_j^{p,n}}{2} + \delta_{k0}\frac{\beta_{s_{j-1/2}} + \mathrm{u_I}_j^{0,n}}{2} \right), \right.$$
$$\left. \frac{1}{\omega_0}\left(\frac{(\beta_{s_{j-1/2}} - \overline{u}_{i,j-1/2})\hat{\rho}_{i,j-1/2}}{2\rho_{i,j}^{0,n}} + \frac{\epsilon_{\nu_{j-1/2}}}{\alpha_{i,j}^{0,n}} \right), \frac{1}{\omega_p}\left(\frac{(\beta_{s_{j+1/2}} + \overline{u}_{i,j+1/2})\hat{\rho}_{i,j+1/2}}{2\rho_{i,j}^{p,n}} + \frac{\epsilon_{\nu_{j+1/2}}}{\alpha_{i,j}^{p,n}} \right) \right) < \frac{1}{2}, \tag{4.32}$$

where $\overline{u}_{i,j+1/2} = \frac{u_{i,j}^{p,n} + u_{i,j+1}^{0,n}}{2}$, $\hat{\rho}_{i,j+1/2} = \frac{\rho_{i,j+1}^{0,n} - \rho_{i,j}^{p,n}}{\ln \rho_{i,j+1}^{0,n} - \ln \rho_{i,j}^{p,n}}$, *we have for the cell averaged solution at time* $t^{(n+1)}$

$$\langle \alpha_{i,h}\rho_{i,h}\rangle_j^{(n+1)} > 0, \quad \langle \alpha_{i,h}\rangle_j^{(n+1)} > 0, \quad i = 1,2, \quad j \in \mathbb{Z}.$$

Furthermore,

$$\begin{aligned} \langle \alpha_{i,h}\rangle_j^{(n+1)} = \sum_{k=0}^{p} \left(\frac{\omega_k}{2} - \lambda \left(\langle \mathrm{u_I}_h^{(n)}, d_x\phi_j^k\rangle_j^p + \delta_{kp}\frac{\beta_{s_{j+1/2}} - \mathrm{u_I}_j^{p,n}}{2} + \delta_{k0}\frac{\beta_{s_{j-1/2}} + \mathrm{u_I}_j^{0,n}}{2} \right) \right) \alpha_{i,j}^{k,n} \\ + \lambda \frac{\beta_{s_{j+1/2}} - \mathrm{u_I}_j^{p,n}}{2} \alpha_{i,j+1}^{0,n} + \lambda \frac{\beta_{s_{j-1/2}} + \mathrm{u_I}_j^{0,n}}{2} \alpha_{i,j-1}^{p,n} \end{aligned} \tag{4.33}$$

is a convex combination of DOFs at time $t^{(n)}$.

Proof. Summing over $0 \leqslant k \leqslant p$ the first component of (4.30) for the void fraction we obtain

$$\begin{aligned} &\langle \alpha_{i,h}\rangle_j^{(n+1)} \\ &= \sum_{k=0}^{p} \frac{\omega_k}{2} \alpha_{i,j}^{k,n+1} \\ &= \sum_{k=0}^{p} \frac{\omega_k}{2} \alpha_{i,j}^{k,n} - \lambda \Bigg(\sum_{l=0}^{p} \omega_k D_{kl} \mathrm{u_I}_j^{k,n} \alpha_{i,j}^{l,n} + \delta_{kp}\frac{\mathrm{u_I}_j^{p,n} - \beta_{s_{j+1/2}}}{2}(\alpha_{i,j+1}^{0,n} - \alpha_{i,j}^{p,n}) \\ &+ \delta_{k0}\frac{\mathrm{u_I}_j^{0,n} + \beta_{s_{j-1/2}}}{2}(\alpha_{i,j}^{0,n} - \alpha_{i,j-1}^{p,n}) \Bigg) \\ &\overset{(3.35)}{=} \sum_{k=1}^{p-1} \left(\frac{\omega_k}{2} - \lambda \langle \mathrm{u_I}_h^{(n)}, d_x\phi_j^k\rangle_j^p \right) \alpha_{i,j}^{k,n} + \left(\frac{\omega_0}{2} - \lambda \left(\langle \mathrm{u_I}_h^{(n)}, d_x\phi_j^0\rangle_j^p + \frac{\beta_{s_{j-1/2}} + \mathrm{u_I}_j^{0,n}}{2} \right) \right) \alpha_{i,j}^{0,n} \\ &+ \left(\frac{\omega_p}{2} - \lambda \left(\langle \mathrm{u_I}_h^{(n)}, d_x\phi_j^p\rangle_j^p + \frac{\beta_{s_{j+1/2}} - \mathrm{u_I}_j^{p,n}}{2} \right) \right) \alpha_{i,j}^{p,n} + \lambda \frac{\beta_{s_{j-1/2}} + \mathrm{u_I}_j^{0,n}}{2} \alpha_{i,j-1}^{p,n} \\ &+ \lambda \frac{\beta_{s_{j+1/2}} - \mathrm{u_I}_j^{p,n}}{2} \alpha_{i,j+1}^{0,n}, \end{aligned}$$

which is a convex combination of DOFs at time n with (4.31) and the following restriction

on the time-step:

$$\lambda\left(\langle \mathrm{u_I}_h^{(n)}, d_x\phi_j^k\rangle_j^p + \delta_{kp}\frac{\beta_{s_{j+1/2}} - \mathrm{u_I}_j^{p,n}}{2} + \delta_{k0}\frac{\beta_{s_{j-1/2}} + \mathrm{u_I}_j^{0,n}}{2}\right) < \frac{\omega_k}{2}, \quad 0 \leqslant k \leqslant p,$$

since from (4.6) we have $\beta_{s_{j+1/2}} \geqslant \max(|\mathrm{u_I}_j^{p,n}|, |\mathrm{u_I}_{j+1}^{0,n}|)$.

For the cell-averaged partial densities, we use a similar technique to [104, 145] and sum over $0 \leqslant k \leqslant p$ the second component in (4.30) for the partial densities to get

$$\begin{aligned}
&\langle \alpha_{i,h}\rho_{i,h}\rangle_j^{(n+1)} \\
&= \sum_{k=0}^{p}\frac{\omega_k}{2}\alpha_{i,j}^{k,n}\rho_{i,j}^{k,n} \\
&- \lambda\left(\left(\overline{u}_{i,j+1/2}\frac{\alpha_{i,j}^{p,n} + \alpha_{i,j+1}^{0,n}}{2} - \frac{\beta_{s_{j+1/2}}}{2}\left(\alpha_{i,j+1}^{0,n} - \alpha_{i,j}^{p,n}\right)\right)\hat{\rho}_{i,j+1/2} - \epsilon_{\nu_{i,j+1/2}}\left(\rho_{i,j+1}^{0,n} - \rho_{i,j}^{p,n}\right)\right) \\
&+ \lambda\left(\left(\overline{u}_{i,j-1/2}\frac{\alpha_{i,j-1}^{p,n} + \alpha_{i,j}^{0,n}}{2} - \frac{\beta_{s_{j-1/2}}}{2}\left(\alpha_{i,j}^{0,n} - \alpha_{i,j-1}^{p,n}\right)\right)\hat{\rho}_{i,j-1/2} - \epsilon_{\nu_{i,j-1/2}}\left(\rho_{i,j}^{0,n} - \rho_{i,j-1}^{p,n}\right)\right) \\
&= \sum_{k=1}^{p-1}\frac{\omega_k}{2}\alpha_{i,j}^{k,n}\rho_{i,j}^{k,n} \\
&+ \left(\frac{\omega_p}{2} - \lambda\left(\frac{\beta_{s_{j+1/2}} + \overline{u}_{i,j+1/2}}{2}\frac{\hat{\rho}_{i,j+1/2}}{\rho_{i,j}^{p,n}} + \frac{\epsilon_{\nu_{i,j+1/2}}}{\alpha_{i,j}^{p,n}}\right)\right)\alpha_{i,j}^{p,n}\rho_{i,j}^{p,n} \\
&+ \lambda\left(\frac{\beta_{s_{j+1/2}} - \overline{u}_{i,j+1/2}}{2}\frac{\hat{\rho}_{i,j+1/2}}{\rho_{i,j+1}^{0,n}} + \frac{\epsilon_{\nu_{i,j+1/2}}}{\alpha_{i,j+1}^{0,n}}\right)\alpha_{i,j+1}^{0,n}\rho_{i,j+1}^{0,n} \\
&+ \left(\frac{\omega_0}{2} - \lambda\left(\frac{\beta_{s_{j-1/2}} - \overline{u}_{i,j-1/2}}{2}\frac{\hat{\rho}_{i,j-1/2}}{\rho_{i,j}^{0,n}} + \frac{\epsilon_{\nu_{i,j-1/2}}}{\alpha_{i,j}^{0,n}}\right)\right)\alpha_{i,j}^{0,n}\rho_{i,j}^{0,n} \\
&+ \lambda\left(\frac{\beta_{s_{j-1/2}} + \overline{u}_{i,j-1/2}}{2}\frac{\hat{\rho}_{i,j-1/2}}{\rho_{i,j-1}^{p,n}} + \frac{\epsilon_{\nu_{i,j-1/2}}}{\alpha_{i,j-1}^{p,n}}\right)\alpha_{i,j-1}^{p,n}\rho_{i,j-1}^{p,n},
\end{aligned}$$

and is positive if

$$\lambda\left(\frac{\beta_{s_{j-1/2}} - \overline{u}_{i,j-1/2}}{2}\frac{\hat{\rho}_{i,j-1/2}}{\rho_{i,j}^{0,n}} + \frac{\epsilon_{\nu_{i,j-1/2}}}{\alpha_{i,j}^{0,n}}\right) \leqslant \frac{\omega_0}{2}, \quad \lambda\left(\frac{\beta_{s_{j+1/2}} + \overline{u}_{i,j+1/2}}{2}\frac{\hat{\rho}_{i,j+1/2}}{\rho_{i,j}^{p,n}} + \frac{\epsilon_{\nu_{i,j+1/2}}}{\alpha_{i,j}^{p,n}}\right) \leqslant \frac{\omega_p}{2},$$

provided $\epsilon_{\nu_{i,j\pm1/2}} \geqslant 0$ and (4.31). □

4.4.3 A POSTERIORI LIMITERS

The properties of Theorem 4.4.2 hold only for the cell averaged value of the numerical solution at time $t^{(n+1)}$, which can be extended to nodal values by using a posteriori limiters [145, 146]. We here limit the void fraction with the bounds of its initial value over the whole domain, while we enforce positivity of the partial densities, similar to [108]. The limiter reads

$$\tilde{\mathbf{U}}_j^{k,n+1} = \theta_j\big(\mathbf{U}_j^{k,n+1} - \langle \mathbf{u}_h \rangle_j^{(n+1)}\big) + \langle \mathbf{u}_h \rangle_j^{(n+1)}, \quad 0 \leqslant k \leqslant p, \quad j \in \mathbb{Z}, \tag{4.34}$$

with $0 \leqslant \theta_j \leqslant 1$ defined by $\theta_j := \min(\theta_j^{\rho_i}, \theta_j^{\alpha_i} : i = 1, 2)$ where

$$\begin{aligned}
\theta_j^{\rho_i} &= \min\left(\frac{\langle \alpha_{i,h}\rho_{i,h}\rangle_j^{(n+1)} - \epsilon}{\langle \alpha_{i,h}\rho_{i,h}\rangle_j^{(n+1)} - (\alpha_i\rho_i)_j^{min}}, 1\right), \quad (\alpha_i\rho_i)_j^{min} = \min_{0\leqslant k\leqslant p}(\alpha_i\rho_i)_j^{k,n+1}, \\
\theta_j^{\alpha_i} &= \min\left(\frac{\langle \alpha_{i,h}\rangle_j^{(n+1)} - m_{i,j}^{\alpha}}{\langle \alpha_{i,h}\rangle_j^{(n+1)} - \alpha_{i,j}^{min}}, \frac{M_{i,j}^{\alpha} - \langle \alpha_{i,h}\rangle_j^{(n+1)}}{\alpha_{i,j}^{max} - \langle \alpha_{i,h}\rangle_j^{(n+1)}}, 1\right), \quad \alpha_{i,j}^{min} = \min_{0\leqslant k\leqslant p}\alpha_{i,j}^{k,n+1}, \quad \alpha_{i,j}^{max} = \max_{0\leqslant k\leqslant p}\alpha_{i,j}^{k,n+1},
\end{aligned} \tag{4.35}$$

$0 < \epsilon \ll 1$ is a parameter (we set $\epsilon = 10^{-8}$ in our numerical tests), and

$$m_{i,j}^{\alpha} = \min_{j\in\mathbb{Z}}\min_{0\leqslant k\leqslant p}\alpha_{i,j}^{k,0}, \quad M_{i,j}^{\alpha} = \max_{j\in\mathbb{Z}}\max_{0\leqslant k\leqslant p}\alpha_{i,j}^{k,0}.$$

The limiter (4.35) guarantees that $\tilde{\rho}_j^{0\leqslant k\leqslant p,n+1} > 0$ together with the following bounds on the void fractions $m_{i,j}^{\alpha} \leqslant \tilde{\alpha}_{i,j}^{0\leqslant k\leqslant p,n+1} \leqslant M_{i,j}^{\alpha}$.

4.5 NUMERICAL TESTS IN ONE SPACE DIMENSION

In this section we assess the high-order accuracy, robustness, and nonlinear stability of the numerical scheme for the Baer-Nunziato model by considering numerical tests for the initial value problem (4.1). We recall the numerical scheme in A.1. We use $\mathrm{u_I} = u_2$ and $\mathrm{p_I} = \mathrm{p}_1$ as the interfacial variables (4.6). Unless stated otherwise, all numerical tests are performed with fourth-order accuracy in space, $p = 3$, on a unit domain $\Omega = [-0.5, 0.5]$ discretized with a uniform mesh of 100 cells. The values of the numerical dissipation parameter ϵ_ν in (4.29) lie in the range $[0.1, 0.5]$. The time integration is performed by using the three-stage third-order strong stability-preserving Runge-Kutta scheme by Shu and Osher by [121], refer section 3.7. The limiter (4.34) is applied at the end of each stage. The time step is computed through (4.32). The numerical experiments of sections 4.5 and 4.6 have been obtained with the CFD code *Aghora* developed at ONERA [112].

4.5.1 ADVECTION OF DENSITY AND VOID FRACTION WAVES

We first test the high-order accuracy of the scheme (3.54). Let us consider a unit domain with periodic conditions and the following initial condition $\mathbf{u}_0(x)$

$$\alpha_{1,0}(x) = \frac{1}{2} + \frac{1}{4}\sin(4\pi x), \quad \rho_{i,0}(x) = 1 + \frac{1}{2}\sin(2\pi x), \quad u_{i,0}(x) = 1, \quad \mathrm{p}_{i,0}(x) = 1, \quad i = 1, 2,$$

which results in a density wave and a void fraction wave with different frequencies and amplitudes that are purely advected in a uniform flow. The EOS parameters in (4.5) are $\gamma_1 = 1.4, \mathrm{p}_{\infty_1} = 2.0$ and $\gamma_2 = 3.0, \mathrm{p}_{\infty_2} = 5.0$.

Table 4.1 indicates the values of the norms of the error on $\frac{1}{2}(\rho_1+\rho_2)$ obtained at final time $T_{max} = 5$ with different polynomial degrees and grid refinements, as well as the associated orders of convergence. We observe, as the mesh is refined, that the expected $p+1$ order of convergence is recovered with the present scheme.

p	h	$\|e_h\|_{L^1(\Omega_h)}$	$\mathcal{O}_1$	$\|e_h\|_{L^2(\Omega_h)}$	$\mathcal{O}_2$	$\|e_h\|_{L^\infty(\Omega_h)}$	$\mathcal{O}_\infty$
1	1/32	4.51E-02	-	5.08E-02	-	8.52E-02	-
	1/64	7.71E-03	2.55	9.75E-03	2.38	2.05E-02	2.05
	1/128	2.90E-03	1.41	3.38E-03	1.53	6.79E-03	1.59
	1/256	7.67E-04	1.92	8.88E-04	1.93	1.71E-03	1.99
2	1/32	2.08E-04	-	2.24E-04	-	5.41E-04	-
	1/64	1.93E-05	3.43	2.49E-05	3.29	5.88E-05	3.20
	1/128	2.59E-06	2.90	3.29E-06	2.92	8.16E-06	2.85
	1/256	3.43E-07	2.92	4.40E-07	2.90	1.25E-06	2.71
3	1/32	1.33E-06	-	1.74E-06	-	5.57E-06	-
	1/64	4.21E-08	4.98	6.19E-08	4.81	2.49E-07	4.48
	1/128	2.28E-09	4.21	3.55E-09	4.12	1.53E-08	4.03
	1/256	1.41E-40	4.02	2.22E-10	3.99	1.00E-09	3.93

Table 4.1: Test for high-order accuracy: different norms of the error on densities under p- and h-refinements and associated orders of convergence at final time $T_{max} = 5$.

4.5.2 Riemann Problems

We now consider a series of Riemann problems from [15, 36, 132] to assess the entropy conservation, robustness, and stability properties of the present scheme. The initial condition reads

$$\mathbf{u}_0(x) = \begin{cases} \mathbf{u}_L, & x < x_0, \\ \mathbf{u}_R, & x > x_0. \end{cases}$$

Table 4.2 contains the initial conditions for the different Riemann problems, while the physical parameters are given in Table 4.3.

Test for entropy conservation

The property of entropy conservation of the numerical fluxes (3.47) in the modified scheme (3.54) is validated based from the experimental setup introduced in [15]. Here we only focus on entropy conservative fluxes, so we set $\epsilon_\nu = 0$ in (4.29). The initial condition corresponds to the test case EC in Table 4.2 which generates discontinuities of moderate strength in each phase. We impose periodic boundary conditions and the global entropy should remain constant over the computational domain, while being modified only as a result

Test case		α_1	ρ_1	u_1	p_1	ρ_2	u_2	p_2
EC	$\mathbf{u}_L$	0.5	1.0	0.0	1.0	1.0	0.0	1.0
	$\mathbf{u}_R$	0.5	1.125	0.0	1.1	1.125	0.0	1.1
RP1	$\mathbf{u}_L$	0.1	1.0	1.0	1.0	1.5	1.0	1.0
	$\mathbf{u}_R$	0.9	2.0	1.0	1.0	1.0	1.0	1.0
RP2	$\mathbf{u}_L$	0.8	2.0	0.0	3.0	1900.0	0.0	10.0
	$\mathbf{u}_R$	0.1	1.0	0.0	1.0	1950.0	0.0	1000.0
RP3	$\mathbf{u}_L$	0.2	0.99988	-1.99931	0.4	0.99988	-1.99931	0.4
	$\mathbf{u}_R$	0.5	0.99988	1.99931	0.4	0.99988	1.99931	0.4
RP4	$\mathbf{u}_L$	0.3	1.0	-19.59741	1000.0	1.0	-19.59716	1000.0
	$\mathbf{u}_R$	0.8	1.0	-19.59741	0.01	1.0	-19.59741	0.01
RP5	$\mathbf{u}_L$	0.999	1.6	1.79057	5.0	2.0	1.0	10.0
	$\mathbf{u}_R$	0.001	2.0	1.0	10.0	2.67183	1.78888	15.0

Table 4.2: Initial conditions for the Riemann problems.

	EC	RP1	RP2	RP3	RP4	RP5
x_0	0.0	0.0	0.0	0.0	0.3	0.0
T_{max}	0.15	0.25	0.15	0.15	0.007	0.05
γ_1	1.4	3.0	1.35	1.4	1.4	3.0
γ_2	1.4	1.4	3.0	1.4	3.0	1.4
p_{∞_1}	0.1	0.1	0.0	0.0	0.0	0.0
p_{∞_2}	0.0	0.0	3400.0	0.0	100.0	0.0

Table 4.3: Location of discontinuity on Ω_h, final time, EOS parameters from (4.5).

of the time integration. We thus introduce the entropy budget

$$\mathcal{E}_{\Omega_h}(t) := h\Big|\sum_{\kappa_j\in\Omega_h} \langle\eta(\mathbf{u}_h)\rangle_j - \langle\eta(\mathbf{u}_0)\rangle_j\Big|, \tag{4.36}$$

which evaluates the variations in the computation of the cell-averaged entropy over the domain Ω_h. The results in Table 4.4 show that the error (4.36) decreases to machine accuracy when refining the time step, with the order of convergence corresponding to the theoretical approximation order of the time integration scheme. This validates the entropy conservation of the numerical fluxes (3.47).

time step	$\mathcal{E}_{\Omega_h}(t)$	$\mathcal{O}$
Δt	6.85E-06	–
$\Delta t/2$	2.08E-06	2.94
$\Delta t/4$	2.65E-07	2.97
$\Delta t/8$	3.31E-08	2.99
$\Delta t/16$	4.14E-09	3.00
$\Delta t/32$	5.14E-10	3.00

Table 4.4: Global entropy budget and the corresponding order of convergence $\mathcal{O}$ when refining the time step at final time $T_{max} = 0.15$.

Riemann problems

The results of the Riemann problems in Table 4.2 are shown in Figures 4-1 to 4-5, where we compare the numerical results with the exact solutions from [36, 132].

Here the test RP1 consists in the advection of a material interface in a uniform flow and the results in Figure 4-1 show that the velocity and pressure of both phases remain uniform in time which may be related to the so-called criterion of Abgrall [1]. The observed smearing of the contact is a consequence of the limiter (4.34) which is a common remark for all Riemann problems that we will consider.

The results for tests RP2 and RP3 in Figures 4-2 and 4-3 contain the development of shocks, rarefaction and contacts in both phases. The scheme captures the correct solutions, but the intermediate states contain small oscillations at the shock and rarefaction waves in phase 1 of RP2. It is however observed that as the mesh is refined all the intermediate states are accurately captured and the DG solution converges to the exact weak entropy solution. The scheme also proves to maintain the positivity of the partial densities in the near vacuum region of RP3, see Figure 4-3.

The capabilities of the scheme to resolve strong shocks are demonstrated in Figure 4-4 for the RP4 test case. Here the left-traveling rarefaction waves and the material discontinuity are well captured, whereas small oscillations are observed around the right-traveling shock in both phases. A possible reason could be that, as the dissipation is introduced in the numerical scheme through the interfaces, the internal DOFs may suffer from a lack of stabilization mechanism.

Finally, the test case RP5 probes the numerical scheme close to resonance (4.15) mimicking pure phases separated by a material interface. Numerical experiments are given for two different grids. Note that we do not consider pure phases in this work and restrict ourselves to conditions close to resonance (see [36] about the numerical difficulties associated to resonance effects and the derivation of a robust scheme handling such phenomena). The design of the present scheme is based on entropy variables (4.20) requiring the map $\mathbf{u} \mapsto \mathbf{v}(\mathbf{u})$ to be one-to-one and thus excluding pure phases. We indicate in Figure 4-5 the regions where the corresponding phases exist. The results show a correct approximation of the intermediate states where either phase exists, while spurious oscillations occur but in regions where the corresponding phase is absent. As the mesh is refined, we observe a damping of the oscillations where the phase exist, but oscillations in the regions of vanishing phase persist.

4.6 Numerical tests in multiple space dimensions

The Baer-Nunziato model in multiple space dimensions reads

$$\partial_t \mathbf{u} + \nabla \cdot \mathbf{f}(\mathbf{u}) + \mathbf{c}(\mathbf{u}) \nabla \mathbf{u} = 0, \quad \mathbf{x} \in \mathbb{R}^d, \, t \geqslant 0, \tag{4.37}$$

where

$$\mathbf{u} := \begin{pmatrix} \alpha_i \\ \alpha_i\rho_i \\ \alpha_i\rho_i\mathbf{v}_i \\ \alpha_i\rho_i E_i \end{pmatrix}, \quad \mathbf{f}(\mathbf{u}) := \begin{pmatrix} 0 \\ \alpha_i\rho_i\mathbf{v}_i^\top \\ \alpha_i(\rho_i\mathbf{v}_i\mathbf{v}_i^\top + \mathrm{p}_i\mathbf{I}) \\ \alpha_i(\rho_i E_i + \mathrm{p}_i)\mathbf{v}_i^\top \end{pmatrix}, \quad \mathbf{c}(\mathbf{u})\nabla\mathbf{u} := \begin{pmatrix} \mathbf{v}_\mathrm{I}{}^\top \\ 0 \\ -\mathrm{p}_\mathrm{I}\mathbf{I} \\ -\mathrm{p}_\mathrm{I}\mathbf{v}_\mathrm{I}{}^\top \end{pmatrix}\nabla\alpha_i, \quad i = 1, 2,$$

with $\mathbf{v}_i = (u_i, v_i, w_i)^\top$ the velocity vector of the ith phase, $\mathrm{p}_i = \mathrm{p}_i(\rho_i, e_i)$ given by (4.5) and $e_i = E_i - \frac{1}{2}\mathbf{v}_i \cdot \mathbf{v}_i$ the specific internal energy.

The DGSEM scheme (3.54) can be extended to (4.37). The derivation of the scheme for Cartesian meshes is introduced in 3.6, while the numerical fluxes for the above model are presented in A.2. Unless stated otherwise, the time step is computed with the CFL condition in A.3 and was seen to maintain positivity of the solution though it does not guaranty positivity of the partial internal energies.

Numerical experiments in two-space dimensions are given in the remainder of this section including tests on high-order accuracy, entropy conservation, kinetic energy preservation, together with the simulation of a shock-bubble interaction problem.

4.6.1 Advection of density and void fraction waves

We here reproduce the test on accuracy from section 4.5.1 and consider the pure advection of oblique void fraction and density waves in a uniform flow in a unit square with periodic boundary conditions. The initial condition reads

$$\begin{aligned} &\alpha_{1,0}(\mathbf{x}) = \frac{1}{2} + \frac{1}{4}\sin\big(4\pi(x+y)\big),\ \rho_{i,0}(\mathbf{x}) = 1 + \frac{1}{2}\sin\big(2\pi(x+y)\big), \\ &u_{i,0}(\mathbf{x}) = 1,\ v_{i,0}(\mathbf{x}) = 1,\ \mathrm{p}_{i,0}(\mathbf{x}) = 1,\ i = 1, 2. \end{aligned} \tag{4.38}$$

The EOS parameters in (4.5) are $\gamma_1 = 1.4, \mathrm{p}_{\infty_1} = 2.0$ and $\gamma_2 = 3.0, \mathrm{p}_{\infty_2} = 5.0$. The obtained results are presented in Table 4.5. It is again observed that the expected $p+1$ order of convergence is achieved.

p	h	$\|e_h\|_{L^1(\Omega_h)}$	$\mathcal{O}_1$	$\|e_h\|_{L^2(\Omega_h)}$	$\mathcal{O}_2$	$\|e_h\|_{L^\infty(\Omega_h)}$	$\mathcal{O}_\infty$
1	1/32	1.00E-01	1.83	1.11E-01	1.82	1.83E-01	1.65
	1/64	1.67E-02	2.58	2.03E-02	2.45	3.98E-02	2.20
	1/128	4.86E-03	1.78	5.83E-03	1.80	1.16E-02	1.78
2	1/32	4.84E-04	3.67	5.90E-04	3.65	1.22E-03	3.59
	1/64	3.81E-05	3.66	4.92E-05	3.58	1.00E-04	3.61
	1/128	2.77E-06	3.78	3.77E-06	3.71	1.06E-05	3.55
3	1/32	2.77E-06	6.37	3.53E-06	6.28	1.32E-05	5.75
	1/64	8.04E-08	5.11	1.03E-07	5.10	5.38E-07	4.61
	1/128	4.18E-09	4.26	5.27E-09	4.29	2.96E-08	4.18

Table 4.5: Test for high-order accuracy with initial condition (4.38): different norms of the errors on $\frac{1}{2}(\rho_1 + \rho_2)$ under grid and polynomial degree refinements and associated orders of convergence at final time $T_{max} = 5$.

4.6.2 Entropy conservation

We also check entropy conservation by using the same procedure as in section 4.5.2 on the unit square with periodic boundary conditions. The initial condition is EC in Table 4.2 with zero transverse velocity, $v_i = 0$ for $i = 1, 2$, and we keep the same EOS parameters. The global entropy budget, similar to (4.36), is displayed in Table 4.6 when refining the time step. Again the conservation of entropy by the space discretization is observed.

time step	$\mathcal{E}_\Omega(t)$	$\mathcal{O}$
Δt	7.49E-04	-
$\Delta t/2$	1.07E-04	2.81
$\Delta t/4$	1.37E-05	2.97
$\Delta t/8$	1.72E-06	2.99
$\Delta t/16$	2.15E-07	3.00
$\Delta t/32$	2.67E-08	3.01
$\Delta t/64$	3.19E-09	3.06

Table 4.6: Global entropy budget (4.36) in two space dimensions and the corresponding order of convergence $\mathcal{O}$ at final time $T_{max} = 0.15$.

4.6.3 Kinetic energy preservation

The property of kinetic energy preservation in Theorem 4.4.1 is here investigated. We propagate material and contact discontinuities in a unit square with periodic boundary conditions, following the initial condition $\mathbf{u}_0(x, y) = \mathbf{u}_R$ if $0 \leq x, y \leq \frac{1}{2}$ or $\frac{1}{2} \leq x, y \leq 1$, else $\mathbf{u}_0(x, y) = \mathbf{u}_L$ (see Table 4.7). The EOS parameters for the two-phases are $\gamma_1 = \gamma_2 = 1.4$, $\mathrm{p}_{\infty,1} = 0.1$, and $\mathrm{p}_{\infty,2} = 0$. For this test, the pressure fields are uniform and equal so that the kinetic energy is conserved.

Figure 4-6 presents the temporal variations of the global kinetic energy of the domain $KE(t) = \int_{\Omega_h} \sum_{i=1}^{2} \frac{1}{2}\alpha_i \rho_i u_i^2 dx$ from its initial value and we observe that $KE(t)$ does not vary in time. We conclude that $KE(t)$ is not changed by the advective terms, but only by the pressure work, which validates Theorem 4.4.1.

Test case		α_1	ρ_1	u_1	v_1	p_1	ρ_2	u_2	v_2	p_2
KEP	$\mathbf{u}_L$	0.4	1.0	1.0	1.0	1.0	1.5	1.0	1.0	1.0
	$\mathbf{u}_R$	0.6	2.0	1.0	1.0	1.0	1.0	1.0	1.0	1.0

Table 4.7: Initial conditions for the kinetic energy preservation test case.

4.6.4 Shock-bubble interaction

This numerical test involves the interaction between a shock wave and a material discontinuity. The test was introduced by Haas and Sturtevant [65] to experimentally study the interaction of a shock wave with a single discrete gas inhomogeneity. Later it was adopted as a numerical benchmark to validate the robustness and accuracy of various numerical schemes for compressible two-phase flows, see [60, 74, 80, 83, 107, 110, 116, 129] and references therein.

The computational domain $\Omega_h = [0, 6.5] \times [0, 1.78]$ is discretized using a Cartesian mesh with 1300×356 elements. The initial condition involves a bubble of unit diameter containing a mixture of 95% of helium by volume ($\alpha_1 = 0.95$) and 5% of air, to exclude resonance effects (4.15), in a domain filled with 5% of air. The center of the bubble is located at $\mathbf{x} = (3.5, 0.89)$. A left moving shock is initially placed at the rightmost edge of the bubble, $x_0 = 4$, and then moves to the left and interacts with the bubble. The initial condition is provided in Table 4.8.

	α_1	ρ_i	u_i	v_i	p_i
Pre-shock air ($i = 2$)	0.05	1.3764	-0.3336	0.0	1.1213
Helium bubble ($i = 1$)	0.95	0.1819	0.0	0.0	0.7143
Post-shock air ($i = 2$)	0.05	1.0	0.0	0.0	0.7143

Table 4.8: Physical parameters for the initial condition of the shock-bubble interaction problem.

The EOS parameters for helium and air are $\gamma_1 = 1.648$ and $\mathrm{C_{v1}} = 6.06$, and $\gamma_2 = 1.4$ and $\mathrm{C_{v2}} = 1.786$, respectively. The physical model does not involve viscous effects so to avoid oscillations of the interface we smoothen the initial condition around the material interface following [14, 73, 83]. The numerical test is performed using periodic boundary conditions at the top and bottom boundaries, and non-reflective conditions on the left and right boundaries.

Figure 4-7 illustrates the deformation of the He bubble as the shock passes through it. The plotted fields are those of the void fraction for phase 1, the total pressure and numerical Schlieren. It is observed that the material interface and the shock are accurately captured without excessive smearing of the contact. Note however that, for the Baer-Nunziato model, the pressure field shows the presence of a secondary shock inside the bubble (see e.g. the Schlieren at $t = 62\mu$s). This secondary shock is due to the presence of air inside the bubble. Furthermore, as the shock leaves the bubble, vortices are generated on the bubble interface as a result of the Kevin-Helmoltz instability.

Figure 4-8 shows the space-time diagram for three characteristic points on the interface of the bubble. We compare the results obtained with the DGSEM scheme to reference data from [83]. The deformation of the bubble shows complete agreement with the reference data and indicate that the smooth initial condition does not affect the global deformation of the bubble.

Finally, we compare results obtained under mesh refinement in Figure 4-9. We observe a sharpening of the material interface and the excitation of Kelvin-Helmoltz vortices as the mesh is refined. The positions of the three characteristic points in Figure 4-8 are clearly unaffected by the mesh refinement.

4.7 Summary

In this work, we derive a high-order entropy stable scheme for the Baer-Nunziato model [7, 115] for flows of two separated immiscible fluids in complete disequilibria with respect to the chemical, mechanical, thermal, and thermodynamic processes. Here we focus on the discretization of the convective part of the model and neglect the modelling source terms. The exchange of information at the interfaces of the fluids is governed through interface variables of pressure and velocity, for which we choose general closure laws [34, 56] that allow the material interface to be associated to a LD field and an entropy inequality in conservative form to be derived from the model. The model is closed with stiffened gas EOS relevant for both gas and liquid phases.

The space discretization is performed by using the semi-discrete entropy stable DGSEM framework proposed in [108], which involves modifying the integration over cell elements by replacing the physical fluxes with two point entropy conservative fluxes in fluctuation form [24, 103], while employing entropy stable fluctuation fluxes at the cell interfaces. This framework is here generalized to include both conservative and nonconservative terms to allow a conservative discretization of the former ones. The entropy conservative fluxes are derived by using the condition in [24], to which we add upwind type dissipation to obtain the entropy stable fluxes. The semi-discrete scheme is high-order accurate for smooth solutions, satisfies an entropy inequality, and is kinetic energy preserving.

We use a method of lines with an explicit time integration and propose conditions on the numerical parameters that guarantee the positivity of the cell-averaged partial densities and a maximum principle on the void fraction for the fully discrete scheme coupled with a first-order forward Euler discretization. High-order integration in time is performed using strong stability-preserving explicit Runge-Kutta schemes [121]. The positivity of the solution is then extended to nodal values using a posteriori limiters adapted from [104, 145, 146].

The numerical tests involve specific test cases that support the high-order accuracy, stability and robustness of the semi-discrete scheme in one and two space dimensions. Riemann problems are performed in one space dimension involving the development of strong shocks, contacts, near vacuum regions, and vanishing phases. The results obtained with a fourth-order scheme show that the present method captures the physically relevant entropy weak solution. The intermediate states are well resolved, as well as the shocks and contacts and the computation is shown to be robust in situations close to either vacuum, or resonance. Furthermore, the application to the simulation of a shock-bubble interaction problem in two space dimensions confirm the accurate approximation of the shock and material interfaces.

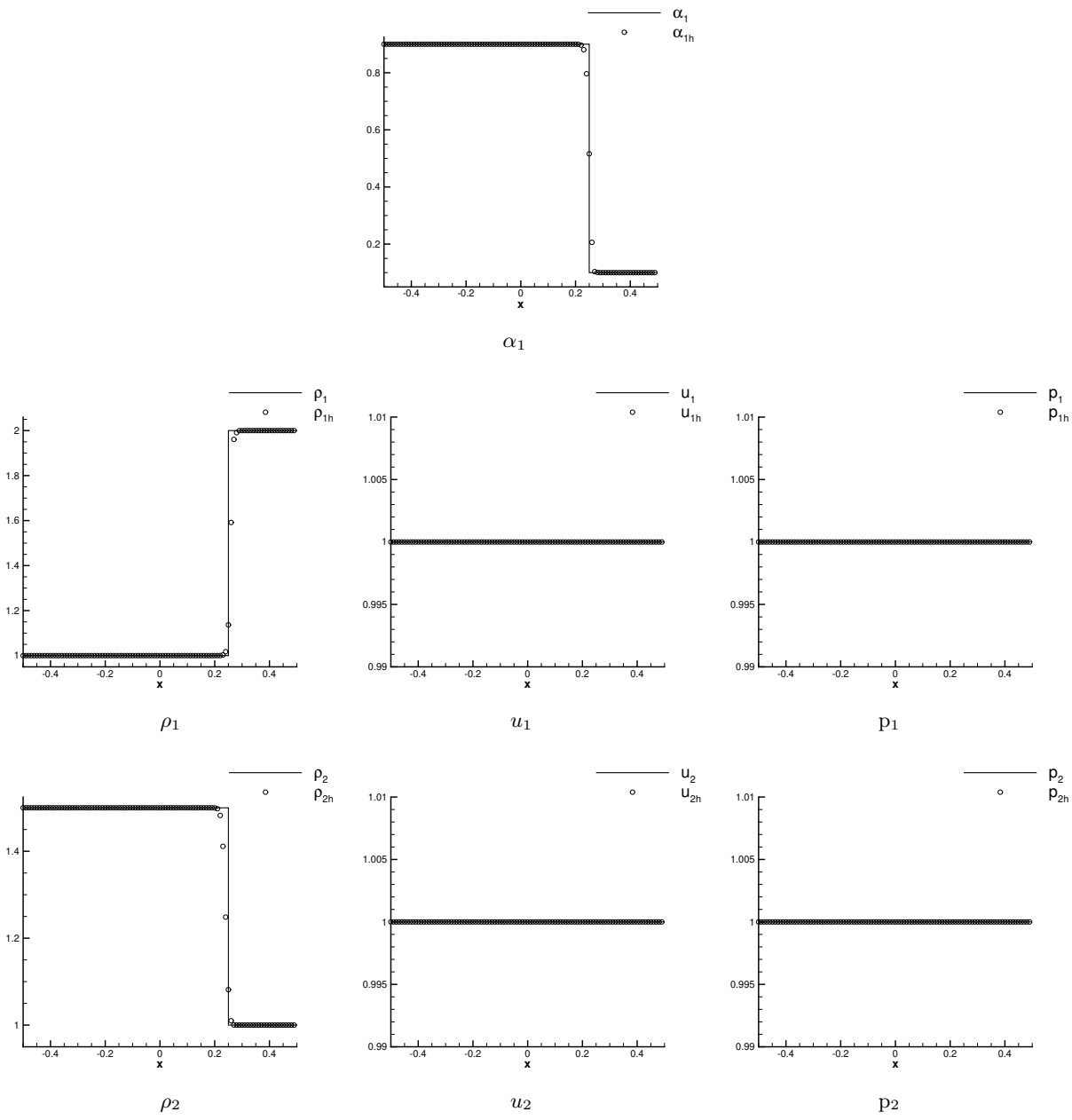

Figure 4-1: Comparison of the fourth-order accurate numerical solution to the exact solution for test case RP1 at final time $T_{max} = 0.25$.

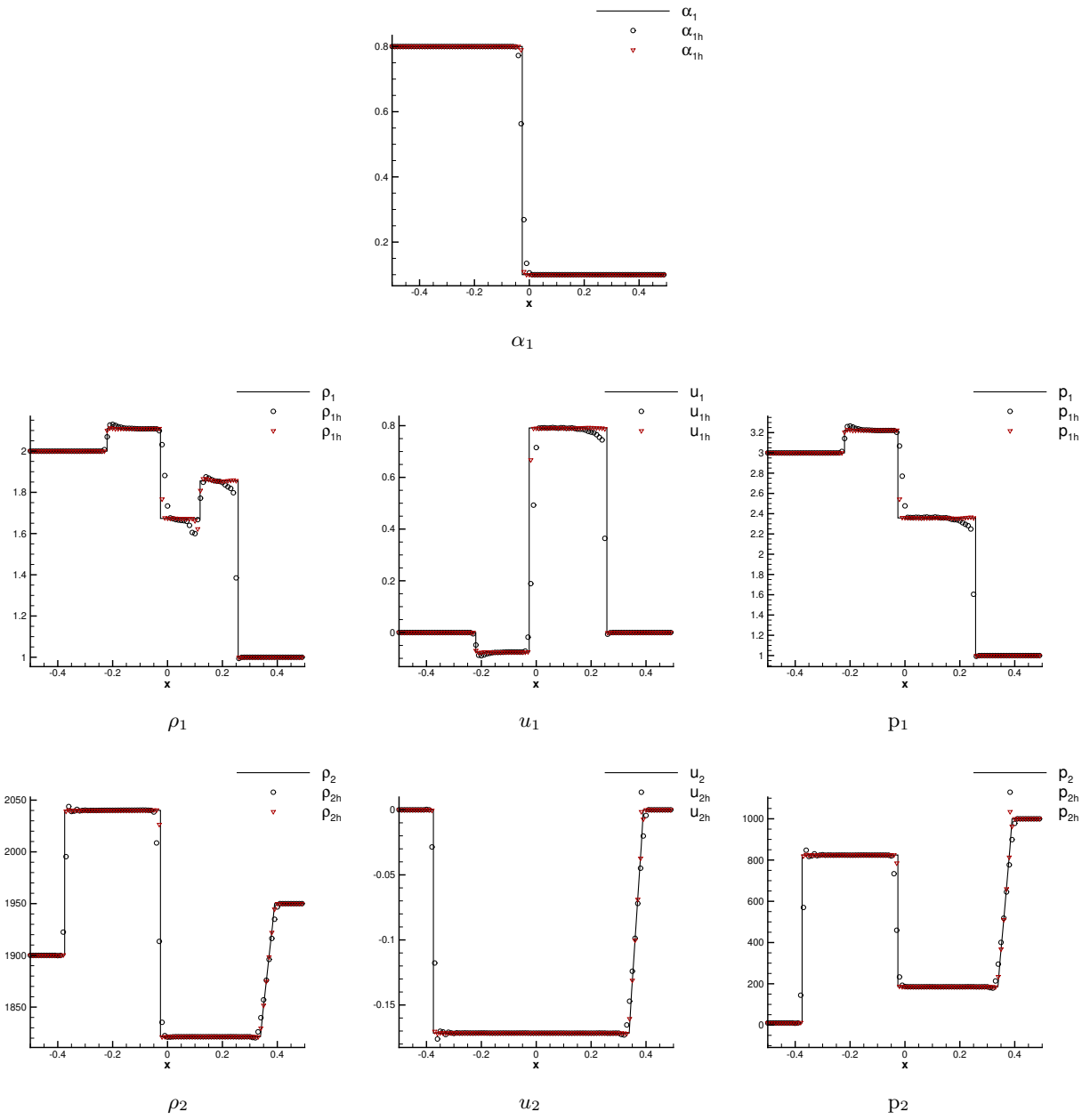

Figure 4-2: Test for convergence of solution through mesh refinement: RP2 at at final time T_{max} = 0.15. The black symbols represent solutions on a mesh with 100 elements, whereas the symbols in red represent solutions on a mesh with 400 elements.

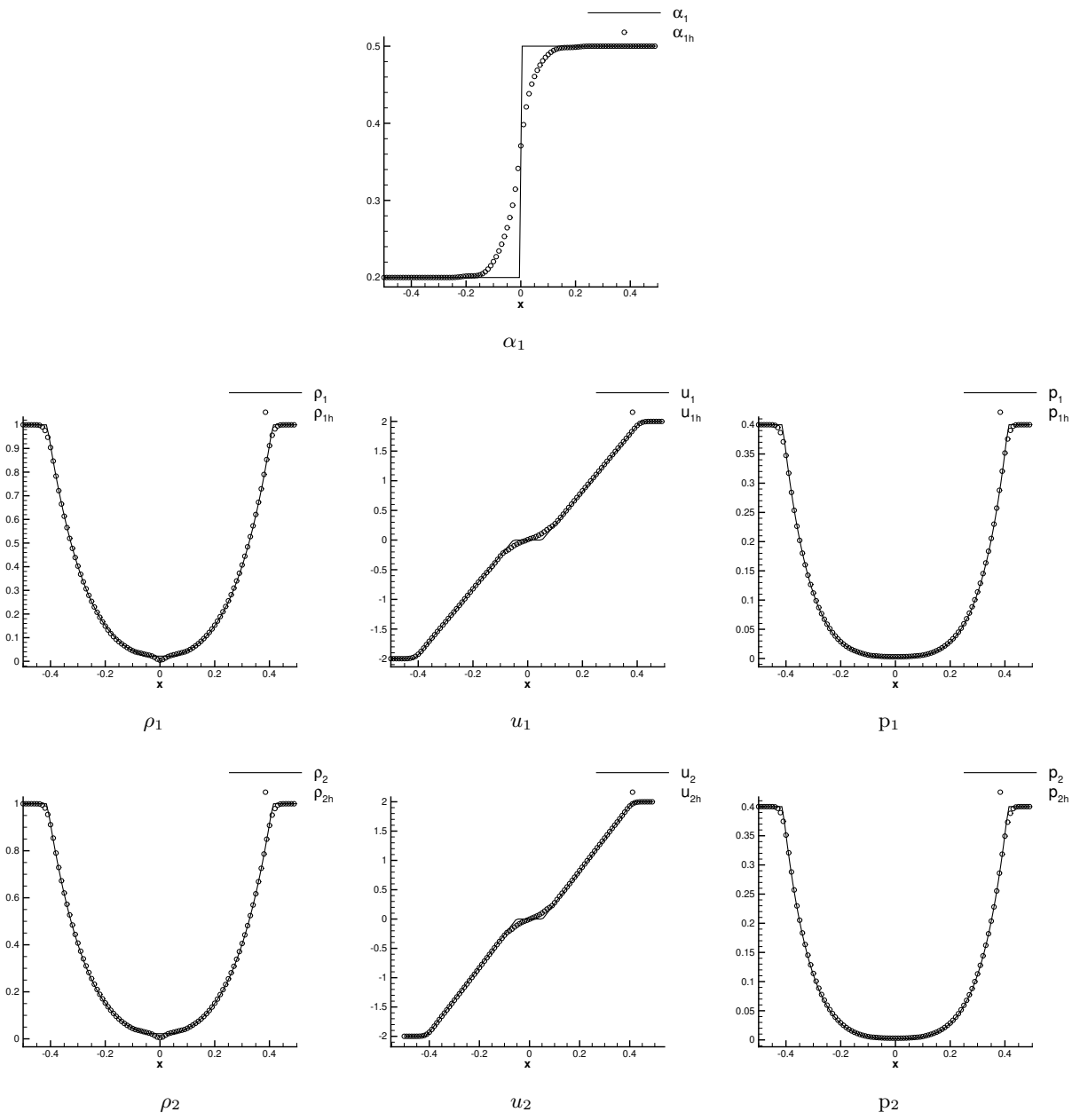

α_1 ρ_1 u_1 p1 ρ_2 u_2 p2

Figure 4-3: Comparison of the fourth-order accurate numerical solution to the exact solution for test case RP3 at final time $T_{max} = 0.15$.

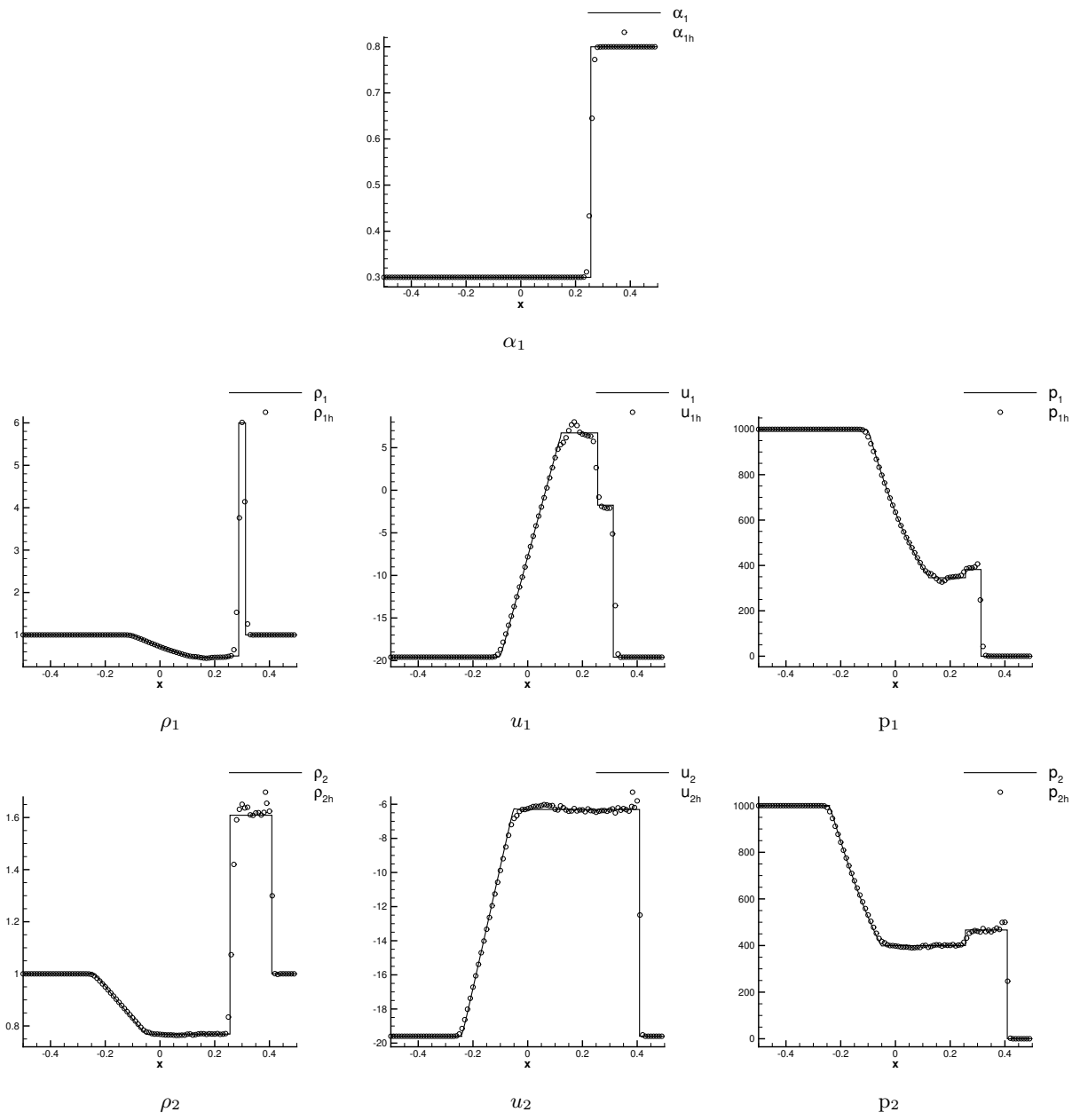

Figure 4-4: Comparison of the fourth-order accurate numerical solution to the exact solution for test case RP4 at final time $T_{max} = 0.007$.

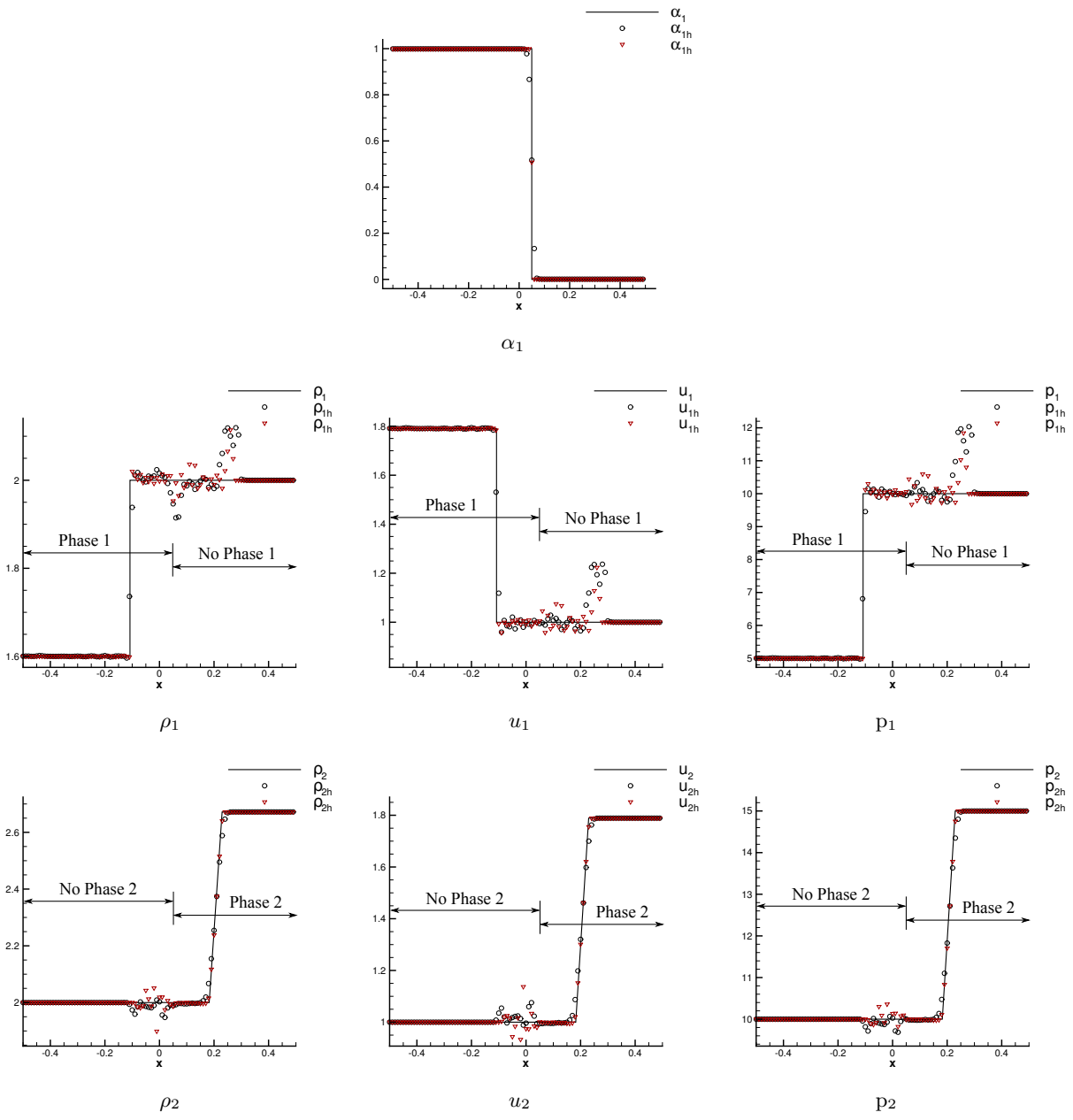

Figure 4-5: Comparison of the fourth-order accurate numerical solution of test case RP5 to the exact solution on meshes with 100 elements (black symbols) and 400 elements (red symbols) at final time $T_{max} = 0.05$.

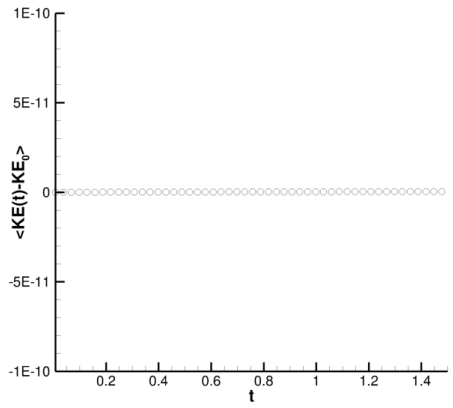

Figure 4-6: The demonstration of kinetic energy preservation for the test case KEP, where $< \mathrm{KE}(t) - \mathrm{KE}_0 >$ is the difference in the kinetic energies of the initial state and those calculated along the physical time until $T_{max} = 1.5$.

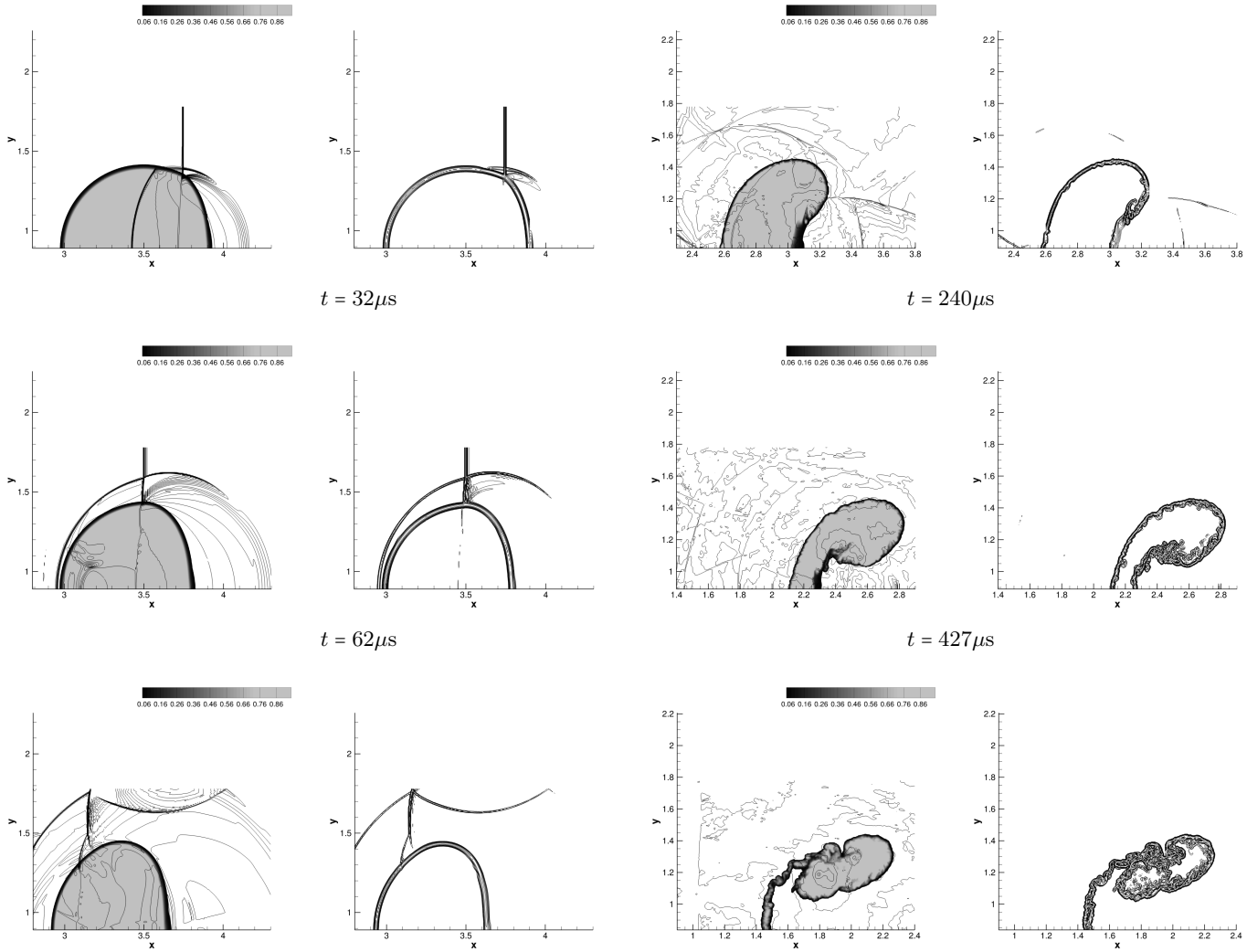

Figure 4-7: The snapshots of the deformation of the He bubble due to the left traveling shock at various physical times. For each snapshot, the left plot displays contours of the void fraction α_1 and of the total pressure $\mathrm{p} = \alpha_1 \mathrm{p}_1 + \alpha_2 \mathrm{p}_2$, while the right plot shows the Schlieren $\phi = \exp(|\nabla\rho|/|\nabla\rho|_{\max})$, with $\rho = \alpha_1\rho_1 + \alpha_2\rho_2$, obtained with a polynomial degree $p = 3$.

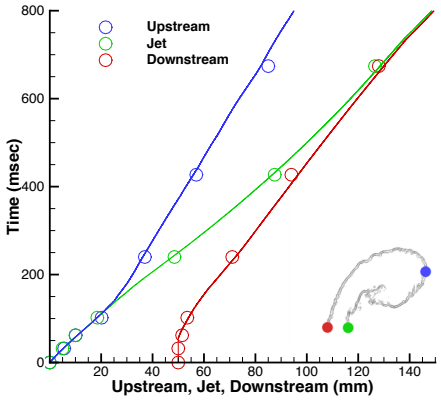

Figure 4-8: Space-time diagram for three characteristic points on the interface of the He bubble. The solid lines are the reference data from [83], while the symbols are the results obtained with the present DGSEM scheme for polynomial of degree $p = 3$ and on a 1300×356 mesh.

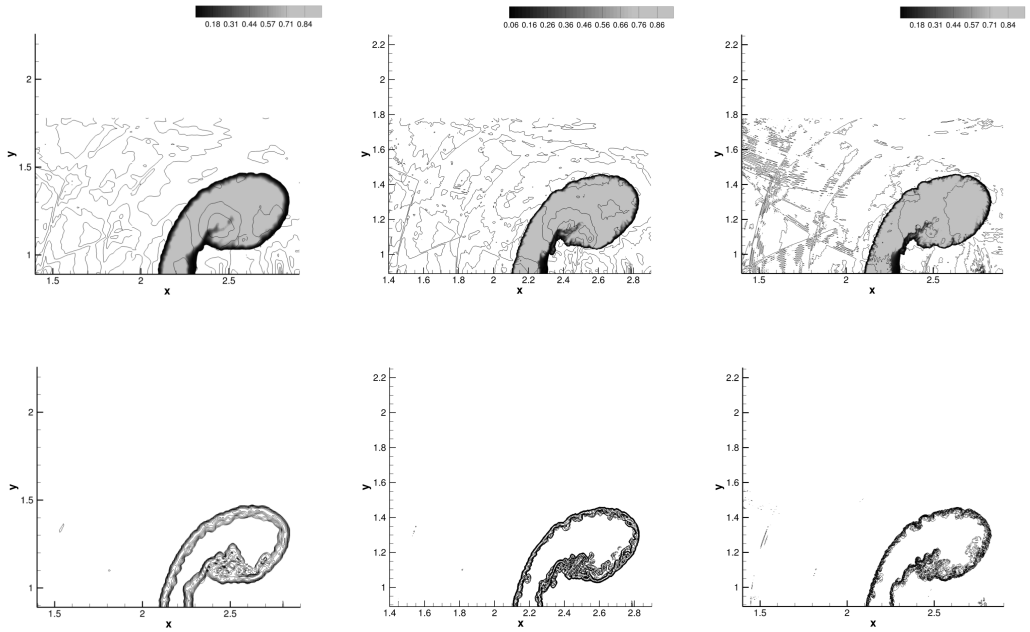

Mesh: 650×178 Mesh: 1300×356 Mesh: 2600×712

Figure 4-9: Comparison of the deformation of the He bubble at the physical time of $427\mu s$ for different mesh refinements. The top figures display contours of the void fraction α_1 and of the total pressure $\mathrm{p} = \alpha_1 \mathrm{p}_1 + \alpha_2 \mathrm{p}_2$, while the bottom figures show Schlieren $\phi = \exp(|\nabla\rho|/|\nabla\rho|_{\max})$, with $\rho = \alpha_1\rho_1 + \alpha_2\rho_2$, obtained with a polynomial degree $p = 3$.

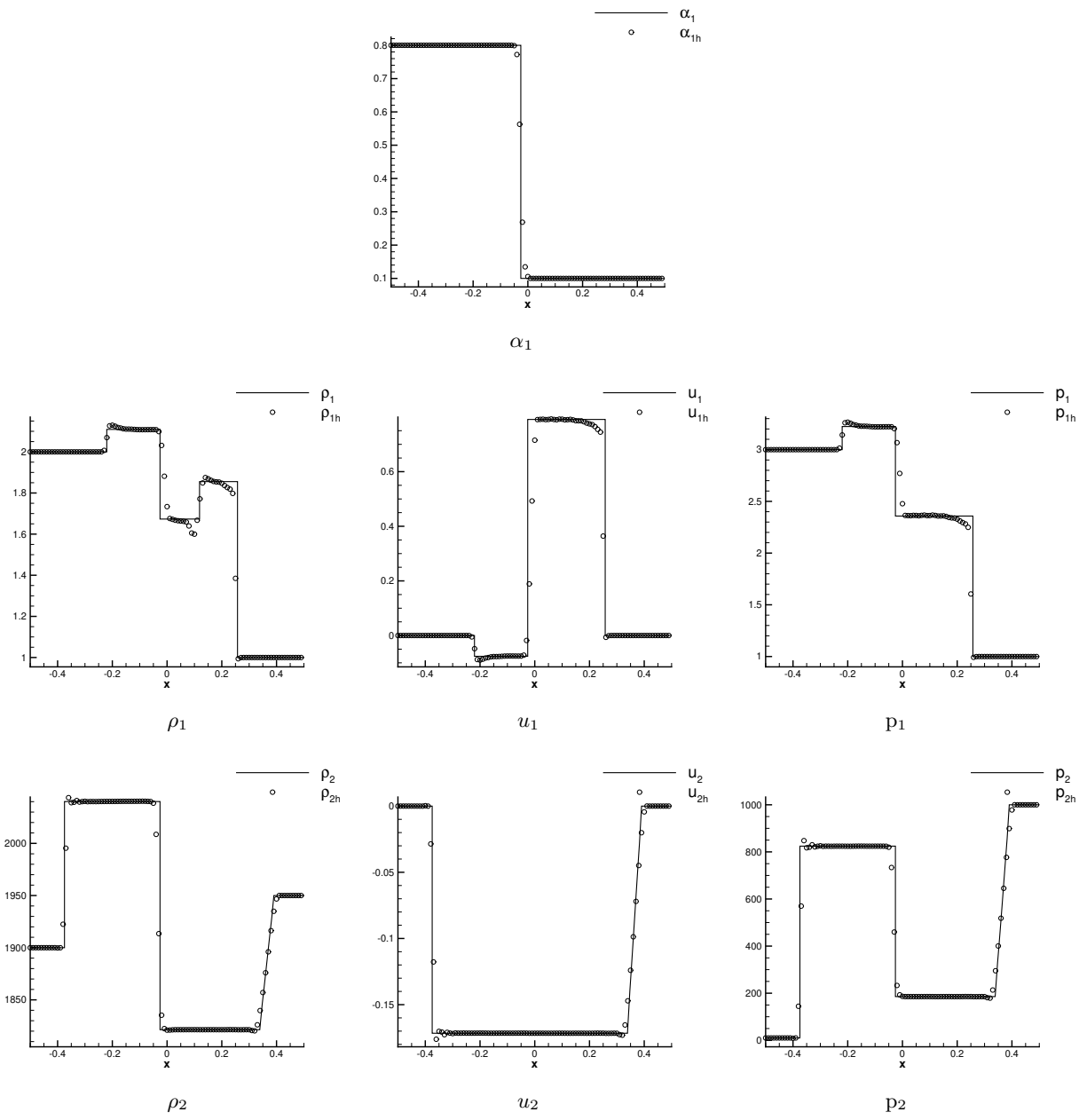

Figure 4-10: Comparison of the fourth-order accurate numerical solution to the exact solution for test case RP2 at final time $T_{max} = 0.15$.

Chapter 5

A contact preserving and entropy stable DGSEM for multicomponent flows

Résumé du chapitre

Dans ce chapitre, nous nous intéressons à la discrétisation du modèle d'écoulement multicomposant proposé dans [122] où l'état thermodynamique de chaque espèce est modélisé par une équation d'état (EOS) de type gaz raidi. Ce modèle est une extension du travail original d'Abgrall [1], qui était limité à l'équation d'état polytropique. Nous appellerons ici ce modèle le modèle gamma. Ce modèle possède deux qualités essentielles qui rendent son étude intéressante. Premièrement, le nombre d'équations du modèle ne dépend pas du nombre d'espèces, cette qualité du modèle est en contraste avec le modèle Baer-Nunziato qui a été discuté dans Chapter 2 et Chapter 4. Et deuxièmement, la forme non-conservative du modèle permet de préserver les interfaces matérielles et les discontinuités de contact. Nous discrétisons le modèle gamma [122] en utilisant le cadre DGSEM introduit dans Chapter 3, dans le but de proposer un schéma DG précis d'ordre élevé qui préserve les discontinuités de contact, tout en satisfaisant également à une inégalité d'entropie semi-discrète au travers des chocs au sens de Theorem 3.5.1.

Nous appliquons le schéma DGSEM semi-discret (3.54) au modèle gamma et considérons la conception des flux numériques pour l'intégrale de volume et pour les flux d'interface séparément. La condition d'inégalité d'entropie de Theorem 3.5.1 impose que des flux conservant l'entropie [24] doivent être appliqués dans l'intégrale de volume. Cependant, il apparaît dans ce travail que les flux conservant l'entropie pour le modèle gamma ne préservent pas la pression et la vitesse uniformes à travers les discontinuités de contact. Nous introduisons donc un deuxième jeu de flux numériques préservant les contacts pour l'intégrale de volume, qui satisfont le critère d'Abgrall [1]. Cependant, les flux numériques préservant les contacts ne satisfont pas la condition de conservation de l'entropie proposée dans [24]. Dans ce travail, nous appliquons des flux conservant l'entropie dans l'intégrale de volume uniquement lorsqu'un choc est détecté, tandis que des flux préservant le contact sont appliqués partout ailleurs. Le schéma numérique alterne entre les flux par le biais d'un senseur de choc basé sur la distribution de pression dans la cellule [78, 126].

Nous dérivons ensuite des flux de type HLL et HLLC [134, 136] pour le modèle gamma qui sont appliqués aux interfaces des cellules. Nous montrons que le solveur HLLC satisfait la

condition de stabilité de l'entropie [12] sous une condition CFL donnée et préserve les profils uniformes à travers les discontinuités de contact. De plus, nous proposons des estimations des vitesses d'onde pour le solveur HLLC qui maintiennent la positivité de la solution [9, 16]. La positivité est renforcée aux valeurs nodales par l'application de limiteurs a posteriori, similaires à [37, 139, 145, 146]. L'intégration temporelle d'ordre élevé est effectuée à l'aide de schémas Runge Kutta préservant la stabilité, voir section 3.7. L'extension du schéma DGSEM à plusieurs dimensions d'espace sur maillages cartésiens est effectuée par le biais de tensorisations des fonctions de base et des règles de quadrature comme en section 3.6. Les capacités du schéma à préserver les discontinuités de contact et à maintenir la stabilité non linéaire à travers les chocs avec une précision d'ordre élevé sont démontrées par plusieurs expériences numériques en une et deux directions de l'espace.

5.1 SHORT DESCRIPTION AND OUTLINE OF THE CHAPTER

In this work, we discretize the multicomponent flow model, called the gamma model, proposed in [122] where each species is considered as a stiffened gas. This model is an extension of the original work by Abgrall [1], which was limited to the polytropic equation of state (EOS). The interest is discretizing such multicomponent models are twofolds. First, the number of equations in the model is independent of the number of species, this quality of the model is in contrast to the Baer-Nunziato model which was discussed in Chapter 2 and Chapter 4. One consequence, however, is the lack of information on each species. And second, the nonconservative form of the model allows to preserve the material interface and contact discontinuities. We discretize the gamma-model [122] using the DGSEM framework introduced in Chapter 3, with the aim to propose a high-order accurate DG scheme that preserves contact discontinuities, while also satisfying an entropy inequality across shocks in the sense of Theorem 3.5.1.

To this purpose, we apply the semi-discrete DG scheme (3.54) to the gamma-model and consider the design of the numerical fluxes for the volume integral and for the interface fluxes separately. The entropy inequality condition from Theorem 3.5.1 dictates that entropy conservative fluxes [24] must be applied in the volume integral. However, the entropy conservative fluxes derived in this work for the gamma-model do not preserve uniform pressure and velocity across contact discontinuities, hence contact preserving numerical fluxes for the volume integral, that satisfy the Abgrall criterion [1], are designed separately. However, contract preserving numerical fluxes fail to satisfy the entropy conservation condition proposed in [24]. We thus apply entropy conservative fluxes within the volume integral only when a shock is detected, while contact preserving fluxes are applied everywhere else. The numerical scheme alternates between the fluxes through a pressure-based troubled-cell indicator function [78, 126].

We then derive HLL and HLLC like fluxes [134, 136] for the gamma model that are applied at the cell interfaces. We show that the HLLC solver satisfies the entropy stability condition [12] under a given CFL condition and preserves the uniform profiles across contact discontinuities. Furthermore, we propose wave speed estimates for the HLLC solver that maintain positivity of the solution [9, 16]. The positivity is further enforced at the nodal values by applying a posteriori limiters, similar to [37, 139, 145, 146]. High-order time integration is performed using strong-stability preserving Runge Kutta schemes, see section 3.7. The DGSEM is easily extended to several space dimensions with Cartesian meshes by using

tensor products of basis functions and quadrature rules as detailed in section 3.6.

This chapter is organised as follow. The gamma-model and the definition of the mixture quantities are introduced in section 5.2. In section 5.3 we derive contact preserving fluxes and entropy conservative fluxes that are applied to the volume integral, together with the troubled-cell indicator function. The HLL and HLLC fluxes for the cell interface are derived in section 5.4. In section 5.4.3 we provide details on the properties of the HLLC solver. The a posteriori limiter has been described in section 5.6 and we summarize the properties of the DGSEM scheme in section 5.5 . Numerical experiments in one and two spatial dimensions are given in section 5.7. Finally, the results of this chapter are summarised in section 5.8.

5.2 The gamma model

In this work, we are interested in the multicomponent model proposed in [122], where each species is considered as a stiffened gas. The model comprises of the compressible Euler equations for the mixture which are supplemented by the transport equations for the equation of state (EOS) state parameters.

For the sake of simplicity, let us consider the Cauchy problem for the SG-gamma model in one-space dimension

$$\partial_t \mathbf{u} + \partial_x \mathbf{f}(\mathbf{u}) + \mathbf{c}(\mathbf{u})\partial_x \mathbf{u} = 0, \qquad x \in \mathbb{R}, t > 0, \tag{5.1a}$$

$$\mathbf{u}(x,0) = \mathbf{u}_0(x), \quad x \in \mathbb{R}, \tag{5.1b}$$

where

$$\mathbf{u} = \begin{pmatrix} \rho \\ \rho u \\ \rho E \\ \Gamma \\ \Pi \end{pmatrix}, \quad \mathbf{f}(\mathbf{u}) = \begin{pmatrix} \rho u \\ \rho u^2 + \mathrm{p} \\ (\rho E + \mathrm{p})u \\ 0 \\ 0 \end{pmatrix}, \quad \mathbf{c}(\mathbf{u})\partial_x \mathbf{u} = u \begin{pmatrix} 0 \\ 0 \\ 0 \\ \partial_x \Gamma \\ \partial_x \Pi \end{pmatrix}. \tag{5.2}$$

represent the vector of state variables, the physical fluxes and the nonconservative products, respectively.

In (5.2), the density, momentum and the total energy of the mixture are defined as

$$\rho = \sum_{i=1}^{n} \alpha_i \rho_i, \tag{5.3a}$$

$$\rho u = \sum_{i=1}^{n} \alpha_i \rho_i u_i, \tag{5.3b}$$

$$\rho E = \sum_{i=1}^{n} \alpha_i \rho_i E_i, \tag{5.3c}$$

where ρ_i, u_i, and E_i represent the density, velocity and specific total energy of the ith species, respectively, and n represents the number of species. The species are coupled through the void fraction α_i which satisfies the saturation condition

$$\sum_{i=1}^{n} \alpha_i = 1. \tag{5.4}$$

The pressure of each species is related to the density and specific internal energy e_i of the species through the stiffened gas EOS (SG-EOS)

$$\mathrm{p}_i(\rho_i, e_i) = (\gamma_i - 1)\rho_i e_i - \gamma_i \mathrm{p}_{\infty_i}, \quad i = 1, \cdots, n, \tag{5.5}$$

where $\gamma_i = \mathrm{C}_{\mathrm{p}_i}/\mathrm{C}_{\mathrm{v}i} > 1$ is the ratio of specific heats and $\mathrm{p}_{\infty_i} \geq 0$ is a pressure-like constant that introduces incompressibility in the species. Observe that if $\mathrm{p}_{\infty_i} = 0$ in (5.5) then we recover the polytropic EOS. The total pressure of the mixture is defined as

$$\frac{\mathrm{p} + \gamma \mathrm{p}_\infty}{(\gamma - 1)} = \mathrm{p}\Gamma + \Pi = \rho e, \tag{5.6}$$

where

$$\rho e = \sum_{i=1}^{n} \alpha_i \rho_i e_i, \tag{5.7}$$

is the mixture total internal energy and the EOS parameters of the mixture, Γ and Π, are defined as

$$\Gamma = \frac{1}{\gamma - 1} = \sum_{i=1}^{n} \frac{\alpha_i}{\gamma_i - 1}, \tag{5.8a}$$

$$\Pi = \frac{\gamma \mathrm{p}_\infty}{\gamma - 1} = \sum_{i=1}^{n} \frac{\alpha_i \gamma_i \mathrm{p}_{\infty_i}}{\gamma_i - 1}. \tag{5.8b}$$

Hyperbolicity of the SG-gamma model requires that the solutions to the Cauchy problem (5.1) belong to the phase space

$$\Omega_{\mathrm{GM}} = \left\{ \mathbf{u} \in \mathbb{R}^5 : \rho > 0, u \in \mathbb{R}, \rho e > \mathrm{p}_\infty, \Gamma > 0, \Pi \geq 0 \right\}, \tag{5.9}$$

for all time, and, for smooth solutions, the matrix-valued function $\mathbf{A} : \Omega_{\mathrm{GM}} \ni \mathbf{u} \mapsto \mathbf{A}(\mathbf{u}) = \mathbf{f}'(\mathbf{u}) + \mathbf{c}(\mathbf{u}) \in \mathbb{R}^{5\times 5}$ admits real eigenvalues

$$\lambda_1(\mathbf{u}) = u - c, \quad \lambda_2(\mathbf{u}) = u, \quad \lambda_3(\mathbf{u}) = u, \quad \lambda_4(\mathbf{u}) = u, \quad \lambda_5(\mathbf{u}) = u + c, \tag{5.10}$$

where $c = \sqrt{\gamma(\gamma - 1)(\rho e - \mathrm{p}_\infty)/\rho}$ is the speed of sound of the mixture. Observe here that, in (5.10), λ_2, λ_3 and λ_4 are associated to linearly degenerate (LD) fields, while λ_1 and λ_5 are associated to genuinely nonlinear (GNL) fields, and the eigenvalues are not distinct, hence (5.1a) is not strictly hyperbolic.

Uniqueness of solution for (5.1a) requires satisfying an entropy condition, where physically relevant weak solutions of (5.1a) must satisfy

$$\partial_t \eta(\mathbf{u}) + \partial_x q(\mathbf{u}) \leq 0, \tag{5.11}$$

for a given convex entropy function $\eta(\mathbf{u})$ and an entropy flux $q(\mathbf{u})$. However, during the course of this work we realised that the derivation of a strictly convex function for the model (5.1a) is a very challenging task, and in our efforts were unable to prove that there exists a $\eta(\mathbf{u})$ for (5.1a) for which the Hessian $\eta''(\mathbf{u})$ is symmetric positive-definite.

Alternatively, we know that the involved species, in (5.1a), are endowed with a physical

entropy function

$$s_i(\rho_i, \theta) = -\mathrm{C_{v}}_i \left(\ln \theta + (\gamma_i - 1) \ln \rho_i \right), \quad i = 1, \cdots, n, \tag{5.12}$$

where $\theta = 1/T$ is the inverse of the temperature T and that the physical entropy satisfies the second law of thermodynamics

$$T ds_i = de_i - \frac{\mathrm{p}_i}{\rho_i^2} d\rho_i. \tag{5.13}$$

Note that the SG-gamma model was derived under the assumption that species are in thermal equilibrium

$$T(\rho, e) \equiv T_1(\rho_1, e_1) \equiv \cdots \equiv T_n(\rho_n, e_n). \tag{5.14}$$

In our work, we set the entropy pair as

$$\eta(\mathbf{u}) = -\rho s, \quad q(\mathbf{u}) = -\rho s u, \tag{5.15}$$

where

$$s = \mathrm{C_v} \ln \left(\frac{\mathrm{p} + \mathrm{p}_\infty}{\rho^\gamma} \right), \tag{5.16}$$

is the specific physical entropy of the immiscible mixture and in the case of smooth solutions of (5.1a), the total physical entropy is conserved

$$\partial_t \rho s + \partial_x \rho s u = 0. \tag{5.17}$$

In (5.16), the term $\mathrm{C_v}$ is defined as

$$\mathrm{C_v} = \sum_{i=1}^{n} Y_i \mathrm{C_{v}}_i, \tag{5.18}$$

where $Y_i = \frac{\alpha_i \rho_i}{\rho}$ is the mass fraction of the ith species that satisfy

$$\sum_{i=1}^{n} Y_i = 1. \tag{5.19}$$

Remark 5.2.1. *We must emphasize that the convexity of the entropy pair (5.15) holds only for pure phases, i.e. regions in the physical domain where both α_i and Y_i are uniform and the species become uncoupled. This restriction on the convexity has implications when deriving the entropy variables $\mathbf{v}(\mathbf{u}) = \eta'(\mathbf{u})$ as the map $\mathbf{u} \mapsto \mathbf{v}(\mathbf{u})$ is one-to-one only in regions containing pure phases.*

We end this section by deriving the entropy variables for the SG-gamma model through the below lemma.

Lemma 5.2.1. *Under the choice of the entropy function $\eta(\mathbf{u})$ in (5.15), the SG-gamma*

model (5.1a) admits the following entropy variables for pure phases:

$$\mathbf{v}(\mathbf{u}) = \frac{\partial}{\partial \mathbf{u}}\eta(\mathbf{u}) = \begin{pmatrix} \gamma \mathrm{C_v} - s - \zeta \frac{u^2}{2} \\ \zeta u \\ -\zeta \\ 0 \\ 0 \end{pmatrix}, \quad \forall \mathbf{u} \in \Omega_{\mathrm{GM}} \tag{5.20}$$

where $\zeta = \frac{(\gamma-1)\mathrm{C_v}\rho}{\mathrm{p}+\mathrm{p}_\infty}$.

Proof. The physical entropy of the mixture (5.16) be reformulated as

$$\begin{aligned} s &= \mathrm{C_v} \ln\left(\frac{\mathrm{p}+\mathrm{p}_\infty}{\rho^\gamma}\right) \\ &= -\mathrm{C_v}\ln\zeta - (\gamma-1)\mathrm{C_v}\ln\rho + \mathrm{C_v}\ln((\gamma-1)\mathrm{C_v}), \end{aligned} \tag{5.21}$$

and using the definition of $\eta(\mathbf{u})$ from (5.15), we have

$$\begin{aligned} d\eta &= -\rho ds - s d\rho \\ &\overset{(5.21)}{=} -\rho \mathrm{C_v} \frac{d(\mathrm{p}+\mathrm{p}_\infty)}{\mathrm{p}+\mathrm{p}_\infty} + \gamma \mathrm{C_v} d\rho - s d\rho \\ &\overset{(5.6)}{=} -\rho \mathrm{C_v}(\gamma-1)\frac{d\rho e}{\mathrm{p}+\mathrm{p}_\infty} + \gamma \mathrm{C_v} d\rho - s d\rho \\ &= -\rho \frac{(\gamma-1)\mathrm{C_v}}{\mathrm{p}+\mathrm{p}_\infty}\left(d\rho E - u d\rho u + \frac{u^2}{2} d\rho\right) + \gamma \mathrm{C_v} d\rho - s d\rho \\ &= -\zeta d\rho E + \zeta u d\rho u + \left(\gamma \mathrm{C_v} - s - \zeta \frac{u^2}{2}\right) d\rho. \end{aligned} \tag{5.22}$$

It is direct to get (5.20) from the above relation, where γ can be computed from (5.8). □

5.3 NUMERICAL FLUXES FOR THE VOLUME INTEGRAL

For the sake of clarity, let us first recall the semi-discrete DG scheme (3.54), for general hyperbolic system with nonconservative product, over the cell κ_j with cell size $h > 0$:

$$\frac{\omega_k h}{2}\frac{d\mathbf{U}_j^k}{dt} + \omega_k \sum_{l=0}^{p} D_{kl}\tilde{\mathbf{D}}(\mathbf{U}_j^k, \mathbf{U}_j^l) + \delta_{kp}\mathbf{D}^-(\mathbf{U}_j^p, \mathbf{U}_{j+1}^0) + \delta_{k0}\mathbf{D}^+(\mathbf{U}_{j-1}^p, \mathbf{U}_j^0) = 0, \qquad 0 \le k \le p, \quad j \in \mathbb{Z}, \tag{5.23}$$

where $\omega_k > 0$ are the quadrature weights, $\mathbf{U}_j^{0\le k\le p}$ are the $p+1$ degrees of freedom in cell κ_j, $\mathbf{D}^\pm$ are the numerical fluxes at the interfaces and

$$\tilde{\mathbf{D}}(\mathbf{u}^-, \mathbf{u}^+) := \mathbf{D}_X^-(\mathbf{u}^-, \mathbf{u}^+) - \mathbf{D}_X^+(\mathbf{u}^+, \mathbf{u}^-), \tag{5.24a}$$

$$= \mathbf{h}_X(\mathbf{u}^-, \mathbf{u}^+) + \mathbf{h}_X(\mathbf{u}^+, \mathbf{u}^-) + \mathbf{d}^-(\mathbf{u}^-, \mathbf{u}^+) - \mathbf{d}^+(\mathbf{u}^+, \mathbf{u}^-). \tag{5.24b}$$

In (5.24), $\mathbf{D}_X^{\pm}$ are numerical fluxes in fluctuation form that are applied in the volume integral. They are defined as

$$\mathbf{D}_X^-(\mathbf{u}^-,\mathbf{u}^+) = \mathbf{h}_X(\mathbf{u}^-,\mathbf{u}^+) - \mathbf{f}(\mathbf{u}^-) + \mathbf{d}^-(\mathbf{u}^-,\mathbf{u}^+), \tag{5.25a}$$
$$\mathbf{D}_X^+(\mathbf{u}^-,\mathbf{u}^+) = -\mathbf{h}_X(\mathbf{u}^-,\mathbf{u}^+) + \mathbf{f}(\mathbf{u}^+) + \mathbf{d}^+(\mathbf{u}^-,\mathbf{u}^+), \tag{5.25b}$$

where $\mathbf{h}_X(\mathbf{u}^-,\mathbf{u}^+)$ is the vector of numerical fluxes, $\mathbf{f}(\mathbf{u}^{\pm})$ are the approximation of the traces of the physical flux at the interfaces, and $\mathbf{d}^{\pm}(\mathbf{u}^-,\mathbf{u}^+)$ is the vector of fluctuation fluxes for approximating the nonconservative product. In the forthcoming discussions, the suffix X attached to the numerical fluxes may be replaced by *cp* or *ec*, which signifies that the numerical fluxes exhibit the property of either contract-preservation of entropy conservation, respectively. Note that entropy stability of (5.23) requires that $\tilde{\mathbf{D}}$ should be replaced by entropy conservative fluxes $\mathbf{D}_{ec}^{\pm}$, while $\mathbf{D}^{\pm}$ must be entropy stable fluxes, see Theorem 3.5.1 for details.

In this section, we will specifically focus on designing numerical fluxes that will be applied to the volume integral for the scheme (5.23). Numerical fluxes at the interface will be dealt separately in section 5.4. An essential tool which would help in the algebraic manipulations are the Leibniz identities, which we recall here. Let $a^+, a^-, b^+, b^-, c^+, c^-$ in $\mathbb{R}$ have finite values, then we have

$$[\![ab]\!] = \overline{a}[\![b]\!] + \overline{b}[\![a]\!], \quad [\![abc]\!] = \overline{a}(\overline{b}[\![c]\!] + \overline{c}[\![b]\!]) + \overline{bc}[\![a]\!], \tag{5.26}$$

where $\overline{a} = \frac{a^+ + a^-}{2}$ is the arithmetic mean and $[\![a]\!] = a^+ - a^-$.

5.3.1 Contact preserving numerical fluxes

Here, we focus on deriving conditions that will ensure that the numerical fluxes maintain uniform pressure and velocity profiles across an isolated contact discontinuity. To this purpose, we introduce *contact preserving* fluctuation fluxes of the form

$$\mathbf{D}_{cp}^-(\mathbf{u}^-,\mathbf{u}^+) = \mathbf{h}_{cp}(\mathbf{u}^-,\mathbf{u}^+) - \mathbf{f}(\mathbf{u}^-) + \mathbf{d}^-(\mathbf{u}^-,\mathbf{u}^+), \tag{5.27a}$$
$$\mathbf{D}_{cp}^+(\mathbf{u}^-,\mathbf{u}^+) = -\mathbf{h}_{cp}(\mathbf{u}^-,\mathbf{u}^+) + \mathbf{f}(\mathbf{u}^+) + \mathbf{d}^+(\mathbf{u}^-,\mathbf{u}^+), \tag{5.27b}$$

where $\mathbf{h}_{cp}(\mathbf{u}^-,\mathbf{u}^+) = (h_{cp}^{\rho}, h_{cp}^{\rho u}, h_{cp}^{\rho E}, 0, 0)^{\top}$ is the numerical flux for the conservative equations of mass, momentum and energy, $\mathbf{f}(\mathbf{u}^{\pm})$ are the traces of the physical flux function, and $\mathbf{d}^{\pm}(\mathbf{u}^-,\mathbf{u}^+) = (0,0,0,d_{\Gamma}^{\pm}, d_{\Pi}^{\pm})^{\top}$ are fluctuation fluxes for the nonconservative product.

The semi-discrete scheme for (5.1a) using (5.27) in the volume integral reads

$$\frac{\omega_k h}{2} d_t \rho_{cp,j}^k + 2\omega_k \sum_{l=0}^{p} h_{cp}^{\rho}(\mathbf{U}_j^k, \mathbf{U}_j^l) D_{kl} + \delta_{kp} D_{\rho}^-(\mathbf{U}_j^p, \mathbf{U}_{j+1}^0) + \delta_{k0} D_{\rho}^+(\mathbf{U}_{j-1}^p, \mathbf{U}_j^0) = 0, \tag{5.28a}$$

$$\frac{\omega_k h}{2} d_t (\rho u)_j^k + 2\omega_k \sum_{l=0}^{p} h_{cp}^{\rho u}(\mathbf{U}_j^k, \mathbf{U}_j^l) D_{kl} + \delta_{kp} D_{\rho u}^+(\mathbf{U}_j^p, \mathbf{U}_{j+1}^0) + \delta_{k0} D_{\rho u}^+(\mathbf{U}_{j-1}^p, \mathbf{U}_j^0) = 0, \tag{5.28b}$$

$$\frac{\omega_k h}{2} d_t (\rho E)_j^k + 2\omega_k \sum_{l=0}^{p} h_{cp}^{\rho E}(\mathbf{U}_j^k, \mathbf{U}_j^l) D_{kl} + \delta_{kp} D_{\rho E}^-(\mathbf{U}_j^p, \mathbf{U}_{j+1}^0) + \delta_{k0} D_{\rho E}^+(\mathbf{U}_{j-1}^p, \mathbf{U}_j^0) = 0, \tag{5.28c}$$

$$\frac{\omega_k h}{2} d_t \Gamma_j^k + \omega_k \sum_{l=0}^{p} \Big(d_\Gamma^-(\mathbf{U}_j^k, \mathbf{U}_j^l) - d_\Gamma^+(\mathbf{U}_j^l, \mathbf{U}_j^k) \Big) D_{kl} + \delta_{kp} D_\Gamma^-(\mathbf{U}_j^p, \mathbf{U}_{j+1}^0) + \delta_{k0} D_\Gamma^+(\mathbf{U}_{j-1}^p, \mathbf{U}_j^0) = 0, \tag{5.28d}$$

$$\frac{\omega_k h}{2} d_t \Pi_j^k + \omega_k \sum_{l=0}^{p} \Big(d_\Pi^-(\mathbf{U}_j^k, \mathbf{U}_j^l) - d_\Pi^+(\mathbf{U}_j^l, \mathbf{U}_j^k) \Big) D_{kl} + \delta_{kp} D_\Pi^-(\mathbf{U}_j^p, \mathbf{U}_{j+1}^0) + \delta_{k0} D_\Pi^+(\mathbf{U}_{j-1}^p, \mathbf{U}_j^0) = 0, \tag{5.28e}$$

where, for the moment, we assume that the interface fluxes $D_{(\cdot)}^-(\mathbf{U}_{j-1}^p, \mathbf{U}_j^0)$ and $D_{(\cdot)}^+(\mathbf{U}_j^p, \mathbf{U}_{j+1}^0)$ at the right and left interfaces of the cell, respectively, are contact preserving. We will address this assumption on the interfaces fluxes in section 5.4.3.

Now let us suppose that the scheme encounters an isolated contact discontinuity, across which the velocity and pressure must be uniform, $u_j^k = u$ and $\mathrm{p}_j^k = \mathrm{p}$, respectively, for all $0 \le k \le p$, and ρ, Γ and Π are allowed to be discontinuous. For such a case, we are interested in deriving conditions for the numerical fluxes (5.27) that will be sufficient to maintain the uniform states in time.

We can derive a semi-discrete scheme for the evolution of velocity in time from (5.28) following the differential relation

$$\rho du = d\rho u - u d\rho, \tag{5.29}$$

and we get

$$\begin{aligned} \frac{\omega_k h}{2} \rho_j^k d_t u_j^k + 2\omega_k \sum_{l=0}^{p} \Big(h_{cp}^{\rho u}(\mathbf{U}_j^k, \mathbf{U}_j^l) - u h_{cp}^{\rho}(\mathbf{U}_j^k, \mathbf{U}_j^l) \Big) D_{kl} \\ + \delta_{kp} \Big(D_{\rho u}^-(\mathbf{U}_j^p, \mathbf{U}_{j+1}^0) - u D_\rho^-(\mathbf{U}_j^p, \mathbf{U}_{j+1}^0) \Big) \\ + \delta_{k0} \Big(D_{\rho u}^+(\mathbf{U}_{j-1}^p, \mathbf{U}_j^0) - u D_\rho^-(\mathbf{U}_{j-1}^p, \mathbf{U}_j^0) \Big) = 0, \end{aligned} \tag{5.30}$$

where we observe that in order to maintain uniform velocity in time, the following condition on the numerical fluxes (5.27)

$$h_{cp}^{\rho u}(\mathbf{u}^-, \mathbf{u}^+) = u h_{cp}^{\rho}(\mathbf{u}^-, \mathbf{u}^+) + \tilde{\mathrm{p}}(\mathbf{u}^-, \mathbf{u}^+), \quad \forall \mathbf{u}^\pm \in \Omega_{\text{GM}}, \tag{5.31}$$

are sufficient enough to ensure that the volume integral does not perturb the uniform velocity. Note that we have added $\tilde{\mathrm{p}}$ in (5.31) which acts as a consistent contribution from the discrete pressure and is essential in order to maintain homogeneity. Although, if the pressure is uniform within the cell then, owing to consistency, the contribution of $\tilde{\mathrm{p}}(\mathbf{u}^-, \mathbf{u}^+)$ vanishes

$$\sum_{l=0}^{p} \tilde{\mathrm{p}}_j(\mathbf{U}^k, \mathbf{U}^k) D_{kl} \overset{(3.37)}{=} 0, \quad 0 \le k, l \le p, \quad j \in \mathbb{Z}. \tag{5.32}$$

In a similar manner, a semi-discrete equation for the evolution of pressure (5.6) can be obtained following the differential relation

$$\Gamma d\mathrm{p} \underset{(5.8)}{\overset{(5.6)}{=}} d\rho E - \left(\frac{u^2}{2} d\rho + \mathrm{p} d\Gamma + d\Pi \right), \tag{5.33}$$

$$
\begin{aligned}
&\frac{\omega_k h}{2}\Gamma_j^k d_t \mathrm{p}_j^k + 2\omega_k \sum_{l=0}^{p}\Bigg(h_{cp}^{\rho E}(\mathbf{U}_j^k, \mathbf{U}_j^l) \\
&- \frac{1}{2}\Bigg(u^2 h_{cp}^{\rho}(\mathbf{U}_j^k, \mathbf{U}_j^l) + \mathrm{p}(d_\Gamma^-(\mathbf{U}_j^k, \mathbf{U}_j^l) - d_\Gamma^+(\mathbf{U}_j^l, \mathbf{U}_j^k)) + d_\Pi^-(\mathbf{U}_j^k, \mathbf{U}_j^l) - d_\Pi^+(\mathbf{U}_j^l, \mathbf{U}_j^k)\Bigg)\Bigg) D_{kl} \\
&+ \delta_{kp}\left(D_{\rho E}^-(\mathbf{U}_j^p, \mathbf{U}_{j+1}^0) - \left(\frac{u^2}{2} D_\rho^-(\mathbf{U}_j^p, \mathbf{U}_{j+1}^0) + \mathrm{p} D_\Gamma^-(\mathbf{U}_j^p, \mathbf{U}_{j+1}^0) + D_\Pi^-(\mathbf{U}_j^p, \mathbf{U}_{j+1}^0) \right) \right) \\
&+ \delta_{k0}\left(D_{\rho E}^+(\mathbf{U}_{j-1}^p, \mathbf{U}_j^0) - \left(\frac{u^2}{2} D_\rho^+(\mathbf{U}_{j-1}^p, \mathbf{U}_j^p) + \mathrm{p} D_\Gamma^+(\mathbf{U}_{j-1}^p, \mathbf{U}_j^0) + D_\Pi^+(\mathbf{U}_{j-1}^p, \mathbf{U}_j^0) \right) \right) = 0,
\end{aligned}
\tag{5.34}
$$

where the evolution of uniform pressure, in time, remains unaffected by the volume integral if the numerical fluxes satisfy

$$
\begin{aligned}
&h_{cp}^{\rho E}(\mathbf{u}^-, \mathbf{u}^+) \\
&= \frac{1}{2}\left(u^2 h_{cp}^{\rho}(\mathbf{u}^-, \mathbf{u}^+) + \mathrm{p}\left(d_\Gamma^-(\mathbf{u}^-, \mathbf{u}^+) - d_\Gamma^+(\mathbf{u}^+, \mathbf{u}^-) \right) + d_\Pi^-(\mathbf{u}^-, \mathbf{u}^+) - d_\Pi^+(\mathbf{u}^+, \mathbf{u}^-) \right), \ \forall \mathbf{u}^\pm \in \Omega_{\text{GM}}.
\end{aligned}
\tag{5.35}
$$

Following conditions (5.31) and (5.35), we can now propose contact preserving fluxes for the volume integral.

Proposition 5.3.1. *Numerical fluxes of the form*

$$
\mathbf{D}_{cp}^\pm(\mathbf{u}^-, \mathbf{u}^+) = \mp \mathbf{h}_{cp}(\mathbf{u}^-, \mathbf{u}^+) \pm \mathbf{f}(\mathbf{u}^\pm) + \mathbf{d}^\pm(\mathbf{u}^-, \mathbf{u}^+),
\tag{5.36}
$$

where

$$
\mathbf{h}_{cp}(\mathbf{u}^-, \mathbf{u}^+) = \begin{pmatrix} \overline{\rho}\,\overline{u} \\ \overline{\rho}\,\overline{u}^2 + \overline{\mathrm{p}} \\ (\overline{\rho E} + \overline{\mathrm{p}})\overline{u} \\ 0 \\ 0 \end{pmatrix}, \quad \mathbf{d}^\pm(\mathbf{u}^-, \mathbf{u}^+) = \frac{u^\pm}{2}\begin{pmatrix} 0 \\ 0 \\ 0 \\ [\![\Gamma]\!] \\ [\![\Pi]\!] \end{pmatrix},
\tag{5.37}
$$

preserve the uniform pressure and velocity fields across an contact discontinuities and material interfaces for the SG-gamma model (5.1a)-(5.2), with the mixture EOS (5.6).

Proof. Let us assume the situation of encountering an isolated contact discontinuity, across which the velocity and pressure are uniform in space

$$
u_j^k = u, \quad \mathrm{p}_j^k = \mathrm{p}, \quad 0 \le k \le p, j \in \mathbb{Z}.
\tag{5.38}
$$

It is evident from (5.37) that the momentum flux directly satisfies (5.31) and the contribution from $\overline{\mathrm{p}}_j$ will vanish owing to consistency and (5.32). In order to prove that (5.36) satisfy (5.35), we first introduce the following relation for (5.6) as it will simplify the proof

$$
\mathrm{p}[\![\Gamma]\!] + [\![\Pi]\!] \overset{(5.26)}{=} [\![\rho E]\!] - \frac{u^2}{2}[\![\rho]\!].
\tag{5.39}
$$

Using the numerical fluxes (5.36) in the volume integral of (5.34), (5.35) reduces to

$$h_{cp}^{\rho E}(\mathbf{U}_j^k, \mathbf{U}_j^l) D_{kl} = \frac{u}{2} (\rho E)_j^l D_{kl}. \tag{5.40}$$

Furthermore

$$\begin{aligned}
&\frac{1}{2}\left(u^2 h_{cp}^{\rho}(\mathbf{U}^k, \mathbf{U}^l) + \mathrm{p}\left(d_\Gamma^-(\mathbf{U}_j^k, \mathbf{U}_j^l) - d_\Gamma^+(\mathbf{U}_j^l, \mathbf{U}_j^k)\right) + d_\Pi^-(\mathbf{U}_j^k, \mathbf{U}_j^l) - d_\Pi^+(\mathbf{U}^l, \mathbf{U}^k)\right) D_{kl}, \\
&\overset{(5.36)}{=} \frac{u}{2}\left(u^2 \overline{\rho} + \mathrm{p}[\![\Gamma]\!] + [\![\Pi]\!]\right) D_{kl}, \\
&\overset{(5.39)}{=} \frac{u}{2}\left(u^2 \overline{\rho} + [\![\rho E]\!] - \frac{u^2}{2}[\![\rho]\!]\right) D_{kl}, \\
&= \frac{u}{2} (\rho E)_j^l D_{kl},
\end{aligned} \tag{5.41}$$

which is equal to (5.40).

Hence $d_t u_j^k = 0$ and $d_t \mathrm{p}_j^k = 0$ are maintained which concludes the proof. □

Remark 5.3.1. *The contact preserving numerical fluxes (5.36) are similar to the one proposed in [85], where we have modified the contributions towards the energy equation to satisfy our requirements.*

5.3.2 ENTROPY CONSERVATIVE NUMERICAL FLUXES FOR THE GAMMA MODEL

We now recall the definition of entropy conservative fluctuation fluxes as stated in section 3.5. Fluctuation fluxes of the form

$$\mathbf{D}_{ec}^-(\mathbf{u}^-, \mathbf{u}^+) = \mathbf{h}_{ec}(\mathbf{u}^-, \mathbf{u}^+) - \mathbf{f}(\mathbf{u}^-) + \mathbf{d}^-(\mathbf{u}^-, \mathbf{u}^+), \tag{5.42a}$$

$$\mathbf{D}_{ec}^+(\mathbf{u}^-, \mathbf{u}^+) = -\mathbf{h}_{ec}(\mathbf{u}^-, \mathbf{u}^+) + \mathbf{f}(\mathbf{u}^+) + \mathbf{d}^+(\mathbf{u}^-, \mathbf{u}^+), \tag{5.42b}$$

are said to entropy conservative if they satisfy

$$\begin{aligned}
\Delta Q(\mathbf{u}^-, \mathbf{u}^+) = &-\mathbf{h}_{ec}(\mathbf{u}^-, \mathbf{u}^+)^\top [\![\mathbf{v}]\!] + \mathbf{v}(\mathbf{u}^-)^\top \mathbf{d}^-(\mathbf{u}^-, \mathbf{u}^+) + \mathbf{v}(\mathbf{u}^+)^\top \mathbf{d}^+(\mathbf{u}^-, \mathbf{u}^+) \\
&+ [\![\mathbf{v}^\top(\mathbf{u})\mathbf{f}(\mathbf{u}) - q(\mathbf{u})]\!] = 0 \quad \forall \mathbf{u}^\pm \in \Omega_{\mathrm{GM}},
\end{aligned} \tag{5.43}$$

where $\Delta Q(\mathbf{u}^-, \mathbf{u}^+)$ is the discrete entropy dissipation at the interface.

In this work, we design entropy conservative fluxes for pure phases, thus excluding contact discontinuities. This restriction is necessary as the entropy is not convex for the complete mixture.

Proposition 5.3.2. *Entropy conservative fluxes (5.42) with the following definition of its components*

$$\mathbf{h}_{ec}(\mathbf{u}^-, \mathbf{u}^+) = \begin{pmatrix} h_{ec}^{\rho} \\ h_{ec}^{\rho u} \\ h_{ec}^{\rho E} \\ 0 \\ 0 \end{pmatrix}, \quad \mathbf{d}^\pm(\mathbf{u}^-, \mathbf{u}^+) = \frac{u^\pm}{2} \begin{pmatrix} 0 \\ 0 \\ 0 \\ [\![\Gamma]\!] \\ [\![\Pi]\!] \end{pmatrix}, \tag{5.44}$$

where

$$h_{ec}^{\rho} = \hat{\rho}\overline{u}, \quad h_{ec}^{\rho u} = \overline{u}h_{ec}^{\rho} + \overline{\rho}\overline{(\gamma-1)}\overline{\left(\frac{\mathrm{C_v}}{\zeta}\right)} - \overline{\mathrm{p}_\infty}, \quad h_{ec}^{\rho E} = \left(\widehat{\left(\frac{\mathrm{C_v}}{\zeta}\right)} + \frac{u^- u^+}{2}\right)h_{ec}^{\rho} + \overline{\rho}\,\overline{u}\,\overline{(\gamma-1)}\overline{\left(\frac{\mathrm{C_v}}{\zeta}\right)},$$

and $\zeta = \frac{(\gamma-1)\mathrm{C_v}\rho}{\mathrm{p}+\mathrm{p}_\infty}$ *satisfy (5.43), for the EOS (5.6), and hence conserve the cell entropy for pure phases.*

The void fraction is uniform in pure phases, therefore (5.8) along with (5.26) gives $[\![\Gamma]\!] \equiv [\![\Pi]\!] \equiv 0$.

Proof. As we intend to design entropy conservative fluxes for pure phases, the system (5.1a) can be considered as conservative. This reduces (5.43) to the Tadmor condition [128]:

$$\Delta Q(\mathbf{u}^-, \mathbf{u}^+) = \mathbf{h}_{ec}(\mathbf{u}^-, \mathbf{u}^+) \cdot [\![\mathbf{v}]\!] - [\![\psi(\mathbf{u})]\!] = 0, \quad \forall \mathbf{u}^\pm \in \Omega_{\mathrm{GM}}, \tag{5.45}$$

where $\psi(\mathbf{u}) = \mathbf{v}^\top \mathbf{f} - q$ is the entropy potential.

Let us now resolve each term in (5.45) and show that the numerical fluxes (5.44) indeed conserve the entropy. The entropy potential reads

$$\begin{aligned}
\psi(\mathbf{u}) &\overset{(5.20)}{=} -\zeta(\rho E + \mathrm{p})u + \zeta u(\rho u^2 + \mathrm{p}) + (\gamma \mathrm{C_v} - s - \zeta\frac{u^2}{2})\rho u + \rho s u \\
&= (\gamma \mathrm{C_v} - \zeta e)\rho u \\
&= (\gamma - 1)\mathrm{C_v}\rho u - \mathrm{p}_\infty \zeta u
\end{aligned} \tag{5.46}$$

and

$$[\![\psi(\mathbf{u})]\!] \overset{(5.26)}{=} \overline{(\gamma-1)\mathrm{C_v}}[\![\rho u]\!] - \overline{\mathrm{p}_\infty}[\![\zeta u]\!]. \tag{5.47}$$

Then we have

$$\begin{aligned}
\mathbf{h}_{ec}^\top(\mathbf{u}^-, \mathbf{u}^+)[\![\mathbf{v}(\mathbf{u})]\!] &= [\![\gamma \mathrm{C_v} - s - \zeta\frac{u^2}{2}]\!]\overline{u}\hat{\rho} + [\![\zeta u]\!]\left(\overline{u}^2\hat{\rho} + \frac{(\gamma-1)\mathrm{C_v}\overline{\rho}}{\overline{\zeta}} - \mathrm{p}_\infty\right) \\
&\quad - [\![\zeta]\!]\left(\left(\frac{\mathrm{C_v}}{\hat{\zeta}} + \frac{u^- u^+}{2}\right)\hat{\rho} + \frac{(\gamma-1)\mathrm{C_v}}{\overline{\zeta}}\overline{\rho}\right)\overline{u} \\
&\overset{(5.21)}{\underset{(5.26)}{=}} \left(\frac{[\![\zeta]\!]}{\hat{\zeta}} + (\gamma-1)\frac{[\![\rho]\!]}{\hat{\rho}}\right)\mathrm{C_v}\overline{u}\hat{\rho} + [\![\zeta u]\!]\left(\overline{u}^2\hat{\rho} + \frac{(\gamma-1)\mathrm{C_v}\overline{\rho}}{\overline{\zeta}} - \mathrm{p}_\infty\right) \\
&\quad - [\![\zeta]\!]\left(\left(\frac{\mathrm{C_v}}{\hat{\zeta}} + \frac{u^- u^+}{2}\right)\hat{\rho} + \frac{(\gamma-1)\mathrm{C_v}}{\overline{\zeta}}\overline{\rho}\right)\overline{u} \\
&= (\gamma-1)\mathrm{C_v}[\![\rho u]\!] - \mathrm{p}_\infty[\![\zeta u]\!].
\end{aligned} \tag{5.48}$$

It is clear that (5.47) cancels (5.48) and $\Delta Q(\mathbf{u}^-, \mathbf{u}^+)$ is zero in (5.45). Hence the discrete entropy is conserved and it concludes the proof. □

5.3.3 A TROUBLED-CELL INDICATOR BASED SELECTION OF NUMERICAL FLUXES

We have introduced two numerical fluxes for the volume integral: the contact preserving fluxes (5.36) and the entropy conservative fluxes (5.44). It must be noted that these fluxes fail to satisfy each others purpose. Thus, the contact preserving numerical fluxes (5.36) do not conserve the entropy across an isolated shock, while the entropy conservative fluxes (5.44) fail to preserve uniform pressure and velocity profiles across a contact or material discontinuity.

In view of this inflexible behaviour of the numerical fluxes, we choose to apply the contact preserving numerical fluxes (5.36)-(5.37) or the entropy conservative fluxes (5.44) based on the following troubled-cell indicator (TCI) function, which was originally proposed in [78] and here it has been adapted to the DG framework:

$$\mathrm{TCI}_j = \sum_{k=0}^{p} \frac{\omega_k}{2} \left| \frac{\mathrm{p}_{\min} - 2\mathrm{p}_j^k + \mathrm{p}_{\max}}{\mathrm{p}_{\min} + 2\mathrm{p}_j^k + \mathrm{p}_{\max}} \right|, \quad j \in \mathbb{Z}, \tag{5.49}$$

where $\mathrm{p}_{\min} = \min_k \mathrm{p}_j^k$ and $\mathrm{p}_{\max} = \max_k \mathrm{p}_j^k$.

The essential idea of the pressure-based indicator function (5.49) is that it is expected to generate large values across shocks, due to the jump in pressure, while the function vanishes across contact discontinuities. In our implementation, we impose a pre-determined threshold value of the TCI function as the selection criteria for the numerical fluxes. As a result, if the TCI function generates values exceeding the threshold within a cell then entropy conservative fluxes (5.44) are applied in the volume integral and for all other cases contact preserving numerical fluxes (5.36)-(5.37) are applied.

5.4 INTERFACE FLUXES FOR THE GAMMA-MODEL

We are now concerned with designing HLL and HLLC numerical fluxes for the gamma-model, which will be applied at the cell interfaces. Following [69], we consider the integral form of (5.1a)

$$\int_0^{\Delta t} \int_{-h/2}^{h/2} \partial_t \mathbf{u} + \partial_x \mathbf{f}(\mathbf{u}) + \mathbf{c}(\mathbf{u}) \partial_x \mathbf{u} dx dt = 0, \tag{5.50}$$

with Riemann initial data

$$\mathbf{u}_0(x) = \begin{cases} \mathbf{u}_L, & x < 0, \\ \mathbf{u}_R, & x > 0, \end{cases} \tag{5.51}$$

where h is the cell size of the mesh and $\Delta t > 0$ is the time step. Referring to Figure 5-1, we integrate over $\left[-\frac{h}{2}, \frac{h}{2}\right] \times [0, \Delta t]$, which gives

$$\begin{aligned} \int_{-h/2}^{h/2} \mathcal{W}\left(\frac{x}{\Delta t}; \mathbf{u}_L, \mathbf{u}_R\right) dx - \frac{h}{2}(\mathbf{u}_L + \mathbf{u}_R) + \Delta t \left(\mathbf{f}(\mathbf{u}_R) - \mathbf{f}(\mathbf{u}_L)\right) \\ + \int_0^{\Delta t} \int_{-h/2}^{h/2} \mathbf{c}(\mathbf{u}) \partial_x \mathbf{u} dx dt = 0, \end{aligned} \tag{5.52}$$

where $\boldsymbol{\mathcal{W}}\left(\frac{x}{\Delta t}, \mathbf{u}_L, \mathbf{u}_R\right)$ denotes the exact Riemann weak solution of (5.1a) with initial data (5.51). Applying $\mathbf{c}(\mathbf{u})\partial_x \mathbf{u} = u(\partial_x \Gamma \mathbf{e}_\Gamma + \partial_x \Pi \mathbf{e}_\Pi)$, where $\mathbf{e}_\Gamma = (0,0,0,1,0)^\top$ and $\mathbf{e}_\Pi = (0,0,0,0,1)^\top$, with both Γ and Π continuous across shocks, we obtain

$$
\begin{aligned}
&\int_0^{\Delta t}\int_{-h/2}^{h/2} \mathbf{c}(\mathbf{u})\partial_x \mathbf{u} dx dt \\
&= \int_0^{\Delta t}\int_{-h/2}^{h/2} u\partial_x \left(\Gamma \mathbf{e}_\Gamma + \Pi \mathbf{e}_\Pi\right) dx dt \\
&= \int_0^{\Delta t}\int_{-h/2}^{h/2} \partial_x u \left(\Gamma \mathbf{e}_\Gamma + \Pi \mathbf{e}_\Pi\right) - \left(\Gamma \mathbf{e}_\Gamma + \Pi \mathbf{e}_\Pi\right)\partial_x u dx dt \\
&= \Delta t \left((u_R\Gamma_R - u_L\Gamma_L)\mathbf{e}_\Gamma + (u_R\Pi_R - u_L\Pi_L)\mathbf{e}_\Pi\right) - \Delta t(\Gamma_R \mathbf{e}_\Gamma + \Pi_R \mathbf{e}_\Pi)\left(u_R - u^*\right) \\
&- \Delta t(\Gamma_L \mathbf{e}_\Gamma + \Pi_L \mathbf{e}_\Pi)\left(u^* - u_L\right) \\
&= \Delta t u^* \left((\Gamma_R - \Gamma_L)\mathbf{e}_\Gamma + (\Pi_R - \Pi_L)\mathbf{e}_\Pi\right),
\end{aligned}
\tag{5.53}
$$

where u_L and u_R are the velocities in the left and right states $\mathbf{u}_L$ and $\mathbf{u}_R$, respectively and u^* is veclocity in the intermediate state. Substituting (5.53) in (5.52), leads to the integral form for (5.1a):

$$
\begin{aligned}
\frac{1}{\Delta t}\int_{-h/2}^{h/2} \boldsymbol{\mathcal{W}}\left(\frac{x}{\Delta t}; \mathbf{u}_L, \mathbf{u}_R\right) dx - \frac{h}{2\Delta t}(\mathbf{u}_L + \mathbf{u}_R) + \mathbf{f}(\mathbf{u}_R) - \mathbf{f}(\mathbf{u}_L) \\
+ u^*(\Gamma_R - \Gamma_L)\mathbf{e}_\Gamma + u^*(\Pi_R - \Pi_L)\mathbf{e}_\Pi = 0.
\end{aligned}
\tag{5.54}
$$

We now introduce Godunov fluxes in fluctuation form for (5.50)

$$
\begin{aligned}
\mathbf{D}^-(\mathbf{u}^-, \mathbf{u}^+) &:= \mathbf{f}(\mathbf{u}_L) + \mathbf{f}\left(\boldsymbol{\mathcal{W}}\left(0; \mathbf{u}_L, \mathbf{u}_R\right)\right) + u^{*,-}(\Gamma_R - \Gamma_L)\mathbf{e}_\Gamma + u^{*,-}(\Pi_R - \Pi_L)\mathbf{e}_\Pi \\
&= \frac{h}{2\Delta t}\mathbf{u}_L - \frac{1}{\Delta t}\int_{-h/2}^{0} \boldsymbol{\mathcal{W}}\left(\frac{x}{\Delta t}; \mathbf{u}_L, \mathbf{u}_R\right) dx,
\end{aligned}
\tag{5.55a}
$$

$$
\begin{aligned}
\mathbf{D}^+(\mathbf{u}^-, \mathbf{u}^+) &:= -\mathbf{f}(\mathbf{u}_R) - \mathbf{f}\left(\boldsymbol{\mathcal{W}}\left(0; \mathbf{u}_L, \mathbf{u}_R\right)\right) + u^{*,+}(\Gamma_R - \Gamma_L)\mathbf{e}_\Gamma + u^{*,+}(\Pi_R - \Pi_L)\mathbf{e}_\Pi \\
&= \frac{h}{2\Delta t}\mathbf{u}_R - \frac{1}{\Delta t}\int_{0}^{h/2} \boldsymbol{\mathcal{W}}\left(\frac{x}{\Delta t}; \mathbf{u}_L, \mathbf{u}_R\right) dx,
\end{aligned}
\tag{5.55b}
$$

which are obtained by integrating (5.1a) over the control volumes $\left[-\frac{h}{2}, 0\right] \times [0, \Delta t]$ and $\left[0, \frac{h}{2}\right] \times [0, \Delta t]$, respectively, where $(\cdot)^+ = \max(\cdot, 0)$ and $(\cdot)^- = \min(\cdot, 0)$ denote the positive and negative parts, respectively.

Note that summing up (5.55a) and (5.55b) leads to

$$
\mathbf{D}^-(\mathbf{u}^-, \mathbf{u}^+) + \mathbf{D}^+(\mathbf{u}^-, \mathbf{u}^+) = u^*\left((\Gamma_R - \Gamma_L)\mathbf{e}_\Gamma + (\Gamma_R - \Gamma_L)\mathbf{e}_\Pi\right),
\tag{5.56}
$$

which corresponds to the path-conservative property [103] for a nonconservative product $u\partial_x(\Gamma \mathbf{e}_\Gamma + \Pi \mathbf{e}_\Pi) = u^*\partial_x(\Gamma \mathbf{e}_\Gamma + \Pi \mathbf{e}_\Pi)$.

The cell-averaged solution at time $t^{n+1} = (n+1)\Delta t$ in the cell κ_j, is defined as

$$\begin{aligned}\mathbf{U}_j^{n+1} &= \frac{1}{h}\left(\int_{x_{j-1/2}}^{x_j} \boldsymbol{\mathcal{W}}\left(\frac{x}{\Delta t};\mathbf{U}_{j-1}^n,\mathbf{U}_j^n\right)dx + \int_{x_j}^{x_{j+1/2}} \boldsymbol{\mathcal{W}}\left(\frac{x}{\Delta t};\mathbf{U}_j^n,\mathbf{U}_{j+1}^n\right)dx\right),\\ &\overset{(5.55)}{=} \mathbf{U}_j^n - \frac{\Delta t}{h}\left(\mathbf{D}^+(\mathbf{U}_{j-1}^n,\mathbf{U}_j^n) + \mathbf{D}^-(\mathbf{U}_j^n,\mathbf{U}_{j+1}^n)\right),\end{aligned} \tag{5.57}$$

where $x_j = \frac{x_{j-1/2}+x_{j+1/2}}{2}$ is the cell centre, and $x_{j-1/2}$ and $x_{j+1/2}$ are the left and right interfaces of cell κ_j, respectively, see Figure 3-1.

The numerical scheme needs to be consistent with the integral form of the entropy inequality (5.11) over the control volume $\left[-\frac{h}{2},\frac{h}{2}\right]\times[0,\Delta t]$:

$$\frac{1}{\Delta t}\int_{-h/2}^{h/2}\eta\left(\boldsymbol{\mathcal{W}}\left(\frac{x}{\Delta t};\mathbf{u}_L,\mathbf{u}_R\right)\right)dxdt - \frac{h}{2\Delta t}\left(\eta(\mathbf{u}_L)+\eta(\mathbf{u}_R)\right) + q(\mathbf{u}_R) - q(\mathbf{u}_L) \le 0. \tag{5.58}$$

Therefore, in the case when the entropy function (5.15) is convex, we invoke the Jensen's inequality and show that a discrete entropy inequality can be obtained which is consistent with (5.11):

$$\begin{aligned}\eta(\mathbf{U}_j^{n+1}) &\overset{(5.57)}{\le} \frac{1}{h}\left(\int_{x_{j-1/2}}^{x_j}\eta\left(\boldsymbol{\mathcal{W}}\left(\frac{x}{\Delta t};\mathbf{U}_{j-1}^n,\mathbf{U}_j^n\right)\right)dx + \int_{x_j}^{x_{j+1/2}}\eta\left(\boldsymbol{\mathcal{W}}\left(\frac{x}{\Delta t};\mathbf{U}_j^n,\mathbf{U}_{j+1}^n\right)\right)dx\right)\\ &= \frac{\Delta t}{h}\left(Q(\mathbf{U}_{j-1}^n,\mathbf{U}_j^n) - q(\mathbf{U}_j^n) + \frac{h}{2\Delta t}\eta(\mathbf{U}_j^n) + q(\mathbf{U}_j^n) - Q(\mathbf{U}_j^n,\mathbf{U}_{j+1}^n) + \frac{h}{2\Delta t}\eta(\mathbf{U}_j^n)\right)\\ &= \eta(\mathbf{U}_j) - \frac{\Delta t}{h}\left(Q(\mathbf{U}_j^n,\mathbf{U}_{j+1}^n) - Q(\mathbf{U}_{j-1}^n,\mathbf{U}_j^n)\right),\end{aligned} \tag{5.59}$$

where in the second step, we have integrated (5.13) over the control volumes $\left[-\frac{h}{2},0\right]\times[0,\Delta t]$ and $\left[0,\frac{h}{2}\right]\times[0,\Delta t]$, and considered

$$Q(\mathbf{U}_{j-1}^n,\mathbf{U}_j^n) = q\left(\boldsymbol{\mathcal{W}}(0;\mathbf{U}_{j-1}^n,\mathbf{U}_j^n)\right) \tag{5.60a}$$

$$Q(\mathbf{U}_j^n,\mathbf{U}_{j+1}^n) = q\left(\boldsymbol{\mathcal{W}}(0;\mathbf{U}_j^n,\mathbf{U}_{j+1}^n)\right), \tag{5.60b}$$

as the entropy flux at the left and right interfaces, respectively.

5.4.1 HLL Riemann solver

We are interested in an approximate Riemann solver of the form

$$\boldsymbol{\mathcal{W}}^{\text{HLL}}\left(\frac{x}{t};\mathbf{u}_L,\mathbf{u}_R\right) = \begin{cases}\mathbf{u}_L, & \frac{x}{t} < s_L,\\ \mathbf{u}^\star, & s_L < \frac{x}{t} < s_R,\\ \mathbf{u}_R, & s_R < \frac{x}{t},\end{cases} \tag{5.61}$$

for which (5.54) and (5.58) are still satisfied, while replacing the exact Riemann solver by (5.61). Note that here we assume a two wave configuration that splits the state vector $\mathbf{u}$ into three constant states, see Figure 5-1, where s_L is the speed of the leftmost wave and

s_R is the rightmost wave. Therefore, the integral of the approximate solution over $\left[\frac{-h}{2}, \frac{h}{2}\right]$ is computed as

$$\int_{-h/2}^{h/2} \boldsymbol{\mathcal{W}}^{\text{HLL}}\left(\frac{x}{\Delta t}; \mathbf{u}_L, \mathbf{u}_R\right) dx = \left(\frac{h}{2} - s_R \Delta t\right)\mathbf{u}_R + \Delta t(s_R - s_L)\mathbf{u}^* + \left(s_L \Delta t + \frac{h}{2}\right)\mathbf{u}_L. \quad (5.62)$$

If (5.62) is introduced into (5.54), we get

$$-s_R\mathbf{u}_R + (s_R - s_L)\mathbf{u}^* + s_L\mathbf{u}_L + \mathbf{f}(\mathbf{u}_R) - \mathbf{f}(\mathbf{u}_L) + s^*(\Gamma_R - \Gamma_L)\mathbf{e}_\Gamma + s^*(\Pi_R - \Pi_L)\mathbf{e}_\Pi = 0, \quad (5.63)$$

which leads to a definition of the state vector in the *star region*:

$$\mathbf{u}^* = \frac{s_R\mathbf{u}_R - s_L\mathbf{u}_L - \mathbf{f}(\mathbf{u}_R) + \mathbf{f}(\mathbf{u}_L)}{s_R - s_L} - \frac{s^*(\Gamma_R - \Gamma_L)}{s_R - s_L}\mathbf{e}_\Gamma - \frac{s^*(\Pi_R - \Pi_L)}{s_R - s_L}\mathbf{e}_\Pi, \quad (5.64)$$

where s^* is the approximate velocity in the star region, which is defined as

$$s^* = \frac{(\rho u)^*}{\rho^*} = \frac{\mathrm{p}_L - \mathrm{p}_R - \rho_L u_L(s_L - u_L) + \rho_R u_R(s_R - u_R)}{\rho_R(s_R - u_R) - \rho_L(s_L - u_L)}. \quad (5.65)$$

The expressions for Γ and Π in the star region can be obtained directly from (5.64) as

$$\Gamma^* = \frac{(s_R - s^*)\Gamma_R - (s_L - s^*)\Gamma_L}{s_R - s_L}, \quad (5.66a)$$

$$\Pi^* = \frac{(s_R - s^*)\Pi_R - (s_L - s^*)\Pi_L}{s_R - s_L}. \quad (5.66b)$$

We now define the numerical fluxes at interfaces so as to satisfy a discrete version of (5.55).

Theorem 5.4.1. *The HLL fluctuation fluxes (5.55) take the following form for the gamma model (5.1a):*

$$\mathbf{D}^-(\mathbf{u}_L, \mathbf{u}_R) = \begin{cases} \mathbf{f}(\mathbf{u}_L), & s_L > 0, \\ \mathbf{D}^{*,-}(\mathbf{u}^-, \mathbf{u}^+), & s_L < 0 < s_R, \\ \mathbf{f}(\mathbf{u}_R) + s^*(\Gamma_R - \Gamma_L)\mathbf{e}_\Gamma + s^*(\Pi_R - \Pi_L)\mathbf{e}_\Pi, & s_R < 0, \end{cases} \quad (5.67a)$$

$$\mathbf{D}^+(\mathbf{u}_L, \mathbf{u}_R) = \begin{cases} -\mathbf{f}(\mathbf{u}_L) - s^*(\Gamma_R - \Gamma_L)\mathbf{e}_\Gamma - s^*(\Pi_R - \Pi_L)\mathbf{e}_\Pi, & s_L > 0, \\ \mathbf{D}^{*,+}(\mathbf{u}^-, \mathbf{u}^+), & s_L < 0 < s_R, \\ -\mathbf{f}(\mathbf{u}_R), & s_R < 0, \end{cases} \quad (5.67b)$$

where $\boldsymbol{e}_\Gamma = (0,0,0,1,0)^\top$ *and* $\boldsymbol{e}_\Pi = (0,0,0,0,1)^\top$ *and* $\mathbf{D}^{\star,\pm}$ *are defined in (5.68) below.*

Proof. To derive fluctuation fluxes for the HLL solver, we substitute (5.61) with (5.64) where $u^\star$ is replaced by $s^\star$, and consider three different possibilities for the wave speeds.

If $s_L < 0 < s_R$:

$$\begin{aligned}
\mathbf{D}^{*,-}(\mathbf{u}^-,\mathbf{u}^+) &= \mathbf{f}(\mathbf{u}_L) - \frac{1}{\Delta t}\left(-s_L\Delta t\mathbf{u}^* + \left(s_L\Delta t + \frac{h}{2}\right)\mathbf{u}^*\right) + \frac{h}{2\Delta t}\mathbf{u}_L,\\
&= \mathbf{f}(\mathbf{u}_L) - s_L\mathbf{u}_L + s_L\left(\frac{s_R\mathbf{u}_R - s_L\mathbf{u}_L + \mathbf{f}(\mathbf{u}_L) - \mathbf{f}(\mathbf{u}_R)}{s_R - s_L}\right.\\
&\quad \left. - s^*\frac{\Gamma_R - \Gamma_L}{s_R - s_L}\mathbf{e}_\Gamma - s^*\frac{\Pi_R - \Pi_L}{s_R - s_L}\mathbf{e}_\Pi\right),\\
&= \frac{s_R\mathbf{f}(\mathbf{u}_L) - s_L\mathbf{f}(\mathbf{u}_R) + s_Rs_L(\mathbf{u}_R - \mathbf{u}_L)}{s_R - s_L} - \frac{s^*s_L}{s_R - s_L}(\Gamma_R - \Gamma_L)\mathbf{e}_\Gamma\\
&\quad - \frac{s^*s_L}{s_R - s_L}(\Pi_R - \Pi_L)\mathbf{e}_\Pi.
\end{aligned} \tag{5.68a}$$

$$\begin{aligned}
\mathbf{D}^{*,+}(\mathbf{u}^-,\mathbf{u}^+) &= -\mathbf{f}(\mathbf{u}_R) - \frac{1}{\Delta t}\left(\left(\frac{h}{2} - s_R\Delta t\right)\mathbf{u}_R + s_R\Delta t\mathbf{u}^*\right) + \frac{h}{2\Delta t}\mathbf{u}_R,\\
&= -\mathbf{f}(\mathbf{u}_R) + s_R\mathbf{u}_R - s_R\frac{s_R\mathbf{u}_R - s_L\mathbf{u}_L - \mathbf{f}(\mathbf{u}_R) + \mathbf{f}(\mathbf{u}_L)}{s_R - s_L}\\
&\quad + \frac{s^*s_R}{s_R - s_L}(\Gamma_R - \Gamma_L)\mathbf{e}_\Gamma + \frac{s^*s_R}{s_R - s_L}(\Pi_R - \Pi_L)\mathbf{e}_\Pi,\\
&= -\frac{s_R\mathbf{f}(\mathbf{u}_L) - s_L\mathbf{f}(\mathbf{u}_R) + s_Ls_R(\mathbf{u}_R - \mathbf{u}_L)}{s_R - s_L}\\
&\quad + \frac{s^*s_R}{s_R - s_L}(\Gamma_R - \Gamma_L)\mathbf{e}_\Gamma + \frac{s^*s_R}{s_R - s_L}(\Pi_R - \Pi_L)\mathbf{e}_\Pi.
\end{aligned} \tag{5.68b}$$

If $0 < s_L$:

$$\mathbf{D}^-(\mathbf{u}^-,\mathbf{u}^+) = \mathbf{f}(\mathbf{u}_L). \tag{5.68c}$$

$$\begin{aligned}
\mathbf{D}^+(\mathbf{u}^-,\mathbf{u}^+) &= -\mathbf{f}(\mathbf{u}_R) - \frac{1}{\Delta t}\left(\left(\frac{h}{2} + s_R\Delta t\right)\mathbf{u}_R + (s_R - s_L)\Delta t\mathbf{u}^* + s_L\Delta t\mathbf{u}_L\right) + \frac{h}{2\Delta t}\mathbf{u}_R,\\
&\overset{(5.64)}{=} -\mathbf{f}(\mathbf{u}_R) + s_R\mathbf{u}_R - s_L\mathbf{u}_L - s_R\mathbf{u}_R + s_L\mathbf{u}_L + \mathbf{f}(\mathbf{u}_R) - \mathbf{f}(\mathbf{u}_L)\\
&\quad + s^*(\Gamma_R - \Gamma_L)\mathbf{e}_\Gamma + s^*(\Pi_R - \Pi_L)\mathbf{e}_\Pi,\\
&= -\mathbf{f}(\mathbf{u}_L) + s^*(\Gamma_R - \Gamma_L)\mathbf{e}_\Gamma + s^*(\Pi_R - \Pi_L)\mathbf{e}_\Pi.
\end{aligned} \tag{5.68d}$$

If $s_R < 0$:

$$\begin{aligned}
\mathbf{D}^-(\mathbf{u}^-,\mathbf{u}^+) &= \mathbf{f}(\mathbf{u}_L) - \frac{1}{\Delta t}\left(-s_R\Delta t\mathbf{u}_R + (s_R - s_L)\Delta t\mathbf{u}^* + \left(s_L\Delta t + \frac{h}{2}\right)\mathbf{u}_L\right) + \frac{h}{2\Delta t}\mathbf{u}_L,\\
&\overset{(5.64)}{=} \mathbf{f}(\mathbf{u}_L) + s_R\mathbf{u}_R - s_L\mathbf{u}_L - s_R\mathbf{u}_R + s_L\mathbf{u}_L + \mathbf{f}(\mathbf{u}_R) - \mathbf{f}(\mathbf{u}_L)\\
&\quad + s^*(\Gamma_R - \Gamma_L)\mathbf{e}_\Gamma + s^*(\Pi_R - \Pi_L)\mathbf{e}_\Pi,\\
&= \mathbf{f}(\mathbf{u}_R) + s^*(\Gamma_R - \Gamma_L)\mathbf{e}_\Gamma + s^*(\Pi_R - \Pi_L)\mathbf{e}_\Pi.
\end{aligned} \tag{5.68e}$$

$$\mathbf{D}^+(\mathbf{u}^-,\mathbf{u}^+) = -\mathbf{f}(\mathbf{u}_R). \tag{5.68f}$$

□

Note that the contribution from the nonconservative term in (5.54) prevents the proof of entropy consistency of the HLL solver with (5.58). Indeed from (5.54) we have

$$\begin{aligned}\int_{-h/2}^{h/2} \mathbf{W}^{\text{HLL}}\left(\frac{x}{\Delta t};\mathbf{u}_L,\mathbf{u}_R\right)dx = \int_{-h/2}^{h/2}\mathbf{W}\left(\frac{x}{\Delta t};\mathbf{u}_L,\mathbf{u}_R\right)dx \\ + (u^*-s^*)\left((\Gamma_R-\Gamma_L)\mathbf{e}_\Gamma + (\Pi_R-\Pi_L)\mathbf{e}_\Pi\right),\end{aligned} \tag{5.69}$$

where consistency with (5.54) would require s^* to be equal to u^* and thus one needs to solve the exact Riemann problem. Here $\mathbf{u}^*$ is not the avarage of the exact Riemann solution over $(s_L\Delta t, s_R\Delta t)$ and we cannot apply the Jensen's inequality to prove that $\mathbf{W}^{\text{HLL}}\left(\frac{x}{\Delta t};\mathbf{u}_L,\mathbf{u}_R\right)$ satisfies (5.58) as done in [69].

Moreover, this solver is known to smear contacts [136] and has to be modified to preserve uniform velocity and pressure profiles across material interfaces. We thus consider a HLLC like solver in the next section.

5.4.2 HLLC Riemann solver

The HLLC solver [9, 136] considers a three wave configuration that splits the state vector into four constant states, see Figure 5-1. Therefore, the approximate solution takes the following form:

$$\mathcal{W}^{\text{HLLC}}\left(\frac{x}{t};\mathbf{u}_L,\mathbf{u}_R\right) = \begin{cases} \mathbf{u}_L, & \frac{x}{t} < s_L, \\ \mathbf{u}_L^*, & s_L < \frac{x}{t} < s^*, \\ \mathbf{u}_R^*, & s^* < \frac{x}{t} < s_R, \\ \mathbf{u}_R, & s_R < \frac{x}{t}, \end{cases} \tag{5.70}$$

where the speed of the central wave, s^*, is considered, which approximates a contact wave, along with s_L and s_R. The integral of the approximate solution (5.70) over $\left[\frac{-h}{2},\frac{h}{2}\right]$ at time Δt can be split as

$$\begin{aligned}\int_{-h/2}^{h/2}\mathcal{W}^{\text{HLLC}}\left(\frac{x}{\Delta t};\mathbf{u}_L,\mathbf{u}_R\right)dx = \left(\frac{h}{2}-s_R\Delta t\right)\mathbf{u}_R + \Delta t(s_R-s^*)\mathbf{u}_R^* \\ + \Delta t(s^*-s_L)\mathbf{u}_L^* + \left(s_L\Delta t+\frac{h}{2}\right)\mathbf{u}_L.\end{aligned} \tag{5.71}$$

We now, explicitly, define the intermediate states. We impose

$$\int_{s_L\Delta t}^{s_R\Delta t}\mathcal{W}^{\text{HLLC}}\left(\frac{x}{\Delta t};\mathbf{u}_L,\mathbf{u}_R\right)dx = \int_{s_L\Delta t}^{s_R\Delta t}\mathcal{W}^{\text{HLL}}\left(\frac{x}{\Delta t};\mathbf{u}_L,\mathbf{u}_R\right)dx, \tag{5.72}$$

which results in

$$(s_R-s_L)\mathbf{u}^* = (s^*-s_L)\mathbf{u}_L^* + (s_R-s^*)\mathbf{u}_R^*. \tag{5.73}$$

If we introduce the definition of the HLL state vector in the star region (5.64), we obtain

$$\begin{aligned} s_R\mathbf{u}_R - s_L\mathbf{u}_L - \mathbf{f}(\mathbf{u}_R) + \mathbf{f}(\mathbf{u}_L) - s^*(\Gamma_R - \Gamma_L)\mathbf{e}_\Gamma - s^*(\Pi_R - \Pi_L)\mathbf{e}_\Pi \\ = (s^* - s_L)\mathbf{u}_L^* + (s_R - s^*)\mathbf{u}_R^*, \end{aligned} \tag{5.74}$$

and considering the terms related to Γ and Π, and using (5.66) we get

$$(s_R - s^*)\Gamma_R + (s^* - s_L)\Gamma_L = (s^* - s_L)\Gamma_L^* + (s_R - s^*)\Gamma_R^*, \tag{5.75a}$$
$$(s_R - s^*)\Pi_R + (s^* - s_L)\Pi_L = (s^* - s_L)\Pi_L^* + (s_R - s^*)\Pi_R^*, \tag{5.75b}$$

from where it is evident that

$$\begin{aligned} \Gamma_L^* = \Gamma_L, \quad \Gamma_R^* = \Gamma_R, \\ \Pi_L^* = \Pi_L, \quad \Pi_R^* = \Pi_R, \end{aligned} \tag{5.76}$$

meaning that Γ and Π are continuous across shocks and may be discontinuous across intermediate waves.

We now define the intermediate states for the HLLC solver, where the conserved quantities in $\mathbf{u}_L^*$ and $\mathbf{u}_R^*$ can be computed by imposing the Rankine-Hugoniot relations across s_L and s_R

$$\begin{aligned} \mathbf{f}(\mathbf{u}_L^*) - \mathbf{f}(\mathbf{u}_L) = s_L(\mathbf{u}_L^* - \mathbf{u}_L), \\ \mathbf{f}(\mathbf{u}_R^*) - \mathbf{f}(\mathbf{u}_R) = s_R(\mathbf{u}_R^* - \mathbf{u}_R). \end{aligned} \tag{5.77}$$

Let us introduce the mass fluxes [135] as

$$Q_L = \rho_L(u_L - s_L) > 0, \quad Q_R = \rho_R(s_R - u_R) > 0, \tag{5.78}$$

which leads to the following definition of the velocity in the star regions:

$$u_L^* = u_L - \frac{\mathrm{p}_L^* - \mathrm{p}_L}{Q_L}, \quad u_R^* = u_R + \frac{\mathrm{p}_R^* - \mathrm{p}_R}{Q_R}. \tag{5.79}$$

If we further impose the continuity of the velocity and the pressure across the intermediate wave, $u_L^\star = u_R^\star = u^\star$ and $p_L^\star = p_R^\star = p^\star$, we obtain

$$\frac{\mathrm{p}^* - \mathrm{p}_R}{Q_R} + \frac{\mathrm{p}^* - \mathrm{p}_L}{Q_L} + u_R - u_L = 0, \tag{5.80}$$

which gives the expression for the pressure in the intermediate states

$$\mathrm{p}^* = \frac{Q_L\mathrm{p}_R + Q_R\mathrm{p}_L + Q_RQ_L(u_L - u_R)}{Q_L + Q_R}. \tag{5.81}$$

Similarly by equating the pressure in (5.79), we have

$$s^* = \frac{\mathrm{p}_L - \mathrm{p}_R + Q_Lu_L + Q_Ru_R}{Q_L + Q_R}. \tag{5.82}$$

Note that the value of s^* in (5.82) corresponds to the one in the HLL fluxes (5.65).

The other states can directly be obtained following the Rankine-Hugoniot relation (5.77),

also see [135]:

$$\rho_L^* = \frac{u_L - s_L}{s^* - s_L}\rho_L, \tag{5.83a}$$

$$e_L^* = e_L + (s^* - u_L)\left(\frac{s^* - u_L}{2} - \frac{\mathrm{p}_L}{Q_L}\right), \tag{5.83b}$$

$$E_L^* = E_L + (s^* - u_L)(s^* - \frac{\mathrm{p}_L}{Q_L}), \tag{5.83c}$$

$$\rho_R^* = \frac{s_R - u_R}{s_R - s^*}\rho_R, \tag{5.83d}$$

$$e_R^* = e_R + (s^* - u_R)\left(\frac{s^* - u_R}{2} + \frac{\mathrm{p}_R}{Q_R}\right), \tag{5.83e}$$

$$E_R^* = E_R + (s^* - u_R)\left(s^* + \frac{\mathrm{p}_R}{Q_R}\right). \tag{5.83f}$$

Again, the numerical fluxes at interfaces are defined so as to satisfy a discrete version of (5.55):

$$\mathbf{D}^-(\mathbf{u}^-, \mathbf{u}^+) = \begin{cases} \mathbf{f}(\mathbf{u}_L), & 0 < s_L, \\ \mathbf{f}(\mathbf{u}_L) + s_L(\mathbf{u}_L^* - \mathbf{u}_L), & s_L < 0 < s*, \\ \mathbf{f}(\mathbf{u}_R) + s_R(\mathbf{u}_R^* - \mathbf{u}_R) + s^*(\Gamma_R - \Gamma_L)\mathbf{e}_\Gamma + s^*(\Pi_R - \Pi_L)\mathbf{e}_\Pi, & s^* < 0 < s_R, \\ \mathbf{f}(\mathbf{u}_R) + s^*(\Gamma_R - \Gamma_L)\mathbf{e}_\Gamma + s^*(\Pi_R - \Pi_L)\mathbf{e}_\Pi, & s_R < 0, \end{cases} \tag{5.84a}$$

$$\mathbf{D}^+(\mathbf{u}^-, \mathbf{u}^+) = \begin{cases} \mathbf{f}(\mathbf{u}_L) - s^*(\Gamma_R - \Gamma_L)\mathbf{e}_\Gamma - s^*(\Pi_R - \Pi_L)\mathbf{e}_\Pi, & 0 < s_L, \\ \mathbf{f}(\mathbf{u}_L) + s_L(\mathbf{u}_L^* - \mathbf{u}_L) - s^*(\Gamma_R - \Gamma_L)\mathbf{e}_\Gamma - s^*(\Pi_R - \Pi_L)\mathbf{e}_\Pi, & s_L < 0 < s*, \\ \mathbf{f}(\mathbf{u}_R) + s_R(\mathbf{u}_R^* - \mathbf{u}_R), & s^* < 0 < s_R, \\ \mathbf{f}(\mathbf{u}_R), & s_R < 0. \end{cases} \tag{5.84b}$$

Note that by construction the numerical fluxes (5.84) satisfy

$$\begin{aligned} \mathbf{D}^-(\mathbf{u}_L, \mathbf{u}_R) &= \mathbf{f}\left(\boldsymbol{\mathcal{W}}^{\mathrm{HLLC}}\left(\frac{x}{\Delta t}, \mathbf{u}_L, \mathbf{u}_R\right)\right) + s^{*^-}(\Gamma_R - \Gamma_L)\mathbf{e}_\Gamma + s^{*^-}(\Pi_R - \Pi_L)\mathbf{e}_\Pi, \\ \mathbf{D}^+(\mathbf{u}_L, \mathbf{u}_R) &= -\mathbf{f}\left(\boldsymbol{\mathcal{W}}^{\mathrm{HLLC}}\left(\frac{x}{\Delta t}, \mathbf{u}_L, \mathbf{u}_R\right)\right) + s^{*^+}(\Gamma_R - \Gamma_L)\mathbf{e}_\Gamma + s^{*^+}(\Pi_R - \Pi_L)\mathbf{e}_\Pi. \end{aligned} \tag{5.85}$$

Finally, the HLLC solver (5.70) satisfies the consistency condition (5.54) with $u^\star$ replaced by $s^\star$and the three-point scheme reads

$$\mathbf{U}_j^{n+1} - \mathbf{U}_j^n + \frac{\Delta t}{\Delta x}\left(\mathbf{D}^-(\mathbf{U}_j^n, \mathbf{U}_{j+1}^n) + \mathbf{D}^+(\mathbf{U}_{j-1}^n, \mathbf{U}_j^n)\right) = 0, \tag{5.86}$$

with

$$\mathbf{U}_j^{n+1} = \frac{1}{\Delta x}\int_{x_{j-1/2}}^{x_j} \boldsymbol{\mathcal{W}}^{\text{HLLC}}\left(\frac{x}{\Delta t}; \mathbf{U}_{j-1}^n, \mathbf{U}_j^n\right) dx + \frac{1}{\Delta x}\int_{x_j}^{x_j+1/2} \boldsymbol{\mathcal{W}}^{\text{HLLC}}\left(\frac{x}{\Delta t}; \mathbf{U}_j^n, \mathbf{U}_{j+1}^n\right) dx. \tag{5.87}$$

5.4.3 PROPERTIES OF THE HLLC SOLVER

In this section, we analyse the properties of the numerical scheme (5.86) using fluxes (5.84), where the time step $\Delta t > 0$ is assumed to satisfy the CFL condition

$$\frac{\Delta t}{\Delta x}\max_{j\in\mathbb{Z}}\left(\left|s_R(\mathbf{U}_j^n)\right|, \left|s_L(\mathbf{U}_j^n)\right|\right) \le \frac{1}{2}, \tag{5.88}$$

with Δt small enough so that the left and right waves do not interact. The wave speeds s_L and s_R are defined in section 5.4.3.

Discrete entropy inequality

We are interested in the nonlinear stability of the scheme (5.86). Here we use the technique from [12] to prove the entropy inequality in integral form (5.59) for the HLLC solution (5.70) and propose sufficient conditions on the intermediate states that enforce the required stability.

Note that in the following theorem we refer to the physical entropy $s_i(\rho_i, \theta) \to s_i(\tau_i, e_i)$ as a strictly convex function, where $\tau_i = 1/\rho_i$.

Theorem 5.4.2. *Suppose that condition (5.88) on the time step holds. Assume that the intermediate states in the HLLC solver (5.70), $\mathbf{u}_L^\star$ and $\mathbf{u}_R^\star$, satisfy $\mathbf{u}_L^*, \mathbf{u}_R^* \in \Omega_{\text{GM}}$ together with*

$$s(\mathbf{u}_L^*) \ge s(\mathbf{u}_L), \quad s(\mathbf{u}_R^*) \ge s(\mathbf{u}_R), \tag{5.89}$$

for the physical entropy of the mixture (5.16), then the numerical scheme (5.86) satisfies the entropy inequality (5.59) with the consistent numerical fluxes

$$Q(\boldsymbol{U}_{j-1}^n, \boldsymbol{U}_j^n) = q(\boldsymbol{U}_j^n) + \frac{1}{\Delta t}\int_{x_{j-1/2}}^{x_j} \eta\left(\boldsymbol{\mathcal{W}}^{\text{HLLC}}\left(\frac{x}{\Delta t}; \boldsymbol{U}_{j-1}^n, \boldsymbol{U}_j^n\right)\right) dx - \frac{\Delta x}{2\Delta t}\eta\left(\boldsymbol{U}_j^n\right). \tag{5.90}$$

Proof. We first prove the entropy inequality in integral form (5.58) using (5.71), so we have

$$
\begin{aligned}
&\int_{-h/2}^{h/2} \eta\left(\boldsymbol{\mathcal{W}}^{\text{HLLC}}\left(\frac{x}{\Delta t};\mathbf{u}_L,\mathbf{u}_R\right)\right)dx \\
&= \left(s_L\Delta t+\frac{h}{2}\right)\eta(\mathbf{u}_L)+(s^*-s_L)\Delta t\eta(\mathbf{u}_L^*)+(s_R-s^*)\Delta t\eta(\mathbf{u}_R^*)+\left(\frac{h}{2}-s_R\Delta t\right)\eta(\mathbf{u}_R), \\
&\overset{(5.15)}{=} \frac{h}{2}(\eta(\mathbf{u}_L)+\eta(\mathbf{u}_R))-\Delta t\Big(s_L\rho_L s(\mathbf{u}_L)+(s^*-s_L)\rho_L^* s(\mathbf{u}_L^*)\Big) \\
&\qquad\qquad -\Delta t\Big((s_R-s^*)\rho_R^* s(\mathbf{u}_R^*)-s_R\rho_R s(\mathbf{u}_R)\Big), \\
&\overset{(5.89)}{\leq} \frac{h}{2}\big(\eta(\mathbf{u}_L)+\eta(\mathbf{u}_R)\big)-\Delta t s(\mathbf{u}_L)\big(s_L\rho_L+(s^*-s_L)\rho_L^*\big)-\Delta t((s_R-s^*)\rho_R^*-s_R\rho_R)s(\mathbf{u}_R), \\
&= \frac{h}{2}(\eta(\mathbf{u}_L)+\eta(\mathbf{u}_R))-\Delta t(\rho_R u_R s(\mathbf{u}_R)-\rho_L u_L s(\mathbf{u}_L)),
\end{aligned}
\tag{5.91}
$$

where we have used the first component of the Rankine-Hugoniot relations (5.77).

As a consequence, setting $\mathbf{u}_L = \mathbf{U}_j^n$ and $\mathbf{u}_R = \mathbf{U}_{j+1}^n$, the numerical flux (5.90) satisfies

$$
Q(\mathbf{U}_j^n,\mathbf{U}_{j+1}^n) \leq q(\mathbf{U}_j^n)-\frac{1}{\Delta x}\int_{x_j}^{x+1/2}\eta\left(\boldsymbol{\mathcal{W}}^{\text{HLLC}}\left(\frac{x}{\Delta t};\mathbf{U}_j^n,\mathbf{U}_{j+1}^n\right)\right)dx+\frac{\Delta x}{2\Delta t}\eta(\mathbf{U}_j^n), \tag{5.92}
$$

and using (5.87) we have the following relation through Jensen's inequality for the convex entropy function (5.15)

$$
\begin{aligned}
\eta(\mathbf{U}_j^{n+1}) &\leq \frac{1}{\Delta x}\int_{x_{j-1/2}}^{x_j}\eta\left(\boldsymbol{\mathcal{W}}^{\text{HLLC}}\left(\frac{x}{\Delta t};\mathbf{U}_{j-1}^n,\mathbf{U}_j^n\right)\right)dx \\
&\qquad +\frac{1}{\Delta x}\int_{x_j}^{x_{j+1/2}}\eta\left(\boldsymbol{\mathcal{W}}^{\text{HLLC}}\left(\frac{x}{\Delta t};\mathbf{U}_j^n,\mathbf{U}_{j+1}^n\right)\right)dx, \\
&\underset{(5.92)}{\overset{(5.90)}{\leq}} \frac{\Delta t}{\Delta x}\left(Q(\mathbf{U}_{j-1}^n,\mathbf{U}_j^n)-q(\mathbf{U}_j^n)+\frac{\Delta x}{2\Delta t}\eta(\mathbf{U}_j^n))\right) \\
&\qquad +\frac{\Delta t}{\Delta x}\left(-Q(\mathbf{U}_j^n,\mathbf{U}_{j+1}^n)+q(\mathbf{U}_j^n)+\frac{\Delta x}{2\Delta t}\eta(\mathbf{U}_j^n)\right), \\
&= \eta(\mathbf{U}_j^n)-\frac{\Delta t}{\Delta x}\Big(Q(\mathbf{U}_j^n,\mathbf{U}_{j+1}^n)-Q(\mathbf{U}_{j-1}^n,\mathbf{U}_j^n)\Big).
\end{aligned}
\tag{5.93}
$$

□

We now clarify the conditions on the wave speed estimates under which (5.89) hold.

Lemma 5.4.1. *There exist wave speed estimates s_L and s_R large enough so that they are bounds of the minimum and maximum wave speeds in the exact Riemann weak solution of (5.1a) with initial data (5.51), and so that (5.89) holds.*

Proof. The first result is obvious by the finiteness of the wave speeds in the exact Riemann solution. Then, we need to check that $\mathbf{u}_L^*$ and $\mathbf{u}_R^*$ satisfy the local entropy minimum principle (5.89) introduced in [11, §4.2], which is a wave-by-wave condition provided the scheme is consistent with the integral form of (5.1a). Using $\Gamma_X^* = \Gamma_X$ and $\Pi_X^* = \Pi_X$, the invariance

principle in [11, Theorem 3.3] reads

$$\mathrm{p}^* + \frac{Q_X^2}{\rho_X^*} = \mathrm{p}_X + \frac{Q_X^2}{\rho_X}, \tag{5.94a}$$

$$e_X^* - \frac{(\mathrm{p}^*)^2}{2Q_X^2} = e_X - \frac{\mathrm{p}_X^2}{2Q_X^2}, \quad X = L, R. \tag{5.94b}$$

The first is a direct consequence of (5.79) and (5.83a,5.83d), while eliminating p^* from the above relations and using (5.83a,5.83d) give (5.83b,5.83e). So the assumptions of [12, Theorem 2.3] are met. □

We finally link the discrete entropy inequality (5.58) to the entropy stable character of the numerical fluxes (3.52), so that the HLLC fluxes can be used at the interfaces in the DGSEM scheme to prove a semi-discrete entropy inequality.

Corollary 5.4.1. *Let a three-point scheme of the form (5.86) for the discretization of (5.1a). Then, the entropy inequality (5.58) implies the entropy stability of the numerical fluxes in the sense of [24]:*

$$\boldsymbol{\eta}'(\mathbf{u}_L)^\top \mathbf{D}^-(\mathbf{u}_L, \mathbf{u}_R) + \boldsymbol{\eta}'(\mathbf{u}_R)^\top \mathbf{D}^+(\mathbf{u}_L, \mathbf{u}_R) \geq q(\mathbf{u}_R) - \boldsymbol{\eta}'(\mathbf{u}_R)^\top \mathbf{f}(\mathbf{u}_R) - q(\mathbf{u}_L) + \boldsymbol{\eta}'(\mathbf{u}_L)^\top \mathbf{f}(\mathbf{u}_L), \tag{5.95}$$

for all $\mathbf{u}_L, \mathbf{u}_R \in \Omega_\star$.

Proof. Indeed, let $\mathbf{U}_{j-1}^n = \mathbf{U}_j^n = \mathbf{u}_L$ and $\mathbf{U}_{j+1}^n = \mathbf{u}_R$ then from (5.58) and (5.86), we obtain

$$\mathbf{U}_j^{n+1} = \mathbf{u}_L - \frac{\Delta t}{\Delta x} \mathbf{D}^-(\mathbf{u}_L, \mathbf{u}_R), \tag{5.96}$$

and

$$\eta\left(\mathbf{u}_L - \frac{\Delta t}{\Delta x} \mathbf{D}^-(\mathbf{u}_L, \mathbf{u}_R)\right) \leq \eta(\mathbf{u}_L) - \frac{\Delta t}{\Delta x}\left(Q(\mathbf{u}_L, \mathbf{u}_R) - q(\mathbf{u}_L)\right). \tag{5.97}$$

Likewise, using $\mathbf{U}_{j-1}^n = \mathbf{u}_L$ and $\mathbf{U}_j^n = \mathbf{U}_{j+1}^n = \mathbf{u}_R$, we get

$$\mathbf{U}_j^{n+1} = \mathbf{u}_R - \frac{\Delta t}{\Delta x} \mathbf{D}^+(\mathbf{u}_L, \mathbf{u}_R) \tag{5.98}$$

and

$$\eta\left(\mathbf{u}_R - \frac{\Delta t}{\Delta x} \mathbf{D}^+(\mathbf{u}_L, \mathbf{u}_R)\right) \leq \eta(\mathbf{u}_R) - \frac{\Delta t}{\Delta x}\left(q(\mathbf{u}_R) - Q(\mathbf{u}_L, \mathbf{u}_R)\right). \tag{5.99}$$

Summing (5.97) and (5.99) gives

$$\begin{aligned} \eta\left(\mathbf{u}_L - \frac{\Delta t}{\Delta x} \mathbf{D}^-(\mathbf{u}_L, \mathbf{u}_R)\right) + \eta\left(\mathbf{u}_R - \frac{\Delta t}{\Delta x} \mathbf{D}^+(\mathbf{u}_L, \mathbf{u}_R))\right) \\ \leq \eta(\mathbf{u}_L) + \eta(\mathbf{u}_R) - \frac{\Delta t}{\Delta x}\left(q(\mathbf{u}_R) - q(\mathbf{u}_L)\right), \end{aligned} \tag{5.100}$$

and letting $\Delta t \to 0^+$ with fixed Δx, we obtain (5.95). □

Preservation of uniform states

We, first, verify that the three-point scheme (5.86), with numerical fluxes (5.84), satisfy the Abgrall criterion [1].

Let us consider that the left and right states satisfy $u_L = u_R = u$ and $\mathrm{p}_L = \mathrm{p}_R = \mathrm{p}$, then (5.81) and (5.82) gives $\mathrm{p}^* = \mathrm{p}$ and $s^* = u$, respectively. As a result, the requirements (5.31) and (5.35)

$$D^{\pm}_{\rho u} - u D^{\pm}_{\rho} = \mathrm{p}, \quad D^{\pm}_{\rho E} - \frac{u^2}{2} D^{\pm}_{\rho} = u\left(\mathrm{p}\Gamma + \Pi\right), \tag{5.101}$$

are satisfied, respectively.

Now assume that $\Gamma_L = \Gamma_R$ and $\Pi_L = \Pi_R$, then $D^{\pm}_{\Gamma} = 0$ and $D^{\pm}_{\Pi} = 0$ and the fluxes reduce to the conservative HLLC solver for the Euler equations so pure phases are preserved.

Wave speed estimates

We propose wave speeds for the scheme [16]:

$$s_L = u_L - \tilde{c}_L, \quad s_R = u_R + \tilde{c}_R, \tag{5.102}$$

where

$$\left.\begin{aligned} \tilde{c}_L &= c_L + \tfrac{\gamma+1}{2}\left(\tfrac{\mathrm{p}_R - \mathrm{p}_L}{\rho_R c_R} + u_L - u_R\right)^+, \\ \tilde{c}_R &= c_R + \tfrac{\gamma+1}{2}\left(\tfrac{\mathrm{p}_L - \mathrm{p}_R}{\rho_L \tilde{c}_L} + u_L - c_L\right)^+, \end{aligned}\right\} \quad \text{if } \mathrm{p}_R \geq \mathrm{p}_L. \tag{5.103}$$

$$\left.\begin{aligned} \tilde{c}_R &= c_R + \tfrac{\gamma+1}{2}\left(\tfrac{\mathrm{p}_L - \mathrm{p}_R}{\rho_L c_L} + u_L - u_R\right)^+, \\ \tilde{c}_L &= c_L + \tfrac{\gamma+1}{2}\left(\tfrac{\mathrm{p}_R - \mathrm{p}_L}{\rho_R \tilde{c}_R} + u_L - u_R\right)^+, \end{aligned}\right\} \quad \text{if } \mathrm{p}_L \geq \mathrm{p}_R, \tag{5.104}$$

and $\gamma = \max_X \gamma_X$, $c_X = \sqrt{\gamma(\mathrm{p}_X + \mathrm{p}_{\infty_X})/\rho_X}$ for $X = L, R$.

These wave speeds estimates will also bound the exact Riemann solution for pure phases. In the general case when $\Gamma_L \neq \Gamma_R$ and $\Pi_L \neq \Pi_r$, it is difficult to guaranty such properties. We refer to [98] for such an analysis in the case of a conservative multi-species model. However, these estimates are sufficient for our purpose since the entropy inequality is relevant for pure phases only.

Positivity of solution

According to [9], a numerical scheme preserves positivity of solution if it updates values from a convex averaging [50] of the states that appear in the exact or approximate solution to the Riemann problem.

Indeed, from (5.87), $\mathbf{U}_j^{n+1}$ results from the cell average of the HLLC solution at left and right interfaces. Therefore, assuming that the left and right states are positive, we first show that the density and the total internal energy in the intermediate states are positive.

The proof for positivity of density in the star region can be directly stated following its definition in (5.83a) and (5.83d), where s_X is always greater than u_X and s^* for $X = L, R$.

Positivity of the internal energy in the star region requires satisfying the following condition

$$\rho_X^* e_X^* > \mathrm{p}_{\infty_X}, \quad X = L, R, \tag{5.105}$$

to hold in the intermediate states. We now consider the left star state $\mathbf{u}_L^*$, with the corresponding results for the right star state following in a similar way. Therefore, we have from (5.105)

$$\begin{aligned}
&\rho_L^* \left(E_L^* - \frac{(s_L^*)^2}{2} \right) > \mathrm{p}_{\infty_L}, \\
\overset{(5.83)}{\Leftrightarrow}\ &\rho_L^* \left(E_L + s^*(s^* - u_L) - \frac{(s^*)^2}{2} + (s^* - u_L)\frac{\mathrm{p}_L}{\rho_L(s_L - u_L)} \right) > \mathrm{p}_{\infty_L}, \\
\Leftrightarrow\ &\rho_L^* \left(e_L + \frac{(u_L - s^*)^2}{2} + (s^* - u_L)\frac{\mathrm{p}_L}{\rho_L(u_L - s_L)} \right) > \mathrm{p}_{\infty_L}, \\
\overset{(5.83)}{\Leftrightarrow}\ &\left(\frac{u_L - s_L}{s^* - s_L} \right) \left(\frac{\mathrm{p}_L + \gamma_L \mathrm{p}_{\infty_L}}{\gamma_L - 1} \right) + \left(\frac{u_L - s_L}{s^* - s_L} \right) \frac{\rho_L (u_L - s^*)^2}{2} - \left(\frac{s^* - u_L}{s^* - s_L} \right) \mathrm{p}_L - \mathrm{p}_{\infty_L} > 0, \\
\Leftrightarrow\ &(u_L - s_L) \left(\frac{\mathrm{p}_L + \gamma_L \mathrm{p}_{\infty_L}}{\gamma_L - 1} \right) + (u_L - s_L)\frac{\rho_L}{2}\sigma^2 + \sigma \mathrm{p}_L - (s^* - s_L)\mathrm{p}_{\infty_L} > 0,
\end{aligned} \tag{5.106}$$

where $\sigma = u_L - s*$. Upon further simplification we get the following quadratic inequality

$$(u_L - s_L)\frac{\rho_L}{2}\sigma^2 - (\mathrm{p}_L + \mathrm{p}_{\infty_L})\sigma + (u_L - s_L)\left(\frac{\mathrm{p}_L + \mathrm{p}_{\infty_L}}{\gamma_L - 1} \right) > 0, \tag{5.107}$$

where the sign for the inequality holds for all $\sigma \in \mathbb{R}$ if the discriminant of (5.107) is negative

$$\begin{aligned}
\mathcal{D} &= (\mathrm{p}_L + \mathrm{p}_{\infty_L})^2 - 2\rho_L(u_L - s_L)^2 \left(\frac{\mathrm{p}_L + \gamma_L \mathrm{p}_{\infty_L}}{\gamma_L - 1} \right) < 0, \\
&= (\mathrm{p}_L + \mathrm{p}_{\infty_L})^2 - 2(u_L - s_L)^2 \frac{(\rho_L c_L)^2}{\gamma_L(\gamma_L - 1)} < 0.
\end{aligned} \tag{5.108}$$

The inequality (5.108) reveals the following bounds on the left wave speed

$$s_L < u_L - \sqrt{\frac{\gamma_L - 1}{2\gamma_L}} c_L, \tag{5.109}$$

which is satisfied by the wave speed estimates in section 5.4.3, since $\frac{\gamma_L - 1}{2\gamma_L} < 1$.

We also show that the fully discrete three-point scheme preserves the positivity of Γ and Π at time t^{n+1} and also satisfies a maximum principle. Here we demonstrate this for Γ, however a similar argument can be stated for Π.

Let us discretize the equation for Γ using forward Euler in time and the HLLC solver at the interface. Then we have,

$$\begin{aligned}
\Gamma_j^{n+1} &= \Gamma_j^n - \frac{\Delta t}{\Delta x} \left(s_{j+1/2}^{*,-} \left(\Gamma_{j+1}^n - \Gamma_j^n \right) + s_{j-1/2}^{*,+} \left(\Gamma_{j-1}^n - \Gamma_j^n \right) \right), \\
&= \left(1 - \frac{\Delta t}{\Delta x} \left(s_{j-1/2}^{*,+} - s_{j+1/2}^{*,-} \right) \right) \Gamma_j^n - \frac{\Delta t}{\Delta x} s_{j+1/2}^{*,-} \Gamma_{j+1}^n + \frac{\Delta t}{\Delta x} s_{j-1/2}^{*,+} \Gamma_{j-1}^n,
\end{aligned} \tag{5.110}$$

which shows that Γ at time $n+1$ is a convex combination of the cell-averaged Γ at time n. Hence Γ satisfies the discrete max-principle.

5.5 Properties of the DGSEM scheme

We recall here the main properties of the DGSEM scheme for the discretization of the gamma model with the numerical fluxes from section 5.3 and section 5.4.

First, the semi-discrete scheme (3.54) with the entropy conservative fluxes (5.44) in the volume integral and the HLLC flux (5.84) at the interface satisfy the semi-discrete entropy inequality (3.57) in the case of pure phases, see Theorem 3.5.1.

Then, we consider the fully discrete scheme (3.68) with forward Euler time-stepping. The scheme with the contact-preserving fluxes (5.36)-(5.37) in the volume integral, along with the HLLC solver at the interfaces, preserves uniform pressure and velocity profiles across material interfaces.

Finally, for both contact-preserving and entropy conservative numerical fluxes in the volume integral, the DGSEM (5.23) guarantees the positivity of the cell-averaged solution

$$\mathbf{U}_j^{k,n} \in \Omega_{\text{GM}} \forall 0 \leq k \leq p, \quad \Rightarrow \quad \langle \mathbf{u}_h^{n+1} \rangle \in \Omega_{\text{GM}}, \quad \forall j \in \mathbb{Z},$$

provided that the time step satisfies the following conditions

$$\frac{\Delta t}{h} \max_{j\in\mathbb{Z}} \left(\left| s^n_{L_{j+1/2}} \right|, \left| s^n_{R_{j-1/2}} \right| \right) \leq \frac{1}{p(p+1)}, \tag{5.111a}$$

$$\frac{\Delta t}{h} \max_{j\in\mathbb{Z}} \max_{0\leq k\leq p} \left(\sum_{l=0}^{p} \omega_l D_{lk} \mathbf{u}_j^{k,n} - \delta_{kp} s^{*,-}_{j+1/2} + \delta_{k0} s^{*,+}_{j-1/2} \right) \leq \frac{1}{2}. \tag{5.111b}$$

Indeed, the cell average of (3.68) gives (3.60) according to Theorem 3.5.1. For the first three components of (5.1a), $X = \rho, \rho u, \rho E$, this gives [145]

$$\begin{aligned} \langle X_h \rangle_j^{n+1} &= \langle X_h \rangle_j^n - \frac{\Delta t}{h} \left(h_X \left(\mathbf{U}_j^{p,n}, \mathbf{U}_{j+1}^{0,n} \right) - h_X \left(\mathbf{U}_{j-1}^{p,n}, \mathbf{U}_j^{0,n} \right) \right) \\ &= \sum_{k=1}^{p-1} \frac{\omega_k}{2} X_j^{k,n} + \frac{\omega_p}{2} \left(X_j^{p,n} - \frac{2\Delta t}{\omega_p h} \left(h_X \left(\mathbf{U}_j^{p,n}, \mathbf{U}_{j+1}^{0,n} \right) - h_X \left(\mathbf{U}_j^{0,n}, \mathbf{U}_j^{p,n} \right) \right) \right) \\ &+ \frac{\omega_0}{2} \left(X_j^{0,n} - \frac{2\Delta t}{\omega_0 h} \left(h_X \left(\mathbf{U}_j^{0,n}, \mathbf{U}_j^{p,n} \right) - h_X \left(\mathbf{U}_{j-1}^{p,n}, \mathbf{U}_j^{0,n} \right) \right) \right), \end{aligned} \tag{5.112}$$

which is a convex combination of positive quantities under (5.111a), since the HLLC solver is positive under (5.88) and $\omega_0 = \omega_p = \frac{p(p+1)}{2}$.

Moreover, the last two components, now $X = \Gamma, \Pi$ satisfy

$$\begin{aligned}\langle X_h\rangle_j^{n+1} &= \langle X_h\rangle_j^n - \frac{\Delta t}{h}\left(\sum_{k,l=0}^{p}\omega_k D_{kl}u_j^{k,n}X_j^{l,n} + s_{j+1/2}^{*,-}\left(X_{j+1}^{0,n} - X_j^{p,n}\right) + s_{j-1/2}^{*,+}\left(X_j^{0,n} - X_{j-1}^{p,n}\right)\right)\\ &= \sum_{k=0}^{p}\left(\frac{\omega_k}{2} - \frac{\Delta t}{h}\left(\sum_{l=0}^{p}\omega_l D_{kl}u_j^{l,n} - \delta_{kp}s_{j+1/2}^{*,-} + \delta_{k0}s_{j-1/2}^{*,+}\right)\right)X_j^{k,n}\\ &+ \frac{\Delta t}{h}\left(-s_{j+1/2}^{*,-}X_{j+1}^{0,n} + s_{j-1/2}^{*,+}X_{j-1}^{p,n}\right),\end{aligned} \tag{5.113}$$

which is indeed positive under (5.111a).

We further enforce the positivity of the solution at the nodal values by the use of limiters which are introduced in section 5.6.

5.6 A POSTERIORI LIMITERS

We impose positivity of the solution at the nodal values by using a posteriori limiters as proposed in [37, 139, 145, 146]. In this work we limit the mixture density, the total internal energy and the Γ and Π terms. The solution at time $n+1$ after applying the limiter reads

$$\tilde{\mathbf{U}}_j^{k,n+1} = \theta_j\left(\mathbf{U}_j^{k,n+1} - \langle \mathbf{u}_h\rangle_j^{(n+1)}\right) + \langle \mathbf{u}_h\rangle_j^{(n+1)}, \quad 0 \le k \le p, \quad j \in \mathbb{Z}, \tag{5.114}$$

where

$$\langle \mathbf{u}_h\rangle_j^{(n+1)} = \sum_{k=0}^{p}\frac{\omega_k}{2}\mathbf{U}_j^k(t), \quad 0 \le k \le p, \tag{5.115}$$

is the cell-averaged solution and $0 \le \theta_j \le 1$ is the limiter which is defined based on the variable that needs limiting $\theta_j = \min(\theta_j^{\rho}, \theta_j^{\rho e}, \theta_j^{\Gamma})$.

- Limiting the mixture density:

$$\tilde{\rho}_j^{k,n+1} = \theta_j^{\rho}\left(\rho_j^{k,n+1} - \langle \rho_h\rangle_j^{(n+1)}\right) + \langle \rho_h\rangle_j^{(n+1)}, \quad 0 \le k \le p, \quad j \in \mathbb{Z}, \tag{5.116}$$

  where

$$\theta_j^{\rho} = \min\left(\frac{\langle \rho_h\rangle_j^{(n+1)} - \epsilon}{\langle \rho_h\rangle_j^{(n+1)} - \rho_j^{\min}}, 1\right), \quad \rho_j^{\min} = \min_{0\le k\le p}\rho_j^{k,n+1}. \tag{5.117}$$

- Limiting the mixture total internal energy:

$$\begin{pmatrix}\tilde{\rho}\\ \tilde{\rho u}\\ \tilde{\rho E}\end{pmatrix}_j^{k,n+1} = \theta_j^{\rho e}\begin{pmatrix}\rho_j^{k,n+1} - \langle \rho_h\rangle_j^{(n+1)}\\ \rho u_j^{k,n+1} - \langle \rho u_h\rangle_j^{(n+1)}\\ \rho E_j^{k,n+1} - \langle \rho E_h\rangle_j^{(n+1)}\end{pmatrix} + \begin{pmatrix}\langle \rho_h\rangle_j^{(n+1)}\\ \langle \rho u_h\rangle_j^{(n+1)}\\ \langle \rho E_h\rangle_j^{(n+1)}\end{pmatrix}, \quad 0 \le k \le p, \quad j \in \mathbb{Z}, \tag{5.118}$$

where

$$\theta_j^{\rho e} = \min\left(\frac{\rho e_h(\langle \mathbf{u}_h\rangle_j^{n+1}) - \langle \mathrm{p}_\infty\rangle_j^{n+1} + \epsilon}{\rho e_h(\langle \mathbf{u}_h\rangle_j^{n+1}) - \rho e_j^{\min}}, 1\right), \quad \rho e_j^{\min} = \min_{0\le k\le p} \rho e_j^{k,n+1}, \tag{5.119}$$

and $\rho e_h(\langle \mathbf{u}_h\rangle_j^{n+1}) = \rho E_h(\langle \mathbf{u}_h\rangle_j^{n+1}) - \frac{(\rho u_h(\langle \mathbf{u}_h\rangle_j^{n+1}))^2}{2\rho(\langle \mathbf{u}_h\rangle_j^{n+1})}$, see [139].

- Limiting Γ:

$$\tilde{\Gamma}_j^{k,n+1} = \theta_j^{\Gamma}\left(\Gamma_j^{k,n+1} - \langle \Gamma_h\rangle_j^{(n+1)}\right) + \langle \Gamma_h\rangle_j^{(n+1)}, \tag{5.120}$$

where

$$\theta_j^{\Gamma} = \min\left(\frac{\langle \Gamma_h\rangle_j^{(n+1)} - m_\Gamma}{\langle \Gamma_h\rangle_j^{(n+1)} - \Gamma_j^{\min}}, \frac{M_\Gamma - \langle \Gamma_h\rangle_j^{(n+1)}}{\Gamma_j^{\max} - \langle \Gamma_h\rangle_j^{(n+1)}}, 1\right), \tag{5.121}$$

and

$$\Gamma_j^{\min} = \min_{0\le k\le p} \Gamma_j^{k,n+1}, \quad \Gamma_j^{\max} = \max_{0\le k\le p} \Gamma_j^{k,n+1}, \quad m_\Gamma = \min_{i=1,2} \frac{1}{\gamma_i - 1}, \quad M_\Gamma = \max_{i=1,2} \frac{1}{\gamma_i - 1}, \tag{5.122}$$

Note that in (5.117) and (5.119), $0 < \epsilon \ll 1$ is a small parameter, which we set as $\epsilon = 10^{-8}$ in our numerical tests. The limiter (5.116) and (5.118) guarantees that $\tilde{\rho}_j^{0\le k\le p,n+1} > 0$ and $\tilde{\rho e}_j^{0\le k\le p,n+1} > 0$, respectively. Recalling (5.8), it is understood that

$$\min_{i=1,2} \frac{1}{\gamma_i - 1} \le \Gamma \le \max_{i=1,2} \frac{1}{\gamma_i - 1}, \tag{5.123}$$

as the void fraction is assumed to satisfy $0 \le \alpha_i \le 1$ and (5.4). Therefore, (5.120) imposes the following maximum principle

$$m_\Gamma \le \tilde{\Gamma}_j^{0\le k\le p,n+1} \le M_\Gamma, \tag{5.124}$$

following (5.8), where the above inequalities also hold on Π hold for two species only.

5.7 Numerical tests

We, now, perform some numerical tests using the semi-discrete scheme (5.23) for the SG-gamma model (5.1)-(5.2) to assess its qualities of contact preservation, high-order accuracy and the nonlinear stability, as described in section 5.5. The numerical scheme was implemented in the in-house CFD code *Aghora* at ONERA [112], and we subject it to numerical tests which are borrowed from [31, 37, 38, 42, 80]. Note that, as part of our algorithm, the numerical fluxes in the volume integral switches between contact preserving numerical fluxes (5.36)-(5.37) and entropy conservative fluxes (5.44), based on values of the TCI function (5.49) relative to a threshold. We thus set the TCI threshold belongs in the range $[0.01, 0.03]$.

The numerical tests include Riemann problems on one spatial dimension, where we consider a computational domain comprising of 100 elements. All numerical tests are performed at fourth-order accuracy ($p = 3$) in space, while the time integration is performed using a

three-stage third-order strong stability-preserving Runge-Kutta scheme by Shu and Osher [121], where the cell-averaged solution is expected to remain positive under the CFL condition (5.88). The a posteriori limiter, introduced in section 5.6, which further transfers the positivity of the solution to nodal values is applied at the end of each stage. The collection of numerical tests performed as part of this work comprise of both one-dimensional Riemann problems and two dimensional test cases, where in the two-dimensional setting we restrict to Cartesian meshes. However, the numerical scheme (5.23) can easily be extended to unstructured meshes, for higher spatial dimensions, due to the tensor product of function spaces and the quadrature rule, see [37, 86, 111].

The results for each numerical test consists of the profile of the physical quantities at the final time along with a plot of the values of the TCI function at each cell. We also show the regions in the computational domain where contract preserving fluxes and entropy conservative fluxes were applied to compute the volume integral. This can be found in the plot named flux indicator, associated to each test case. We plot a binary flux indicator where a value of 1 indicates the regions where entropy conservative fluxes were applied and 0 for contact preserving fluxes within the volume integral.

5.7.1 Advection of density wave

We begin by validating the claim of high-order accuracy of the scheme (5.23) by advecting a density wave in a uniform flow in a unit square domain $\Omega_h = [0,1]^2$ with periodic conditions. The initial condition $\mathbf{u}_0(x)$ is set as

$$\rho_0(x) = 1 + \frac{1}{2}\sin(2\pi x), \quad u_0(x) = 1, \quad v_0(x) = 1, \quad \mathrm{p}_0(x) = 1,$$

along with a set of EOS parameters

$$\mathrm{C_{v1}} = 1.0, \quad \mathrm{C_{v2}} = 1.0, \quad \gamma_1 = 1.4, \quad \mathrm{p}_{\infty_1} = 2.0, \quad \gamma_2 = 3.0, \quad \mathrm{p}_{\infty_2} = 5.0. \tag{5.125}$$

The numerical test is performed separately using contact preserving fluxes and entropy conservative fluxes in the volume integral, while HLLC fluxes are applied at the interfaces. We compute the values of the error $e_h = \rho_h - \rho$ under different norms at final time $T_{max} = 5.0$, see Tables 5.1 and 5.2, using different polynomial order and grid refinements, and it is observed that the expected $p+1$ order of convergence is recovered by the present scheme.

p	h	$\|e_h\|_{L^1(\Omega_h)}$	$\mathcal{O}_1$	$\|e_h\|_{L^2(\Omega_h)}$	$\mathcal{O}_2$	$\|e_h\|_{L^\infty(\Omega_h)}$	$\mathcal{O}_\infty$
1	1/32	3.63E-01	-	4.01E-01	-	5.80E-01	-
	1/64	1.22E-01	1.5743	1.35E-01	1.5668	1.93E-01	1.5899
	1/128	3.19E-02	1.9352	3.54E-02	1.9351	5.02E-02	1.9399
	1/256	8.02E-03	1.9898	8.91E-03	1.9895	1.26E-02	1.9925
2	1/32	1.02E-03	-	1.23E-03	-	2.14E-03	-
	1/64	7.98E-05	3.67519	9.94E-05	3.6324	2.17E-04	3.2959
	1/128	8.48E-06	3.2357	9.97E-06	3.3176	3.33E-05	2.7064
	1/256	9.66E-07	3.1339	1.16E-06	3.1078	4.55E-06	2.8730
3	1/32	8.67E-06	-	1.21E-05	-	6.56E-05	-
	1/64	5.29E-07	4.0339	7.56E-07	4.0013	4.19E-06	3.9690
	1/128	3.25E-08	4.0238	4.75E-08	3.9901	2.67E-07	3.9717
	1/256	1.97E-09	4.0466	3.05E-09	3.9619	1.73E-08	3.9510

Table 5.1: Test for high-order accuracy using contact preserving (cp) numerical fluxes in the volume integral at final time $T_{max} = 5$. The error on density $e_h = \rho_h - \rho$ is computed for each polynomial order with mesh refinement along with the associated orders of convergence.

p	h	$\|e_h\|_{L^1(\Omega_h)}$	$\mathcal{O}_1$	$\|e_h\|_{L^2(\Omega_h)}$	$\mathcal{O}_2$	$\|e_h\|_{L^\infty(\Omega_h)}$	$\mathcal{O}_\infty$
1	1/32	3.56E-01	-	3.94E-01	-	5.72E-01	-
	1/64	1.20E-01	1.5674	1.34E-01	1.5587	2.29E-01	1.321
	1/128	2.95E-02	2.0254	3.55E-02	1.9151	6.65E-02	1.7851
	1/256	7.55E-03	1.9674	8.94E-03	1.9873	1.68E-02	1.9835
2	1/32	2.35E-03	-	2.87E-03	-	6.98E-03	-
	1/64	2.05E-04	3.5199	2.71E-04	3.4058	7.28E-04	3.2618
	1/128	1.79E-05	3.3516	2.24E-05	3.5987	6.57E-05	3.4689
	1/256	1.50E-06	3.5791	1.87E-06	3.5814	7.02E-06	3.2269
3	1/32	9.74E-05	-	1.17E-04	-	3.10E-04	-
	1/64	3.15E-06	4.9496	4.26E-06	4.7839	2.41E-05	3.6854
	1/128	1.92E-07	4.0337	2.51E-07	4.0858	1.70E-06	3.8248
	1/256	1.07E-08	4.1655	1.43E-08	4.1335	1.09E-07	3.9653

Table 5.2: Test for high-order accuracy using entropy conservative (ec) numerical fluxes in the volume integral at final time $T_{max} = 5$. The error on density $e_h = \rho_h - \rho$ is computed for each polynomial order with mesh refinement along with the associated orders of convergence.

5.7.2 Advection of a material discontinuity

We perform this test to validate the contact preservation property of the present scheme. The computational domain for this test is chosen to be $\Omega_h = [-0.5, 0.5]$ and the Riemann initial data is split at $x = 0$ as

$$(\alpha_1, \rho, u, \mathrm{p}) = \begin{cases} (0.375, 2.0, 1.0, 1.0), & x < 0.0, \\ (0.146342, 1.0, 1.0, 1.0), & x > 0.0, \end{cases} \tag{5.126}$$

with

$$\mathrm{C_{v1}} = 1.0, \quad \mathrm{C_{v2}} = 2.0, \quad \gamma_1 = 1.4, \quad \gamma_2 = 1.5, \quad \mathrm{p}_{\infty_1} = 0.0, \quad \mathrm{p}_{\infty_2} = 0.0. \tag{5.127}$$

The discontinuity in ρ and Γ between the left and right states amounts to an isolated contact discontinuity, see Figure 5-2. The results obtained at the final time $T_{max} = 2.0$ show that the TCI function attains values close to machine accuracy, which aligns well with the expectation, see the comments in section 5.3.3. The algorithm thus applies the contact preserving numerical fluxes in the volume integral, by respecting the threshold, along with HLLC fluxes at the interfaces, and together they maintain uniform velocity and pressure profiles across the contact discontinuity. The results in Figure 5-2 shows that the interface is well captured with minimal oscillations for the ρ profile.

5.7.3 The Lax problem

The Lax problem is performed for pure phases, which results in a rarefaction waves, a contact discontinuity and a shock in each phase. The computational domain is $\Omega_h = [-1.0, 1.0]$ and the Riemann initial data is split at $x = 0$ as

$$(\alpha_1, \rho, u, \mathrm{p}) = \begin{cases} (0.5, 0.445, 0.698, 3.528), & x < 0.0, \\ (0.5, 0.5, 0.0, 0.571), & x > 0.0, \end{cases} \tag{5.128}$$

with

$$\mathrm{C_{v1}} = 1.0, \quad \mathrm{C_{v2}} = 1.0, \quad \gamma_1 = 1.4, \quad \gamma_2 = 1.4, \quad \mathrm{p}_{\infty_1} = 0.0, \quad \mathrm{p}_{\infty_2} = 0.0. \tag{5.129}$$

It is seen that the TCI function gains high values in a small neighbourhood around the shock where the algorithm applies entropy conservative fluxes (5.44) in the volume integral (3.56). The approximate solution, in Figure 5-3, is well captured in the regions of rarefaction and shock, with oscillations of small amplitude appearing at the contact.

We believe that the oscillations at the contact are due to the initial discontinuity. Until some initial time, the scheme fails to distinguish between shocks and contacts, especially when the shock and contact are found in the same cell. The algorithm will thus apply entropy conservative fluxes in the volume integral in such cells which will fail to preserve uniform profiles across contacts. This can be shown through a manufactured example, where we set the initial data in the Lax problem such that shocks do not occur. The results in Figure 5-4 show that, in the absence of the shock, the approximate solution is well captured at high-order accuracy without any oscillations at the contact.

5.7.4 Gas-gas shock-interface interaction problem

This is a classic shock-material interface interaction problem which was originally proposed in [93]. Here a shock wave in Helium gas travels at Mach 8.96 and interacts with air.

The computational domain $\Omega_h = [-1.0, 1.0]$ and the initial conditions are as follows:

$$(\alpha_1, \rho, u, \mathrm{p}) = \begin{cases} (0.0, 0.386, 26.59, 100.0), & x < -0.8, \\ (0.0, 0.1, -0.5, 1.0), & -0.8 < x < -0.2, \\ (1.0, 1.0, -0.5, 1.0), & x > -0.2, \end{cases} \tag{5.130}$$

with

$$\mathrm{C_{v1}} = 1.0, \quad \mathrm{C_{v2}} = 2.5, \quad \gamma_1 = 1.4, \quad \gamma_2 = 1.6667, \quad \mathrm{p_{\infty_1}} = 0.0, \quad \mathrm{p_{\infty_2}} = 0.0. \tag{5.131}$$

The solution, in Figure 5-5, at final time reveals two shocks, one travelling left and the other travelling right, with an advected material interface in between. It is observed that the shocks are well captured, with oscillations of small amplitude occurring near the material interface. This behaviour is akin to the oscillation observed at the wake of the shock during the Lax problem, see Figure 5-3.

5.7.5 Gas-water shock-interface interaction problem

This test case models an underwater explosion, where the initial condition consists of a material interface that separates highly compressed air to the left and water at atmospheric pressure on the right. The computational domain is $\Omega_h = [-5.0, 5.0]$. The initial data is given as

$$(\alpha_1, \rho, u, \mathrm{p}) = \begin{cases} (1.0, 1.241, 0.0, 2.753), & x < 0.0, \\ (0.0, 0.991, 0.0, 3.059 \times 10^{-4}), & x > 0.0, \end{cases} \tag{5.132}$$

with

$$\mathrm{C_{v1}} = 1.2, \quad \mathrm{C_{v2}} = 0.073037, \quad \gamma_1 = 1.4, \quad \gamma_2 = 5.5, \quad \mathrm{p_{\infty_1}} = 0.0, \quad \mathrm{p_{\infty_2}} = 1.505. \tag{5.133}$$

The solution to the Riemann problem in Figure 5-6 shows a right travelling shock, a right travelling contact wave, a right advected material interface and a left rarefaction wave. It is observed that even though the shock is of high amplitude, the velocity and pressure profiles across the contact wave bears little oscillations. The material interface is well captured as can be seen through the plots of Γ and Π.

The TCI values oscillate and attain high values near the right travelling shock. The algorithm correctly detects the shock and applies entropy conservative fluxes in the volume integral. This can be seen in the plot for the flux indicator.

5.7.6 Advection of a Helium bubble in air

The advection of a spherical He bubble (represented as species 1) in air (species 2) demonstrates that the numerical is capable of preserving contact discontinuities which are not aligned with the mesh. Here we have demonstrated this property by considering two spatial dimensions as the scheme can easily be extended to accommodate higher spatial dimensions owing to the tensor product of function spaces and the quadrature rule.

The initial data for the Helium bubble and the air surrounding it is taken from the

shock-bubble interaction problem presented in section 5.7.7, also refer [37, 83], where we set the initial data to disregard the shock for the purpose of this test. Thus the computational domains contains a single discrete gas inhomogeneity. The computational domain $\Omega_h = [0, 6.5] \times [0, 1.78]$ is discretized using 1300×365 elements and the Helium bubble, of unit diameter, is centered at $x = 3.5$ and $y = 0.89$. The EOS parameters are $\gamma_1 = 1.648, \gamma_2 = 1.4, \mathrm{C_{v1}} = 6.0598$ and $\mathrm{C_{v2}} = 1.7857$. Note that the initial data are made nondimensional with the initial bubble diameter and the density, temperature and the sound speed of air. In order to advect the bubble in air, we introduce a unit positive velocity for the bubble and air and allow the bubble to move right from its initial position.

The Figure 5-7 show the advection of the bubble from $t = 0\mu s$ to a final time of $t = 152.38\mu s$. We observe that the material interface is captured sharply as the algorithm applies contact preserving numerical fluxes in the volume integral, which preserves the velocity and pressure profiles across the interface.

5.7.7 SHOCK IN AIR INTERACTS WITH A HELIUM BUBBLE

We perform the standard shock bubble interaction problem with the present scheme, which was originally introduced in [65] through physical experiments. However, since then, this famed test case has been adopted to highlight the robustness and accuracy of numerical schemes for multiphase and multicomponent flows, see [37, 60, 74, 80, 83, 107, 111] to name a few.

The test involves a stationary Helium bubble which is suspended in air while a left moving Mach 1.22 shock in air travels through the bubble and deforms it. The computational domain $\Omega_h = [0.0, 6.5] \times [0, 1.78]$ is discretized into 1300×365 elements. The Helium bubble of unit diameter is centered at $x = 3.5$ and $y = 0.89$ and the left travelling shock is initially located at $x = 4$. The boundary conditions on the computational domain is set as periodic conditions on the top and bottom boundaries, along with non-reflective conditions at the left and right boundaries. While referring to the species in the immiscible mixture, we once again consider the Helium bubble as species 1 and the air surrounding it as species 2. The EOS parameters of the species are $\gamma_1 = 1.648, \gamma_2 = 1.4, \mathrm{C_{v1}} = 6.0598$ and $\mathrm{C_{v2}} = 1.7857$. The initial data are made nondimensional with the initial bubble diameter and the density, temperature and the sound speed of the pre-shock air.

The Figure 5-8 shows the deformation of the bubble at several physical times as the left travelling shock passes through it. The plotted fields are those of the void fraction of the Helium bubble, along with the total pressure, and the numerical Schlieren $\phi = \exp(|\nabla\rho|/|\nabla\rho|_{\max})$. We observe that the scheme allows a sharp resolution of the bubble interface for all physical times and is able to accurately capture the shock dynamics. The bubble interface develops vortices after the shock has left the bubble due to Kelvin-Helmholtz instability. We also highlight the regions in the computational domain where entropy conservative fluxes are applied in the volume integral and, for our choice of threshold of the TCI function, the algorithm is able to detect the shock accurately and apply entropy conservative fluxes in the volume integral along with HLLC fluxes at the interfaces. This allows us to ensure nonlinear stability of the DGSEM scheme at the shock.

Through Figure 5-9, we show the space-time diagram for three characteristic points on the interface of the bubble. Here we compare the results obtained with the present DGSEM scheme to reference data from [83]. The deformation of the bubble shows complete agreement

with the reference data and indicates that the smooth initial condition does not affect the global deformation of the bubble.

5.7.8 Strong shock in air interacts with a Hydrogen bubble

We finally subject the scheme to the simulation of a strong shock ($M = 2.0$) in air and its interaction with a Hydrogen bubble [14, 125]. The strong shock, compared to section 5.7.7, results in a faster shock-bubble interaction. The computational domain $\Omega_h = [0, 22.5] \times [0, 7.5]$ is discretized into 450×300 elements, with the bubble centered at $x = 4$ and $y = 0$, and the right travelling shock located at $x = 7$. The initial data is made nondimensional with the pre-shock density, velocity and temperature of the air and the a length scale of 1mm. The boundaries of the computational domain are defined using symmetry conditions for the top and bottom boundaries, along with supersonic inflow condition at the left boundary and nonreflecting conditions on the right boundary. The species in the mixture are designated as 1 for the Hydrogen gas in the bubble and 2 for the surrounding air. The EOS parameters of these species are $\gamma_1 = 1.41, \gamma_2 = 1.353, \mathrm{C_{v1}} = 7.424$ and $\mathrm{C_{v2}} = 0.523$.

The results obtained as part of Figure 5-10 show the deformation of the bubble as the strong shock passes through it. The plotted field are those of the void fraction of the Hydrogen bubble, the total pressure and the numerical Schlieren $\phi = \exp(|\nabla\rho|/|\nabla\rho|_{\max})$. Here, we once again observe that the numerical scheme is able to resolve the bubble interface well along with the shock. The oscillations at the interface are due to the Kelvin-Helmholtz instability and they were also observed in [14]. The algorithm, under the current TCI threshold, is able to the detect shock accurately and apply entropy conservative fluxes in the volume integral at the shock while applying contact preserving numerical fluxes everywhere else. As a result we were once again able to demonstrate the present scheme's capability to maintain sharp resolution of the interface while also resolving strong shocks.

5.8 Summary

In this work, we propose a high-order entropy stable semi-discrete numerical scheme for the gamma model [122] that preserves uniform profiles of pressure and velocity across contact and material discontinuities. The spatial discretization is performed using the DGSEM framework [37, 108], where the design of the numerical fluxes for the volume integral and those that are applied at the interfaces are considered separately. Following Theorem 3.5.1, entropy stability for the DGSEM requires that entropy conservative fluxes [24] be applied in the volume integral along with entropy stable fluxes at the cell interfaces, however through this work we discovered that entropy conservative fluxes for the gamma model, which are derived using entropy variables, fail to preserve uniform pressure and velocity profiles across contact and material discontinuities. As a result, we design contact preserving numerical fluxes for the gamma model that are applied in the volume integral when encountering contact discontinuities or rarefaction waves. Conversely, contact preserving fluxes do not conserve the discrete entropy within the cell, hence we apply entropy conservative fluxes in the volume integral at shocks. The switching between entropy conservative and contact-preserving fluxes in the volume integral is determined through the values obtained by a pressure-based troubled-cell indicator (TCI) function [78, 126]. The algorithm receives a user-defined threshold and applies entropy conservative numerical fluxes in the volume inte-

gral for cells where the TCI function gains values that exceed the threshold, whereas contact preserving fluxes are applied everywhere else.

We then propose HLL and HLLC approximate Riemann solvers for the gamma model that can be applied at the cell-interfaces. Through this work we show that the HLL solver is not consistent with the integral form of the model as it requires solving the exact Riemann solution. Therefore, in our work we implement the HLLC solver and show that the HLLC solver satisfies a discrete entropy inequality for the three-point scheme, preserves uniform pressure and velocity profiles across contact discontinuities and we propose estimates for the wave speeds that maintains the positivity of the solution. The property of positivity of the solution is further transferred to nodal values by the use of a posteriori limiters [37, 108, 139, 145] where we limit the density, the total internal energy and Γ. Furthermore, to perform high-order integration in time we use strong-stability preserving Runge Kutta schemes [121].

Numerical tests are performed both in one and two spatial dimensions that demonstrate the capabilities of the scheme to maintain high-order accuracy, resolve shocks through entropy stability and the ability to preserve material interfaces and contact discontinuities. The numerical tests comprise of a variety of Riemann problems as well as two different variants of the shock bubble interaction problem. The numerical scheme also reveal the effectiveness of the TCI function to accurately detects shocks and apply entropy conservative numerical fluxes in the volume integral for cell containing the shock. Overall, the numerical results show that the approximate solutions are well capture by the present numerical scheme at high-order accuracy. There are small amplitude oscillations present around contact discontinuities which are linked to the limitations of the TCI based algorithm for switching between the numerical fluxes. However, this also paves the path for the development of more advanced switching strategy for the numerical fluxes.

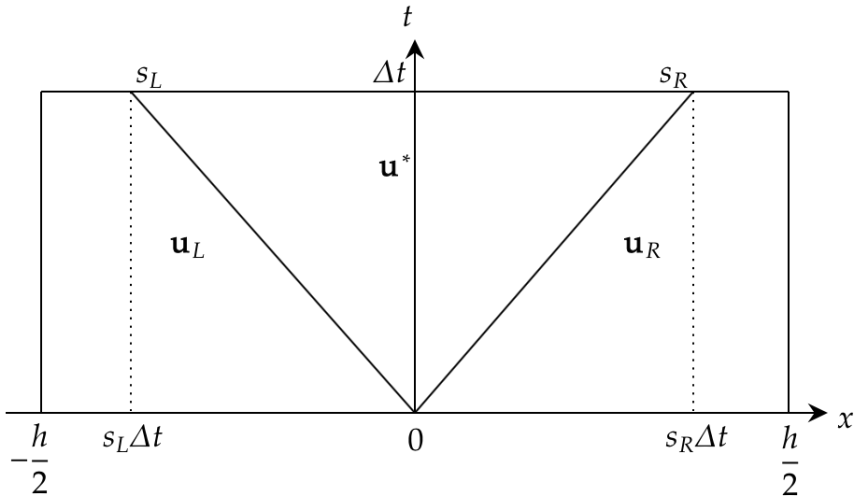

HLL wave configuration

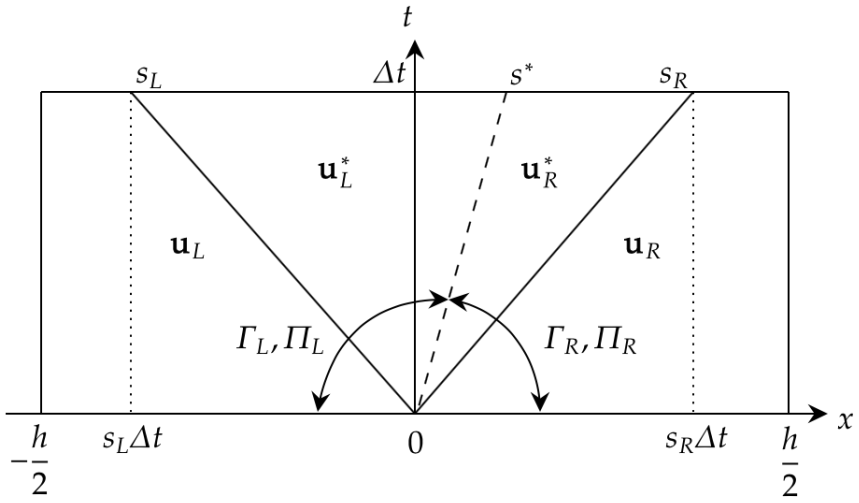

HLLC wave configuration

Figure 5-1: The control volume $\left[-\frac{h}{2}, \frac{h}{2}\right] \times [0, \Delta t]$ on the $x-t$ plane, where s_L and s_R are the slowest and fastest waves emanating from the cell interface.

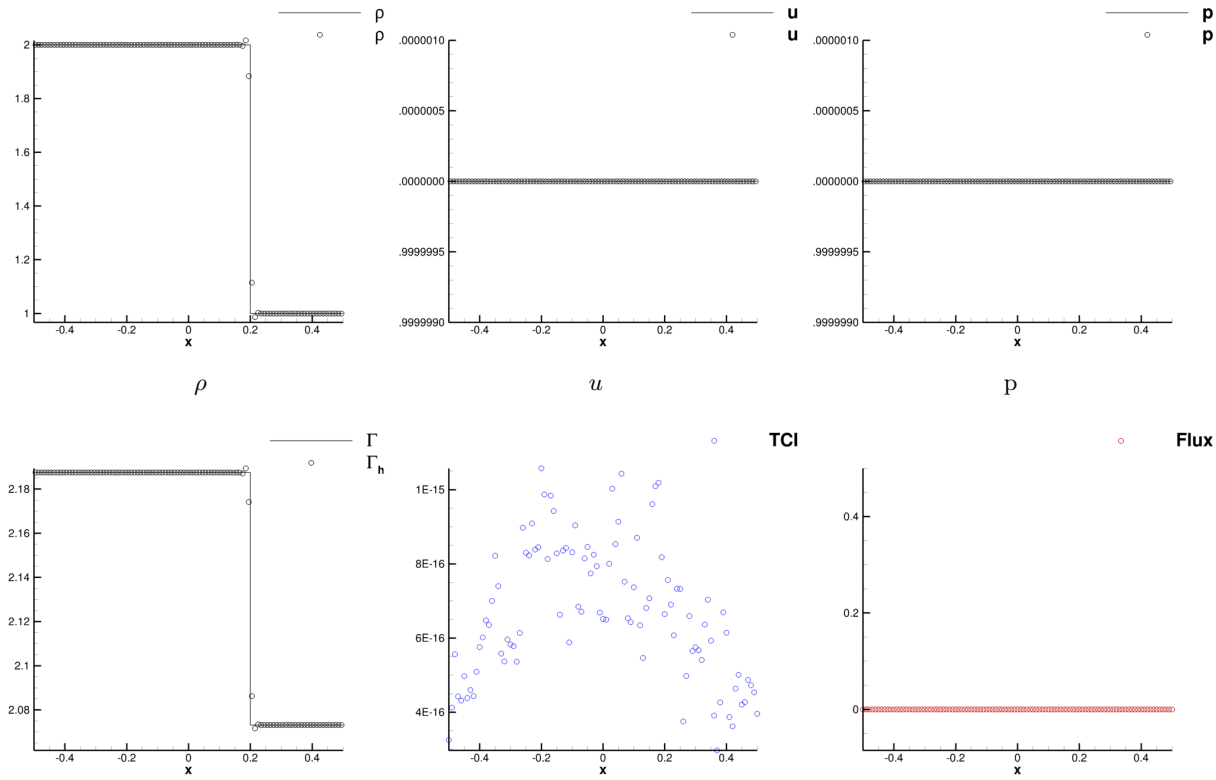

ρ u p

Γ TCI Flux indicator

Figure 5-2: The approximate solution for the advection of contact discontinuities at fourth-order accuracy (p = 3) is compared to the exact solution on a computational domain comprising of 100 elements at T_{max} = 0.2. The plot for the the TCI values indicate the values obtained by the TCI function in the volume integral. A value of 0 (zero) on the flux indicator implies that contact preserving numerical fluxes have been applied in the volume integral.

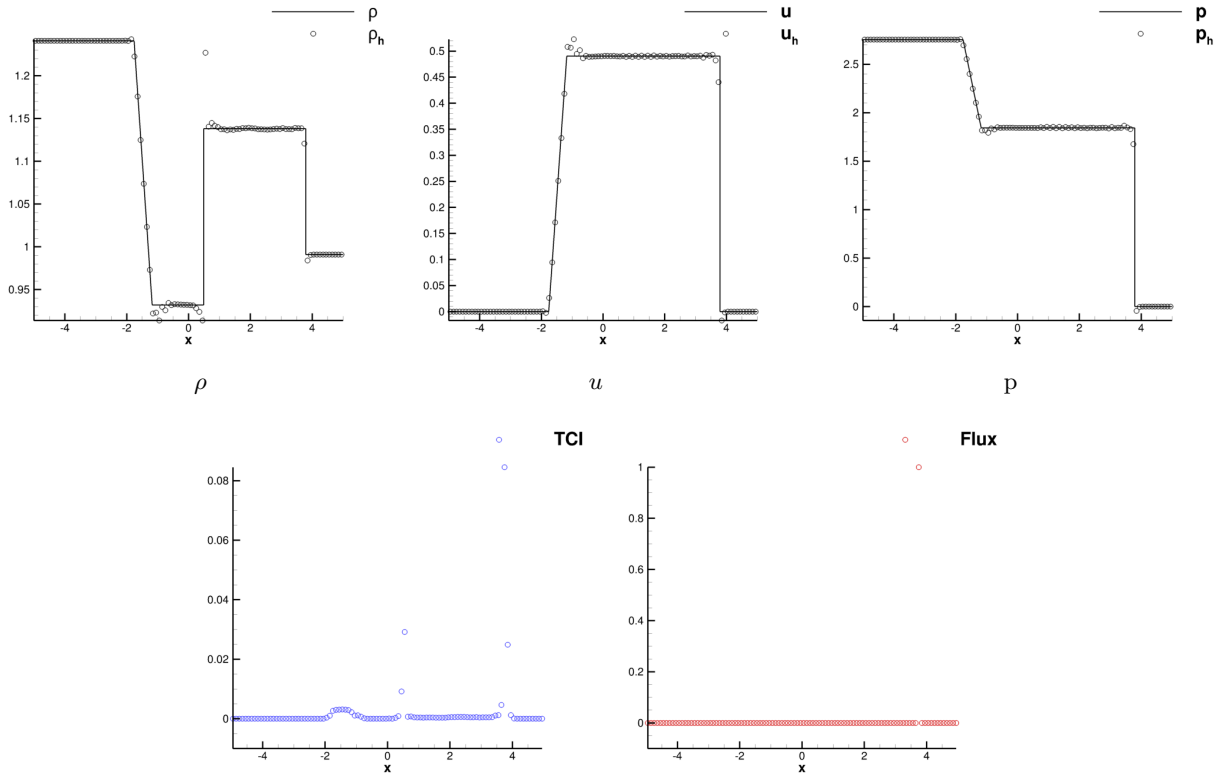

ρ u p

TCI flux indicator

Figure 5-3: The approximate solution for the Lax problem at fourth-order accuracy ($p = 3$) is compared to the exact solution on a computational domain comprising of 100 elements at $T_{max} = 0.26$. The plot for TCI function indicates the oscillation in the TCI values when encountering a shock. The flux indicator shows the regions in the domain where entropy conservative fluxes are applied.

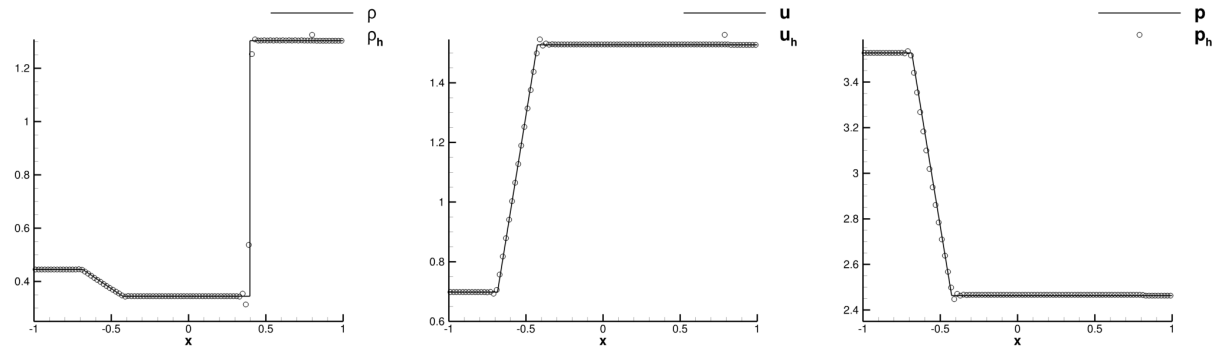

ρ u p

Figure 5-4: The approximate solution for the Lax problem without the shock at fourth-order accuracy $p = 3$ is compared to the exact solution on a computational domain comprising of 100 elements at $T_{max} = 0.26$.

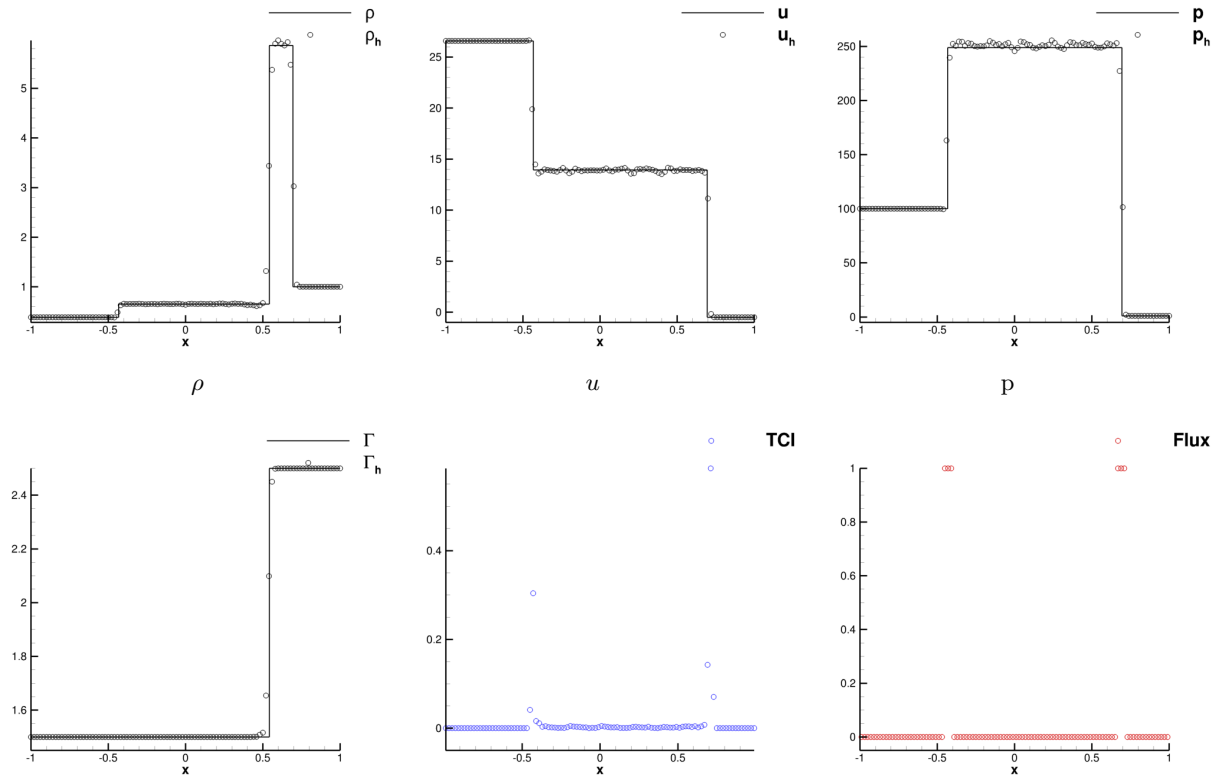

Figure 5-5: The approximate solution for gas-gas shock-interface interaction at fourth-order accuracy ($p = 3$) is compared to the exact solution on a computational domain comprising of 100 elements at $T_{max} = 0.07$. The plot for TCI values indicates the oscillation in the TCI function when encountering a shock. The flux indicator is one when entropy conservative fluxes are applied.

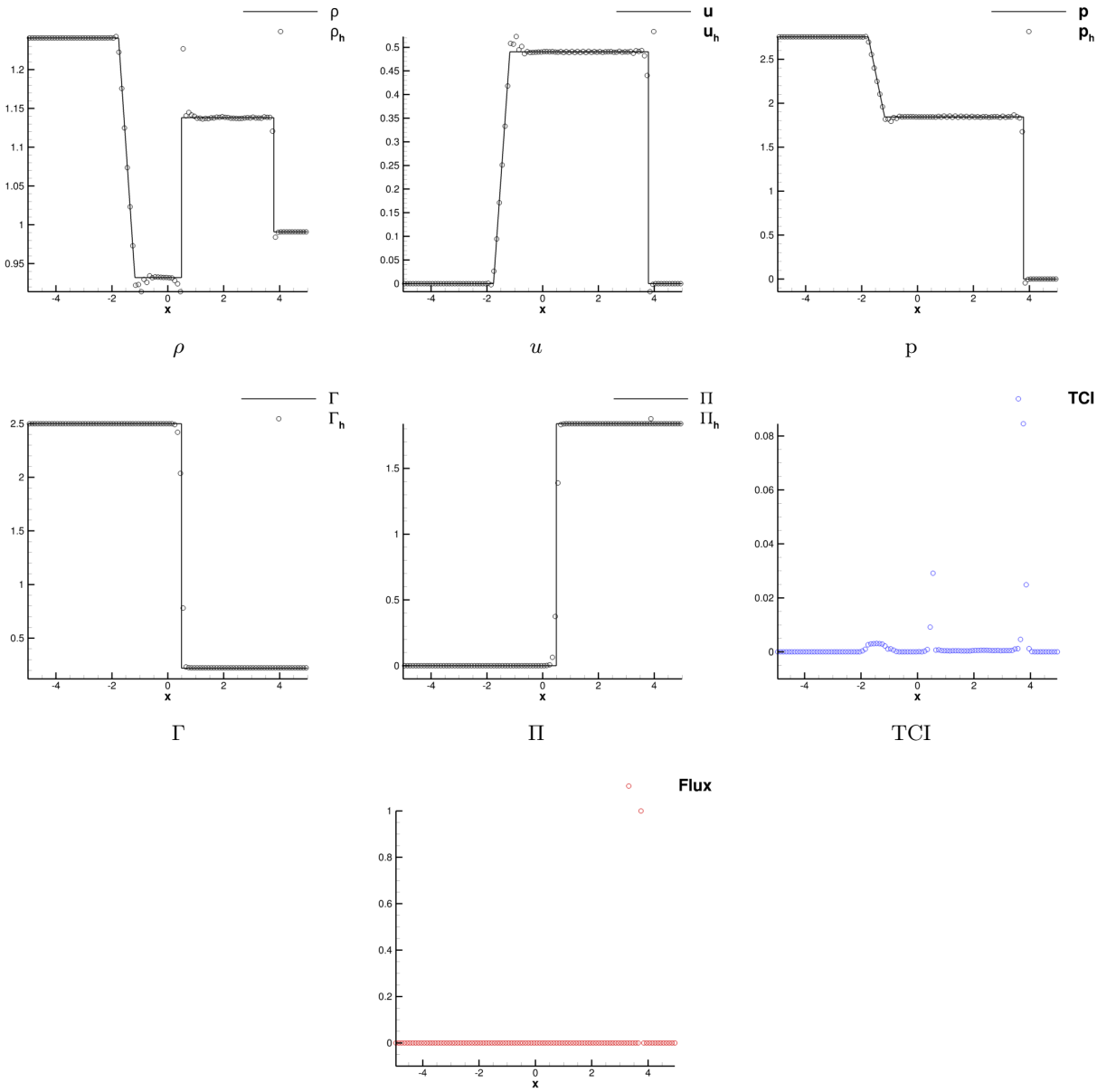

ρ u p

Γ Π TCI

Flux indicator

Figure 5-6: The approximate solution for gas-water shock-interface interaction at fourth-order accuracy ($p = 3$) is compared to the exact solution on a computational domain comprising of 100 elements at $T_{max} = 1.0$. The plot for TCI values indicates the oscillation in the TCI function when encountering a shock. The flux indicator is one when entropy conservative fluxes are applied.

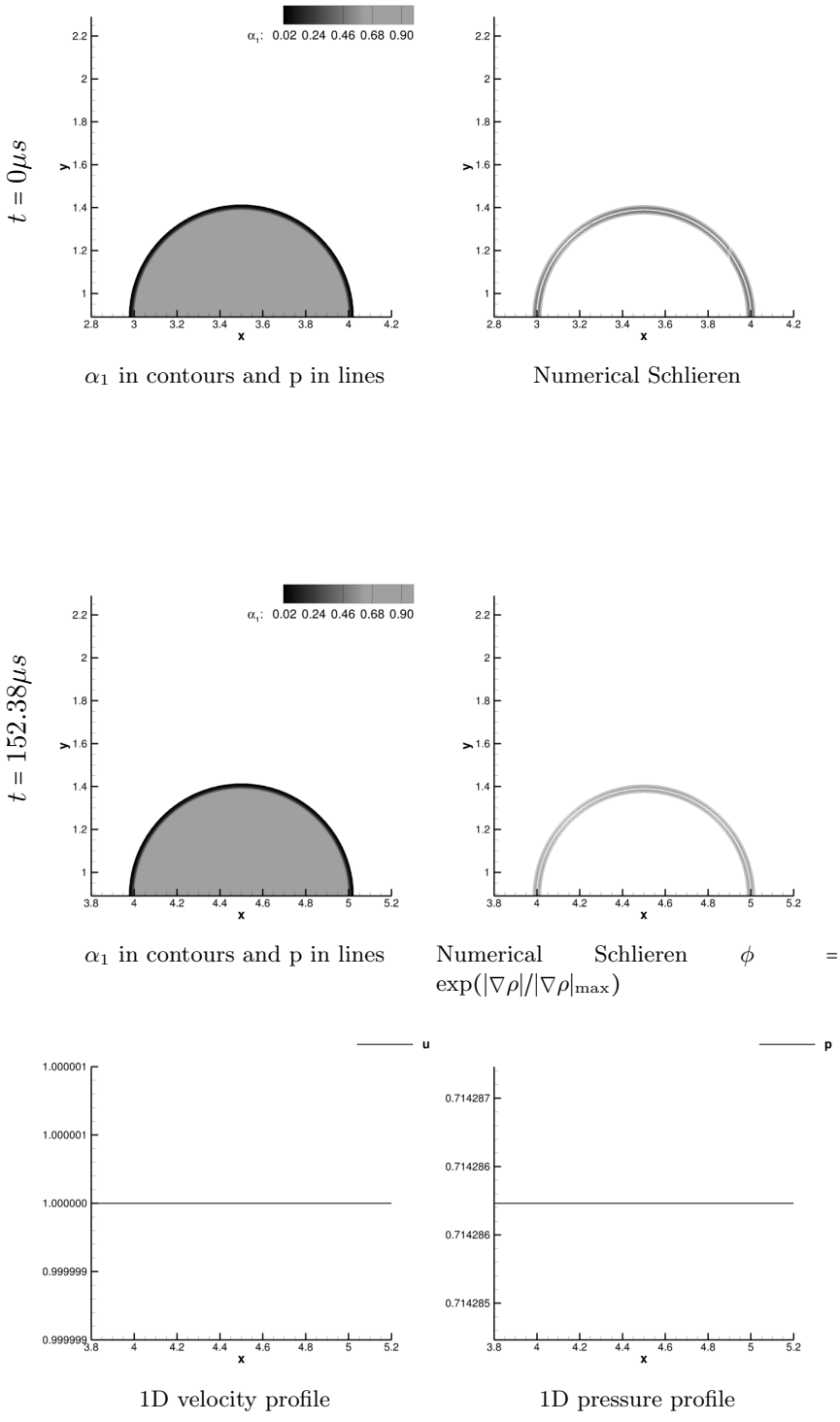

α_1 in contours and p in lines | Numerical Schlieren

α_1 in contours and p in lines | Numerical Schlieren $\phi = \exp(|\nabla\rho|/|\nabla\rho|_{\max})$

1D velocity profile | 1D pressure profile

Figure 5-7: The advection of a Helium bubble in air through a unit distance at fourth order accuracy ($p = 3$) in space on a mesh comprising of 1300×365 elements.

$t = 32\mu s$

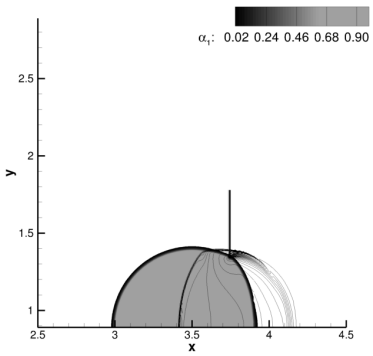

α_1 in contours and p in lines

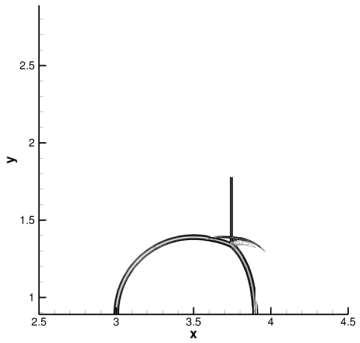

Numerical Schlieren

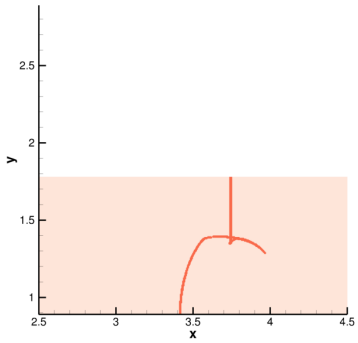

Flux indicator

$t = 102\mu s$

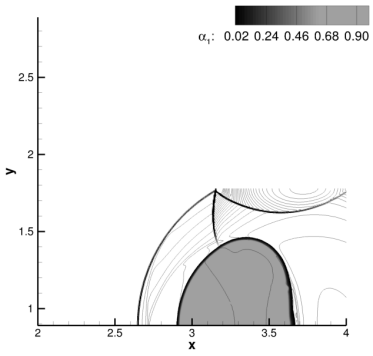

α_1 in contours and p in lines

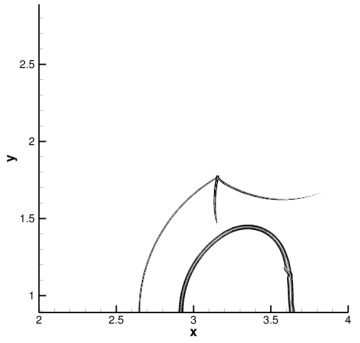

Numerical Schlieren

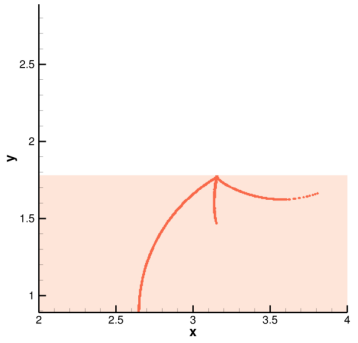

Flux indicator

$t = 427\mu s$

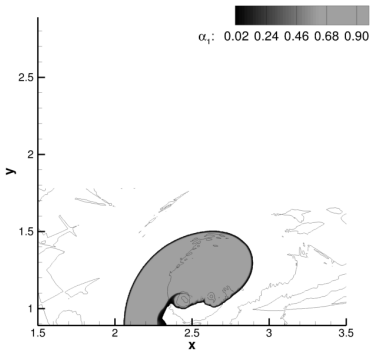

α_1 in contours and p in lines

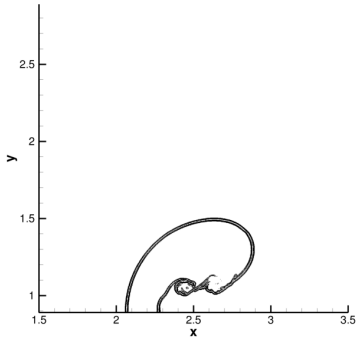

Numerical Schlieren

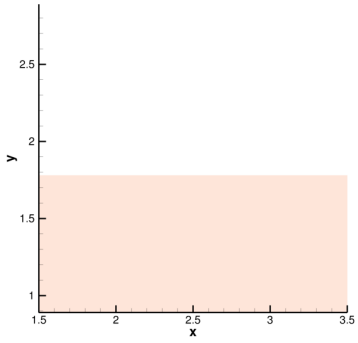

Flux indicator

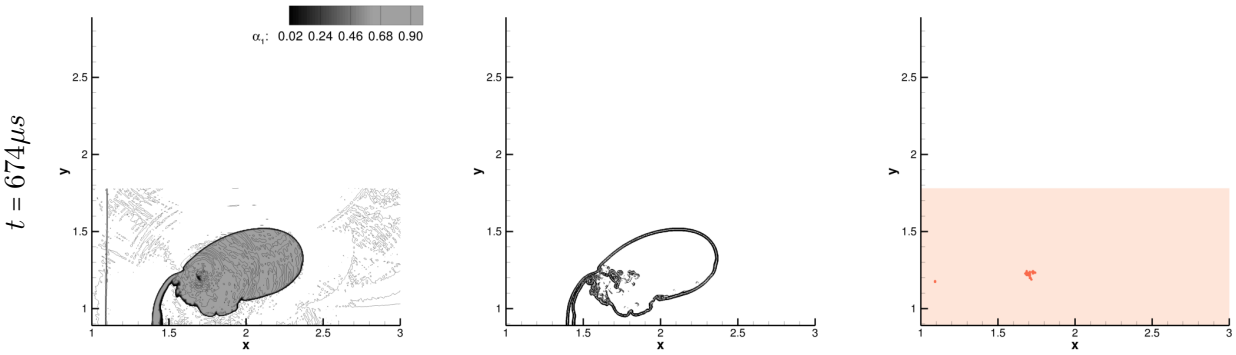

α_1 in contours and p in lines | Numerical Schlieren | Flux indicator

Figure 5-8: The simulation of an interaction of a $M = 1.22$ shock in air with a Helium bubble at fourth order accuracy ($p = 3$) in space on a mesh comprising of 1300×365 elements.

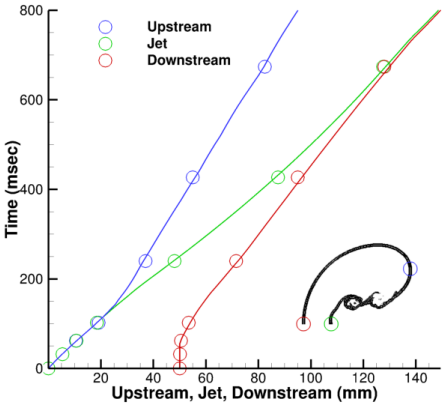

Figure 5-9: Space-time diagram for three characteristic points on the interface of the He bubble. The solid lines are the reference data from [83], while the symbols are the results obtained with the present DGSEM scheme for polynomial of degree $p = 3$ and on a mesh comprising of 1300×356 elements.

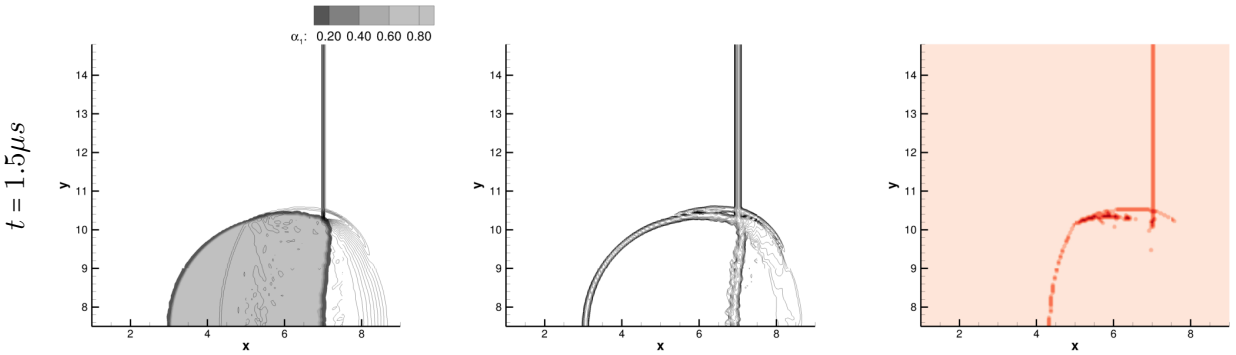

α_1 in contours and p in lines | Numerical Schlieren | Flux indicator

$t = 2.0\mu s$

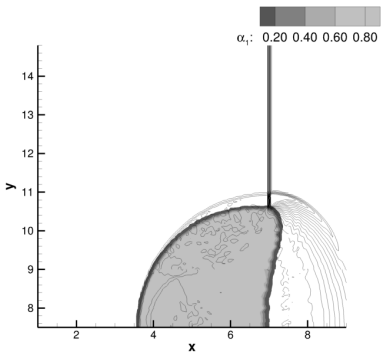

α_1 in contours and p in lines

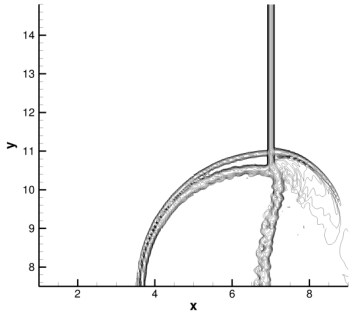

Numerical Schlieren

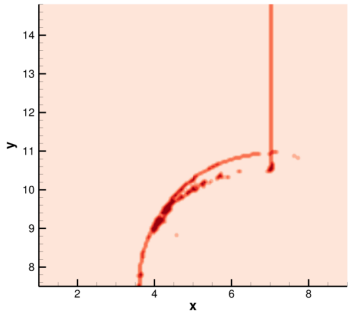

Flux indicator

$t = 2.5\mu s$

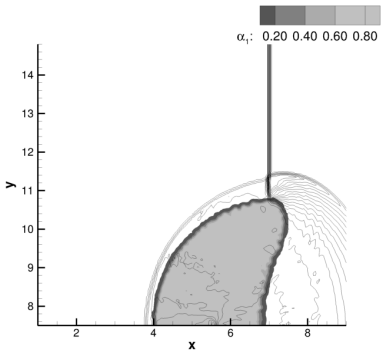

α_1 in contours and p in lines

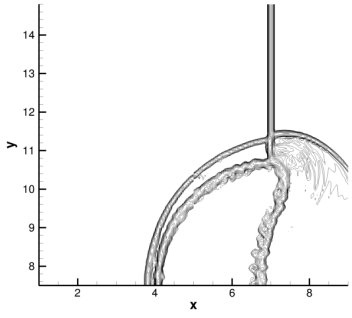

Numerical Schlieren

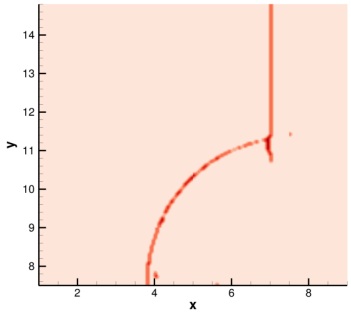

Flux indicator

$t = 3.0\mu s$

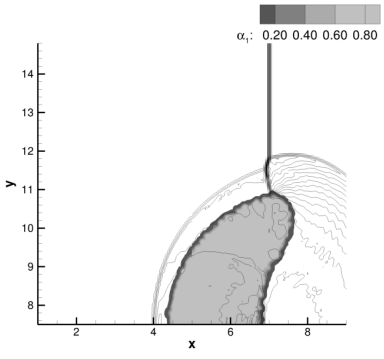

α_1 in contours and p in lines

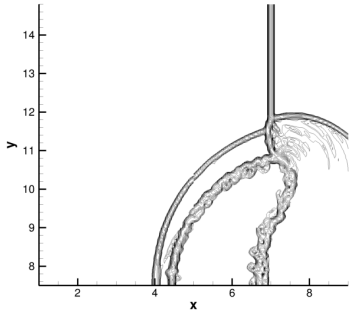

Numerical Schlieren

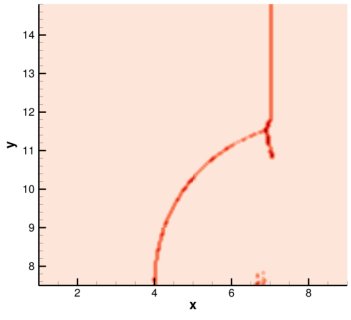

Flux indicator

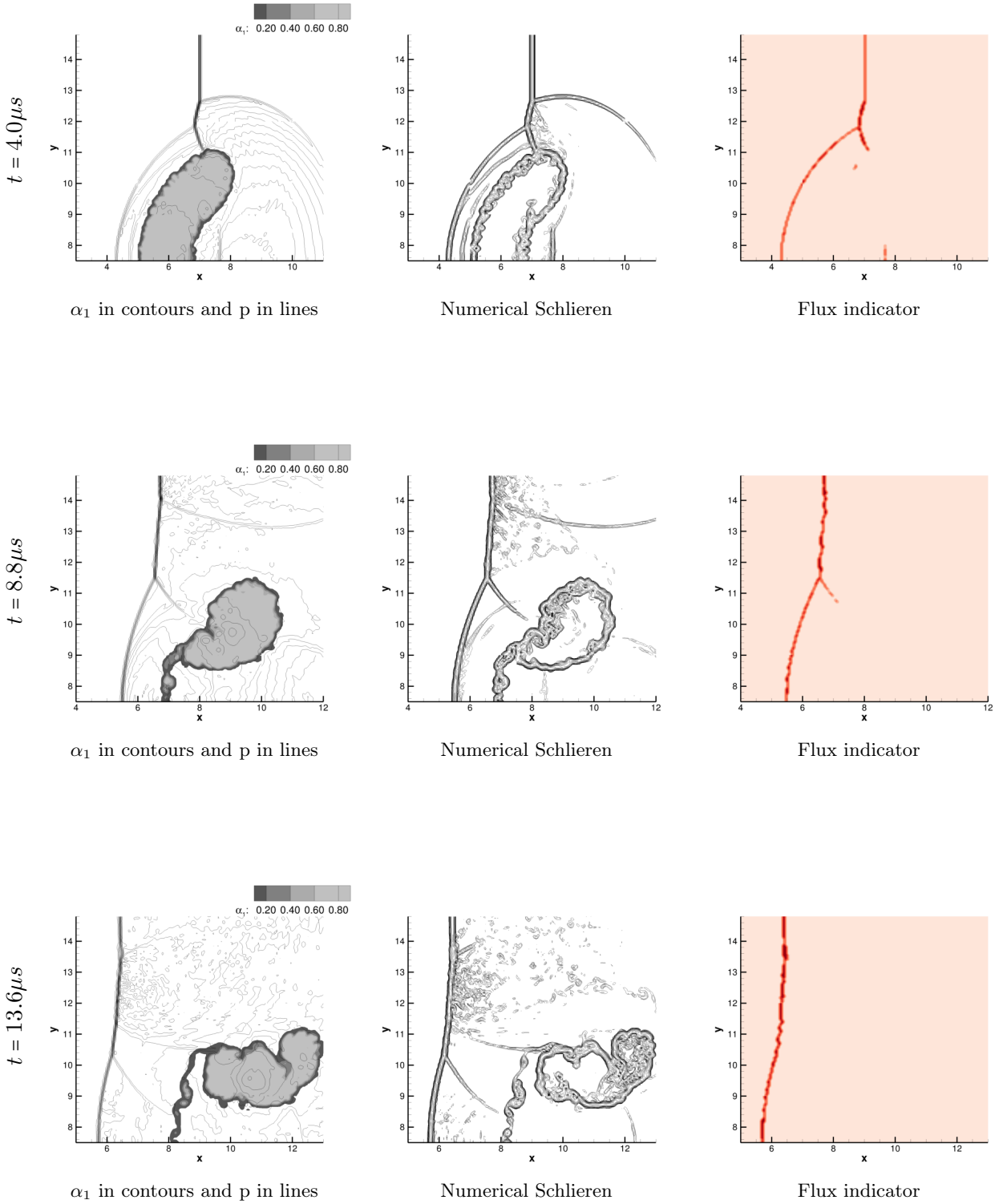

Figure 5-10: The interaction of a $M = 2.0$ shock in air with a Hydrogen bubble at fourth order accuracy $(p = 3)$ in space on a mesh comprising of 450×300 elements.

Chapter 6

Conclusion and perspectives

6.1 Conclusion

The goal of this thesis is to focus on the modelling and the design of novel high-order entropy stable schemes for compressible multiphase and multicomponent flows.

In the context of modelling of compressible multiphase flows, in Chapter 2, we focus on flows involving a reactive mixture of gas and liquid. We recall that there is no general consensus on the choice of models that accurately depicts the physics of such flows, and several works have been proposed over the years for their modelling. To this end, we consider the two-phase flow model proposed by Saurel and Abgrall [115] as a basis, and modify the source terms so that the resulting model accounts for mass transfer, interfacial drag, mechanical non-equilibrium and heat transfer under standard assumptions for reactive flows. We show that including new source terms in a pre-existing model is far from trivial as it affects the well-posedness of the system. Thus, we suggest corrective terms and propose a hyperbolic two-phase flow model that is Galilean invariant and entropy dissipative under complete disequilibria.

We, then, focus on the design of numerical schemes for hyperbolic multiphase and multicomponent models in nonconservative form. In Chapter 3 we briefly recall the notion of weak solutions for nonconservative systems and introduce the DGSEM framework in one and multiple space dimensions. Then, we describe a semi-discrete DG scheme for general nonconservative systems, where we modify the volume integral over cell elements and replace the physical fluxes with two-point entropy conservative fluxes while at the interface we apply entropy stable fluxes. The DGSEM satisfies the SBP-SAT property, and we use it to prove that our modifications lead to a semi-discrete scheme that is both high-order accurate and satisfies a semi-discrete entropy inequality. High-order integration in time is performed using strong-stability preserving Runge-Kutta (SSP-RK) scheme that is also described in this chapter. The SSP-RK are a convex combination of explicit first-order schemes in time. We utilize this property in our discretization and impose restrictions on the numerical parameters to prove that the cell-averaged solution is positive.

In Chapter 4, we discretize the homogeneous Baer-Nunziato model [7] using the semi-discrete DGSEM from Chapter 3. We derive entropy conservative and entropy stable fluxes for the Baer-Nunziato model that satisfy the requirements for high-order accuracy and en-

tropy stability of the DG scheme. The numerical fluxes are also shown to preserve the kinetic energy at the discrete level. We show that our numerical scheme guarantees positivity of the cell-averaged void fraction and partial densities by imposing conditions on the time step and on the numerical parameters. The positivity of the cell-averaged solutions is then transferred to the nodal values through the use of a posteriori limiters. We demonstrate the properties of the scheme by performing numerous tests, involving both one-dimensional Riemann problems and a two-dimensional shock-bubble interaction problem.

We then discretize the gamma-based multicomponent model propose by Shyue [122], with the aim to propose a high-order entropy stable DG scheme for multicomponent flows that also allows for sharp resolution of the material interfaces. The DGSEM requires replacing the physical fluxes in the volume integral with entropy conservative fluxes, as shown in Theorem 3.5.1. However, the gamma-model does not admit a mathematical entropy function that is convex for the entire state vector, instead convexity of the entropy function can only be claimed for pure phases. To this purpose, we design entropy conservative fluxes for pure phases, and, in order to preserve uniform pressure and velocity profiles across contact and material discontinuities, we design contacting-preserving fluxes. It must be noted that the design of a single numerical flux that exhibits the qualities of entropy conservation and preservation of contacts is difficult, as a result our algorithm selects between entropy conservative numerical fluxes and contact-preserving fluxes based on the values generated from a pressure-based troubled-cell indicator function.

The semi-discrete scheme for the gamma-model involves applying a HLLC solver at the interfaces of the cell. We show that a three-point scheme with this solver satisfies a discrete entropy inequality, preserves uniform profiles across contact discontinuities and preserves positivity of the density, the total internal energy and the adiabatic exponent of the mixture. The positivity is further enforced at nodal values through the use of a posteriori limiters.

In this work, we demonstrate the capabilities of our numerical scheme by performing several numerical experiments in one and two space dimensions. For tests in one space dimension, we include Riemann problems that involve strong shocks, vanishing phases and sharp resolution of material interfaces, while at two space dimensions we simulate the interaction of a shock with a Helium bubble in space[107].

6.2 PERSPECTIVES

The research conducted in the course of this thesis creates a foundation for further development in the modelling of compressible multiphase flows and the design of high-order entropy stable numerical schemes for numerical approximation of these flows. Here we briefly describe the planned extension of the present work.

The non-equilibrium model proposed in Chapter 2 contains stiff relaxation source terms and it is of interest to derive an equilibrium model under instantaneous relaxation. To this end, a small parameter $0 < \varepsilon \ll 1$ can be introduced that quantifies the different relaxation time scales for the source terms when perturbed close to an equilibrium. The source terms in (2.38) can then be scaled with respect to ε as

$$\Theta^{\varepsilon}(\mathbf{u}) = \frac{\Theta(\mathbf{u})}{\varepsilon^3}, \quad \Lambda^{\varepsilon}(\mathbf{u}) = \frac{\Lambda(\mathbf{u})}{\varepsilon^2}, \quad \mathcal{K}^{\varepsilon}(\mathbf{u}) = \frac{\mathcal{K}(\mathbf{u})}{\varepsilon}.$$

The above choice of scaling for the coefficients of the source terms lead to a cascading relaxation towards equilibrium, where the pressure relaxes the fastest followed by the relaxation in velocity and then in temperature. Such cascading relaxation behaviour is attributed to physical considerations and is classical in the context of reactive systems, see section 2.2. Note that the coefficient for mass transfer $\mathcal{M}$ is not scaled with respect to ε, as one can derive a homogeneous relaxation model [13], from the present model, at the limit of instantaneous relaxation. Here, an important open question arises in the form of the well-posedness of the relaxation process to the equilibrium.

In order to prove that the relaxation is stable, one needs show that the eigenvalues of the equilibrium model satisfy the subcharacteristic condition [140]. Furthermore, equilibrium state should minimize the convex entropy function and constitutes an analogue of the Gibbs lemma from kinetic theory, while the entropy of the spatially homogeneous (perturbed) disequilibrium system must be shown to decrease in time as $\varepsilon \downarrow 0$ and reaches a unique minimum in the sense of Lyapunov. Thus proving an analogue of the H-theorem.

In Chapters 4 and 5, it was observed that the numerical scheme is prone to spurious oscillations in the neighbourhood of discontinuities, which may be attributed to some of the drawbacks of the present approach, such as the scheme is entropy stable only at the semi-discrete level and the entropy stability holds only for cell-averaged quantities, and only for one convex entropy function. The stabilization of the numerical schemes is introduced only through the numerical fluxes at the interface that do not stabilize internal degrees of freedom. Furthermore, positivity of the solution is not guaranteed in the whole element with the Lagrange interpolation polynomials, even if the nodal values are positive. One possible way to alleviate these issues would be to consider a fully discrete scheme under the DGSEM framework and include entropy diminishing projections which was introduced in [18] for scalar conservation laws and in [32] for system of conservation laws using the MUSCL scheme. An important result in this aspect would be the dissipation of all convex entropies for the system. In [18, 32], these projections are used within a splitting procedure to re-project the solution in the function space after an evolution step. One possible way to apply these projections in the context of the DGSEM would be to introduce a posteriori nonlinear limiters to the solution in contrast to the limiters used in the present work. Another possibility to improve stability would be to extend the introduction of shock capture and artificial dissipation terms, as done in [70], to the DGSEM setting by considering a space-time DGSEM formulation.

In Chapter 5, we show that entropy consistency requires wave speed estimates that bound the exact Riemann solution, which is necessary for consistency of the HLLC solver. However, if the EOS differs in the left and right states, due to different species compositions, estimation of maximum wave speeds may require the use of time-consuming Newton-Raphson iterations. One possibility would be to use the energy relaxation technique introduced in [33] for the approximation of the monocomponent compressible Euler equations with a general EOS. In this method, one considers a decomposition of the internal energy including the energy for a polytropic gas thus relaxing the general EOS. The method then allows the design of numerical schemes by using classical numerical fluxes for polytropic gases. This method has been extended to the compressible multispecies Euler equations in conservative form in [98] and it would be interesting to check if this approach can be extended also to the nonconservative mutlicomponent model by Shyue [122]. Works in [43, 109] tend to highlight some difficulties with this approach in the case of fluid mixtures.

Chapter 7

Conclusion générale

L'objectif de cette thèse porte sur la modélisation des écoulements compressibles multi-phases et multicomposants, et de concevoir de nouveaux schémas d'ordre élevé qui dissipe l'entropie mathématique.

Dans le contexte de la modélisation des écoulements multi-phasiques compressibles, nous nous concentrons sur les écoulements impliquant un mélange réactif de gaz et de liquide. Nous rappelons qu'il n'y a pas de consensus général sur le choix des modèles qui décrivent avec précision la physique de tels écoulements, et plusieurs travaux ont été présentés au cours des années en ce sens. Dans ce but, nous considérons le modèle d'écoulement diphasique proposé par Saurel et Abgrall [115], et nous modifions les termes sources afin que le modèle résultant tienne compte du transfert de masse, de la traînée interfaciale, du non-équilibre mécanique et du transfert de chaleur sous des hypothèses standards pour les écoulements réactifs. Nous montrons que l'ajout de nouveaux termes sources dans un modèle préexistant est loin d'être trivial car cela affecte le caractère bien posé du système. Nous suggérons donc des termes correctifs et proposons un modèle d'écoulement diphasique hyperbolique qui est invariant par transformations galiléennes et dissipe d'entropie en cas de déséquilibres complets.

Nous nous concentrons ensuite sur la conception de schémas numériques pour les modèles hyperboliques multi-phasique et multi-composants sous forme non conservative. Dans Chapter 3 nous rappelons brièvement la notion de solutions faibles pour les systèmes non-conservatifs et introduisons le cadre DGSEM en une et plusieurs dimensions d'espace. Nous décrivons ici un schéma DG semi-discret pour les systèmes non-conservatifs généraux, où nous modifions l'intégrale de volume sur les éléments de la cellule et remplaçons les flux physiques par des flux conservant l'entropie à deux points tandis qu'à l'interface nous appliquons des flux dissipant l'entropie. Le schéma DGSEM se base sur des opérateurs satisfaisant les propriétés SBP-SAT, et nous les utilisons pour prouver que nos modifications conduisent à un schéma semi-discret qui est à la fois précis à l'ordre élevé et satisfait une inégalité d'entropie semi-discrète. L'intégration temporelle d'ordre élevé est réalisée à l'aide d'un schéma de Runge-Kutta préservant la stabilité (SSP-RK) qui est également décrit dans ce chapitre. Les schémas SSP-RK sont une combinaison convexe de schémas explicites au premier ordre en temps. Nous utilisons cette propriété dans notre discrétisation et imposons des restrictions sur les paramètres numériques et le pas de temps pour prouver que la solution moyenne dans la cellule est positive.

Dans l'article Chapter 4, nous discrétisons le modèle homogène de Baer-Nunziato [7] en utilisant la méthode DGSEM de Chapter 3. Nous dérivons des flux conservant et dissipant l'entropie physique pour le modèle de Baer-Nunziato qui satisfont aux exigences de précision d'ordre élevé et de stabilité en entropie du schéma DG. Nous montrons également que les flux numériques préservent l'énergie cinétique au niveau discret. Nous montrons que notre schéma numérique garantit la positivité de la fraction volumique et des densités moyennes dans la cellule en imposant des conditions sur le pas de temps. La positivité des solutions moyennes de la cellule est ensuite transférée aux valeurs nodales par l'utilisation de limiteurs a posteriori. Nous illustrons les propriétés du schéma en effectuant de nombreux cas tests impliquant à la fois des problèmes de Riemann unidimensionnels et un problème d'interaction choc-bulle.

Nous discrétisons ensuite le modèle multi-composant proposé par Shyue [122], dans le but de proposer un schéma DG d'ordre élevé qui dissipe l'entropie pour les écoulements multi-composants qui permet également une résolution fine de l'interface matérielle. Le DGSEM nécessite de remplacer les flux physiques dans l'intégrale de volume par des flux conservant l'entropie, comme le montre le Theorem 3.5.1. Cependant, le modèle gamma n'admet une fonction d'entropie mathématique n'est convexe que pour les phases pures. À cette fin, nous concevons des flux conservant l'entropie pour les phases pures. Afin de préserver des profils de pression et de vitesse uniformes à travers les interfaces matérielles, nous concevons des flux préservant ces interfaces matérielles. Il faut noter qu'il est difficile de trouver un flux numérique unique qui présente les qualités de conservation de l'entropie et de préservation des contacts. Par conséquent, notre algorithme sélectionne entre les flux numériques conservateurs de l'entropie et les flux préservant les contacts dans l'intégrale de volume en se basant sur les valeurs générées par un senseur de chocs basé sur la pression.

À l'interface du schéma semi-discret pour le modèle gamma, nous appliquons un solveur HLLC. Nous montrons qu'un schéma à trois points basé sur ce solveur satisfait à une inégalité d'entropie discrète, préserve des profils uniformes à travers les discontinuités de contact et préserve la positivité de la densité, de l'énergie interne totale et de l'exposant adiabatique du mélange. La positivité est renforcée aux valeurs nodales par l'utilisation de limiteurs a posteriori.

Nous illustrons les propriétés de notre schéma numérique en réalisant plusieurs expériences numériques en une et deux dimensions spatiales. Pour les tests en une dimension, nous incluons des problèmes de Riemann qui impliquent des chocs forts, des phases évanescentes et des interfaces matérielles, tandis qu'en deux dimensions d'espace, nous simulons l'interaction d'un choc avec une bulle d'Hélium suspendue dans l'air[107].

Appendix A

Appendices

A.1 The semi-discrete DGSEM for the Baer-Nunziato model

Here we recall the semi-discrete scheme (3.54)

$$\frac{\omega_k h}{2}\frac{d\mathbf{U}_j^k}{dt} + \omega_k \sum_{l=0}^{p} \tilde{\mathbf{D}}(\mathbf{U}_j^k, \mathbf{U}_j^l) D_{kl} + \delta_{kp}\mathbf{D}^-(\mathbf{U}_j^p, \mathbf{U}_{j+1}^0) + \delta_{k0}\mathbf{D}^+(\mathbf{U}_{j-1}^p, \mathbf{U}_j^0) = 0,$$

where

$$\tilde{\mathbf{D}}(\mathbf{u}^-, \mathbf{u}^+) = 2\mathbf{h}(\mathbf{u}^-, \mathbf{u}^+) + \mathbf{d}^-(\mathbf{u}^-, \mathbf{u}^+) - \mathbf{d}^+(\mathbf{u}^+, \mathbf{u}^-),$$

and to which we apply the numerical fluxes from Propositions 4.3.1 and 4.2) at each DOF k of cell j at time n:

$$\frac{\omega_k h}{2}\frac{d}{dt}\alpha_{1,j}^{k,n} + \omega_k \sum_{l=0}^{p} \mathrm{u}_{\mathrm{I}}{}_j^{k,n} \alpha_{1,j}^{l,n} D_{kl} + \delta_{kp}\left((\mathrm{u}_{\mathrm{I}}{}_j^{p,n} - \beta_{sj+1/2}) \frac{[\![\alpha_1]\!]_{j+1/2}}{2} \right) + \delta_{k0}\left((\mathrm{u}_{\mathrm{I}}{}_j^{0,n} + \beta_{s_{j-1/2}}) \frac{[\![\alpha_1]\!]_{j-1/2}}{2} \right) = 0,$$

$$\begin{aligned}
&\frac{\omega_k h}{2}\frac{d}{dt}(\alpha_i\rho_i)_j^{k,n} + \omega_k \sum_{l=0}^{p} 2h_{\rho_i}(\mathbf{U}_j^{k,n}, \mathbf{U}_j^{l,n}) D_{kl} \\
&+ \delta_{kp}\left(h_{\rho_{i,j+1/2}} - \beta_{s_{j+1/2}} \frac{[\![\alpha_i]\!]_{j+1/2}}{2} \tilde{h}_{\rho_{i,j+1/2}} - (\alpha_i\rho_i u_i)_j^{p,n} - \frac{\epsilon_{\nu_{j+1/2}}}{2} \max\left(\rho_{\mathbf{A}}(\mathbf{u}_j^{p,n}), \rho_{\mathbf{A}}(\mathbf{u}_{j+1}^{0,n})\right) [\![\rho_i]\!]_{j+1/2} \right) \\
&+ \delta_{k0}\left(\beta_{s_{j-1/2}} \frac{[\![\alpha_i]\!]_{j-1/2}}{2} \tilde{h}_{\rho_{i,j-1/2}} - h_{\rho_{i,j-1/2}} + (\alpha_i\rho_i u_i)_j^{0,n} + \frac{\epsilon_{\nu_{j-1/2}}}{2} \max\left(\rho_{\mathbf{A}}(\mathbf{u}_{j-1}^{0,n}), \rho_{\mathbf{A}}(\mathbf{u}_j^{0,n})\right) [\![\rho_i]\!]_{j-1/2} \right) \\
&= 0, \quad i = 1, 2, \\
&\frac{\omega_k h}{2}\frac{d}{dt}(\alpha_i\rho_i u_i)_j^{k,n} + \omega_k \sum_{l=0}^{p} \left(2h_{\rho u_i}(\mathbf{U}_j^{k,n}, \mathbf{U}_j^{l,n}) - \mathrm{p}_{\mathrm{I}}{}_j^{k,n} \alpha_j^{l,n} \right) D_{kl}
\end{aligned}$$

$$
\begin{aligned}
&+\delta_{kp}\Bigg(h_{\rho u_{i,j+1/2}}-\Big(\beta_{s_{j+1/2}}\tilde{h}_{\rho u_{i,j+1/2}}+\mathrm{p}_{\mathrm{I}_j}^{p,n}\Big)\frac{[\![\alpha_i]\!]_{j+1/2}}{2}-\alpha_{i,j}^{p,n}(\rho_i u_i+\mathrm{p}_i)_j^{p,n}\\
&-\frac{\epsilon_{\nu_{j+1/2}}}{2}\max\big(\rho_{\mathbf{A}}(\mathbf{u}_j^{p,n}),\rho_{\mathbf{A}}(\mathbf{u}_{j+1}^{0,n})\big)[\![\rho_i u_i]\!]_{j+1/2}\Bigg)\\
&+\delta_{k0}\Bigg(\Big(\beta_{s_{j-1/2}}\tilde{h}_{\rho u_{i,j-1/2}}-\mathrm{p}_{\mathrm{I}_j}^{0,n}\Big)\frac{[\![\alpha_i]\!]_{j-1/2}}{2}-h_{\rho u_{i,j-1/2}}+\alpha_{i,j}^{0,n}(\rho_i u_i+\mathrm{p}_i)_j^{0,n}\\
&+\frac{\epsilon_{\nu_{j-1/2}}}{2}\max\big(\rho_{\mathbf{A}}(\mathbf{u}_{j-1}^{0,n}),\rho_{\mathbf{A}}(\mathbf{u}_j^{p,n})\big)[\![\rho_i u_i]\!]_{j-1/2}\Bigg)=0,\quad i=1,2,\\
&\frac{\omega_k h}{2}\frac{d}{dt}(\alpha_i\rho_i E_i)_j^{k,n}+\omega_k\sum_{l=0}^{p}\Big(2h_{\rho E_i}(\mathbf{U}_j^{k,n},\mathbf{U}_j^{l,n})-\mathrm{p}_{\mathrm{I}_j}^{k,n}\mathrm{u}_{\mathrm{I}_j}^{k,n}\alpha_{i,j}^{l,n}\Big)D_{kl}\\
&+\delta_{kp}\Bigg(h_{\rho E_{i,j+1/2}}-\Big(\beta_{s_{j+1/2}}\tilde{h}_{\rho E_{i,j+1/2}}+\mathrm{p}_{\mathrm{I}_j}^{p,n}\mathrm{u}_{\mathrm{I}_j}^{p,n}\Big)\frac{[\![\alpha_i]\!]_{j+1/2}}{2}-\alpha_{i,j}^{p,n}u_{i,j}^{p,n}(\rho_i E_i+\mathrm{p}_i)_j^{p,n}\\
&-\frac{\epsilon_{\nu_{j+1/2}}}{2}\max\big(\rho_{\mathbf{A}}(\mathbf{u}_j^{p,n}),\rho_{\mathbf{A}}(\mathbf{u}_{j+1}^{0,n})\big)\Bigg(\Big(\frac{\mathrm{C_v}_i}{\hat{\theta}_{i,j+1/2}}+\frac{u_{i,j}^{p,n}u_{i,j+1}^{0,n}}{2}\Big)[\![\rho_i]\!]_{j-1/2}+\overline{\rho}_{i,j+1/2}[\![E_i]\!]_{j+1/2}\Bigg)\Bigg)\\
&+\delta_{k0}\Bigg(\Big(\beta_{s_{j-1/2}}\tilde{h}_{\rho E_{i,j-1/2}}-\mathrm{p}_{\mathrm{I}_j}^{0,n}\mathrm{u}_{\mathrm{I}_j}^{0,n}\Big)\frac{[\![\alpha_i]\!]_{j-1/2}}{2}-h_{\rho E_{i,j-1/2}}+\alpha_{i,j}^{0,n}u_{i,j}^{0,n}(\rho_i E_i+\mathrm{p}_i)_j^{0,n}\\
&+\frac{\epsilon_{\nu_{j-1/2}}}{2}\max\big(\rho_{\mathbf{A}}(\mathbf{u}_{j-1}^{0,n}),\rho_{\mathbf{A}}(\mathbf{u}_j^{p,n})\big)\Bigg(\Big(\frac{\mathrm{C_v}_i}{\hat{\theta}_{i,j-1/2}}+\frac{u_{i,j-1}^{p,n}u_{i,j}^{0,n}}{2}\Big)[\![\rho_i]\!]_{j-1/2}+\overline{\rho}_{i,j-1/2}[\![E_i]\!]_{j-1/2}\Bigg)\Bigg)\\
&=0,\quad i=1,2,
\end{aligned}
$$

where $\epsilon_{\nu_{i,j\pm1/2}}\geqslant 0$, $\rho_{\mathbf{A}}(\mathbf{u})=\max_{i=1,2}(|u_i|+c_i)$, $\beta_{s_{j\pm1/2}}$ is defined is (4.31), while the numerical fluxes $(h_{\rho_i},h_{\rho u_i},h_{\rho E_i})$ and $(\tilde{h}_{\rho_i},\tilde{h}_{\rho u_i},\tilde{h}_{\rho E_i})$ are defined from (4.18).

A.2 Entropy conservative and entropy stable fluxes in multiple space dimensions

In multidimensional space, for solutions belonging to the phase space

$$\Omega_{\text{BNM}}=\big\{\mathbf{u}\in\mathbb{R}^{5+2d}:\,0<\alpha_i<1,\,\rho_i>0,\,\mathbf{v}_i\in\mathbb{R}^d,\,\rho_i e_i>\mathrm{p}_{\infty,i},\,i=1,2\big\},$$

the entropy conservative fluxes (3.47) are defined as follows:

$$\mathbf{D}_{ec}^{\mp}(\mathbf{u}^-,\mathbf{u}^+,\mathbf{n})=\pm\mathbf{h}(\mathbf{u}^-,\mathbf{u}^+,\mathbf{n})\mp\mathbf{f}(\mathbf{u}^{\mp})\cdot\mathbf{n}+\mathbf{d}^{\mp}(\mathbf{u}^-,\mathbf{u}^+,\mathbf{n}),$$

for the system (4.37). They are assumed to be consistent, $\mathbf{h}(\mathbf{u},\mathbf{u},\mathbf{n}) = \mathbf{f}(\mathbf{u})\cdot\mathbf{n}$ and $\mathbf{d}^{\mp}(\mathbf{u},\mathbf{u},\mathbf{n}) = 0$, and are defined as follows:

$$\mathbf{h}(\mathbf{u}^-,\mathbf{u}^+,\mathbf{n}) := \begin{pmatrix} 0 \\ \overline{\alpha}_i\hat{\rho}_i\overline{\mathbf{v}}_i\cdot\mathbf{n} \\ \overline{\alpha}_i\left(\hat{\rho}_i(\overline{\mathbf{v}}_i\cdot\mathbf{n})\overline{\mathbf{v}}_i + \dfrac{\overline{\mathrm{p}_i\theta_i}}{\overline{\theta}_i}\mathbf{n}\right) \\ \overline{\alpha}_i\left(\hat{\rho}_i\left(\dfrac{\mathrm{C_{v}}i}{\hat{\theta}_i} + \dfrac{\mathbf{v}_i^-\cdot\mathbf{v}_i^+}{2}\right) + \dfrac{\overline{\mathrm{p}_i\theta_i}}{\overline{\theta}_i} + \mathrm{p}_{\infty,i}\right)\overline{\mathbf{v}}_i\cdot\mathbf{n} \end{pmatrix} - \beta_s\frac{[\![\alpha_i]\!]}{2}\begin{pmatrix} 1 \\ \hat{\rho}_i \\ \hat{\rho}_i\overline{\mathbf{v}}_i \\ \hat{\rho}_i\left(\dfrac{\mathrm{C_{v}}i}{\hat{\theta}_i} + \dfrac{\mathbf{v}_i^-\cdot\mathbf{v}_i^+}{2}\right) + \mathrm{p}_{\infty,i} \end{pmatrix},$$

$$\mathbf{d}^{\pm}(\mathbf{u}^-,\mathbf{u}^+,\mathbf{n}) := \frac{[\![\alpha_i]\!]}{2}\begin{pmatrix} \mathbf{v}_{\mathrm{I}}^{\pm}\cdot\mathbf{n} \\ 0 \\ -\mathrm{p_I}^{\pm}\mathbf{n} \\ -\mathrm{p_I}^{\pm}\mathbf{v}_{\mathrm{I}}^{\pm}\cdot\mathbf{n} \end{pmatrix}, \quad i\in\{1,2\}.$$

The entropy stable fluxes read

$$\mathbf{D}^{\pm}(\mathbf{u}^-,\mathbf{u}^+,\mathbf{n}) = \mathbf{D}_{ec}^{\pm}(\mathbf{u}^-,\mathbf{u}^+,\mathbf{n}) \pm \mathbf{D}_{\nu}(\mathbf{u}^-,\mathbf{u}^+,\mathbf{n}),$$

with

$$\mathbf{D}_{\nu}(\mathbf{u}^-,\mathbf{u}^+,\mathbf{n}) = \frac{\epsilon_\nu}{2}\max\left(\rho_{\mathbf{A}}(\mathbf{u}^-,\mathbf{n}),\rho_{\mathbf{A}}(\mathbf{u}^+,\mathbf{n})\right)\begin{pmatrix} 0 \\ [\![\rho_i]\!] \\ [\![\rho_i\mathbf{v}_i]\!] \\ \left(\dfrac{\mathrm{C_{v}}i}{\hat{\theta}_i} + \dfrac{\mathbf{v}_i^-\cdot\mathbf{v}_i^+}{2}\right)[\![\rho_i]\!] + \overline{\rho_i}[\![E_i]\!] \end{pmatrix}, \quad i\in\{1,2\},$$

where $\epsilon_\nu \geqslant 0$ and $\rho_{\mathbf{A}}(\mathbf{u},\mathbf{n}) = \max_{i=1,2}(|\mathbf{v}_i\cdot\mathbf{n}| + c_i)$.

A.3 Condition for positivity of the cell-averaged solution in multiple space dimensions

The condition for positivity of the solution is based on the extension of Theorem 4.4.2. We introduce $\lambda_x = \frac{\Delta t}{h_x}$ and $\lambda_y = \frac{\Delta t}{h_y}$ with $\Delta t > 0$ the time step. Let $\rho_{i,j}^{0\leqslant k,l\leqslant p,n} > 0, 1 > \alpha_{i,j}^{0\leqslant k,l\leqslant p,n} > 0$, then the cell-averaged partial densities and void fraction are positive, at time $t^{(n+1)}$, under the following CFL condition:

$$(\lambda_x+\lambda_y)\max_{\kappa\in\Omega_h}\max_{\mathbf{u}=\mathbf{u}_1,\mathbf{u}_2}\max_{0\leqslant m\leqslant p}\left(\max_{0\leqslant k\leqslant p}\frac{1}{\omega_k}\left(\sum_{l=0}^{p}\omega_l D_{lk}\mathrm{u}_{\mathrm{I}}{}_{i,j}^{lm}+\delta_{kp}\frac{\beta^m_{s_{i+1/2}}-\mathrm{u}_{\mathrm{I}}{}_{i,j}^{pm}}{2}+\delta_{k0}\frac{\beta^m_{s_{i-1/2}}+\mathrm{u}_{\mathrm{I}}{}_{i,j}^{0m}}{2}\right),\right.$$
$$\max_{0\leqslant l\leqslant p}\frac{1}{\omega_l}\left(\sum_{k=0}^{p}\omega_k D_{kl}\mathrm{v}_{\mathrm{I}}{}_{i,j}^{mk}+\delta_{lp}\frac{\beta^m_{s_{j+1/2}}-\mathrm{v}_{\mathrm{I}}{}_{i,j}^{mp}}{2}+\delta_{l0}\frac{\beta^m_{s_{j-1/2}}+\mathrm{v}_{\mathrm{I}}{}_{i,j}^{m0}}{2}\right),$$
$$\frac{1}{\omega_0}\left(\frac{(\beta^m_{s_{i-1/2}}-\overline{u}^m_{i-1/2})\hat{\rho}^m_{i-1/2}}{2\rho^{0m}_{i,j}}+\frac{\epsilon^m_{\nu_{i-1/2}}}{\alpha^{0m}_{i,j}}\right),\frac{1}{\omega_p}\left(\frac{(\beta^m_{s_{i+1/2}}+\overline{u}^m_{i+1/2})\hat{\rho}^m_{i+1/2}}{2\rho^{pm}_{i,j}}+\frac{\epsilon^m_{\nu_{i+1/2}}}{\alpha^{pm}_{i,j}}\right),$$
$$\left.\frac{1}{\omega_0}\left(\frac{(\beta^m_{s_{j-1/2}}-\overline{v}^m_{j-1/2})\hat{\rho}^m_{j-1/2}}{2\rho^{m0}_{i,j}}+\frac{\epsilon^m_{\nu_{j-1/2}}}{\alpha^{m0}_{i,j}}\right),\frac{1}{\omega_p}\left(\frac{(\beta^m_{s_{j+1/2}}+\overline{v}^m_{j+1/2})\hat{\rho}^m_{j+1/2}}{2\rho^{mp}_{i,j}}+\frac{\epsilon^m_{\nu_{j+1/2}}}{\alpha^{mp}_{i,j}}\right)\right)^{(n)}<\frac{1}{2},$$

where u, v, and ρ refer either to phase $\mathbf{u}_1$, or to $\mathbf{u}_2$ and

$$\beta^m_{s_{i+1/2}}=\max_{i_p=1,2}\left(|u^{pm,n}_{i_p,i,j}|,|u^{0m,n}_{i_p,i+1,j}|\right),\quad \beta^m_{s_{j+1/2}}=\max_{i_p=1,2}\left(|v^{mp,n}_{i_p,i,j}|,|v^{m0,n}_{i_p,i,j+1}|\right),\quad 0\leqslant m\leqslant p,$$
$$\overline{u}^m_{i+1/2}=\frac{u^{pm,n}_{i,j}+u^{0m,n}_{i+1,j}}{2},\quad \overline{v}^m_{j+1/2}=\frac{v^{mp,n}_{i,j}+v^{m0,n}_{i+1,j}}{2},\quad 0\leqslant m\leqslant p,$$
$$\hat{\rho}^m_{i+1/2}=\frac{\rho^{0m,n}_{i+1,j}-\rho^{pm,n}_{i,j}}{\ln\rho^{0m,n}_{i+1,j}-\ln\rho^{pm,n}_{i,j}},\quad \hat{\rho}^m_{j+1/2}=\frac{\rho^{m0,n}_{i,j+1}-\rho^{mp,n}_{i,j}}{\ln\rho^{m0,n}_{i,j+1}-\ln\rho^{mp,n}_{i,j}},\quad 0\leqslant m\leqslant p.$$

Bibliography

[1] R. Abgrall. How to prevent pressure oscillations in multicomponent flow calculations: a quasi conservative approach. *J. Comput. Phys.*, 125(1):150–160, 1996.

[2] R. Abgrall and S. Karni. Computations of compressible multifluids. *J. Comput. Phys.*, 169(2):594–623, 2001.

[3] R. Abgrall and S. Karni. A comment on the computation of non-conservative products. *J. Comput. Phys.*, 229(8):2759–2763, 2010.

[4] G. Allaire, S. Clerc, and S. Kokh. A five-equation model for the simulation of interfaces between compressible fluids. *J. Comput. Phys.*, 181(2):577–616, 2002.

[5] A. Ambroso, C. Chalons, and P.-A. Raviart. A Godunov-type method for the seven-equation model of compressible two-phase flow. *Comput. Fluids*, 54:67–91, 2012.

[6] N. Andrianov and G. Warnecke. The Riemann problem for the Baer–Nunziato two-phase flow model. *J. Comput. Phys.*, 195(2):434–464, 2004.

[7] M. R. Baer and J. W. Nunziato. A two-phase mixture theory for the deflagration-to-detonation transition (DDT) in reactive granular materials. *Int. J. Multiphase Flow*, 12(6):861–889, 1986.

[8] D. S. Bale, R. J. Leveque, S. Mitran, and J. A. Rossmanith. A wave propagation method for conservation laws and balance laws with spatially varying flux functions. *SIAM J. Sci. Comput.*, 24(3):955–978, 2003.

[9] P. Batten, N. Clarke, C. Lambert, and D. M. Causon. On the choice of wavespeeds for the HLLC Riemann solver. *J. Sci. Comput.*, 18(6):1553–1570, 1997.

[10] J. B. Bdzil, R. Menikoff, S. F. Son, A. K. Kapila, and D. S. Stewart. Two-phase modeling of deflagration-to-detonation transition in granular materials: A critical examination of modeling issues. *Phys. Fluids*, 11(2):378–402, 1999.

[11] C. Berthon, B. Dubroca, and A. Sangam. A local entropy minimum principle for deriving entropy preserving schemes. *SIAM J. Numer. Anal.*, 50(2):468–491, 2012.

[12] C. Berthon, B. Dubroca, and A. Sangam. An entropy preserving relaxation scheme for ten-moments equations with source terms. *Comm. Math. Sci.*, 13(8):2119–2154, 2015.

[13] Z. Bilicki and J. Kestin. Physical aspects of the relaxation model in two-phase flow. *Proc. Royal Society of London. A. Mathematical and Physical Sciences*, 428(1875): 379–397, 1990.

[14] G. Billet, V. Giovangigli, and G. De Gassowski. Impact of volume viscosity on a shock–hydrogen-bubble interaction. *Combust. Theory Model.*, 12(2):221–248, 2008.

[15] M. Bohm, A. Winters, G. Gassner, D. Derigs, F. Hindenlang, and J. Saur. An entropy stable nodal discontinuous Galerkin method for the resistive MHD equations. Part I: Theory and numerical verification. *J. Comput. Phys.*, 2018.

[16] F. Bouchut. *Nonlinear stability of finite Volume Methods for hyperbolic conservation laws: And Well-Balanced schemes for sources.* Springer Science & Business Media, 2004.

[17] F. Bouchut. A reduced stability condition for nonlinear relaxation to conservation laws. *J. Hyperbolic Diff. Equations*, 1(01):149–170, 2004.

[18] F. Bouchut, C. Bourdarias, and B. Perthame. A MUSCL method satisfying all the numerical entropy inequalities. *Math. Comput.*, 65(216):1439–1461, 1996.

[19] J. C. Butcher. *The numerical analysis of ordinary differential equations: Runge-Kutta and general linear methods.* Wiley-Interscience, 1987.

[20] M. H. Carpenter, T. C. Fisher, E. J. Nielsen, and S. H. Frankel. Entropy stable spectral collocation schemes for the Navier–Stokes equations: Discontinuous interfaces. *SIAM J. Sci. Comput.*, 36(5):B835–B867, 2014.

[21] M. J. Castro, J. Gallardo, and C. Parés. High order finite volume schemes based on reconstruction of states for solving hyperbolic systems with nonconservative products. applications to shallow-water systems. *Math. Comput.*, 75(255):1103–1134, 2006.

[22] M. J. Castro, P. G. LeFloch, M. Muñoz-Ruiz, and C. Parés. Why many theories of shock waves are necessary: Convergence error in formally path-consistent schemes. *J. Comput. Phys.*, 227(17):8107–8129, 2008.

[23] M. J. Castro, C. Parés, G. Puppo, and G. Russo. Central schemes for nonconservative hyperbolic systems. *SIAM J. Sci. Comput.*, 34(5):B523–B558, 2012.

[24] M. J. Castro, U. S. Fjordholm, S. Mishra, and C. Parés. Entropy conservative and entropy stable schemes for nonconservative hyperbolic systems. *SIAM J. Numer. Anal.*, 51(3):1371–1391, 2013.

[25] M. J. Castro, T. M. de Luna, and C. Parés. Well-balanced schemes and path-conservative numerical methods. In *Handbook of Numer. Anal.*, volume 18, pages 131–175. Elsevier, 2017.

[26] C. Chalons and F. Coquel. A new comment on the computation of non-conservative products using Roe-type path conservative schemes. *J. Comput. Phys.*, 335:592 – 604, 2017. ISSN 0021-9991.

[27] C. Chalons, F. Coquel, S. Kokh, and N. Spillane. Large time-step numerical scheme for the seven-equation model of compressible two-phase flows. In *Finite Volumes for Complex Applications VI Problems & Perspectives*, pages 225–233. Springer, 2011.

[28] P. Chandrashekar. Kinetic energy preserving and entropy stable finite volume schemes for compressible Euler and Navier-Stokes equations. *Comm. Comput. Phys.*, 14(5): 1252–1286, 2013.

[29] G.-Q. Chen, C. D. Levermore, and T.-P. Liu. Hyperbolic conservation laws with stiff relaxation terms and entropy. *Comm. Pure Appl. Math.*, 47(6):787–830, 1994.

[30] T. Chen and C.-W. Shu. Entropy stable high order discontinuous Galerkin methods with suitable quadrature rules for hyperbolic conservation laws. *J. Comput. Phys.*, 345:427–461, 2017.

[31] J. Cheng, F. Zhang, and T. Liu. A discontinuous Galerkin method for the simulation of compressible gas-gas and gas-water two-medium flows. *J. Computat. Phys.*, 403: 109059, 2020.

[32] F. Coquel and P. G. Le Floch. Convergence of finite difference schemes for conservation laws in several space dimensions: a general theory. *SIAM J. Numer. Anal.*, 30(3):675–700, 1993.

[33] F. Coquel and B. t. Perthame. Relaxation of energy and approximate riemann solvers for general pressure laws in fluid dynamics. *SIAM J. Numer. Anal.*, 35(6):2223–2249, 1998.

[34] F. Coquel, T. Gallouët, J.-M. Hérard, and N. Seguin. Closure laws for a two-fluid two-pressure model. *C. R. Acad. Sci. Paris*, 334(10):927–932, 2002.

[35] F. Coquel, J.-M. Hérard, K. Saleh, and N. Seguin. Two properties of two-velocity two-pressure models for two-phase flows. *Comm. Math. Sci.*, 12(3), 2014.

[36] F. Coquel, J.-M. Hérard, and K. Saleh. A positive and entropy-satisfying finite volume scheme for the Baer–Nunziato model. *J. Comput. Phys.*, 330:401–435, 2017.

[37] F. Coquel, C. Marmignon, P. Rai, and F. Renac. An entropy stable high-order discontinuous Galerkin spectral element method for the Baer-Nunziato two-phase flow model. *J. Comput. Phys.*, 431:110135, 2021.

[38] V. Coralic and T. Colonius. Finite-volume WENO scheme for viscous compressible multicomponent flows. *J. Computat. Phys.*, 274:95–121, 2014.

[39] C. Dafermos. *Hyperbolic conservation laws in continuum physics*, volume 3. Springer, 2005.

[40] G. Dal Maso, P. G. LeFloch, and F. Murat. Definition and weak stability of nonconservative products. *J. Math. Pures Appl.*, 74:483–548, 1995.

[41] F. Daude and P. Galon. On the computation of the Baer–Nunziato model using ale formulation with hll-and HLLC-type solvers towards fluid–structure interactions. *J. Comput. Phys.*, 304:189–230, 2016.

[42] M. T. H. de Frahan, S. Varadan, and E. Johnsen. A new limiting procedure for discontinuous Galerkin methods applied to compressible multiphase flows with shocks and interfaces. *J. Comput. Phys.*, 280:489–509, 2015.

[43] S. Dellacherie. Relaxation schemes for the multicomponent euler system. *Math. Model. Numer. Anal.*, 37(6):909–936, 2003.

[44] D. A. Drew. Mathematical modeling of two-phase flow. *Annu. Rev. Fluid Mech.*, 15 (1):261–291, 1983.

[45] D. A. Drew and L. A. Segel. Averaged equations for two-phase flows. *Studies Appl. Math.*, 50(3):205–231, 1971.

[46] M. Dumbser and W. Boscheri. High-order unstructured Lagrangian one-step WENO finite volume schemes for non-conservative hyperbolic systems: applications to compressible multi-phase flows. *Comput. Fluids*, 86:405–432, 2013.

[47] M. Dumbser and R. Loubère. A simple robust and accurate a posteriori sub-cell finite volume limiter for the discontinuous Galerkin method on unstructured meshes. *J. Comput. Phys.*, 319:163–199, 2016.

[48] M. Dumbser and E. F. Toro. A simple extension of the Osher Riemann solver to non-conservative hyperbolic systems. *SIAM J. Sci. Comput.*, 48(1-3):70–88, 2011.

[49] M. Dumbser, M. Castro, C. Parés, and E. F. Toro. ADER schemes on unstructured meshes for nonconservative hyperbolic systems: Applications to geophysical flows. *Comput. Fluids*, 38(9):1731–1748, 2009.

[50] B. Einfeldt, C.-D. Munz, P. L. Roe, and B. Sjögreen. On godunov-type methods near low densities. *J. Comput. Phys.*, 92(2):273–295, 1991.

[51] S. Fechter and C.-D. Munz. A discontinuous Galerkin-based sharp-interface method to simulate three-dimensional compressible two-phase flow. *Int. J. Numer. Methods Fluids*, 78(7):413–435, 2015.

[52] T. C. Fisher and M. H. Carpenter. High-order entropy stable finite difference schemes for nonlinear conservation laws: Finite domains. *J. Comput. Phys.*, 252:518–557, 2013.

[53] T. Flåtten and H. Lund. Relaxation two-phase flow models and the subcharacteristic condition. *Math. Models Methods Appl. Sci.*, 21(12):2379–2407, 2011.

[54] E. Franquet and V. Perrier. Runge–Kutta discontinuous Galerkin method for the approximation of Baer and Nunziato type multiphase models. *J. Comput. Phys.*, 231 (11):4096–4141, 2012.

[55] F. Fraysse, C. Redondo, G. Rubio, and E. Valero. Upwind methods for the Baer–Nunziato equations and higher-order reconstruction using artificial viscosity. *J. Comput. Phys.*, 326:805–827, 2016.

[56] T. Gallouët, J.-M. Hérard, and N. Seguin. Numerical modeling of two-phase flows using the two-fluid two-pressure approach. *Math. Models Methods Appl. Sci.*, 14(05): 663–700, 2004.

[57] G. J. Gassner. A skew-symmetric discontinuous Galerkin spectral element discretization and its relation to SBP-SAT finite difference methods. *SIAM J. Sci. Comput.*, 35 (3):A1233–A1253, 2013. doi: 10.1137/120890144.

[58] G. J. Gassner. A kinetic energy preserving nodal discontinuous Galerkin spectral element method. *Int. J. Numer. Methods Fluids*, 76(1):28–50, 2014.

[59] G. J. Gassner, A. R. Winters, and D. A. Kopriva. Split form nodal discontinuous Galerkin schemes with summation-by-parts property for the compressible Euler equations. *J. Comput. Phys.*, 327:39–66, 2016.

[60] J. Giordano and Y. Burtschell. Richtmyer-Meshkov instability induced by shock-bubble interaction: Numerical and analytical studies with experimental validation. *Phys. Fluids*, 18(3):036102, 2006.

[61] E. Godlewski and P.-A. Raviart. *Numerical approximation of hyperbolic systems of conservation laws*, volume 118. Springer Science & Business Media, 2013.

[62] S. K. Godunov. An interesting class of quasilinear systems. In *Dokl. Acad. Nauk SSSR*, volume 139, pages 521–523, 1961.

[63] S. Gottlieb, C.-W. Shu, and E. Tadmor. Strong stability-preserving high-order time discretization methods. *SIAM review*, 43(1):89–112, 2001.

[64] L. D. Gryngarten and S. Menon. A generalized approach for sub-and super-critical flows using the local discontinuous Galerkin method. *Comput. Method. Appl. Mech. Eng.*, 253:169–185, 2013.

[65] J. F. Haas and B. Sturtevant. Interaction of weak shock waves with cylindrical and spherical gas inhomogeneities. *J. Fluid Mech.*, 181:41–76, 1987.

[66] E. Hairer, S. P. Noersett, and G. Wanner. *Solving Ordinary Differential Equations I: Nonstiff Problems: With 105 Figures*. Springer-Verlag, 1987.

[67] B. Hanouzet and R. Natalini. Global existence of smooth solutions for partially dissipative hyperbolic systems with a convex entropy. *Arch. Rational Mech. Anal.*, 169 (2):89–117, 2003.

[68] M. Hantke and S. Müller. Closure conditions for a one temperature non-equilibrium multi-component model of Baer-Nunziato type. *ESAIM: Proceedings and Surveys*, 66: 42–60, 2019.

[69] A. Harten, P. D. Lax, and B. V. Leer. On upstream differencing and Godunov-type schemes for hyperbolic conservation laws. *SIAM review*, 25(1):35–61, 1983.

[70] A. Hiltebrand and S. Mishra. Entropy stable shock capturing space–time discontinuous Galerkin schemes for systems of conservation laws. *Numer. Math.*, 126(1):103–151, 2014.

[71] A. Hiltebrand, S. Mishra, and C. Parés. Entropy-stable space–time DG schemes for non-conservative hyperbolic systems. *ESAIM: M2AN*, 52(3):995–1022, 2018.

[72] S. Hou and X.-D. Liu. Solutions of multi-dimensional hyperbolic systems of conservation laws by square entropy condition satisfying discontinuous Galerkin method. *J. Sci. Comput.*, 31(1-2):127–151, 2007.

[73] R. W. Houim and K. K. Kuo. A low-dissipation and time-accurate method for compressible multi-component flow with variable specific heat ratios. *J. Comput. Phys.*, 230(23):8527–8553, 2011.

[74] X. Y. Hu, B. Khoo, N. A. Adams, and F. L. Huang. A conservative interface method for compressible flows. *J. Comput. Phys.*, 219(2):553–578, 2006.

[75] M. Ishii. Thermo-fluid dynamic theory of two-phase flow. *NASA Sti/recon Technical Report A*, 75, 1975.

[76] F. Ismail and P. L. Roe. Affordable, entropy-consistent Euler flux functions ii: Entropy production at shocks. *J. Comput. Phys.*, 228(15):5410–5436, 2009.

[77] A. Jameson. Formulation of kinetic energy preserving conservative schemes for gas dynamics and direct numerical simulation of one-dimensional viscous compressible flow in a shock tube using entropy and kinetic energy preserving schemes. *J. Sci. Comput.*, 34(2):188–208, 2008.

[78] A. Jameson, W. Schmidt, and E. Turkel. Numerical solution of the euler equations by finite volume methods using Runge Kutta time stepping schemes. In *14th fluid and plasma dynamics conference*, page 1259, 1981.

[79] G. S. Jiang and C.-W. Shu. On a cell entropy inequality for discontinuous Galerkin methods. *Math. Comput.*, 62(206):531–538, 1994.

[80] E. Johnsen and T. Colonius. Implementation of WENO schemes in compressible multicomponent flow problems. *J. Comput. Phys.*, 219(2):715–732, 2006.

[81] A. K. Kapila, R. Menikoff, J. B. Bdzil, S. F. Son, and D. S. Stewart. Two-phase modeling of deflagration-to-detonation transition in granular materials: Reduced equations. *Phys. fluids*, 13(10):3002–3024, 2001.

[82] S. Karni and G. Hernández-Dueñas. A hybrid algorithm for the Baer-Nunziato model using the riemann invariants. *J. Sci. Comput.*, 45(1):382–403, 2010.

[83] S. Kawai and H. Terashima. A high-resolution scheme for compressible multicomponent flows with shock waves. *Int. J. Numer. Methods. Fluids*, 66(10):1207–1225, 2011.

[84] F. Kemm, E. Gaburro, F. Thein, and M. Dumbser. A simple diffuse interface approach for compressible flows around moving solids of arbitrary shape based on a reduced Baer–Nunziato model. *Computers & Fluids*, 204:104536, 2020.

[85] C. A. Kennedy and A. Gruber. Reduced aliasing formulations of the convective terms within the navier–stokes equations for a compressible fluid. *J. Comput. Phys.*, 227(3): 1676–1700, 2008.

[86] D. A. Kopriva and G. Gassner. On the quadrature and weak form choices in collocation type discontinuous Galerkin spectral element methods. *J. Sci. Comput.*, 44(2):136–155, 2010.

[87] Y. Kuya, K. Totani, and S. Kawai. Kinetic energy and entropy preserving schemes for compressible flows by split convective forms. *J. Comput. Phys.*, 375:823–853, 2018.

[88] P. Lax and B. Wendroff. Systems of conservation laws. *Comm. Pure Appl. Math.*, 13 (2):217–237, 1960.

[89] P. D. Lax. *Hyperbolic systems of conservation laws and the mathematical theory of shock waves*. SIAM, 1973.

[90] P. G. LeFloch. Shock waves for nonlinear hyperbolic systems in nonconservative form. *IMA Preprint Series*, 593, 1989.

[91] P. G. LeFloch and S. Mishra. Numerical methods with controlled dissipation for small-scale dependent shocks. *Acta Numerica*, 23:743–816, 2014.

[92] G. Linga. A hierarchy of non-equilibrium two-phase flow models. *arXiv preprint arXiv:1804.05241*, 2018.

[93] T. G. Liu, B. C. Khoo, and K. S. Yeo. Ghost fluid method for strong shock impacting on material interface. *J. Comput. Phys.*, 190(2):651–681, 2003.

[94] Y. Liu, C.-W. Shu, and M. Zhang. Entropy stable high order discontinuous Galerkin methods for ideal compressible MHD on structured meshes. *J. Comput. Phys.*, 354: 163–178, 2018.

[95] C. Lowe. Two-phase shock-tube problems and numerical methods of solution. *J. Comput. Phys.*, 204(2):598–632, 2005.

[96] H. Lu, J. Zhu, D. Wang, and N. Zhao. Runge–Kutta discontinuous Galerkin method with front tracking method for solving the compressible two-medium flow. *Comput. Fluids*, 126:1–11, 2016.

[97] H. Lund. A hierarchy of relaxation models for two-phase flow. *J. Appl. Math.*, 72(6): 1713–1741, 2012.

[98] C. Marmignon, F. Naddei, and F. Renac. Energy relaxation approximation for the compressible multicomponent flows in thermal nonequilibrium. *arXiv:2103.03731 [math.NA]*, 2021.

[99] J. Massoni, R. Saurel, B. Nkonga, and R. Abgrall. Some models and eulerian methods for interface problems between compressible fluids with heat transfer. *Int. J. Heat and Mass Transfer*, 45(6):1287–1307, 2002.

[100] M. S. Mock. Systems of conservation laws of mixed type. *J. Differ. Equ.*, 37(1):70–88, 1980.

[101] A. Murrone and H. Guillard. A five equation reduced model for compressible two phase flow problems. *J. Comput. Phys.*, 202(2):664–698, 2005.

[102] A. K. Pandare, J. Waltz, and J. Bakosi. A reconstructed discontinuous Galerkin method for multi-material hydrodynamics with sharp interfaces. *Int. J. Numer. Methods Fluids*, 92(8):874–898, 2020.

[103] C. Parés. Numerical methods for nonconservative hyperbolic systems: a theoretical framework. *SIAM J. Numer. Anal.*, 44(1):300–321, 2006.

[104] B. Perthame and C.-W. Shu. On positivity preserving finite volume schemes for euler equations. *Numer. Math.*, 73(1):119–130, 1996.

[105] J. Qiu, T. Liu, and B. C. Khoo. Runge–Kutta discontinuous Galerkin methods for compressible two-medium flow simulations: One-dimensional case. *J. Comput. Phys.*, 222(1):353–373, 2007.

[106] J. Qiu, T. G. Liu, B. C. Khoo, et al. Simulations of compressible two-medium flow by Runge-Kutta discontinuous Galerkin methods with the ghost fluid method. *Comm. Comput. Phys.*, 3(2):479–504, 2008.

[107] J. J. Quirk and S. Karni. On the dynamics of a shock–bubble interaction. *J. Fluid Mech.*, 318:129–163, 1996.

[108] F. Renac. Entropy stable DGSEM for nonlinear hyperbolic systems in nonconservative form with application to two-phase flows. *J. Comput. Phys.*, 382:1–26, 2019.

[109] F. Renac. Entropy stable, positive DGSEM with sharp resolution of material interfaces for a 4×4 two-phase flow system: a legacy from three-point schemes. *arXiv preprint arXiv:2001.05710*, 2019.

[110] F. Renac. Entropy stable, robust and high-order DGSEM for the compressible multicomponent Euler equations. *submitted*, 2020.

[111] F. Renac. Entropy stable, robust and high-order dgsem for the compressible multicomponent euler equations. *J. Comput. Phys.*, page 110584, 2021.

[112] F. Renac, M. de la Llave Plata, E. Martin, J. B. Chapelier, and V. Couaillier. *Aghora: A High-Order DG Solver for Turbulent Flow Simulations*, pages 315–335. Springer International Publishing, Cham, 2015. doi: 10.1007/978-3-319-12886-3_15.

[113] S. Rhebergen, O. Bokhove, and J. van der Vegt. Discontinuous Galerkin finite element methods for hyperbolic nonconservative partial differential equations. *J. Comput. Phys.*, 227(3):1887–1922, 2008.

[114] L. Sainsaulieu. Finite volume approximation of two phase-fluid flows based on an approximate Roe-type Riemann solver. *J. Comput. Phys.*, 121(1):1–28, 1995.

[115] R. Saurel and R. Abgrall. A multiphase Godunov method for compressible multifluid and multiphase flows. *J. Comput. Phys.*, 150(2):425–467, 1999.

[116] R. Saurel, S. Gavrilyuk, and F. Renaud. A multiphase model with internal degrees of freedom: application to shock–bubble interaction. *J. Fluid Mech.*, 495:283–321, 2003.

[117] R. Saurel, O. Le Metayer, J. Massoni, and S. Gavrilyuk. Shock jump relations for multiphase mixtures with stiff mechanical relaxation. *Shock waves*, 16(3):209–232, 2007.

[118] R. Saurel, F. Petitpas, and R. Abgrall. Modelling phase transition in metastable liquids: Application to cavitating and flashing flows. *J. Fluid Mech.*, 607:313–350, 2008.

[119] R. Saurel, F. Petitpas, and R. A. Berry. Simple and efficient relaxation methods for interfaces separating compressible fluids, cavitating flows and shocks in multiphase mixtures. *J. Comput. Phys.*, 228(5):1678–1712, 2009.

[120] R. Saurel, A. Chinnayya, and Q. Carmouze. Modelling compressible dense and dilute two-phase flows. *Phys. fluids*, 29(6):063301, 2017.

[121] C.-W. Shu and S. Osher. Efficient implementation of essentially non-oscillatory shock-capturing schemes. *J. Comput. Phys.*, 77(2):439–471, 1988.

[122] K.-M. Shyue. An efficient shock-capturing algorithm for compressible multicomponent problems. *J. Comput. Phys.*, 142(1):208–242, 1998.

[123] K.-M. Shyue. A fluid-mixture type algorithm for compressible multicomponent flow with van der waals equation of state. *J. Comput. Phys.*, 156(1):43–88, 1999.

[124] K.-M. Shyue. A fluid-mixture type algorithm for compressible multicomponent flow with mie–grüneisen equation of state. *J. Comput. Phys.*, 171(2):678–707, 2001.

[125] B. Sjögreen and H. C. Yee. Grid convergence of high order methods for multiscale complex unsteady viscous compressible flows. *J. Comput. Phys.*, 185(1):1–26, 2003.

[126] M. Sonntag and C.-D. Munz. Efficient parallelization of a shock capturing for discontinuous Galerkin methods using finite volume sub-cells. *J. Sci. Comput.*, 70(3): 1262–1289, 2017.

[127] Z. Sun, J. A. Carrillo, and C.-W. Shu. An entropy stable high-order discontinuous Galerkin method for cross-diffusion gradient flow systems. *arXiv preprint arXiv:1810.03221*, 2018.

[128] E. Tadmor. The numerical viscosity of entropy stable schemes for systems of conservation laws. I. *Math. Comput.*, 49(179):91–103, 1987.

[129] H. Terashima and G. Tryggvason. A front-tracking/ghost-fluid method for fluid interfaces in compressible flows. *J. Comput. Phys.*, 228(11):4012–4037, 2009.

[130] M. D. Thanh, D. Kröner, and N. T. Nam. Numerical approximation for a Baer–Nunziato model of two-phase flows. *Appl. Numer. Math.*, 61(5):702–721, 2011.

[131] M. D. Thanh, D. Kröner, and C. Chalons. A robust numerical method for approximating solutions of a model of two-phase flows and its properties. *Appl. Math. Comput.*, 219(1):320–344, 2012.

[132] S. A. Tokareva and E. F. Toro. HLLC-type Riemann solver for the Baer–Nunziato equations of compressible two-phase flow. *J. Comput. Phys.*, 229(10):3573–3604, 2010.

[133] S. A. Tokareva and E. F. Toro. A flux splitting method for the Baer–Nunziato equations of compressible two-phase flow. *J. Comput. Phys.*, 323:45–74, 2016.

[134] E. F. Toro. Riemann-problem-based techniques for computing reactive two-phased flows. In *Numer. Combustion*, pages 472–481. Springer, 1989.

[135] E. F. Toro. *Riemann solvers and numerical methods for fluid dynamics: a practical introduction*. Springer Science & Business Media, 2013.

[136] E. F. Toro, M. Spruce, and W. Speares. Restoration of the contact surface in the hll-riemann solver. *Shock waves*, 4(1):25–34, 1994.

[137] A. Volpert. The spaces bv and quasilinear equations, ussr math. *Sb*, 2:225–267, 1967.

[138] C. Wang and C.-W. Shu. An interface treating technique for compressible multi-medium flow with Runge–Kutta discontinuous Galerkin method. *J. Comput. Phys.*, 229(23):8823–8843, 2010.

[139] C. Wang, X. Zhang, C.-W. Shu, and J. Ning. Robust high order discontinuous Galerkin schemes for two-dimensional gaseous detonations. *J. Comput. Phys.*, 231(2):653–665, 2012.

[140] G. B. Whitham. *Linear and nonlinear waves*, volume 42. John Wiley & Sons, 2011.

[141] N. Wintermeyer, A. R. Winters, G. J. Gassner, and D. A. Kopriva. An entropy stable nodal discontinuous Galerkin method for the two dimensional shallow water equations on unstructured curvilinear meshes with discontinuous bathymetry. *J. Comput. Phys.*, 340:200–242, 2017.

[142] A. R. Winters and G. J. Gassner. Affordable, entropy conserving and entropy stable flux functions for the ideal MHD equations. *J. Comput. Phys.*, 304:72–108, 2016.

[143] W.-A. Yong. Entropy and global existence for hyperbolic balance laws. *Arch. Rat. Mech. Anal.*, 172(2):247–266, 2004.

[144] A. Zein, M. Hantke, and G. Warnecke. Modeling phase transition for compressible two-phase flows applied to metastable liquids. *J. Comput. Phys.*, 229(8):2964–2998, 2010.

[145] X. Zhang and C. Shu. On positivity-preserving high order discontinuous Galerkin schemes for compressible Euler equations on rectangular meshes. *J. Comput. Phys.*, 229(23):8918–8934, 2010.

[146] X. Zhang and C.-W. Shu. On maximum-principle-satisfying high order schemes for scalar conservation laws. *J. Comput. Phys.*, 229(9):3091–3120, 2010.

ECOLE
DOCTORALE
DE MATHEMATIQUES
HADAMARD

Titre : Modélisation et simulation numérique d'écoulements multi-composants compressibles

Mots clés : Écoulements multiphasiques compressibles, écoulement multi-componsants, EDP hyperbolique sous forme non-conservative, Galerkin discontinu

Résumé : Cette thèse a deux objectifs principaux : la modélisation des écoulements compressibles multiphasiques et multi-composants, et la conception de nouveaux schémas numériques pour leur simulation d'ordre élevé.Dans la première partie de ce travail, nous proposons un nouveau modèle hyperbolique de type Baer-Nunziato pour les écoulements réactifs gaz-liquide en non-équilibre, qui présente un transfert de masse, une résistance interfaciale, un non-équilibre mécanique et un transfert thermique entre les phases. Le modèle est fermé en utilisant des lois de fermeture générales pour l'interface matérielle. Nous montrons que notre modèle est invariant par transformation galiléenne et dissipe l'entropie et qu'il maintient ces propriétés à l'état de non-équilibre.
En ce qui concerne la conception de nouveaux schémas pour les écoulements compressibles, nous nous concentrons sur les modèles hyperboliques d'écoulement multiphasiques et multi-composants sous forme non-conservative. Nous choisissons comme cadre de discrétisation la méthode des éléments spectraux de Galerkin discontinus (DG-SEM), basée sur la collocation des points de quadrature et d'interpolation. La méthode DGSEM utilise des opérateurs de sommation par parties (SBP) dans la quadrature numérique pour approcher les intégrales sur les éléments de discrétisation. Dans notre cas, nous modifions l'intégrale sur les éléments de la cellule en remplaçant les flux physiques par des flux aux fluctuations conservant l'entropie tout en appliquant des flux dissipant l'entropie aux interfaces du maillage. Cela nous permet d'établir un schéma semi-discret qui est précis à l'ordre élevé et qui satisfait à une inégalité d'entropie semi-discrète. Pour l'intégration temporelle d'ordre élevé, nous nous appuyons sur des schémas explicites de Runge-Kutta préservant la stabilité et conservant les propriétés des schémas d'intégration temporelle au premier ordre.Dans ce travail, le DGSEM semi-discret est appliqué au modèle homogène de Baer-Nunziato et au modèle multi-composant de Shyue (1998). On montre que les schémas numériques maintiennent la positivité de la solution moyenne de la cellule, qui est renforcée aux valeurs nodales en utilisant des limiteurs a posteriori.

Title : Modelling and numerical simulation of compressible multicomponent flows

Keywords : Compressible multiphase flows, multicomponent flows, hyperbolic PDEs, nonconservative product, discontinuous Galerkin method

Abstract : This thesis addresses two main objectives: the modelling of compressible multiphase and multicomponent flows, and the design of novel numerical schemes for their accurate simulation. In the first part of this work, we propose a novel Baer-Nunziato-like hyperbolic model for reactive non-equilibrium gas-liquid flows, that accounts for mass transfer, interfacial drag, mechanical nonequilibrium and thermal transfer between the phases. The model is closed using general closure laws for the interfaces. We show that our model is Galilean invariant and entropy dissipative and maintain these properties at compete non-equilibrium.
We, then, focus on designing novel high-order, positivity preserving and entropy stable numerical schemes for hyperbolic multiphase and multicomponent flows, involving nonconservative products, using the discontinuous Galerkin spectral elements method (DGSEM). The DGSEM satisfies the summation-by-parts property, and we use the SBP operators to modify the volume integral over cell elements and replace the physical fluxes with entropy conservative fluxes in fluctuation form, while applying entropy stable fluxes at the cell interfaces. This modification allows us to establish a semi-discrete entropy inequality, for a given entropy function, while still ensuring high-order accuracy of the numerical scheme. For high-order integration in time, we rely on explicit strong-stability preserving Runge-Kutta schemes that retain the properties of first order time integration schemes. Here the semi-discrete DGSEM is applied to thehomogeneous Baer-Nunziato model and the multicomponent model of Shyue (1998). The numerical schemes are shown to maintain positivity of the cell-averaged solution which is further enforced at nodal values using a posteriori limiters.

Institut Polytechnique de Paris
91120 Palaiseau, France